



University of HUDDERSFIELD

University of Huddersfield Repository

Finch, Catherine Vanessa

Chemical modification of skin mimic systems

Original Citation

Finch, Catherine Vanessa (2017) Chemical modification of skin mimic systems. Post-Doctoral thesis, The University of Huddersfield.

This version is available at <http://eprints.hud.ac.uk/id/eprint/34645/>

The University Repository is a digital collection of the research output of the University, available on Open Access. Copyright and Moral Rights for the items on this site are retained by the individual author and/or other copyright owners. Users may access full items free of charge; copies of full text items generally can be reproduced, displayed or performed and given to third parties in any format or medium for personal research or study, educational or not-for-profit purposes without prior permission or charge, provided:

- The authors, title and full bibliographic details is credited in any copy;
- A hyperlink and/or URL is included for the original metadata page; and
- The content is not changed in any way.

For more information, including our policy and submission procedure, please contact the Repository Team at: E.mailbox@hud.ac.uk.

<http://eprints.hud.ac.uk/>

CHEMICAL MODIFICATION OF SKIN MIMIC SYSTEMS

CATHERINE VANESSA FINCH

A thesis submitted to the University of Huddersfield in partial fulfilment of the requirements for the
degree of Doctor of Philosophy

The University of Huddersfield

December 2017

Copyright statement

- i. The author of this thesis (including any appendices and/or schedules to this thesis) owns any copyright in it (the “Copyright”) and s/he has given The University of Huddersfield the right to use such copyright for any administrative, promotional, educational and/or teaching purposes.
- ii. Copies of this thesis, either in full or in extracts, may be made only in accordance with the regulations of the University Library. Details of these regulations may be obtained from the Librarian. This page must form part of any such copies made.
- iii. The ownership of any patents, designs, trademarks and any and all other intellectual property rights except for the Copyright (the “Intellectual Property Rights”) and any reproductions of copyright works, for example graphs and tables (“Reproductions”), which may be described in this thesis, may not be owned by the author and may be owned by third parties. Such Intellectual Property Rights and Reproductions cannot and must not be made available for use without the prior written permission of the owner(s) of the relevant Intellectual Property Rights and/or Reproductions.

Abstract

This thesis investigates the effect of various physical and chemical surface modification methods on the permeation of topically applied pharmaceutical compounds through poly(dimethylsiloxane) (PDMS), a polymer frequently employed as a model barrier in *in vitro* skin permeation studies. Such studies are essential for safety, risk assessment, and quality control purposes, in addition to assisting in the design and development of efficacious topically applied medicines. The commercial availability, legal status, ease of handling, and the reproducibility of the permeation data associated with polymeric skin mimics renders them an attractive alternative to biological tissue. However, over-predictions of percutaneous absorption observed following the use of such membranes are a significant disadvantage when attempting to obtain quantitative toxicological data. Accordingly, the aims of the work presented in this thesis were to both reduce the permeability of PDMS to pharmaceutical compounds, and to increase correlation between permeation data obtained using the synthetic substitute and data obtained similarly using suitable biological tissue.

Primarily, the potential of an air plasma pre-treatment to produce a lamellae-type structure in PDMS, endeavouring to more accurately model the architectural, physical, and chemical properties of the human stratum corneum, was investigated. Reductions in the permeability coefficient of up to 54.4 % were observed, rendering the modified system promising. Correlation analysis revealed an increase in correlation between the data collected using the modified synthetic substitute ($R^2 = 0.86$) and a self-collated library of literature-derived epidermal tissue permeability data, relating to eighteen compounds and spanning a range of typical penetrants, compared to similar analysis using data obtained using the native substitute ($R^2 = 0.75$), suggesting an increase in the predictive capability.

It was hypothesised that an N_2 plasma treatment may provide suitable surface functional groups on the PDMS substrate, namely amine groups, for the covalent attachment of biomolecules via an N,N' -dicyclohexylcarbodiimide (DCC) coupling reaction, enabling the production of a skin mimic displaying enhanced biorelevance. Therefore, the effect of an N_2 plasma pre-treatment on the permeation of a subset of the eighteen compounds investigated. It was found that the N_2 plasma pre-treatment was advantageous in terms of offering a greater reduction in permeability, since longer treatment times could be employed i.e. reductions of up to 61.8 % were observed. However, significant surface oxidation was still observed, with only a marginal increase in nitrogen containing functionalities compared with the air plasma analogue i.e. 0.31 %. Furthermore, the treatment did not offer any additional increase in correlation between epidermal-derived data than previously observed.

Further chemical methods of biomolecule attachment were pursued for use in the development of a lipid-proteinaceous bilayer model, initiated in both cases by surface amination using an alkoxy silane. This was followed by a DCC coupling to an amino acid in the former approach, and use of a glutaraldehyde

linker molecule to attach the same amino acid, namely lysine, in the latter approach. In either case, no further reductions in the permeation of the pharmaceutical compounds tested were observed, with respect to that through plasma treated PDMS.

In summary, the air plasma treatment of PDMS was found to be a promising approach to simultaneously reducing the permeability of a silicone skin mimic and increasing correlation with data obtained in similar studies employing biological tissue. Further, the covalent coupling of biomolecules to the surface of PDMS following surface amine group generation, via both plasma and wet chemical methods, appeared not to compromise the integrity the PDMS membranes relating to such applications, rendering the techniques compatible with the production of biorelevant semi-synthetic skin mimics.

Dedication

This thesis is dedicated to my Mum, Dad, and Lorna. Everything that I have achieved is because of you.

Acknowledgements

I would firstly like to thank my supervisors, Dr Laura Waters and Dr Karl Hemming, for all of their help and guidance throughout my PhD, and without whom completion would not have been possible. I would further like to thank Dr Laura Waters for her unconditional support, for being an inspirational woman in science, and for the multitude of opportunities that you have provided me.

I would like to thank every member the research group for sharing their wealth of knowledge, including the fantastic undergraduate students I have had the opportunity to work with; Faiza and Maria, you made my second year of study not only productive, but enjoyable. I would also like to thank the technical staff in the School of Applied Sciences for being an endless source of knowledge and assistance. I would personally like to thank Dr Richard Hughes for being a fantastic laboratory neighbour, and for not requesting to be relocated. I would also like to thank Dr Deborah Hammond at the Kroto Research Institute for allowing me access to a plethora of resources to support my professional development.

To all my friends in the organic and inorganic chemistry research groups, thank you for always being insightful, kind, and hilarious. Finally, to my best friends, Scarlett and James, I owe you everything for your unfaltering love and support, and for making the last three years a truly enjoyable time to reflect upon. I will not list everything that you have done for me here, instead I promise to spend the next ten years returning all the favours, hopefully closer to the equator.

Table of Contents

Chapter 1 Introduction.....	1
1.1 Topical and Transdermal Drug Delivery.....	1
1.2 The Structure of Human Skin.....	1
1.3 Surpassing the Barrier.....	4
1.4 <i>In Vitro</i> Determination of Percutaneous Absorption.....	5
1.5 Properties of the Permeant.....	10
1.6 Modelling Transdermal Absorption.....	13
1.6.1 Human Tissue.....	13
1.6.2 Animal Tissue.....	14
1.6.3 Alternative Models.....	16
1.6.3.1 Cell Culture Models.....	17
1.6.3.2 Quantitative Structure - Permeability Relationships.....	17
1.6.3.3 Parallel Artificial Membrane Permeability Assay (PAMPA).....	20
1.6.3.4 Strat-M®.....	21
1.6.3.5 Poly(dimethylsiloxane).....	23
1.7 Modification of Poly(dimethylsiloxane).....	28
1.7.1 Properties of Poly(dimethylsiloxane).....	28
1.7.2 Dynamic Modification.....	30
1.7.3 Surface Oxidation.....	31
1.7.4 Covalent Attachment.....	33
1.8 Research Aims.....	35
Chapter 2 Materials and Method.....	45
2.1 Materials.....	45

2.2 Methods.....	50
2.2.1 Air Plasma Modification of Poly(dimethylsiloxane).....	50
2.2.1.1 Membrane Preparation.....	50
2.2.1.2 Water Contact Angle Analysis.....	50
2.2.1.3 Scanning Electron Microscopy.....	50
2.2.1.4 Attenuated Total Reflectance - Fourier Transform Infrared Spectroscopy.....	50
2.2.1.5 X-ray Photoelectron Spectroscopy.....	51
2.2.1.6 Finite Dose Permeability Studies.....	51
2.2.1.7 Infinite Dose Permeability Studies.....	53
2.2.2 N ₂ Plasma Modification of Poly(dimethylsiloxane).....	54
2.2.2.1 Membrane Preparation.....	54
2.2.2.2 Membrane Characterisation.....	55
2.2.2.3 Permeation Studies.....	55
2.2.3 Lysine Functionalisation of Poly(dimethylsiloxane).....	57
2.2.3.1 Lysine attachment to N ₂ plasma treated PDMS using <i>N,N'</i> -Dicyclohexylcarbodiimide (DCC).....	57
2.2.3.2 Lysine Attachment to Alkoxysilane Functionalised PDMS using <i>N,N'</i> -Dicyclohexylcarbodiimide (PDMS-APTMS-Lys).....	58
2.2.3.3 Lysine Attachment to PDMS using Glutaraldehyde Linker (PDMS-APTES-GA-Lys).....	59
2.2.3.4 Lysine-Functionalised PDMS Permeation Study.....	59

Chapter 3 The Effect of Air Plasma Treatment on the Permeation of Pharmaceutical Compounds through Poly(dimethylsiloxane).....62

3.1 Introduction.....	62
3.2 Results and Discussion.....	65

3.2.1 Membrane Characterisation.....	65
3.2.1.1 Water Contact Angle Analysis.....	65
3.2.1.2 Attenuated Total Reflectance - Fourier Transform Infrared Spectroscopy.....	65
3.2.1.3 X-ray Photoelectron Spectroscopy.....	66
3.2.1.4 Scanning Electron Microscopy.....	72
3.2.2 Permeation Studies.....	73
3.2.2.1 Finite Dose.....	73
3.2.2.2 Infinite Dose.....	79
3.2.3 Comparison with Human Skin Data.....	90
3.4 Conclusions.....	98
Chapter 4 The Effect of Nitrogen Plasma Treatment on the Permeation of Pharmaceutical Compounds through Poly(dimethylsiloxane).....	103
4.1 Introduction.....	103
4.2 Results and Discussion.....	105
4.2.1 Membrane Characterisation.....	105
4.2.1.1 Attenuated Total Reflectance - Fourier Transform Infrared Spectroscopy.....	105
4.2.1.2 X-ray Photoelectron Spectroscopy.....	106
4.2.1.3 Scanning Electron Microscopy.....	110
4.2.2 Permeation Studies.....	113
4.2.2.1 Treatment Time Determination.....	113
4.2.2.2 Permeability Coefficient Determination.....	116
4.2.2.3 Comparison with Human Skin Data.....	123
4.3 Conclusions.....	125
Chapter 5 A Comparative Study of Biomolecule Conjugation Methods.....	129
5.1. Introduction.....	129

5.2 Results and Discussion.....	132
5.2.1 Alkoxysilane Layer Formation and <i>N, N'</i> -Dicyclohexylcarbodiimide	
Coupling to Lysine.....	132
5.2.1.1 Alkoxysilane Layer Formation	132
5.2.1.1.1 Attenuated Total Reflectance - Fourier Transform Infrared	
Spectroscopy.....	132
5.2.1.1.2 X-ray Photoelectron Spectroscopy.....	132
5.2.1.1.3 Scanning Electron Microscopy.....	136
5.2.1.2 <i>N, N'</i> -Dicyclohexylcarbodiimide coupling to lysine.....	138
5.2.1.2.1 Attenuated Total Reflectance - Fourier Transform Infrared	
Spectroscopy.....	138
5.2.1.2.2. X-ray Photoelectron Spectroscopy.....	140
5.2.2 Coupling of Lysine to N ₂ plasma treated PDMS.....	142
5.2.2.1 Attenuated Total Reflectance - Fourier Transform Infrared Spectroscopy.....	142
5.2.2.2 X-ray Photoelectron Spectroscopy.....	143
5.2.3 Use of glutaraldehyde linker.....	149
5.2.3.1 Attenuated Total Reflectance - Fourier Transform Infrared Spectroscopy.....	151
5.2.3.2 X-ray Photoelectron Spectroscopy.....	152
5.2.3.3 Scanning Electron Microscopy.....	158
5.3 Conclusion.....	160
Chapter 6 The Effect of Biomolecule Attachment on the Permeation of Pharmaceutical Compounds.....	164
6.1 Introduction.....	164
6.2 Results and Discussion.....	166

6.2.1 <i>N,N'</i> -Dicyclohexylcarbodiimide Coupling of Lysine to Silanised PDMS (PDMS-APTMS-Lys).....	166
6.2.2 Use of Glutaraldehyde Linker (PDMS APTES-GA-Lys).....	170
6.3 Conclusion.....	175
Chapter 7 Conclusions and Future Work.....	178

List of Figures

Figure 1.1 Schematic representation of the structure of human skin, adapted from Powell (Powell, 2007).	2
Figure 1.2 'Bricks and mortar' stratum corneum model and potential penetrant routes, adapted from Benson <i>et al.</i> (Benson <i>et al.</i> , 2011).	5
Figure 1.3 Steady-state diffusion in a typical <i>in vitro</i> permeation experiment, adapted from Avdeef (Avdeef, 2012).	7
Figure 1.4 Typical <i>in vitro</i> permeation data obtained under finite dose conditions,	9
Figure 1.5 Franz type (left) and flow through type (right) diffusion cells.	10
Figure 1.6 General structure of polyorganosiloxanes.	29
Figure 1.7 Oxidation of poly(dimethylsiloxane) following treatment with UV/O ₃ or oxygen-containing plasma, adapted from Chen <i>et al.</i> (Chen <i>et al.</i> , 2007).	33
Figure 1.8 General alkoxy silane structure.	34
Figure 1.9 Self-assembled monolayer (SAM) formation using (3-aminopropyl)triethoxysilane, adapted from Nguyen <i>et al.</i> (Nguyen <i>et al.</i> , 2016).	34
Figure 2.1 Schematic of the flow-through type system setup.	56
Figure 3.1 Intercellular lipid lamellae, taken from Benson <i>et al.</i> (Benson <i>et al.</i> , 2011), modelled using plasma treated PDMS.	63
Figure 3.2 XPS survey scan of native PDMS.	67
Figure 3.3 XPS survey scan of PDMS following a 90 second air plasma treatment.	67
Figure 3.4. High resolution XPS spectrum of the Si 2p orbital in native PDMS.	69
Figure 3.5. High resolution XPS spectrum of the Si 2p orbital in plasma treated PDMS.	69
Figure 3.6. High resolution XPS spectrum of the C 1s orbital in native PDMS.	70
Figure 3.7. High resolution XPS spectrum of the C 1s orbital in plasma treated PDMS.	70
Figure 3.8. High resolution XPS spectrum of the N 1s orbital in native PDMS.	71
Figure 3.9. High resolution XPS spectrum of the N 1s orbital in plasma treated PDMS.	71
Figure 3.10 Scanning Electron Microscopy images of native PDMS (A-C, 500 X, 1000 X, and 1500 X magnification, respectively) and PDMS following 90 seconds plasma treatment (D-F, 500 X, 1000 X and 1500 X magnification, respectively).	72
Figure 3.11 Steady-state flux of benzoic acid through native PDMS and PDMS following air plasma treatment (mean \pm standard deviation, $n = 3$).	81
Figure 3.12 Steady-state flux of lidocaine through native PDMS and PDMS following air plasma treatment (mean \pm standard deviation, $n = 3$).	81
Figure 3.13 Steady-state flux of ibuprofen through native PDMS and PDMS following air plasma treatment (mean \pm standard deviation, $n = 3$).	82
Figure 3.14 Plot of percent reduction in K _p (%) versus polar surface	88

Figure 3.15 Plot of permeability coefficients through native PDMS (K_p^{native}) versus human skin (K_p^{human}) ($R^2 = 0.75$, $n = 16$).	92
Figure 3.16 Plot of permeability coefficients through plasma treated PDMS (K_p^{plasma}) versus human skin (K_p^{human}) ($R^2 = 0.86$, $n = 16$).	93
Figure 3.17 Permeability coefficients of alkyl 4-amino- and 4-hydroxy- benzoates as a function of carbon chain length.	95
Figure 3.18 Permeability coefficients of alkyl 4-aminobenzoates through plasma treated PDMS.	97
Figure 4.1 XPS survey scan of N_2 plasma treated PDMS.	106
Figure 4.2 High resolution XPS spectrum of the C 1s orbital in N_2 plasma treated PDMS.	108
Figure 4.3 High resolution XPS spectrum of the N 1s orbital in N_2 plasma treated PDMS.	109
Figure 4.4 High resolution XPS spectrum of the Si 2p orbital in N_2 plasma treated PDMS.	110
Figure 4.5 Scanning Electron Microscopy images of PDMS following 90 seconds N_2 plasma treatment (A-C, 500 X, 1000 X and 1500 X magnification, respectively) and 150 seconds N_2 plasma treatment (D-F, 500 X, 1000 X and 1500 X magnification respectively).	111
Figure 4.6 Scanning Electron Microscopy images of PDMS following 300 seconds N_2 plasma treatment at 500 X (A), 1000 X (B) and 1500 X (C) magnification.	112
Figure 4.7 Permeation of lidocaine (LID) through native PDMS, and PDMS following a 90 second air and N_2 plasma treatment (mean \pm standard deviation, $n = 3$).	115
Figure 4.8 Effect of temperature on the permeation of butyl paraben (BP) and risocaine (PAB) through native PDMS.	118
Figure 4.9 Permeation of lidocaine (LID) through native PDMS, and PDMS following a 150 second N_2 plasma treatment (mean \pm standard deviation, $n = 3$).	121
Figure 4.10 Plot of permeability coefficients through N_2 plasma treated PDMS (K_p^{plasma}) versus human skin (K_p^{human}) ($R^2 = 0.48$, $n = 11$).	124
Figure 5.1 Permeation of a xenobiotic through PDMS (left) and PDMS-protein biphasic membrane (right).	131
Figure 5.2 High resolution XPS spectrum of the C 1s orbital in APTMS silanised PDMS.	135
Figure 5.3 High resolution XPS spectrum of the N 1s orbital in APTMS silanised PDMS.	136
Figure 5.4 APTMS silanised PDMS at a magnification of 500 X (A), 1000 X (B), and 1500 X (C) Scanning Electron Microscopy images of PDMS following 90 seconds air plasma treatment (A-C, 500 X, 1000 X, and 1500 X magnification, respectively) and APTMS silanised PDMS.	137
Figure 5.5 High resolution XPS spectrum of the C 1s orbital in APTMS-Boc-Lys(Z)-OH functionalised PDMS.	141
Figure 5.6 High resolution XPS spectrum of the N 1s orbital in APTMS-Boc-Lys(Z)-OH functionalised PDMS.	142
Figure 5.7 High resolution XPS spectrum of the C 1s orbital in Boc-Lys(Z)-OH functionalised PDMS (dichloromethane).	145

Figure 5.8 High resolution XPS spectrum of the C 1s orbital in Boc-Lys(Z)-OH functionalised PDMS (ethanol).	146
Figure 5.9 High resolution XPS spectrum of the N 1s orbital in Boc-Lys(Z)-OH functionalised PDMS (dichloromethane).	146
Figure 5.10 High resolution XPS spectrum of the N 1s orbital in Boc-Lys(Z)-OH functionalised PDMS (ethanol).	147
Figure 5.11 PDMS membrane following functionalisation with (3-aminopropyl)triethoxysilane, glutaraldehyde, and Boc-Lys-OH (PDMS-APTES-GA-Lys).	153
Figure 5.12 High resolution XPS spectra of the C 1s orbital in PDMS following (3-aminopropyl)triethoxysilane silanisation (PDMS-APTES).	154
Figure 5.13 High resolution XPS spectrum of the C 1s orbital in PDMS following (3-aminopropyl)triethoxysilane silanisation and glutaraldehyde functionalisation (PDMS-APTES-GA).	155
Figure 5.14 High resolution XPS spectrum of the C 1s orbital of PDMS following (3-aminopropyl)triethoxysilane silanisation, and functionalisation with glutaraldehyde and Boc-Lys-OH (PDMS-APTES-GA-Lys).	156
Figure 5.15 High resolution XPS spectrum of the N 1s orbital of PDMS following (3-aminopropyl)triethoxysilane silanisation (PDMS-APTES).	156
Figure 5.16 High resolution XPS spectrum of the N 1s orbital in PDMS following (3-aminopropyl)triethoxysilane silanisation and glutaraldehyde functionalisation (PDMS-APTES-GA).	157
Figure 5.17 High resolution XPS spectrum of the N 1s orbital in PDMS following (3-aminopropyl)triethoxysilane silanisation and functionalisation with glutaraldehyde and Boc-Lys-OH (PDMS-APTES-GA-Lys).	158
Figure 5.18 Scanning Electron Microscopy images of PDMS-APTES-GA (A-C, magnification 500 X, 100 X and 1500 X, respectively) and PDMS-APTES-GA-Lys (D-F, magnification 500 X, 100 X and 1500 X, respectively)	159
Figure 6.1 Proposed schematic of PDMS-biomolecule composite membrane formation.	166
Figure 6.2 Permeation of methyl 4-aminobenzoate (MAB) through native PDMS, PDMS following air plasma treatment, and APTMS silanised PDMS following lysine functionalisation (PDMS-APTMS-Lys) (mean \pm standard deviation, $n = 3$).	169
Figure 6.3 Permeation of butyl paraben (BP) through native PDMS, PDMS following air plasma treatment, and APTMS silanised PDMS following lysine functionalisation (PDMS-APTMS-Lys) (mean \pm standard deviation, $n = 3$).	169
Figure 6.4 Permeation of methyl 4-aminobenzoate (MAB) through native PDMS, PDMS following air plasma treatment, and APTES silanised PDMS following glutaraldehyde and lysine functionalisation (PDMS-APTES-GA-Lys) (mean \pm standard deviation, $n = 3$).	172

Figure 6.5 Permeation of butyl paraben (BP) through native PDMS, PDMS following air plasma treatment, and APTES silanised PDMS following glutaraldehyde and lysine functionalisation (PDMS-APTES-GA-Lys) (mean \pm standard deviation, $n = 3$). 173

Figure 7.1 The corneocyte patterning of PDMS by use of a ‘grid’ template during plasma processing. 181

List of Tables

Table 2.1 Structure, molecular weight, $\log_{10} P$, charge, and λ_{\max} of pharmaceutical compounds used in permeation studies presented in this thesis.	46
Table 3.1 Water contact angle analysis of native PDMS and PDMS following air plasma treatment.	65
Table 3.2 ATR-FTIR of native PDMS and PDMS following air plasma treatment.	66
Table 3.3 Atomic (%) of oxygen, nitrogen, carbon and silicon taken from XPS survey scans of native PDMS and PDMS following air plasma treatment.	68
Table 3.4 Effect of plasma treatment time on the permeation of the model drug ibuprofen	73
Table 3.5 Cumulative mass of ibuprofen (IBU), lidocaine (LID), caffeine (CAF), benzocaine (EAB), benzoic acid (BA), and benzotriazole (BTA) permeated through native PDMS and PDMS following air plasma treatment (mean \pm standard deviation, 4 sig.fig., $n = 3$).	75
Table 3.6 Steady-state flux (J_{ss}) of ibuprofen (IBU), flurbiprofen (FLP), ketoprofen (KTP), caffeine (CAF), lidocaine (LID), benzoic acid (BA), salicylic acid (SA), acetyl salicylic acid (ASA) aminopyrine (AMP), methyl paraben (MP), ethyl paraben (EP), propyl paraben (PP), butyl paraben (BP), methyl 4-aminobenzoate (MAB), benzocaine (EAB), risocaine (PAB), butamben (BAB) and diclofenac (DF) through native PDMS and PDMS following air plasma treatment (mean \pm standard deviation, 4 sig.fig., $n = 3$).	80
Table 3.7 Concentration of ibuprofen (IBU), flurbiprofen (FLP), ketoprofen (KTP), caffeine (CAF), lidocaine (LID), benzoic acid (BA), salicylic acid (SA), acetyl salicylic acid (ASA) aminopyrine (AMP), methyl paraben (MP), ethyl paraben (EP), propyl paraben (PP), butyl paraben (BP), methyl 4-aminobenzoate (MAB), benzocaine (EAB), risocaine (PAB), butamben (BAB) and diclofenac (DF) in the donor chamber (C_{donor}), and receptor chamber after 6 hours (C_{receptor}) quoted to 4 significant figures (mean \pm standard deviation, 4 sig.fig., $n = 3$), and the time at which the receptor chamber exceeded 10 % saturation.	83
Table 3.8 K_p values of ibuprofen (IBU), flurbiprofen (FLP), ketoprofen (KTP), caffeine (CAF), lidocaine (LID), benzoic acid (BA), salicylic acid (SA), acetyl salicylic acid (ASA) aminopyrine (AMP), methyl paraben (MP), ethyl paraben (EP), propyl paraben (PP), butyl paraben (BP), methyl 4-aminobenzoate (MAB), benzocaine (EAB), risocaine (PAB), butamben (BAB) and diclofenac (DF) obtained with native (K_p^{native}) and air plasma (K_p^{plasma}) treated PDMS. (mean \pm standard deviation,	86
Table 3.9 Percent ionised, polar surface area (PSA), $\log_{10} D$, and $\log_{10} P$, hydrogen bond donor (HBD) and acceptor (HBA) count, and hydrogen bond acidity (HB_{acid}), and basicity (HB_{basic}) of ibuprofen (IBU), flurbiprofen (FLP), ketoprofen (KTP), caffeine (CAF), lidocaine (LID), benzoic acid (BA), salicylic acid (SA), acetyl salicylic acid (ASA) aminopyrine (AMP), methyl paraben (MP), ethyl paraben (EP), propyl paraben (PP), butyl paraben (BP), methyl 4-aminobenzoate (MAB), benzocaine (EAB), risocaine (PAB), butamben (BAB) and diclofenac (DF).....	87

Table 3.10 Permeability coefficients extracted from literature for lidocaine (LID), ibuprofen (IBU), benzoic acid (BA), salicylic acid (SA), acetylsalicylic acid (ASA), aminopyrine (AMP), caffeine (CAF), diclofenac (DF), flurbiprofen (FLP), ketoprofen (KTP), methyl paraben (MP), ethyl paraben (EP), propyl paraben (PP) methyl 4-aminobenzoate (MAB), benzocaine (EAB) and risocaine (PAB).	91
Table 4.1 ATR-FTIR of native PDMS and PDMS following N ₂ plasma treatment.	105
Table 4.2 Atomic percent (%) of oxygen, nitrogen, carbon, and silicon at the surface of native, air plasma treated, and N ₂ plasma treated PDMS taken from XPS survey scans.....	106
Table 4.3 Steady state flux (J _{ss}) of lidocaine (LID) and caffeine (CAF) through N ₂ plasma treated PDMS, at various treatment times.	114
Table 4.4 Steady state flux (J _{ss}) and permeability coefficient (K _p) of methyl paraben (MP), ethyl paraben (EP), propyl paraben (PP), butyl paraben (BP), methyl 4-aminobenzoate (MAB), benzocaine (EAB), risocaine (PAB), butamben (BAB), lidocaine (LID), caffeine (CAF) and benzoic acid (BA) through native and N ₂ plasma treated PDMS (mean ± standard deviation, 4 sig.fig., n = 3).....	119
Table 4.5 Percent reduction in the permeability coefficient (K _p) of methyl paraben (MP), ethyl paraben (EP), propyl paraben (PP), butyl paraben (BP), methyl 4-aminobenzoate (MAB), benzocaine (EAB), risocaine (PAB), butamben (BAB), benzoic acid (BA), lidocaine (LID), and caffeine (CAF) following air and N ₂ plasma treatment.....	120
Table 5.1 Summary of ATR-FTIR spectrum of APTMS silanised PDMS (PDMS-APTMS).....	133
Table 5.2 Atomic percent (%) of oxygen, nitrogen, carbon and silicon at the surface of native PDMS, PDMS following a 90 second air plasma treatment, and subsequent APTMS functionalisation, taken from XPS survey scans.	134
Table 5.3 ATR-FTIR analysis of APTMS functionalised PDMS, Boc-Lys(Z)-OH, and Boc-Lys(Z)-OH functionalised PDMS.	139
Table 5.4 Atomic percent (%) of oxygen, nitrogen, carbon and silicon at the surface of.....	140
Table 5.5 ATR-FTIR analysis of N ₂ plasma treated PDMS prior to, and following, coupling with Boc-Lys(Z)-OH.....	143
Table 5.6 Atomic percent (%) of oxygen, nitrogen, carbon and silicon at the surface of N ₂ plasma treated PDMS following coupling to Boc-Lys(Z)-OH in dichloromethane and ethanol, taken from XPS survey scans.	144
Table 5.7 Effect of exposure of N ₂ plasma treated PDMS to various solvents on the cumulative mass of lidocaine (LID) permeated after 6 hours (mean ± standard deviation, 4 sig.fig. n = 3).....	148
Table 5.8 ATR-FTIR of native PDMS, and APTES silanised PDMS following glutaraldehyde and Boc-Lys(Z)-OH functionalisation (PDMS-APTES-GA-Lys).	151
Table 5.9 Atomic percent (%) of oxygen, nitrogen, carbon and silicon at the surface of APTES functionalised PDMS (PDMS-APTES), APTES-glutaraldehyde functionalised PDMS (PDMS-	

APTES-GA), and PDMS-APTES-GA following functionalisation with Boc-Lys-OH (PDMS-APTES-GA-Lys), taken from XPS survey scans.....	152
Table 6.1 Steady state flux (J_{ss}) of lidocaine (LID), benzoic acid (BA), methyl aminobenzoate (MAB), and butyl paraben (BP) through native PDMS, PDMS following air plasma treatment, and PDMS following APTMS silanisation and lysine functionalisation (PDMS-APTMS-Lys) (mean \pm standard deviation, 4 sig.fig., $n = 3$).....	167
Table 6.2 Steady state flux (J_{ss}) of lidocaine (LID), benzoic acid (BA), methyl aminobenzoate (MAB), and butyl paraben (BP) through native PDMS, PDMS following air plasma treatment, and PDMS following APTMS silanisation, glutaraldehyde and lysine functionalisation (PDMS-APTES-GA-Lys) (mean \pm standard deviation, 4 sig.fig., $n = 3$).	171

Abbreviations

OECD	Organisation for Economic Cooperation and Development
ECVAM	European Centre for the Validation of Alternative Methods
REACH	Registration, Evaluation, Authorisation and Restriction of Chemicals
ECHA	European Chemicals Agency
HSE	Health and Safety Executive
3 R's	Reduce, Refine, and Replace
API	Active Pharmaceutical Ingredient
TDDS	Transdermal Drug Delivery System
HRE	Human Reconstructed Epidermis
LSE	Living Skin Equivalent
FTS	Full Thickness Skin
HtSE	Heat Separated Epidermis
STS	Split Thickness Skin
ISC	Isolated Stratum Corneum
QSPR	Quantitative Structure-Permeability Relationships
PAMPA	Parallel Artificial Membrane Permeability Assay
PDMS	Poly(dimethylsiloxane)
PEG	Poly(ethylene glycol)
PC	Polycarbonate
$\log_{10} K_{O/W}$	Logarithm of the Octanol/Water Partition Coefficient
J_{ss}	Steady-state Flux
K_p	Permeability Coefficient
D	Diffusion Coefficient
K	Partition Coefficient
K_p^{native}	Permeability Coefficient through Native PDMS
K_p^{plasma}	Permeability Coefficient through Plasma Treated PDMS
K_p^{human}	Permeability Coefficient through Human Skin
T_{lag}	Lag Time
PSA	Polar Surface Area
$\log_{10} P$	Logarithm of the Partition Coefficient

HBD	Number of Hydrogen Bond Donor Groups
HBA	Number of Hydrogen Bond Acceptor Groups
ATR-FTIR	Attenuated Total Reflectance - Fourier Transform Infrared Spectroscopy
XPS	X-ray Photoelectron Spectroscopy
SEM	Scanning Electron Microscopy
BA	Benzoic Acid
SA	Salicylic Acid
ASA	Acetylsalicylic Acid
LID	Lidocaine
BTA	Benzotriazole
AMP	Aminopyrine
MP	Methyl Paraben
EP	Ethyl Paraben
PP	Propyl Paraben
BP	Butyl Paraben
MAB	Methyl 4-Aminobenzoate
EAB	Benzocaine
PAB	Risocaine
BAB	Butyl 4-Aminobenzoate
CAF	Caffeine
KTP	Ketoprofen
FLP	Flurbiprofen
DF	Diclofenac
IBU	Ibuprofen
APTMS	(3-Aminopropyl)trimethoxysilane
APTES	(3-Aminopropyl)triethoxysilane
DCC	<i>N,N'</i> -Dicyclohexylcarbodiimide
EDC	<i>N</i> -(3-Dimethylaminopropyl)- <i>N'</i> -ethylcarbodiimide hydrochloride
GA	Glutaraldehyde
DCM	Dichloromethane
EtOH	Ethanol
EtOAc	Ethyl acetate
Boc	tert-Butyloxycarbonyl
Z	Carboxybenzyl

Boc-Lys(Z)-OH

N_{α} - tert-Butoxycarbonyl - N_{ϵ} - Carboxybenzyl -L-lysine

Boc-Lys-OH

N_{α} -(tert-Butoxycarbonyl)-L-lysine

SPPS

Solid phase peptide synthesis

Chapter 1 Introduction

1.1. Topical and Transdermal Drug Delivery

The skin is the largest organ in the human body (Feingold, 2007a), contributing 16 % of the body weight of an individual (Liu *et al.*, 2014), with a multitude of functions ranging from protective and barrier functions, to homeostasis and sensory functions. Regardless of its role in the defence of the internal organs, and the protection from chemicals, ultraviolet radiation, pathogens and allergens (Feingold, 2007c), the skin offers a valuable method of drug administration, in particular under circumstances in which the drug would otherwise degrade in the gastrointestinal tract (Aldwaikat *et al.*, 2015) or be destroyed by the liver following oral administration (Shahzad *et al.*, 2015). Additionally, topical and transdermal drug delivery offers an alternative to oral administration in the hope of improved patient compliance, minimises systemic delivery to other sites (Mahdi *et al.*, 2016), lacks the generation of potentially dangerous medical waste as with hypodermic injections (Liu *et al.*, 2014), and eliminates the risks associated with needle re-use, in particular in developing countries (Bartosova *et al.*, 2012; Partidos *et al.*, 2003). Consequently, the development of novel formulations to overcome the barrier function of the skin has gained an increasing amount of economic support from the pharmaceutical community (Akomeah *et al.*, 2007; Misra *et al.*, 2014), and the ability to evaluate the efficacy of such formulations is as relevant as ever. Furthermore, a rise in awareness of diseases such as skin cancer has consequently caused a rise in the topical application of chemicals, and, in the case of formulations such as sunscreen, the target site may not necessitate full penetration of the agent through the epidermis, and the concept of reapplication and, resultantly, increased exposure places further emphasis on evaluating possible percutaneous absorption (Klimová *et al.*, 2015; Varvaresou, 2006).

1.2. The Structure of Human Skin

The structure of human skin can be described in terms of three distinct layers: the epidermis, the dermis and the underlying subcutaneous tissue (Shahzad *et al.*, 2015) (Figure 1.1). The epidermis is the outermost layer, and can be further divided, from a histological perspective, into the stratum corneum (horny layer), stratum granulosum (granular layer), stratum spinosum (spinous cell layer), and the stratum basale (basal cell layer) (Ng *et al.*, 2015). The lower three layers, i.e. the granular, spinous and

basal cell layer, are collectively referred to as the viable epidermis, 95 % of which consists of viable, keratin-synthesizing cells, namely keratinocytes. Over thirty different molecules of keratin, the key structural protein of the epidermis, have been identified. The keratinocytes originate from the basal cell layer, and simultaneously differentiate and migrate through the epidermal layers towards the outermost layer, the stratum corneum (Tobin, 2006). The keratinocytes become enucleated and flattened as they journey towards the superficial layer, and upon arrival, lack cellular organelles. This principal barrier comprises of 15-26 layers of fully keratinised corneocytes, dependant on anatomic position, surrounded by a lipid rich cornified envelope (Choe *et al.*, 2016; Menon *et al.*, 2012; Tobin, 2006), and consists of approximately 15-20 % lipid and 40 % protein by weight (Lee *et al.*, 2010; Moss *et al.*, 2015). Keratinocytes are significantly involved in the response to physical or pathogenic injury, for example, by secreting cytokines or ‘signalling molecules’, prompting growth and repair, in addition to the synthesis of vitamin D (Powell, 2007) .

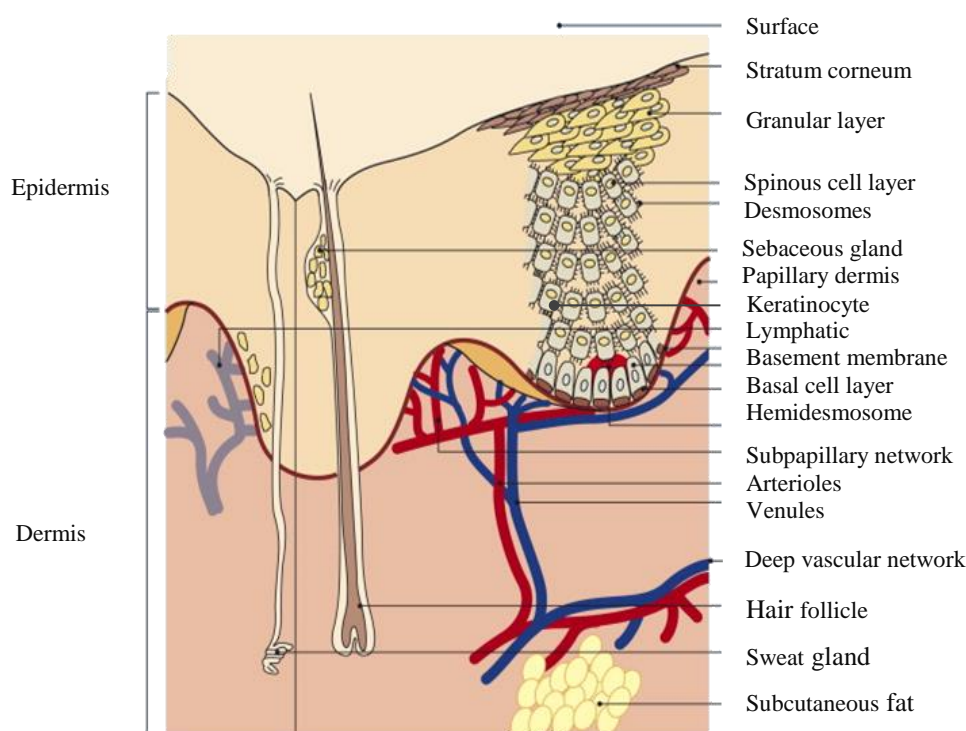


Figure 1.1 Schematic representation of the structure of human skin, adapted from Powell (Powell, 2007).

The barrier function of the skin from exogenous substances is localised in the stratum corneum (Godin *et al.*, 2007; Proksch *et al.*, 2008), thus the rate-limiting step of transdermal absorption is considered to be the passing of molecules across this layer (Godin *et al.*, 2007; Guy, 2013; Herkenne *et al.*, 2006).

At optical microscope level, the organisation of this layer can be represented by a ‘bricks and mortar’ structure, comprising of corneocyte ‘bricks’ and intercellular lipid ‘mortar’ (Hoath, 2014). The ‘mortar’ originates inside lamellar bodies, secretory organelles released prior to cornification, allowing for the complete surrounding of the corneocyte ‘bricks’ (Feingold *et al.*, 2014) (Figure 1.2). The intercellular lipids consists of 15 % free fatty acids, 25 % cholesterol and 50 % ceramides (Barba *et al.*, 2014; Feingold, 2007b), and the profound ability of the stratum corneum to prevent the ingress of xenobiotics can be attributed to the lamellar organisation of the intercellular lipids. Two lamellar phases are known to be present: a short periodicity phase, with a repeat distance of ~ 6 nm, and a long periodicity phase, with a repeat distance of ~ 13 nm (Thakoersing *et al.*, 2012).

Ceramides are the most abundant lipid class in the stratum corneum, the general structure of which consists of a fatty acid amide linked to a sphingoid base. To date, fifteen subclasses of unbound ceramide have been identified in the stratum corneum. Each are the product of one of five sphingoid bases, linked to an α -hydroxy, ω -hydroxy, non-hydroxylated, or ω -esterified fatty acid, along with two other ceramides further acylated at the hydroxyl position on the sphingoid base (Meckfessel *et al.*, 2014; Rabionet *et al.*, 2014). The saturated nature of several ceramide subclasses, along with the occurrence of hydrogen bonding between ceramide head groups, permits tight packing of the lamellae (Notman *et al.*, 2013). As such, the stratum corneum lipids are known to be in the crystalline phase (Mojumdar *et al.*, 2014).

The interactions between the various lipid classes are thought to be incredibly diverse and play an essential role in controlling membrane permeability, and a major driving force for characterisation lies in understanding barrier disruption in a number of diseases. It has been suggested that cholesterol provides much needed fluidity to stacked membrane sheets of stratum corneum lipids in intercellular spaces, which may be brittle in its absence (Madison, 2003; Mojumdar *et al.*, 2015), and ceramides play a central role in the water holding capacity of the stratum corneum. Alterations in the quantities of ceramides in the skin is linked to diseases such as atopic dermatitis and psoriasis, as a result of increased transepidermal water loss (Imokawa *et al.*, 1986). It is thought that unsaturated free fatty acids play a role in disrupting barrier organisation (Meckfessel *et al.*, 2014), along with short chain saturated fatty acids and triglycerides which are suspected of being present only as sebaceous

contaminants (Harding, 2004). Linoleic acid in particular is believed to be integral in the control of transepidermal water loss (Prottey, 1976), and is one of only two unbound unsaturated stratum corneum fatty acids, the other identified as oleic acid (Menon *et al.*, 2012).

1.3. Overcoming the Barrier

Transport across the stratum corneum is known to occur by passive diffusion (Singh *et al.*, 1993), and three potential routes of transport across the stratum corneum are frequently proposed: diffusion through the intercellular lipid lamellae, diffusion through the corneocytes, and diffusion down hair follicles and eccrine sweat glands (Trommer *et al.*, 2006). The relative importance of each route is regularly the subject of debate, in particular the latter, since the appendages represent a mere 0.1 % of the total area of the skin (Lane, 2013), a fraction of which become closed and blocked by dried sebum and corneocytes lost to desquamation. Further, in open follicles, the ingress of permeant must compete with the outward flow of sebum (Moss *et al.*, 2015; Wosicka *et al.*, 2010). Pioneering work by Potts and Guy, aiming to construct a model to predict the skin permeability based on readily obtainable physicochemical properties, observed no requirement to include parameters describing diffusion through an appendageal pathway (Potts *et al.*, 1992). The work is frequently cited, and the large dataset upon which the model was developed has led to many scientists disregarding the contributions of appendageal diffusion. Despite immense doubt surrounding the importance of this route in passive diffusion, great interest surrounds exploiting this potential route for the delivery of xenobiotics that do not possess the adequate physicochemical properties to permeate via the two former routes (Lane, 2013), for example, nanoparticles (Patzelt *et al.*, 2017).

Between 90 and 100 % of the water in the stratum corneum is believed to be deposited intracellularly (Norlén, 2006), therefore, the transcellular route presents a pathway which requires the constant partitioning of the permeant between the hydrated, keratin filament filled corneocytes and the lipophilic intercellular lamellae (Bolzinger *et al.*, 2012). On this basis, it may be understood that few penetrants possess adequate physicochemical properties to transverse the stratum corneum via this route. Moreover, the polar head groups of the intercellular lipids may provide a less disjointed route through the stratum corneum for penetrants able to partition into the corneocyte aqueous environment (Benson *et al.*, 2011; Cannon *et al.*, 2011). The intercellular lipids represent the only continuous route through

the stratum corneum (Hoath, 2014), thus, this route has attracted much attention as the potential pathway for most compounds known to overcome the barrier. Further, the topical application of organic solvents and surfactants is known to simultaneously disrupt the ordered crystalline bilayer organisation of the intercellular lipids and disrupt stratum corneum barrier function (Barba *et al.*, 2016; Barba *et al.*, 2014; Lemery *et al.*, 2015).

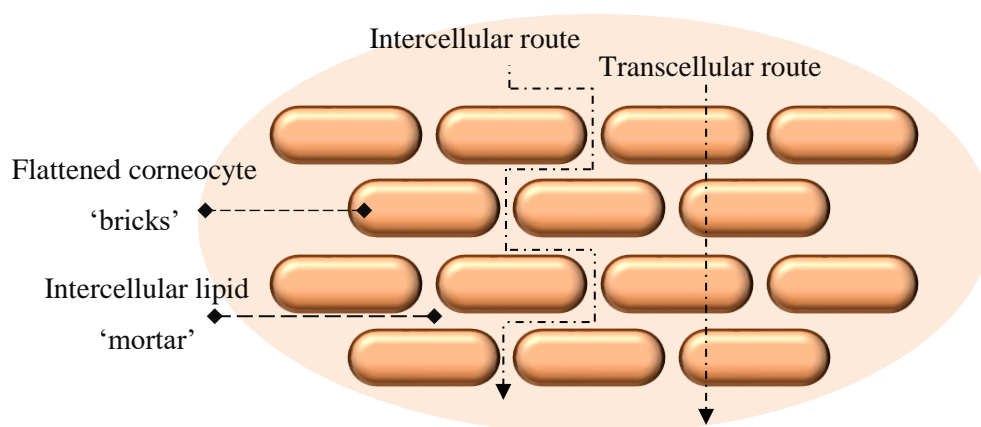


Figure 1.2 'Bricks and mortar' stratum corneum model and potential penetrant routes, adapted from Benson *et al.* (Benson *et al.*, 2011).

1.4. *In Vitro* Determination of Percutaneous Absorption

It is clear that the desire to exploit the benefits of topical administration necessitates a method of quantitatively assessing the ability of a xenobiotic to overcome the barrier, both primitively when considering possible candidates for transdermal delivery, and later during formulation development. The ability to ascertain the performance of topical formulations and transdermal drug delivery systems (TDDS) prior to clinical trials provides a significant financial advantage (Simon *et al.*, 2016). Conversely, the development of cosmetic, dermatologic, and personal care products demands insight into the potential of both active ingredients and excipients to penetrate the skin i.e. the entrance of xenobiotics into the systemic circulation should be considered, even when this is not the intended end point (El Hussein *et al.*, 2007; Klimová *et al.*, 2015; Pineau *et al.*, 2012; Wasukan *et al.*, 2015).

In order to ascertain such information, *in vitro* diffusion cell experiments are routinely undertaken. Typically, the experimental setup includes a donor compartment, containing a reservoir of penetrant, physically separated from a receptor compartment by suitable biological tissue (OECD). Receptor solution is generally an aqueous buffer solution, such as buffered isotonic saline, and the donor

reservoir is often the formulation of interest, a TDDS, or an aqueous solution of a single, or combinations of, active pharmaceutical ingredients (APIs), depending on the desired outcome of the experiment (OECD). The penetrant is, in principle, able to pass from the donor compartment, across the membrane, and into the receptor solution, in the case of skin, by molecular diffusion. The extent of permeation is determined by collection of aliquots of receptor solution at predetermined time intervals, followed by a suitable quantitative spectroscopic assay, or scintillation technique in the case of radiolabelled penetrants (Moss *et al.*, 2015).

Under simplistic experimental conditions, the tissue may be assumed to be an isotropic membrane. If the loss of permeant from the donor region as a result of the transport of permeant across the membrane is negligible, and the concentration of permeant in the receptor region is effectively zero, after a period of time (T_{lag}) flux across the membrane will be constant i.e. steady-state conditions are attained (Avdeef, 2012). Under steady-state conditions, the transfer of permeant across the membrane is described by Fick's first law of diffusion (Avdeef, 2012; Benson *et al.*, 2011; Moss *et al.*, 2015):

$$J = D \frac{\partial C}{\partial x} \quad \text{Equation 1.1}$$

Where J is the permeant flux per membrane unit area, commonly reported in units $\mu\text{g cm}^{-2} \text{s}^{-1}$, D represents the diffusion coefficient, commonly reported in units $\text{cm}^2 \text{s}^{-1}$, C represents the concentration of permeant in units $\mu\text{g cm}^{-3}$, and x is a spatial coordinate normal to the membrane surface in units of cm.

It can be seen that in the system represented in Figure 1.3, whereby steady-state has been attained, the concentration gradient across the membrane, $\delta C/\delta x$, is constant, i.e. a plot of concentration of drug within the membrane as a function of distance across the membrane is linear. Thus, Equation 1.1 can be written:

$$J_{ss} = D \frac{[C^0 - C^h]}{h} \quad \text{Equation 1.2}$$

Where C^0 represents the concentration of permeant within the membrane at position 0 i.e. adjacent to the donor compartment, and C^h represents the concentration of permeant within the membrane at position h , i.e. adjacent to the receiver compartment. From a practical perspective, these concentrations are difficult to ascertain, and for convenience can be approximated using a term describing the

partitioning of permeant between the aqueous solutions and the membrane, permitting the use of the aqueous concentrations, which are more easily ascertained using quantitative spectroscopic methods (Avdeef, 2012). Equation 1.2 becomes:

$$J_{ss} = DK \frac{[C^D - C^R]}{h} \quad \text{Equation 1.3}$$

Where K is the vehicle membrane partition coefficient, C^D and C^R are the permeant concentrations in the donor and receptor compartments, respectively.

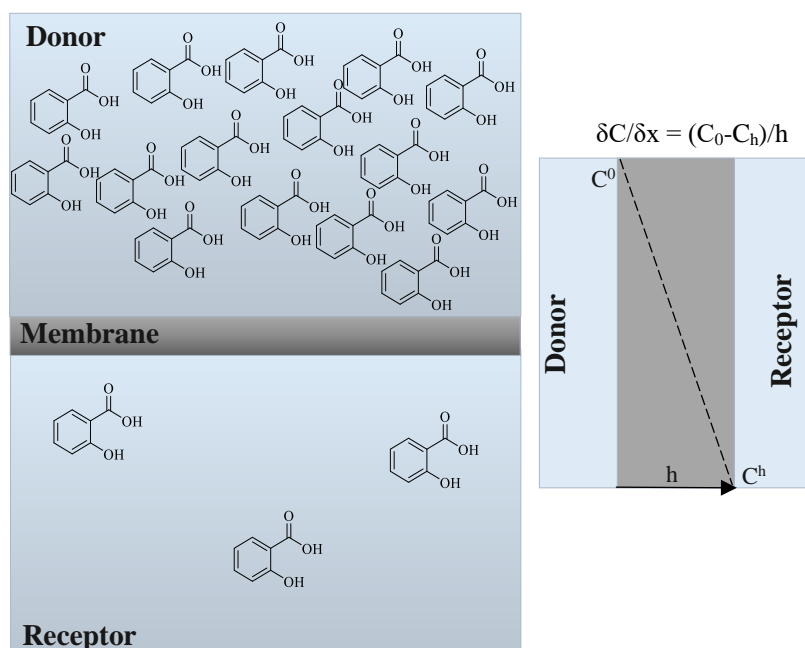


Figure 1.3 Steady-state diffusion in a typical *in vitro* permeation experiment, adapted from Avdeef (Avdeef, 2012).

Equation 1.3 is significantly more employable than Equation 1.2, since K can be determined using simple partitioning experiments. However, determination of D is considerably more difficult. For this reason, the kinetic parameter, D , the thermodynamic parameter, K , along with the membrane thickness, h , in Equation 1.3 are combined yielding the permeability coefficient, K_p . Equation 1.3 can therefore be rewritten:

$$J_{ss} = K_p (C^D - C^R) \quad \text{Equation 1.4}$$

Where K_p represents the permeability coefficient, and C^D and C^R represent the concentration of permeant in the donor and receiver compartment, respectively.

This equation can be further simplified as represented in Equation 1.5 by the equivalence of the term $(C^D - C^R)$, and C^D , since the concentration of permeant in the receptor compartment is effectively zero. In practical terms, to ensure this assumption holds, the concentration of permeant in the receptor medium should not exceed 10 % that of the donor (Moss *et al.*, 2015). Providing this is met, Equation 1.5 can then be applied:

$$J_{ss} = K_p C^D \quad \text{Equation 1.5}$$

Equation 1.5 implies that the permeability coefficient is easily obtained from a diffusion cell experiment, provided the assumptions mentioned previously are met with appropriate experimental design. The permeability coefficient provides a convenient approach to comparing possible candidates for transdermal delivery, and as such, significant quantities of permeability data have been published in this form, such as that by Flynn in 1990, the largest collection of skin permeability data of its time (Flynn, 1990). Since its publication, numerous efforts to extend the dataset have been reported (Mitragotri, 2003; Thomas *et al.*, 2007), and more recently, even larger datasets have been collated, including data of up to 283 compounds (Baba *et al.*, 2015).

K_p can also be described by Equation 1.6, thus it can be seen that its use as a descriptor of membrane permeation enables the separation of the two underlying transport processes: the partition coefficient, K , a thermodynamic quantity describing the partitioning of drug between the donor solution and the membrane, and the diffusion coefficient D , a kinetic parameter describing the mobility of the permeant within the membrane (Du Plessis *et al.*, 2002a):

$$K_p = K \left(\frac{D}{h} \right) \quad \text{Equation 1.6}$$

Data is ordinarily examined as a plot of cumulative quantity of permeant entering the donor chamber per unit area versus time (Figure 1.4). In experiments whereby the donor medium contains a finite dose of drug e.g. a formulation or a defined concentration of drug below the solubility limit in the vehicle, the passing of drug across the membrane, after a period of lag time, T_{lag} , will become constant. The gradient of this section i.e. the cumulative quantity of permeant passing through the membrane per unit area per unit time is defined as the steady state flux, J_{ss} , and the x-intercept of this section of the profile can be used to determine T_{lag} (Cannon *et al.*, 2011). Over time, the concentration of drug in the donor

chamber will become depleted, and the implications of this are that the rate of diffusion through the membrane will be slower, as a result of a reduction in concentration gradient across the membrane (Moss *et al.*, 2015). This experimental setup is most often used as a measure of product performance and the theoretical therapeutic levels which may be achievable *in vivo*, and so many argue this approach provides the most clinically relevant data (Pranitha *et al.*, 2014; Synovec *et al.*, 2013).

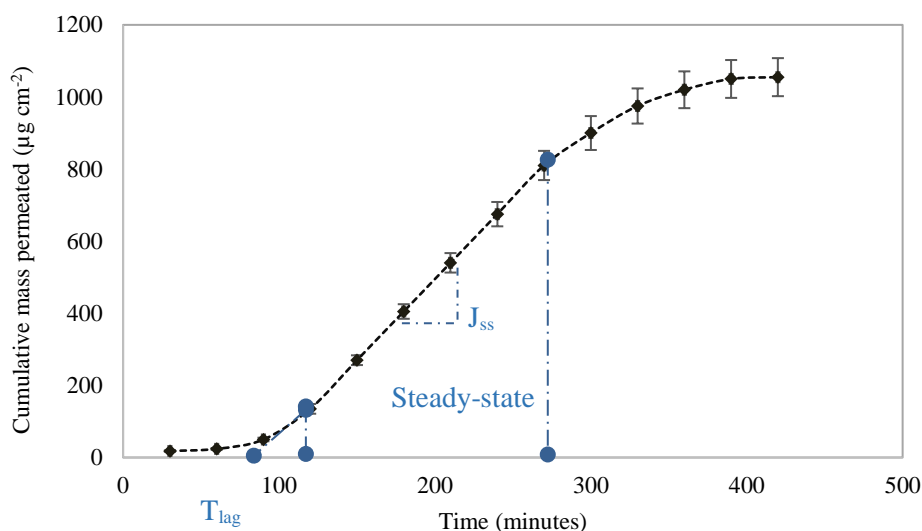


Figure 1.4 Typical *in vitro* permeation data obtained under finite dose conditions, adapted from Mangelsdorf *et al.* (Mangelsdorf *et al.*, 2006).

Since flux is proportional to the concentration gradient, flux generally increases with increasing donor solution concentration until saturation occurs and maximum thermodynamic activity has been reached. Under infinite dose conditions, whereby the donor solution consists of a saturated solution of drug with excess permeant present, the steady-state flux across the membrane will be linear, and can be used to determine D and K as described in Equation 1.6. In practical terms, this implies that the maximum therapeutic dose will be achieved using a formulation in which the drug is at saturation point. Accordingly, super-saturated solutions, in which the thermodynamic activity of the drug is above 1, have been extensively investigated to enhance the likelihood of achieving therapeutic levels of drug *in vivo* (Pellett *et al.*, 1997; Santos *et al.*, 2011).

Two types of vertical diffusion cell are commonly used to obtain this data: static Franz type and flow-through or 'Bronaugh' type cells (Figure 1.5). Franz type cells possess a finite receptor compartment, whereby accumulation of penetrant under the membrane and diffusion layers are avoided by stirring,

typically with a magnetic stirrer bar. Conversely, the receptor compartment of flow through type cells is constantly replenished with fresh receptor solution by means of a pump system. Both cell types can be used to obtain the same information, however, experimental conditions may deem one cell type more appropriate. For example, since the maintenance of sink conditions, generally defined as the receptor solution concentration remaining $\leq 10\%$ that of the donor (Moss *et al.*, 2015), will provide the most accurate representation of the rapid clearance of penetrant from the viable tissue *in vivo*, in cases where permeation is rapid, the flow through type diffusion cells may prove more valuable (Addicks *et al.*, 1987). However, sink conditions in static type diffusion cells may also be controlled by frequent sampling intervals, extraction of large sample volumes and replacement with fresh receptor medium (Ng, Rouse, Sanderson, Meidan, *et al.*, 2010), or the presence of solubility enhancers, such as bovine serum albumin, in the receptor medium (Schreiber *et al.*, 2005).

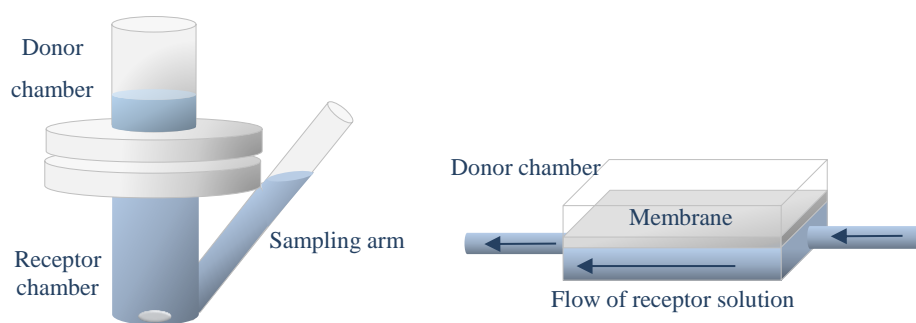


Figure 1.5 Franz type (left) and flow through type (right) diffusion cells.

1.5. Properties of the Permeant

The ability to estimate the diffusion coefficient (D) and partition coefficient (K) in Equation 1.6 by performing *in vitro* studies, in conjunction with an understanding of the properties which influence each parameter, may assist in both the design of appropriate candidates for transdermal drug delivery, and formulation development.

The stratum corneum partition coefficient, K , of a potential penetrant describes the ratio of concentrations of the penetrant in the stratum corneum to that in the vehicle at equilibrium. As such, it is dependent on the relative solubility of the penetrant in each of the phases. Since the stratum corneum is primarily a lipophilic barrier, it is generally accepted that increases in lipophilicity are associated with an increase in transport across the barrier, and that the barrier is orders of magnitude less

permeable to the ionised form of a penetrant (Benson *et al.*, 2011; Moss *et al.*, 2015). The presence of proteins within this principle layer results in the presence of both anionic and cationic groups; these groups, in conjunction with the lipophilic nature of the stratum corneum, render the barrier 1-2 orders of magnitude less permeable to the ionised form of a compound compared with the unionised form of the same compound (Bartosova *et al.*, 2012). In actuality, the permeation of highly lipophilic molecules ($\log_{10} P > 3$) will become limited by poor clearance from the viable tissue as a result of low partitioning into this underlying aqueous environment. It is therefore understood that permeants displaying intermediate lipophilicity, i.e. $1 < \log_{10} P < 3$, are the most suitable candidates for transdermal delivery (Moss *et al.*, 2015). Further, since increasing the quantity of penetrant in a vehicle generally results in an increase in flux, it may be possible to compensate for the lower fluxes observed with ionised compounds with a greater solubility in the vehicle (Hadgraft *et al.*, 2000). Ion-pairing offers an alternative penetration enhancement strategy to overcome the relatively low permeability of the stratum corneum to ionised species; the interaction of a charged API with organic counter-ions has been reported to yield species with greater lipophilicity and, subsequently, higher fluxes (Tan *et al.*, 2009; Trotta *et al.*, 2003).

The diffusion coefficient of a penetrant is heavily influenced by both molecular size and temperature (Akomeah *et al.*, 2004; Shahzad *et al.*, 2015), as described by the Stokes-Einstein equation, i.e. the diffusion coefficient of a penetrant is inversely proportional to the hydrodynamic radius, and proportional to temperature (Moss *et al.*, 2015). Molecular weight is most commonly used as a substitute for molecular size, since this information is substantially easier to obtain. As such, in general, a ceiling of 500 Da is used for transdermal candidates (Benson *et al.*, 2011; Moss *et al.*, 2015). The dependence of D on temperature has also generated substantial interest in thermophoresis as a method to increase the permeation of API across human skin. Increases in drug transport across the skin have been observed with increases in temperature (Shahzad *et al.*, 2015), and a notable study attributed this to both increases in the diffusion coefficient of the API, namely lidocaine, in the vehicle and the barrier, along with temperature-induced structural changes to the intercellular lipids of the stratum corneum (Wood *et al.*, 2012).

The amphipathic structure of the lipid classes that together form the stratum corneum intercellular lipid lamellar has generated substantial interest in the role of hydrogen bonding in the permeation of xenobiotics. Fundamental work by El Tayar *et al.* (Tayar *et al.*, 1991) examined the permeability coefficients of 61 penetrants extracted from literature, subdivided into four datasets, namely alcohols and steroid hormones, hydrocortisone 21-esters, phenolic compounds, and miscellaneous compounds. The authors performed linear regression analysis in order to determine the relationship between K_p values extracted from literature, the stratum corneum partition coefficient (K), and its common surrogate, $\log_{10} P_{\text{oct}}$, the n-heptane-water partition coefficient ($\log_{10} P_{\text{hept}}$), molecular weight, and $\Delta\log_{10} P_{\text{oct-hep}}$. The latter was found, in preliminary analysis, to directly illustrate the hydrogen bond donor acidity of the penetrant.

Analysis of dataset one, containing alcohols and steroid hormones, found that although the permeability coefficients of alcohol and steroid compounds displayed good correlation with $\log_{10} P$ values, correlation existed only within each chemical functionality i.e. alcohols and steroids were considered separately. Further, no correlation was found with water accessible surface areas or molecular weight. The only comprehensive correlation found was with $\Delta\log_{10} P_{\text{oct-hep}}$, indicating the dependence of the permeability coefficient on the hydrogen bonding capacity of the penetrant ($r = 0.901$, $n = 21$). Analysis of dataset two, containing miscellaneous compounds, yielded the same observation ($r = 0.817$, $n = 8$). The authors inferred that the negative dependence of K_p on $\Delta\log_{10} P_{\text{oct-hep}}$ indicates that compounds which are strong hydrogen bond donors permeate more poorly, as a consequence of interactions with the wealth of hydrogen bond accepting groups available in the intercellular lipid lamellae. Analysis of the remaining two datasets found limited correlation with the same parameter, however, noteworthy observations were made. The sharp decline in $\log_{10} K_p$ of hydrocortisone 21-esters at $\Delta\log_{10} P_{\text{oct-hep}} \geq 4$, and the presence of only one out of a total of thirty values > 4 in the two earlier datasets, resulted in the conclusion that above a value of 6, K_p becomes less dependent on $\Delta\log_{10} P_{\text{oct-hep}}$. Further, correlation in the dataset containing phenolic compounds was obtained by the removal of the most lipophilic compounds, and led the authors to conclude that the phenolic compounds are able to permeate by two routes, which the authors found unsurprising taking into account that phenols are known to denature proteins and are subsequently damaging to the skin

(Tayar *et al.*, 1991). This work represents only one example of a large body of literature investigating, and emphasising, the role hydrogen bonding plays in transdermal diffusion (Du Plessis *et al.*, 2002a, 2002b; Pugh *et al.*, 1996).

1.6. Modelling Transdermal Absorption

1.6.1. Human tissue

The use of *ex vivo* human skin obtained from cadavers or cosmetic surgery, typically abdominoplasties and mammoplasties, is often considered the most suitable barrier, since in principle its use will provide the most relevant data. However, availability issues often impede its use, and under circumstances when the tissue is available, deconvolution of the data can be problematic as a result of the various storage conditions employed, such as freezing, and disinfectant procedures exercised previous to the skin entering the laboratory (Abd *et al.*, 2016). The range of skin preparation protocols used for such studies adds further convolution; use of full thickness skin (FTS), split thickness skin (STS), heat separated epidermis (HtSE), and isolated stratum corneum (ISC) have all been reported in permeation studies (Akomeah, 2007; Netzlaff *et al.*, 2007; Roy *et al.*, 1993; Schreiber *et al.*, 2005). The latter three types are all accepted in OECD guideline 428 (OECD), with the former permitted (providing a thickness of < 1 mm is used and adequate justification is provided). STS is typically prepared using a dermatome, and the reproducibility of the product is subject to the consistency of the individual performing the separation (Barbero *et al.*, 2009). ISC membranes are usually enzymatically isolated, for example with trypsin (Netzlaff *et al.*, 2007); the resultant membranes are usually fragile and necessitate an underlying synthetic support, the choice of which must be justified and found not to contribute to the barrier function (Barbero *et al.*, 2009). For these reasons, along with the dependence of skin permeability on age, anatomic location, race and sex (Akomeah *et al.*, 2007; Mohammed *et al.*, 2012; Roskos, 1989), alternatives to human skin are widely employed in these studies, frequently in pursuit of more reproducible data.

1.6.2. Animal Tissue

The wider availability of animal skin has led to its historic use in permeability studies. The most frequently reported substitutes include skin excised from rats (Özgüney *et al.*, 2006), mice (Balakrishnan *et al.*, 2009), guinea pigs (Dalton *et al.*, 2015), rabbits (Nicoli *et al.*, 2006), and pigs

(Qvist *et al.*, 2000). Tissue from more exotic species, such as snakes (Lu *et al.*, 1992; Yuan *et al.*, 2005), have been investigated as potential surrogates, along with skin from various species of fish (Másson *et al.*, 2002), but it is apparent that the availability of such tissues should be questioned. It is generally accepted that the use of animal tissues results in an overestimation of percutaneous absorption (Lu *et al.*, 1992), thought to be as a consequence of differences in lipid composition and morphology (Stahl *et al.*, 2009), thus making it increasingly difficult to extrapolate the data to man. Reported overestimations in skin permeation include 3.5-fold with rabbit skin (Chowhan *et al.*, 1978), 11-fold with rat skin (Ravenzwaay *et al.*, 2004), and 100-fold with nude mouse skin (Lu *et al.*, 1992). Porcine tissue is thought to be the most similar to human skin from a histological perspective (Jacobi *et al.*, 2007), and has subsequently attracted particular interest as a substitute (Barbero *et al.*, 2009). Numerous attempts have been made to characterise the properties of porcine skin, and correlate the data to man (Sekkat *et al.*, 2002). Despite these efforts, overestimations of percutaneous absorption have still been reported with its use (Luo *et al.*, 2016). Moreover, issues with data reproducibility are frequently reported. For example, the preparation technique required for each species may vary; the use of heat separated epidermis (HtSE) poses problems when using skin from certain species, such as the pig, for which the hair shafts are left in the dermis, leaving the epidermis perforated (Barbero *et al.*, 2009). Hair follicle density is also known to differ between species, and the relative importance of this route in the species selected must be accounted for (Stahl *et al.*, 2011).

The last decade has observed a profound move away from the use of animal tissues in the evaluation of the safety and the efficacy of cosmetic products, topical and transdermal formulations, and for risk assessment purposes, both as result of increased criticism of the quality of the data obtained, and quandary surrounding the ethical nature of such studies. Notably, the Registration, Evaluation, Authorisation and restriction of Chemicals (REACH), which came into force on 1st June 2007, necessitates the registration of all chemicals imported into the EU in quantities ≥ 1 tonne per year. The legislation demands the submission of all dossiers containing relevant data, such as dermal toxicity, skin corrosion, and skin irritation, to the European Chemicals Agency (ECHA) by 31st May 2018. The Health and Safety Executive (HSE) estimate that for a single substance, which has undergone no prior testing, obtaining all relevant data for registration may require up to 5,000 laboratory animals. In excess

of 14,000 substances were registered between the introduction of REACH to UK law and June 2016 (www.hse.gov.uk/reach/resources/animaltesting).

The scale of testing has prompted significant ethical consideration regarding the methods by which the necessary data is obtained. REACH recommends, therefore, where appropriate, scientists are to work in line with the principles of the 3Rs i.e. Reduce, Refine, and Replace the usage of laboratory animals. As such, REACH also aims to 'promote the use of alternative methods for the assessment of hazardous properties'. Alternative methods must meet criteria set by the European Centre for the Validation of Alternative Methods (ECVAM) and be appropriately validated prior to acceptance. Four *in vitro* test methods for determining skin corrosivity have been accepted i.e. the use of commercially available reconstructed human skin models EpiSkin™, Epiderm™, SkinEthic™, and epiCS,®. The former three models, along with the LabCyte EPI-MODEL, have all been accepted for use in the skin irritation test, and are outlined in REACH Commission Regulation (EC) No 761/2009, and OECD Test No. 431 and 439.

The acceptance of reconstructed human skin models occasioned the replacement of a test that had historically been performed in laboratory animals, and marked a watershed in reducing the dependence on animal models. For example, ethical dispute surrounding the testing of cosmetics on animal models has led to the prohibition of the entry onto the market of cosmetics for which either the final formulation, or ingredients or combinations of ingredients, have been tested on animal models after the establishment and acceptance of an alternative method by the OECD. The legislation, introduced in 2003, provided a 6 year deadline for the ban on non-compliant products, and a lengthier, 10 year deadline for the completion of toxicological assessment (Salvador *et al.*, 2007). The incorporation of models such as EpiSkin™, a subsidiary of L'Oréal, into OECD Test Guidelines 431 and 439 for skin corrosivity and irritation, has made testing of cosmetics on animals for these endpoints obsolete, and unlawful. To date, no alternative methods have been accepted or validated for use in OECD Test 428 for skin absorption. A change in paradigm and shifting attitudes towards the use of laboratory animals, from a legal, ethical, and data quality perspective, has led to increasing efforts to find alternative models.

1.6.3. Alternative Models

1.6.3.1. Cell Culture Models

The successful displacement of laboratory animal based approaches to evaluating skin irritation, and the widespread acceptance of reconstructed human epidermis (RHE) models for such purpose (OECD) has led to substantial interest in the assessment of their suitability as an alternative to *ex vivo* permeability studies employing animal tissue. The models consist of a three-dimensional tissue culture grown from keratinocytes, and possess an epidermis with a partially differentiated stratum corneum, basal, spinous, and granular layers, and in the case of living skin equivalent (LSE) models, an underlying dermis. These models appear promising from a histological perspective. Nevertheless, there is a stark difference between the requirements of the skin irritation and skin permeability test. The skin irritation test necessitates that the test candidate is able to transverse the model stratum corneum barrier, enabling the assessment of cell viability in underlying layers of tissue. As such, commission regulation (EC) No 761/2009 states ‘the stratum corneum and its lipid composition should be sufficient to resist the rapid penetration of cytotoxic marker substances’. Notably, the regulation does not necessitate that the barrier function of cultured stratum corneum is *equivalent* to that of human tissue, and, as a result of extensive testing, it is generally accepted that skin equivalent models overestimate permeation in comparison to that predicted by equivalent isolated human tissue (Batheja *et al.*, 2009; Roy *et al.*, 1993), reportedly as a consequence of stratum corneum immaturity (Küchler *et al.*, 2013; Williams, 2006). Despite their acceptance in OECD guidelines 431 (OECD) and 439 (OECD) for corrosivity and irritation testing, low reproducibility, poor robustness with regards to direct application of semisolids, along with a high cost, have resulted in the failure of RHE models to obtain widespread acceptance (Batheja *et al.*, 2009; Engesland *et al.*, 2015; Moss *et al.*, 2015). Generally, studies have concluded that currently accessible LSE and RHE models have limited use within *in vitro* permeation studies (Flaten *et al.*, 2015; Netzlaff *et al.*, 2007; Roy *et al.*, 1993; Schmook *et al.*, 2001).

An example of these studies aimed to compare the permeation of two penetrants, namely caffeine and testosterone, through cadaver skin, porcine skin, SkinEthic™ and EpiDerm™, aiming to devise a standard experimental protocol for the use of HRE models during *in vitro* permeation studies. The use

of testosterone necessitated the presence of solubility enhancers in the receptor medium in order to maintain sink conditions. Upon the inclusion of 0.5 % Ipegal[®], a non-ionic surfactant, the authors reported an 85 % reduction in the EpiDerm[™] model viability, leading the authors to perform a 250 reduction in the dose of testosterone (Schreiber *et al.*, 2005). It is apparent that this approach to overcoming the problems associated with the higher permeability of HRE models, in conjunction with the poor solubility of lipophilic compounds in physiologically conducive receptor medium, is unsuitable should the test aim be to evaluate the performance of a formulation or TDDS.

A further study used hydrocortisone, terbinafine, salicylic acid and clotrimazole to evaluate the barrier function of SkinEthic[™] HRE and Graftskin[™] LSE in comparison to rat, human and porcine skin. It was found that porcine skin modelled human skin most appropriately, since results were in the same order of magnitude for both flux through the skin, and concentrations in the skin. However, although Graftskin[™] displayed substantial barrier properties with regards to salicylic acid, an overestimation of flux and skin concentration in human skin was observed with other, more hydrophobic compounds. A similar scenario was reflected in the use of Skinethic[™], with which a skin concentration of salicylic acid was obtained akin to human skin, despite a sevenfold higher flux. In the case of hydrocortisone, terbinafine and clotrimazole, permeation values overestimated that of human skin by up to a factor of around 800 (Schmook *et al.*, 2001). As of yet, these models are only applicable to comparative studies, analogous to artificial membranes (Williams, 2006).

1.6.3.2. Quantitative Structure-Permeability Relationships

The early recognition that the physicochemical properties of the permeant play a crucial role in the extent of permeation, and the likelihood of achieving therapeutic levels of an API *in vivo*, has led to extensive work aiming to quantify these observations and derive mathematical relationships to aid the prediction of percutaneous absorption. Pioneering work by Potts and Guy (Potts *et al.*, 1992) established a relationship between $\log_{10} K_{OW}$, molecular weight (MW) and permeability coefficient values extracted from the Flynn dataset (Flynn, 1990), and has been described as being the first ‘widely accepted’ QSPR model (Karadzovska, Brooks, *et al.*, 2013). Like many more recent QSPR models, the model was derived on empirical data obtained for steady-state transport across excised human

epidermal tissue (Baba *et al.*, 2017; Lee *et al.*, 2010; Moss *et al.*, 2002), and as such, the model output is the human skin permeability coefficient, K_p . The mechanistic foundations of the model lie in the assumption that steady-state transport across the stratum corneum can be described by Equation 1.6 in Section 1.4. Taking a logarithmic form of this equation, likening the membrane/water partition coefficient to $\log_{10} K_{O/W}$, and assuming an exponential relationship between the membrane diffusivity and molecular weight (i.e. free-volume theory), yielded the following model:

$$\log_{10} K_p = -6.3 + 0.71 \log_{10} K_{O/W} - 0.0061 MW \quad \text{Equation 1.7}$$

The authors found no requirement to include any descriptors to outline permeation through aqueous appendageal routes, and found that the relatively high permeability of more hydrophilic compounds could be accounted for by their low molecular weight, and subsequent high diffusivity in the lipid lamellae (Potts *et al.*, 1992). The model assumes that the stratum corneum is the rate limiting barrier to permeation, any interactions between the stratum corneum and the vehicle have no influence on the permeation of the compound in question, and the absence of chemical and physical permeation enhancers such as surfactants or sonophoresis. The simplicity of the model, partnered with its predictive power ($R^2 = 0.86$), the large dataset upon which it was developed i.e. 90 compounds from a wide range of therapeutic classes, the selection of readily available predictors, and the substantiated mechanistic foundations upon which it was developed, has resulted in the model becoming the most frequently cited of its kind (Mitragotri *et al.*, 2011).

The appeal of replacing labour intensive, time-consuming, and potentially costly permeation studies with predictive models is clear, and QSPRs in particular, may provide mechanistic insight upon the importance of molecular properties on transdermal permeation. As such, a large variety of QSPRs are available in literature, which differ greatly in their mechanistic justification. For example, work by one author alone, namely Mitragotri, proposed four models based on numerous routes through the stratum corneum. Mitragotri anticipated that the over-all permeability coefficient (K_p) of a compound is compiled of four permeability coefficients, each for a different potential route through the stratum corneum. The author postulated that free volume diffusion through lipid bilayers, diffusion along lipid bilayers, diffusion through the appendages, and diffusion through defects in the lipid bilayers were all

feasible routes through the stratum corneum. Mitragotri categorised the permeants into high molecular weight hydrophobic drugs, low molecular weight hydrophobic drugs, high molecular weight hydrophilic drugs, and low molecular weight hydrophilic drugs, and stated that the relative importance of each route was variable and category-dependent (Mitragotri, 2003).

The stark contrast between the Potts and Guy model, and those proposed by Mitragotri, outlines an interesting feature of QSPR models; there is no universal model. Understanding the relative importance of the appendageal route may serve as a prerequisite for selecting a model. Even more simply, care must be taken in considering the nature of the permeation data upon which the model was derived, and what model is the most suitable for not only the compound, but for both the expected level of exposure, and the vehicle or dosage form. For example, work by Moss *et al.* identified that steroidal compounds are frequently observed to be outliers in QSPR models based on the Flynn dataset, such as that by Potts and Guy. The authors acknowledge that the data for these compounds in the Flynn dataset were extracted from a single literature source, which since its publication, has been shown to display poor comparability with more recent data, and thought to be subject to error. Thus, the data for these compounds was replaced by that from more recent sources, resulting in the following model:

$$\log_{10} K_p = -2.39 + 0.74 \log_{10} K_{OW} - 0.0091 MW \quad \text{Equation 1.8}$$

An increased fit of the steroid data to the model led the authors to conclude that the permeability coefficients of steroidal compounds can now be predicted using a QSPR developed on permeation data including that of compounds from other therapeutic classes. The removal of data thought to be subject to error, and its replacement with data from more recent literature, led the authors to conclude that the dataset presented was the most comprehensive ($n = 116$), and appropriate, for the development of QSPRs (Moss *et al.*, 2002).

Multiple models have also been developed upon smaller bodies of compounds, and even single therapeutic classes (Liou *et al.*, 2009), or single penetrants with multiple chemical permeation enhancers (Kang *et al.*, 2007). Further, many models, such as that by Potts and Guy, do not incorporate terms to describe formulation effects, and as such it is increasingly difficult to extrapolate the data to studies comparing existing and innovative TDDS's (Mitragotri *et al.*, 2011). It is apparent that whilst QSPRs provide a useful tool, for example, in the large scale screening of potential candidates for topical

and transdermal delivery, careful consideration of the relevance of the model, and therefore model output, must be made.

1.6.3.3. Parallel Artificial Membrane Permeability Assay (PAMPA)

The PAMPA technique is a less labour intensive, automated alternative to the Franz diffusion cell method, and its high throughput capability provides potential for a primary screening technique. PAMPA, traditionally used to evaluate blood-brain barrier permeability and gastrointestinal absorption (Karadzovska & Riviere, 2013), comprises of a 96-well filter plate coated with a liquid artificial membrane (Ottaviani *et al.*, 2006), and appropriate selection of membrane has allowed for the scope of this technique to be extended to the prediction of human skin permeability. Examples of such membranes include a mixture of 30 % isopropyl and 70 % silicone (Markovic *et al.*, 2012), and ceramide analogues, termed certramides (Sinkó *et al.*, 2012; Sinkó *et al.*, 2009).

The authors of the latter work, endeavoured to determine the effect of the introduction of ceramide analogues to the PAMPA system via the use of three model drugs and lipid-matrix membranes consisting of 55 % certramide, 22.5 % cholesterol and 22.5 % stearic acid. Ceramides represent 50 % of the stratum corneum lipids (Feingold *et al.*, 2014), and as such, are of significant interest in biomimetic systems. However, low storage temperatures (-20 °C) and a high associated cost deem them unsuitable for high throughput systems. The synthesised analogues were all saturated, unlike naturally occurring ceramides, enabling ease of handling, however, possessed similar hydrogen bond donor and acceptor capabilities in a small head group, analogous to naturally occurring ceramides. It was determined that the introduction of certramides resulted in substantial effects on the permeability of the three model compounds, described as being a function of alkyl-chain length (Sinkó *et al.*, 2009), and that the presence of both hydrophilic and hydrophobic species representative of the multi-lamellar assembly of human skin provided a promising method of evaluating percutaneous absorption (Sinkó *et al.*, 2012).

In further work with the system, others evaluated the predictability of the model by the correlation of K_p values, extracted from literature and in house, with the effective permeability coefficients (P_e), obtained as the model output (Ottaviani *et al.*, 2006). The authors note an important feature of literature permeability data; the use of varying experimental protocols has resulted in an apparent lack of highly

standardised skin penetration data. Consequently, the model was developed on smaller, but more standardised collections of data, ranging in size from seven compounds (in-house developed database) to more than one hundred compounds, twenty-two of which were used in the study. Concerning the in-house database, determination coefficients (R^2), representing the correlation between human skin permeability data and PAMPA permeability data, range from 0.05 – 0.88 with varying ratios of components and ceramide alkyl chain length. Because of the use of various skin preparation types, ranging from ISC to FTS, and the use of different experiment temperatures, database three, the most comprehensive database sourced from literature, containing more than one hundred compounds, was further separated into smaller datasets as little as four compounds in size. Although the work provides promise in terms of more accurately representing the multi-lamellar assembly of human skin, and acknowledges the gap in existing literature in terms of highly standardised referenced data, the model is yet to be extended to large bodies of compounds (Sinkó *et al.*, 2012).

1.6.3.4. Strat-M[®]

The removal of lot-to-lot variability, safety, and storage limitations associated with using synthetic membrane based skin mimics has resulted in heightened interest in commercially available membranes, one such example being Strat-M[®]. The Strat-M[®] model consists of two superficial layers of polyethersulfone, offering the greatest diffusional resistance, and an underlying polyolefin layer with greater porosity (www.merckmillipore.com).

Work by Sugibayashi *et al.* aimed to physically characterise the membrane, evaluate the permeability of Strat-M[®], and subsequently, evaluate the membranes suitability as a skin mimic. Using scanning electron microscopy, the authors confirmed the presence of three distinct polymeric layers, decreasing in density towards the bottom of the vertical cross-section. The authors also found varying layer thicknesses, with the outside layer measuring $52.3 \pm 0.5 \mu\text{m}$, the intermediate layer measuring $76.7 \pm 5.07 \mu\text{m}$, and the lower layer measuring $196 \pm 7.37 \mu\text{m}$, and confirmed the presence of lipids, primarily in the top two layers. The authors conducted Franz cell diffusion studies, employing thirteen compounds, each applied to the membrane as saturated solutions in phosphate buffered saline. The Franz cell studies were also conducted using human skin and hairless rat skin as the barrier to diffusion,

and the permeability, diffusion, and partition coefficients were calculated for all three membranes. Good correlation was found between permeability coefficients obtained with all three membranes, but the authors noted, in general, an elevated permeability with regards to Strat-M[®]. Permeation experiments using lidocaine were conducted at varying pH to enable the calculation of the permeability coefficients of the unionised and ionised species. The authors found enhanced permeability of ionised species through Strat-M[®] compared with human skin, in conjunction with elevated diffusion coefficients for hydrophilic compounds. This was attributed to the lower tortuosity of hydrophilic routes through the porous membrane structure. It was concluded that the model appears promising on the basis of good correlation between the permeability coefficients through Strat-M[®] and those through human skin. However, the physicochemical properties of the permeant should be considered, since the relative contribution of diffusion through aqueous routes in the synthetic substitute has been found to be greater. Additionally, it was noted that more extensive studies using TDDS's are necessary before the predictability of the membrane can be extrapolated to formulation design (Uchida *et al.*, 2015).

1.6.3.5. Poly(dimethylsiloxane)

The use of polymeric membranes is an attractive alternative to the use of biological tissue as a result of increased obtainability, reduced cost, and lot-to-lot invariability. Further, polymeric membranes prove particularly useful in large scale studies (Ng, Rouse, Sanderson, Meidan, *et al.*, 2010), whereby studies in animals may be considered unethical, and attaining large quantities of human skin may be unachievable. The use of poly(dimethylsiloxane) in permeation studies is reported as early as the 1980's (Jetzer *et al.*, 1986), since which a significant body of literature reporting its use as a model barrier has been established, including multiple studies successfully correlating the data to that obtained with excised human skin (Mertz *et al.*, 2014; Wasdo *et al.*, 2009).

Silicone membranes have found greater use in skin mimicry than alternative isotropic synthetic membranes, such as cellulose nitrate (Lombardi Borgia *et al.*, 2008), polyethersulfone, or polycarbonate (Ng, Rouse, Sanderson, & Eccleston, 2010), since mechanistically diffusion through the stratum corneum is more accurately represented with non-porous systems. More specifically, diffusion

through PDMS occurs via a solution-diffusion type mechanism, i.e. the penetrant dissolves in the membrane, and transverses the membrane down a concentration gradient. Further, differences in the quantity of permeant passing through the membrane occur as a function of the concentration of permeant in the membrane and the diffusivity of the permeant in the membrane (Wijmans *et al.*, 1995), processes which are described by the partition coefficient, K , and the diffusion coefficient, D , discussed in Section 1.4. As such, diffusion through PDMS is rate limiting, in contrast to diffusion through porous membranes, which occurs via a sieving type mechanism (Ng *et al.*, 2012). The latter membrane type has found extensive use in quality control, such as assessing inter-batch uniformity, whereby the structure allows the formation of vehicle filled pores, resulting in the membrane acting as an extension of the vehicle and only as a physical support to prevent semisolid becoming dispersed within the receptor medium (Ng, Rouse, Sanderson, & Eccleston, 2010). These membrane types allow for the evaluation of the kinetic aspect of mass transport i.e. diffusion, devoid of the thermodynamic aspect i.e. partitioning (Fiala *et al.*, 2008). This scenario is not true *in vivo*, and application of these membrane types to skin mimicry may result in a complete misunderstanding of vehicle effects.

On the contrary, silicone membranes have facilitated an increase in understanding of vehicle effects (Cross *et al.*, 2001; Oliveira *et al.*, 2010; Oliveira *et al.*, 2012), the effect of ion-pairing (Trotta *et al.*, 2003), and excipients, such as surfactants (Waters *et al.*, 2013). Moreover, the use of silicone membranes has provided insight into supersaturation as a prospective method of increasing the thermodynamic activity of the penetrant, and thus increasing the maximum flux of API across a rate-limiting barrier (Pellett *et al.*, 1997; Santos *et al.*, 2011). One example of these studies notes the use of silicone membranes as a convenient approach to separating the influence of supersaturation on the flux of drug, from alterations in flux as a consequence of vehicle interactions with epidermal tissue (Pellett *et al.*, 1997).

Likewise, silicone membranes have facilitated the understanding of thermophoresis, enabling the separation of the concomitant processes occurring during percutaneous adsorption i.e. partitioning and diffusion. The authors note a lack of approved TDDS's which exploit the known positive dependence of percutaneous absorption on increases in temperature. The authors attribute this to a lack of clarity

surrounding the relative influence of heat application on diffusion, partitioning, structural changes to the stratum corneum, and local blood flow, increases in all of which could contribute to greater plasma levels of API. Two synthetic membranes were used, namely regenerated cellulose and silicone, along with human epidermal sheet, to evaluate the effect of temperature increases over the range of 27 – 45 °C, on the diffusion and partitioning of lidocaine, along with structural changes to the stratum corneum lipids. Permeation data gathered using regenerated cellulose membrane indicated increases in permeation with increases in temperature, which were explained by increases in the diffusion coefficient and drug release from the vehicle, since transport is not governed by membrane partitioning in porous membranes. Increases in transport were also observed across silicone membrane, which were explained primarily by increases in membrane diffusivity, since minimal variations in partitioning were observed across the temperature range. The most profound effect of temperature alteration was observed with human epidermal sheet, for which a 519.2 % enhancement in diffusion coefficient was observed (calculated relative to that at 32 °C) following an increase in temperature to 45 °C. The partitioning of lidocaine increased only by 24.2 % across this temperature range, thus, significant increases in permeation were attributed to increases in the diffusion coefficient. The diffusion coefficient of lidocaine in silicone membrane was found to increase only by 29.3 % across this temperature range, and release from the vehicle increased only by 44.6 % (Wood *et al.*, 2012).

The authors concluded that the noteworthy increase in membrane diffusivity observed with epidermal tissue was a consequence of decreased barrier function following structural rearrangement of the stratum corneum intercellular lipids. Previous studies, utilising differential scanning calorimetry (DSC) and Fourier transform - infrared spectroscopy (FTIR), have identified multiple phase transitions of the stratum corneum intercellular lipids in the temperature ranges 35 – 42 °C, 65 – 75 °C, 78 – 86 °C, and 90 – 115 °C, the lowest of which the authors note is most relevant to the development of thermophoretic transdermal drug delivery systems (Harrison *et al.*, 1996; Wood *et al.*, 2012). Within this temperature range, a ‘solid to fluid’ transition of the lipid lamellae is thought to occur as a consequence of the increased mobility of the ceramide, cholesterol and fatty acid acyl chains, along with a change in the crystalline structure from orthombic to hexagonal. Further, the authors highlight that such changes may be capitalised for the purpose of skin permeation enhancement, since phase

transitions below 75 °C are thought to be reversible, allowing for the restoration of barrier function following device removal, and are most likely responsible for the increase in membrane diffusivity observed in this study given the temperature range employed. Interestingly, the authors acknowledge the practicality of using silicone membranes for the deconvolution of permeability data, and note the appropriateness of silicone membranes to model the stratum corneum on the macroscopic scale. However, the authors also note the lack of ‘ordered bilayers’, which may inhibit *in vitro* – *in vivo* correlation (Wood *et al.*, 2012).

Interestingly, the role of hydrogen bonding in skin permeation has been modelled ingeniously in silicone membranes, using PDMS impregnated with toluene to model the scenario where penetrant-membrane hydrogen bonding would be at a minimum, and PDMS impregnated with octanol to emulate the hydrogen bonding capability of the stratum corneum. Six model penetrants were selected over a narrow molecular weight range in order to elucidate the effect of the presence of phenol, ether, carboxylic acid (with and without intramolecular hydrogen bonding), and alcohol functionalities on the permeability coefficient (K_p) and steady state flux (J_{ss}) of penetrant across membranes with, and without, the capacity to hydrogen bond with the penetrant. The authors reported lower diffusion and subsequently, lower K_p values for all 6 penetrants when the barrier was impregnated with octanol, when hydrogen bonding was likely, in comparison to when the barrier was impregnated with toluene, when hydrogen bonding was unlikely. Further, the use of K_p as a descriptor enabled the separation of partition phenomena from diffusion phenomena, which was vital in order to deconvolute the lower permeation data, since a change in membrane environment would induce changes in both partition and diffusion. The authors expressed the variations in each parameter as ratios of toluene/octanol i.e. $K_{\text{toluene}}/K_{\text{octanol}}$ and $D_{\text{toluene}}/D_{\text{octanol}}$ for the partition and diffusion coefficients respectively, and found that the most prevalent change was in the diffusion coefficient, which was attributed to amplified hydrogen bonding effects in the membrane (Du Plessis *et al.*, 2002a). The work is another notable example of when silicone membranes have been used to understand mechanistically the events which may determine the ability of a penetrant to overcome the formidable stratum corneum barrier, and the likelihood of therapeutic levels of API being achieved *in vivo*, without the use of animal skin or cadaver skin.

The use of silicone membranes as substitutes for biological tissue in permeability studies is irrefutably attractive from a data interpretation perspective, since synthetic substitutes offer batch-to-batch uniformity, which human skin lacks, are highly chemically characterised, and are sufficiently available to facilitate large scale studies and thus may minimise expensive clinical studies (Feldstein *et al.*, 1998; Houk *et al.*, 1988; Waters, 2015). Polymeric substitutes that are appropriate, not only from a logistical perspective, but also from a mechanistic perspective, thus are highly attractive. Nonetheless, as with many animal and cell culture models, overestimations of percutaneous adsorption are often observed. The recurrent use of PDMS can be attributed to the materials successful prediction of ‘trends’ in permeability (Geinoz *et al.*, 2002), in a ranking-type approach (Leveque *et al.*, 2006; Sugibayashi *et al.*, 2009). Likewise, since the non-porous nature of PDMS permits diffusion via a solution-diffusion mechanism, parallel to that offered by human skin, PDMS provides an excellent platform on which to base a mechanistically relevant skin mimic. The hydrophobic nature of PDMS provides a reasonable representation of the stratum corneum barrier at the macroscopic level, but the structural homogeneity of PDMS membranes do not offer a highly tortuous barrier analogous to that offered by the stratum corneum. As such, attempts have been made to evaluate more complex, but highly chemically characterised, PDMS-containing ‘skin mimics’.

Polydimethylsiloxane-polycarbonate (PDMS-PC) copolymer membranes have been investigated as potential skin mimics, offering a two-phase type structure of hydrophilic PC regions dispersed within hydrophobic PDMS. The authors reported permeability coefficients of 14 compounds through the synthetic substitute from aqueous donor solutions, and found good correlation with the parameters used in the Potts-Guy equation, namely molecular weight and $\log_{10} K_{O/W}$ ($R^2 = 0.83$, $n = 9$). Further, drug delivery through the copolymer from a hydrogel-based TDDS was evaluated, and a linear correlation was observed between the delivery from the aqueous solution and delivery from the TDDS. Likewise, a linear relationship was observed between delivery from the TDDS and an aqueous solution through human epidermal tissue. A linear relationship was also observed between the logarithm of the ratio of permeability coefficients from aqueous solutions through both barriers, and the respective logarithm obtained from the TDDS. Since epidermal tissue permeability coefficients using aqueous donor solutions are readily available, the authors conclude that the employment of the skin-imitating

copolymer may provide a robust method of predicting transdermal drug delivery from similar hydrogel-based transdermal drug delivery systems (Feldstein *et al.*, 1998).

Additional copolymer membranes have been evaluated as potential skin mimics in permeability studies. Work by Miki *et al.* prepared poly(ethylene terephthalate) and poly(tetrafluoroethylene) membranes, and poly(vinylidene difluoride) membranes impregnated with poly(dimethylsiloxane) and poly(ethylene glycol) (PEG) copolymers, for use in both Franz cell diffusion studies and a 96 – well filter plate model. Membranes were also prepared without PEG units in order to evaluate the relative contribution of hydrophilic PEG-containing routes through the membrane. The membranes were tested using 12 model penetrants in saturated aqueous suspensions, ranging in $\log_{10} K_{O/W}$ from -4.70 – 3.86. It was found that the limited extent of permeation through the membrane devoid of PEG units rendered receptor solution concentrations below the limit of detection of the spectroscopic technique for L-dihydroxyphenylalanine, dopamine hydrochloride, and isoproterenol hydrochloride. The three compounds represented the lowest $\log_{10} K_{O/W}$ values of the dataset, and the detectability of the compounds following the use of the PEG unit containing membrane led the authors to conclude that the inclusion of PEG units to the polymeric structure provided an aqueous route through the membrane, and overall heteropolar structure. Permeability coefficients obtained using both the PDMS and PDMS-PEG membrane were compared with that of epidermal tissue, and an improved correlation was found for the PDMS-PEG membrane ($R^2 = 0.930$, $n = 12$) compared with the PDMS membrane ($R^2 = 0.913$, $n = 9$). Similar correlation was observed with the PDMS-PEG membrane in the 96-well plate system with a subset of the compounds ($R^2 = 0.92$, $n = 6$). The authors conclude the artificial membrane system may provide a useful alternative to RHE models, on the basis of its predictive power, high-throughput nature, and reduced cost (Miki *et al.*, 2015) .

Both bodies of work above, utilising PDMS-PC and PDMS-PEG copolymers, highlight substantial interest in synthetic systems possessing discrete, polar domains dispersed within an overall hydrophobic polymer network, similar to the lamellar structure of the stratum corneum. Despite both models demonstrating that heteropolar structures may provide an enhanced model of the stratum

corneum, since their publication in 1998 and 2015, respectively, both models still remain tested using < 14 compounds.

Alternative ‘biphasic’ silicone based systems have been tested; INTEGRA® regeneration template, an FDA approved membrane for the treatment of burns and for use in reconstructive surgery, has been evaluated as a potential surrogate for human skin in permeation studies. The biphasic membrane consists of a lipophilic polysiloxane layer and an underlying hydrophilic collagen layer, and the rationale underlying the membrane selection resided in the modelling of the highly lipophilic stratum corneum and underlying hydrated viable tissue. A plot of flux of eight model compounds ($\log_{10} D = -4.9 - 2.97$) through the biphasic membrane versus flux through human skin revealed a direct correlation in permeation behaviour ($R^2 = 0.8517$), and it was concluded that the membrane was advantageous in terms of uniformity, reduced safety concerns and storage. However, analogous to the work by Miki *et al.* evaluating the suitability of PDMS-PEG copolymers for permeability studies, the work was limited to eight compounds, and the structure of the membrane was destroyed upon the addition of a hydrophilic surfactant to the receptor solution, namely Brij 98 (Shumilov *et al.*, 2009). Further, the sourcing of the collagen from bovine tendon (www.ilstraining.com/imwd/imwd/imwd_it_03.html) leads to the requirement of animal tissue, thus opposing the ‘3 R’s’ principles.

Surprisingly, this tremendous increase in insight, and the increase in technological advances that have made silicone membrane modification achievable, is not reflected in the number of reported attempts to include biorelevant sites to the structure of PDMS for use in permeability studies.

1.7. Modification of Poly(dimethylsiloxane)

1.7.1. Properties of Poly(dimethylsiloxane)

Poly(dimethylsiloxane) (PDMS) belongs to a group of polymers known as polyorganosiloxanes, or silicones, which possess the general structure represented in Figure 1.6, where $R = CH_3$ in the case of PDMS.

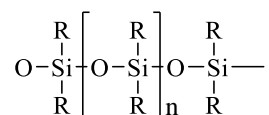


Figure 1.6 General structure of polyorganosiloxanes.

Silicones possess a silicon-oxygen backbone, with bond energies in the range of 450 – 570 kJ mol⁻¹. The high bond energies in the polymeric backbone result in polyorganosiloxanes displaying excellent thermal stability, with degradation of PDMS only occurring at around 350 °C (Jaeger *et al.*, 2008). Silicon is more electropositive than oxygen, displaying values of 1.8 and 3.5 on the Pauling scale of electronegativity, respectively, resulting in Si-O bonds being polar (Brydson, 1999), and partially ionic in nature. The properties of polyorganosiloxanes, are subject to the properties of the R-group substituents, for example, the shielding of the silicon-oxygen backbone by methyl groups in PDMS results in weak intra and intermolecular forces between polymer chains, resulting in high chain mobility and elastomeric properties. The high chain mobility of polysiloxane chains allows the polymer to exhibit the most thermodynamically favoured state, and is responsible for the low surface energy of the polymer (Jaeger *et al.*, 2008). The high conformational freedom of the siloxane chains in PDMS, which can be explained by a lack of steric hindrance as a result of the small molecular volume of the methyl group, and methyl functionalisation occurring at alternate atoms in the siloxane backbone, is further demonstrated by the materials low glass transition temperature (-123 °C) (Karki, 2016). The elastomeric properties of PDMS, along with its non-toxicity, low chemical reactivity, resistance to oxidation, high oxygen permeability (Nishikawa *et al.*, 2008), UV transparency down to 280 nm (Makamba *et al.*, 2003), low cost, and ease of fabrication, has led to substantial interest in the material for use at biological interfaces such as cell culture (Chuah *et al.*, 2015), oesophageal stents (Karakoy *et al.*, 2014), microfluidic devices such as immunoassays (Gunda *et al.*, 2014; Makamba *et al.*, 2003), the transplantation of pancreatic islets in diabetes treatments (Shin *et al.*, 2013), catheters (Sankar *et al.*, 2017; Tyler *et al.*, 2017), and contact lenses (Chen *et al.*, 2017). However, the surface properties of PDMS have limited its aptness for these applications. For example, the materials low surface energy and poor wettability has been shown to encourage bacterial colonisation resulting in greater infection risk following its use in prosthetic devices (Li *et al.*, 2017; Wu *et al.*, 2014), and the surface

hydrophobicity results in difficulty introducing aqueous samples to the small channels in PDMS based microfluidic devices (Zilio *et al.*, 2014).

The plethora of properties of PDMS deeming it an attractive material in the applications listed above have led to the development of an extensive body of literature reporting methods for modifying PDMS. Approaches to modifying PDMS include dynamic approaches exploiting the physical adsorption of hydrophobic and amphiphilic molecules, surface oxidation by exposure to UV/O₃ or plasma treatments (Bodas *et al.*, 2007; Egitto *et al.*, 2006; Fu *et al.*, 2010; Wong *et al.*, 2009), surface oxidation by chemical treatment (Maji *et al.*, 2012), and covalent approaches (Wu *et al.*, 2011).

1.7.2. Dynamic modification

Dynamic methods of modifying the properties of PDMS are frequently reported, attributed to the facile nature of the protocols and lack of demand for expensive benchtop plasma generators. The methods exploit the physical adsorption of hydrophobic, or hydrophobic portions of, amphiphiles onto PDMS, resulting in the display of a specific head group at the polymer surface. Protocols typically utilise surfactants as ‘dynamic modifiers’, and range from the exposure of cured PDMS devices to buffer solutions containing surfactants (Wang *et al.*, 2006), to the introduction of surfactants to the pre-cured monomer mixture (Holczer *et al.*, 2017; Madadi *et al.*, 2013; Seo *et al.*, 2006). Literature reports significant increases in surface hydrophilicity, with post-treatment water contact angles as low as 23° (Madadi *et al.*, 2013), on par with those obtained with low-pressure plasma treatments (Kaczorowski *et al.*, 2015). The substantial increase in hydrophilicity is thought to be a consequence of van der Waals interactions between the lipophilic tail of the surfactant molecule with PDMS, and the presentation of the hydrophilic portion of the amphiphile at the PDMS-aqueous solution interface (Makamba *et al.*, 2003). However, the depletion of ‘dynamic modifier’ as a result of diffusion into the aqueous phase is a detriment to the approach, and surface hydrophilicity has been found to be a function of contact time with aqueous solutions (Seo *et al.*, 2006).

Interestingly, the occurrence of such phenomena has been observed previously in permeation studies, whereby a reduction in permeation of four APIs through PDMS was observed upon inclusion of

surfactants in the donor phase. The effect was observed with anionic, cationic, zwitterionic and neutral charge state surfactants, tested at three concentration levels. Reductions in permeation were observed for the four compounds tested, namely ibuprofen, lidocaine, benzotriazole and benzocaine, and the greatest effects were observed with the highest concentration of surfactant present (Bhuiyan *et al.*, 2017). The findings were in line with previous research published by the same group, whereby a reduction in the permeation of methyl and ethyl paraben was observed in the presence of sodium dodecyl sulphate (SDS) (Waters *et al.*, 2013), reaching an optimum at the highest concentration of SDS tested. In the latter described work, no effect on permeation was observed upon the inclusion of Brij 35, a non-ionic surfactant, to the donor solution. The findings led the group to conclude that the reduction in permeation was a result of the presentation of the anionic head group at the surface of PDMS following the physisorption of the hydrophobic tail (Waters *et al.*, 2013).

1.7.3. Surface Oxidation

The reversible nature of methods exploiting the physical adsorption of molecules onto PDMS has led to research being undertaken endeavouring to establish more robust methods to enhance the properties of PDMS, in terms of both its reactivity and wettability. The activation of PDMS surfaces, and subsequent increased wettability, can be achieved by surface oxidation, resulting in the cleavage of Si-CH₃ bonds, and the formation of silanol groups (Chen *et al.*, 2007).

Wet chemical oxidation of PDMS is carried out by exposure to Piranha solution, which typically consists of mixtures of H₂O₂ and H₂SO₄ in varying ratios (Jang *et al.*, 2006; Koh *et al.*, 2012; Maji *et al.*, 2012). Piranha oxidation of PDMS is an inexpensive alternative to plasma based methods, however is unattractive from a safety perspective. Addition of H₂O₂ to H₂SO₄ is highly exothermic; H₂O₂ must be added dropwise, and the resultant concentration should not exceed 50 %, above which the solution becomes explosive (Wu *et al.*, 2008). Thus, physical methods of oxidation by energy exposure offer an attractive alternative.

UV/O₃, or UV/ozone, treatment of PDMS is frequently reported in literature, as analogous to the use of Piranha solution, surpasses the need for expensive benchtop plasma generators. A typical setup for

UV/O₃ treatment of PDMS includes a low-pressure mercury lamp in an enclosed vessel containing the PDMS sample. Low-pressure mercury lamps emit UV radiation at both 184.9 nm and 253.7 nm, and in the presence of an oxygen containing process gas, produce reactive oxygen species (ROS). Diatomic oxygen is able to absorb UV radiation at 184.9 nm, resulting in the formation of atomic oxygen, which can further react with diatomic oxygen to form ozone. Ozone is also able to absorb UV radiation at 253.7 nm, resulting in its dissociation to diatomic and atomic oxygen (Egitto *et al.*, 2006). Both ozone and atomic oxygen display high reactivity towards PDMS, and the exposure of PDMS to UV radiation also results in the formation of organic radicals which are able to form more volatile species, such as CO₂ and H₂O, with atomic oxygen and ozone. The desorption of volatile organic species from the surface of PDMS following UV/O₃ treatment results in the formation of a thin SiO_x type layer (Fu *et al.*, 2010). UV/ozone treatments are typically milder than plasma treatments (Wong *et al.*, 2009), and require longer treatment times, however, require less financial investment, and can be performed under atmospheric pressure with air as the process gas (Egitto *et al.*, 2006).

The plasma modification of PDMS is widely reported in literature, owing to the simple nature of the process, and the short durations of exposure required, generally below five minutes (George *et al.*, 2017; Keranov *et al.*, 2008; Wu *et al.*, 2011). Plasmas are known as the ‘fourth state of matter’ and are gases containing ionised molecules and free radicals formed following energy exposure, normally radio frequency discharges (Taubert *et al.*, 2013). Oxygen-containing plasma treatments similarly exploit the use of reactive oxygen species (ROS) to form thin SiO_x layers at the surface of PDMS, typically in the top few nm (Béfahy *et al.*, 2010). Both UV/O₃ and oxygen containing plasma treatments result in the formation of a brittle silica-like layer (Cordeiro *et al.*, 2009) (Figure 1.7), with physical properties, such as higher surface energy and wettability (Kaczorowski *et al.*, 2015), that are distinguishable from the bulk material.

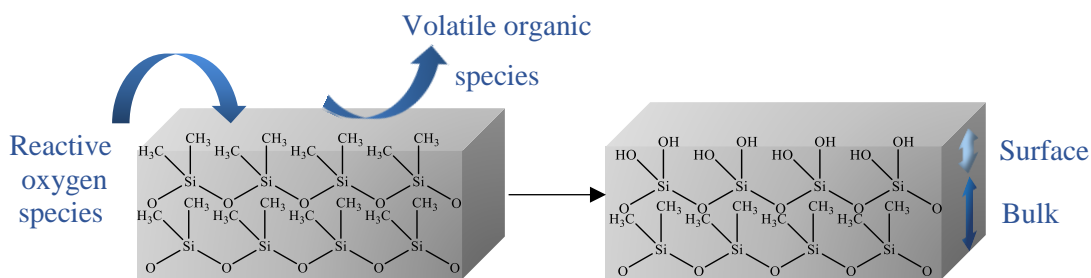


Figure 1.7 Oxidation of poly(dimethylsiloxane) following treatment with UV/O₃ or oxygen-containing plasma, adapted from Chen *et al.* (Chen *et al.*, 2007).

The hydrophobicity of PDMS is known to be restored over time following plasma and UV/O₃ treatments, in a process termed hydrophobic recovery. The hydrophobic recovery of PDMS has been studied extensively, and is thought to be attributed to the diffusion of uncured oligomers through the bulk material to the surface, and the reorientation of polar silanol groups toward the bulk. The UV/O₃ and plasma oxidation of PDMS results in strain between the rigid SiO_x layer and elastomeric bulk, and can lead to crack formation (Lee *et al.*, 2017), which in turn facilitates the diffusion of both oligomers, and other low molecular weight species formed during the treatment, to the surface (Cordeiro *et al.*, 2009; Tan *et al.*, 2010). The exposure of oxidised PDMS to aqueous solutions has been explored as a potential method to extend the lifespan of hydrophilic PDMS surfaces, the success of which is thought to be attributed to hydrogen bonding between surface silanol groups and the solution, which may prevent reorientation towards the bulk (Ma *et al.*, 2011; Zhao *et al.*, 2012). Other attempts to maintain the hydrophilicity of oxidised PDMS include the removal of low molecular weight species, such as cyclic siloxanes, formed during the polymerisation process, which are able to diffuse to the surface and aid hydrophobic recovery (Eddington *et al.*, 2006; Nguyen *et al.*, 2014), and the use of surface silanol groups as a prerequisite to the covalent attachment of hydrophilic molecules.

1.7.4. Covalent Attachment

The generation of silanol groups at the surface of PDMS is frequently followed by covalent bond generation to hydrophilic molecules, endeavouring to lengthen the enhanced surface hydrophilicity, and capitalise the heightened chemical reactivity of oxidised PDMS. Organosilanes, or more specifically, alkoxy silanes, have received substantial attention for such purpose, attributed to the

requirement of moderate reaction conditions, rudimentary protocols, and the inexpensive nature of the reagents (Chuah *et al.*, 2015). The general structure of alkoxy silanes is presented in Figure 1.8.

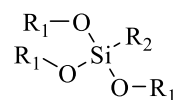


Figure 1.8 General alkoxy silane structure.

Typical procedures involve the use of methoxy- and ethoxysilanes, where $\text{R}_1 = \text{CH}_3$ and $\text{R}_1 = \text{CH}_2\text{CH}_3$, in Figure 1.8, respectively, and result in self-assembled monolayers (SAMs) of alkoxy silanes, represented in Figure 1.9. Protocols generally commence with the plasma oxidation of PDMS, followed by its submersion in a solution of alkoxy silane in aqueous alcohol, typically in concentrations ranging from 1 % to 20 % (Kuddannaya *et al.*, 2013; Nguyen *et al.*, 2016). The reaction precedes with the hydrolysis of the alkoxy silane, producing silanol groups, followed by condensation, leading to the formation of a siloxane linkage between alkoxy silane molecules. The alkoxy silane layers are able to form hydrogen bonds with the PDMS substrate, and further condensation with surface silanols results in Si-O-Si bond formation with the substrate (Gunda *et al.*, 2014).

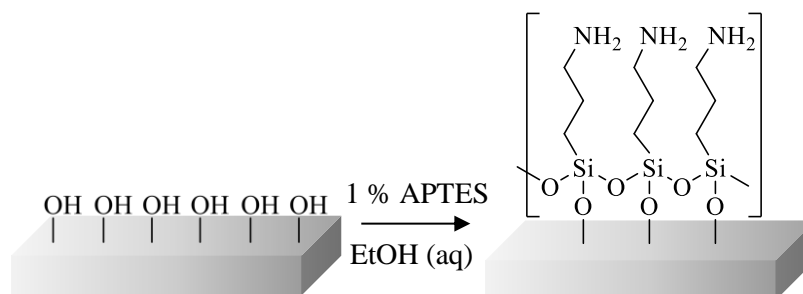


Figure 1.9 Self-assembled monolayer (SAM) formation using (3-aminopropyl)triethoxysilane, adapted from Nguyen *et al.* (Nguyen *et al.*, 2016)

[Methoxy(polyethyleneoxy)propyl]trimethoxysilane, or PEG-silane, has been reported to render microfluidic channels hydrophilic and resistant to non-specific protein adsorption to PDMS microfluidic channels, which is known to be detrimental to device performance (Kovach *et al.*, 2014). Conversely, alkoxy silanes in which R_2 is an amine-containing functionality, such as (3-aminopropyl)trimethoxysilane (APTMS) and (3-aminopropyl)triethoxysilane (APTES), have broadly been used to enhance the interaction of the substrate with biomolecules, such as antibodies in the case

of immunoassay development (Gunda *et al.*, 2014; Pinto *et al.*) and collagen (Wipff *et al.*, 2009), laminin and fibronectin (Kuddannaya *et al.*, 2015) for enhanced substrate biocompatibility in cell culture applications.

Despite the abundance of literature reporting methods of enhancing the properties of PDMS, often endeavouring to render the polymer more comparable to biological tissue in a bid to increase biocompatibility, limited attempts have been made to modify PDMS for use in *in vitro* measurements of percutaneous adsorption.

1.8. Research Aims

The research presented in this thesis endeavours to acknowledge, and to rectify, the current gap in the number of reported attempts to utilise known methods of tailoring the surface properties and chemistry of poly(dimethylsiloxane) to enhance the comparability of the polymer to biological tissue, for use in *in vitro* skin permeability studies. This will be approached according to the following aims:

- ❖ To investigate the potential of an air plasma treatment to produce a lamellar structure of PDMS analogous to that of human skin, and to evaluate the predicting capability of the modified skin mimic by comparison with an appropriate body of literature permeation data obtained using human epidermal tissue.
- ❖ To investigate the potential of a nitrogen plasma treatment to aminate the surface of PDMS, and provide suitable sites for the covalent attachment of biomolecules. Further, the predicting capability of the ‘aminated’ skin mimic will be evaluated on the basis of comparison with the air plasma modified skin mimic, and literature permeation data obtained using human epidermal tissue.
- ❖ To compare three potential methods of immobilising amine group containing biomolecules at the surface of PDMS, to assist in the development of a method of producing a lipid-protein multilayer membrane, similar to the stratum corneum, appropriate for skin permeation assays.

References

- Abd, Yousef, Pastore, Telaprolu, Mohammed, Namjoshi, Grice, & Roberts. (2016). Skin models for the testing of transdermal drugs. *Clinical Pharmacology: Advances and Applications*, 8, 163-176.
- Addicks, Flynn, & Weiner. (1987). Validation of a Flow-Through Diffusion Cell for Use in Transdermal Research. *Pharmaceutical Research*, 4(4), 337-341.
- Akomeah. (2007). Variability in Human Skin Permeability In Vitro: Comparing Penetrants with Different Physicochemical Properties. *Journal of pharmaceutical sciences*, 96(4), 824-834.
- Akomeah, Martin, & Brown. (2007). Variability in human skin permeability in vitro: Comparing penetrants with different physicochemical properties. *Journal of Pharmaceutical Sciences*, 96(4), 824-834.
- Akomeah, Nazir, Martin, & Brown. (2004). Effect of heat on the percutaneous absorption and skin retention of three model penetrants. *European Journal of Pharmaceutical Sciences*, 21(2-3), 337-345.
- Aldwaikat, & Alarjah. (2015). Investigating the sonophoresis effect on the permeation of diclofenac sodium using 3D skin equivalent. *Ultrasonics Sonochemistry*, 22(0), 580-587.
- Avdeef. (2012). *Absorption and Drug Development: Solubility, Permeability, and Charge State* (2 ed.). US: Wiley.
- Baba, Takahara, & Mamitsuka. (2015). In Silico Predictions of Human Skin Permeability using Nonlinear Quantitative Structure–Property Relationship Models. *Pharmaceutical Research*, 32(7), 2360-2371.
- Baba, Ueno, Hashida, & Yamashita. (2017). Quantitative prediction of ionization effect on human skin permeability. *International Journal of Pharmaceutics*, 522(1), 222-233.
- Balakrishnan, Shanmugam, Lee, Lee, Kim, Oh, Kim, Kim, Yoo, Choi, et al. (2009). Formulation and in vitro assessment of minoxidil niosomes for enhanced skin delivery. *International Journal of Pharmaceutics*, 377(1), 1-8.
- Barba, Alonso, Martí, Manich, & Coderch. (2016). Skin barrier modification with organic solvents. *Biochimica et Biophysica Acta (BBA) - Biomembranes*, 1858(8), 1935-1943.
- Barba, Martí, Semenzato, Baratto, Manich, & Coderch. (2014). Effect of lipid modification on stratum corneum permeability. *Journal of Thermal Analysis and Calorimetry*, 120(1), 297-305.
- Barbero, & Frasc. (2009). Pig and guinea pig skin as surrogates for human in vitro penetration studies: A quantitative review. *Toxicology in Vitro*, 23(1), 1-13.
- Bartosova, & Bajgar. (2012). Transdermal drug delivery in vitro using diffusion cells. *Current Medicinal Chemistry*, 19(27), 4671-4677.
- Batheja, Song, Wertz, & Michniak-Kohn. (2009). Effects of growth conditions on the barrier properties of a human skin equivalent. *Pharmaceutical Research*, 26(7), 1689-1700.
- Béfhay, Lipnik, Pardoén, Nascimento, Patris, Bertrand, & Yunus. (2010). Thickness and elastic modulus of plasma treated PDMS silica-like surface layer. *Langmuir*, 26(5), 3372-3375.
- Benson, & Watkinson. (2011). *Topical and Transdermal Drug Delivery : Principles and Practice*. Hoboken, NJ, USA: John Wiley & Sons.
- Bhuiyan, & Waters. (2017). Permeation of pharmaceutical compounds through silicone membrane in the presence of surfactants. *Colloids and Surfaces A: Physicochemical and Engineering Aspects*, 516, 121-128.
- Bodas, & Khan-Malek. (2007). Hydrophilization and hydrophobic recovery of PDMS by oxygen plasma and chemical treatment-An SEM investigation. *Sensors and Actuators, B: Chemical*, 123(1), 368-373.
- Bolzinger, Briançon, Pelletier, & Chevalier. (2012). Penetration of drugs through skin, a complex rate-controlling membrane. *Current Opinion in Colloid & Interface Science*, 17(3), 156-165.
- Brydson. (1999). *Plastics materials* (7 ed.). Oxford: Butterworth-Heinemann.
- Cannon, & Ranade. (2011). *Drug delivery systems*. Boca Raton: CRC Press.
- Chen, & Lindner. (2007). The stability of radio-frequency plasma-treated polydimethylsiloxane surfaces. *Langmuir*, 23(6), 3118-3122.

- Chen, Liu, Tsou, Ting, Tseng, & Wang. (2017). Biopolymer brushes grown on PDMS contact lenses by in situ atmospheric plasma-induced polymerization. *Journal of Polymer Research*, 24(5), 1.
- Choe, Lademann, & Darvin. (2016). A depth-dependent profile of the lipid conformation and lateral packing order of the stratum corneum in vivo measured using Raman microscopy. *Analyst*, 141(6), 1981-1987.
- Chowhan, & Pritchard. (1978). Effect of Surfactants on Percutaneous Absorption of Naproxen I: Comparisons of Rabbit, Rat, and Human Excised Skin. *Journal of Pharmaceutical Sciences*, 67(9), 1272-1274.
- Chuah, Kuddannaya, Lee, Zhang, & Kang. (2015). The effects of poly(dimethylsiloxane) surface silanization on the mesenchymal stem cell fate. *Biomaterials Science*, 3(2), 383-390.
- Cordeiro, Zschoche, Janke, Nitschke, & Werner. (2009). Functionalization of poly(dimethylsiloxane) surfaces with maleic anhydride copolymer films. *Langmuir*, 25(3), 1509-1517.
- Cross, Pugh, Hadgraft, & Roberts. (2001). Probing the effect of vehicles on topical delivery: Understanding the basic relationship between solvent and solute penetration using silicone membranes. *Pharmaceutical Research*, 18(7), 999-1005.
- Dalton, Graham, & Jenner. (2015). Effect of exposure area on nerve agent absorption through skin in vitro. *Toxicology in Vitro*, 30(1), 454-461.
- Du Plessis, Pugh, Judefeind, & Hadgraft. (2002a). The effect of the nature of H-bonding groups on diffusion through PDMS membranes saturated with octanol and toluene. *European Journal of Pharmaceutical Sciences*, 15(1), 63-69.
- Du Plessis, Pugh, Judefeind, & Hadgraft. (2002b). Physico-chemical determinants of dermal drug delivery: Effects of the number and substitution pattern of polar groups. *European Journal of Pharmaceutical Sciences*, 16(3), 107-112.
- Eddington, Puccinelli, & Beebe. (2006). Thermal aging and reduced hydrophobic recovery of polydimethylsiloxane. *Sensors and Actuators B: Chemical*, 114(1), 170-172.
- Egitto, & Matienzo. (2006). Transformation of Poly(dimethylsiloxane) into thin surface films of SiO₂ by UV/Ozone treatment. Part I: Factors affecting modification. *Journal of Materials Science*, 41(19), 6362-6373.
- El Hussein, Muret, Berard, Makki, & Humbert. (2007). Assessment of principal parabens used in cosmetics after their passage through human epidermis–dermis layers (ex-vivo study). *Experimental Dermatology*, 16(10), 830-836.
- Engesland, Škalko-Basnet, & Flaten. (2015). Phospholipid vesicle-based permeation assay and EpiSkin® in assessment of drug therapies destined for skin administration. *Journal of Pharmaceutical Sciences*, 104(3), 1119-1127.
- Feingold. (2007a). The importance of lipids in cutaneous function. *J Lipid Res*, 48(12), 2529-2530.
- Feingold. (2007b). The role of epidermal lipids in cutaneous permeability barrier homeostasis. *Journal of Lipid Research*, 48(12), 2531-2546.
- Feingold. (2007c). Thematic review series: skin lipids. The role of epidermal lipids in cutaneous permeability barrier homeostasis. *J Lipid Res*, 48(12), 2531-2546.
- Feingold, & Elias. (2014). Role of lipids in the formation and maintenance of the cutaneous permeability barrier. *Biochim Biophys Acta*, 1841(3), 280-294.
- Feldstein, Raigorodskii, Iordanskii, & Hadgraft. (1998). Modeling of percutaneous drug transport in vitro using skin-imitating Carbosil membrane. *Journal of Controlled Release*, 52(1-2), 25-40.
- Fiala, Brown, & Jones. (2008). An investigation into the influence of binary drug solutions upon diffusion and partition processes in model membranes. *Journal of Pharmacy and Pharmacology*, 60(12), 1615-1623.
- Flaten, Palac, Engesland, Filipović-Grčić, Vanić, & Škalko-Basnet. (2015). In vitro skin models as a tool in optimization of drug formulation. *European Journal of Pharmaceutical Sciences*, 75, 10-24.
- Flynn. (1990). Physicochemical determinants of skin absorption. In: *Principles of route-to-route extrapolation for risk assessment*. Elsevier, New York.
- Fu, Qui, Liao, Lue, Hu, Lee, & Lai. (2010). Effect of UV-Ozone treatment on poly(dimethylsiloxane) membranes: Surface characterization and gas separation performance. *Langmuir*, 26(6), 4392-4399.

- Geinoz, Rey, Boss, Bunge, Guy, Carrupt, Reist, & Testa. (2002). Quantitative Structure–Permeation Relationships for Solute Transport Across Silicone Membranes. *Pharmaceutical Research*, 19(11), 1622-1629.
- George, Chidangil, & George. (2017). A study on air bubble wetting: Role of surface wettability, surface tension, and ionic surfactants. *Applied Surface Science*, 410, 117-125.
- Godin, & Toutitou. (2007). Transdermal skin delivery: predictions for humans from in vivo, ex vivo and animal models. *Adv Drug Deliv Rev*, 59(11), 1152-1161.
- Gunda, Singh, Norman, Kaur, & Mitra. (2014). Optimization and characterization of biomolecule immobilization on silicon substrates using (3-aminopropyl)triethoxysilane (APTES) and glutaraldehyde linker. *Applied Surface Science*, 305, 522-530.
- Guy. (2013). Skin-'that unfakeable young surface'. *Skin Pharmacology and Physiology*, 26(4-6), 181-189.
- Hadgraft, & Valenta. (2000). pH, pKa and dermal delivery. *International Journal of Pharmaceutics*, 200(2), 243-247.
- Harding. (2004). The stratum corneum: structure and function in health and disease. *Dermatologic Therapy*, 17, 6-15.
- Harrison, Groundwater, Brain, & Hadgraft. (1996). Azone® induced fluidity in human stratum corneum. A fourier transform infrared spectroscopy investigation using the perdeuterated analogue. *Journal of Controlled Release*, 41(3), 283-290.
- Herkenne, Naik, Kalia, Hadgraft, & Guy. (2006). Ibuprofen Transport into and through Skin from Topical Formulations: In Vitro-In Vivo Comparison. *J Invest Dermatol*, 127(1), 135-142.
- Hoath. (2014). Development of the stratum corneum. *British Journal of Dermatology*, 171, 2-5.
- Holczer, & Fürjes. (2017). Effects of embedded surfactants on the surface properties of PDMS; applicability for autonomous microfluidic systems. *Microfluidics and Nanofluidics*, 21(5), 81.
- Houk, & Guy. (1988). Membrane models for skin penetration studies. *Chemical Reviews*, 88(3), 455-471.
- Imokawa, Akasaki, Hattori, & Yoshizuka. (1986). Selective recovery of deranged water-holding properties by stratum corneum lipids. *Journal of Investigative Dermatology*, 87(6), 758-761.
- Jacobi, Kaiser, Toll, Mangelsdorf, Audring, Otberg, Sterry, & Lademann. (2007). Porcine ear skin: an in vitro model for human skin. *Skin Research and Technology*, 13(1), 19-24.
- Jaeger, & Gleria. (2008). *Silicon-based Inorganic Polymers*. New York: Nova Science Publishers, Inc.
- Jang, Oh, & Park. (2006). In situ electrochemical enzyme immunoassay on a microchip with surface-functionalized poly(dimethylsiloxane) channel. *Enzyme and Microbial Technology*, 39(5), 1122-1127.
- Jetzer, Huq, Ho, Flynn, Duraiswamy, & Condie. (1986). Permeation of Mouse Skin and Silicone Rubber Membranes by Phenols: Relationship to In Vitro Partitioning. *Journal of Pharmaceutical Sciences*, 75(11), 1098-1103.
- Kaczorowski, Szymanski, Batory, & Niedzielski. (2015). Effect of plasma treatment on the surface properties of polydimethylsiloxane. *Journal of Applied Polymer Science*, 132(11), 41635.
- Kang, Yap, Lim, Chen, Ho, Chan, Chan, & Wong. (2007). Formulation development of transdermal dosage forms: Quantitative structure-activity relationship model for predicting activities of terpenes that enhance drug penetration through human skin. *Journal of Controlled Release*, 120(3), 211-219.
- Karadzovska, Brooks, Monteiro-Riviere, & Riviere. (2013). Predicting skin permeability from complex vehicles. *Advanced Drug Delivery Reviews*, 65(2), 265-277.
- Karadzovska, & Riviere. (2013). Assessing vehicle effects on skin absorption using artificial membrane assays. *European Journal of Pharmaceutical Sciences*, 50(5), 569-576.
- Karakoy, Gultepe, Pandey, Khashab, & Gracias. (2014). Silane surface modification for improved bioadhesion of esophageal stents. *Applied Surface Science*, 311, 684-689.
- Karki. (2016). Unusual Morphologies of Poly(vinyl alcohol) Thin Films Adsorbed on Poly(dimethylsiloxane) Substrates. *Langmuir*, 32(13), 3191-3198.
- Keranov, Vladkova, Minchev, Kostadinova, & Altankov. (2008). Preparation, characterization, and cellular interactions of collagen-immobilized PDMS surfaces. *Journal of Applied Polymer Science*, 110(1), 321-330.

- Klimová, Hojerová, & Beránková. (2015). Skin absorption and human exposure estimation of three widely discussed UV filters in sunscreens – In vitro study mimicking real-life consumer habits. *Food and Chemical Toxicology*, 83, 237-250.
- Koh, Chin, Chia, & Chiang. (2012). Quantitative studies on PDMS-PDMS interface bonding with piranha solution and its swelling effect. *Micromachines*, 3(2), 427-441.
- Kovach, Kovach, Capadona, Sen Gupta, & Potkay. (2014). The effects of PEG-based surface modification of PDMS microchannels on long-term hemocompatibility. *Journal of biomedical materials research. Part A*, n-a-n/a.
- Küchler, Strüver, & Friess. (2013). Reconstructed skin models as emerging tools for drug absorption studies. *Expert Opinion on Drug Metabolism and Toxicology*, 9(10), 1255-1263.
- Kuddannaya, Bao, & Zhang. (2015). Enhanced In Vitro Biocompatibility of Chemically Modified Poly(dimethylsiloxane) Surfaces for Stable Adhesion and Long-term Investigation of Brain Cerebral Cortex Cells. *ACS Applied Materials & Interfaces*, 7(45), 25529-25538.
- Kuddannaya, Chuah, Lee, Menon, Kang, & Zhang. (2013). Surface chemical modification of poly(dimethylsiloxane) for the enhanced adhesion and proliferation of mesenchymal stem cells. *ACS Applied Materials & Interfaces*, 5(19), 9777-9784.
- Lane. (2013). Skin penetration enhancers. *International Journal of Pharmaceutics*, 447(1–2), 12-21.
- Lee, Conradi, & Shanmugasundaram. (2010). Development of an in silico model for human skin permeation based on a Franz cell skin permeability assay. *Bioorganic and Medicinal Chemistry Letters*, 20(1), 69-73.
- Lee, Hong, Park, Lee, & Kim. (2017). A simple fabrication process for stepwise gradient wrinkle pattern with spatially-controlled wavelength based on sequential oxygen plasma treatment. *Microelectronic Engineering*, 176, 101-105.
- Lemery, Briançon, Chevalier, Oddos, Gohier, Boyron, & Bolzinger. (2015). Surfactants have multi-fold effects on skin barrier function. *European Journal of Dermatology*, 25(5), 424-435.
- Leveque, Raghavan, Lane, & Hadgraft. (2006). Use of a molecular form technique for the penetration of supersaturated solutions of salicylic acid across silicone membranes and human skin in vitro. *International Journal of Pharmaceutics*, 318(1), 49-54.
- Li, Ding, Kuddannaya, Zhang, & Yang. (2017). Anti-bacterial properties of collagen-coated glass and polydimethylsiloxane substrates. *Journal of Materials Science*, 52(17), 9963-9978.
- Liou, Ho, Yang, Lin, & Sheu. (2009). Construction of a quantitative structure-permeability relationship (QSPR) for the transdermal delivery of NSAIDs. *Journal of Controlled Release*, 138(3), 260-267.
- Liu, Kruger, Maibach, Colditz, & Roberts. (2014). Using skin for drug delivery and diagnosis in the critically ill. *Advanced Drug Delivery Reviews*, 77, 40-49.
- Lombardi Borgia, Schlupp, Mehnert, & Schäfer-Korting. (2008). In vitro skin absorption and drug release – A comparison of six commercial prednicarbate preparations for topical use. *European Journal of Pharmaceutics and Biopharmaceutics*, 68(2), 380-389.
- Lu, Lee, & Rao. (1992). Percutaneous Absorption Enhancement of Leuprolide. *Pharmaceutical Research*, 9(12), 1575-1579.
- Luo, Patel, Sinko, Bell, Wibawa, Hadgraft, & Lane. (2016). A comparative study of the in vitro permeation of ibuprofen in mammalian skin, the PAMPA model and silicone membrane. *International Journal of Pharmaceutics*, 505(1), 14-19.
- Ma, Rivera, Hirasaki, & Biswal. (2011). Wettability control and patterning of PDMS using UV-ozone and water immersion. *Journal of Colloid and Interface Science*, 363(1), 371-378.
- Madadi, & Casals-Terré. (2013). Long-term behavior of nonionic surfactant-added PDMS for self-driven microchips. *Microsystem Technologies*, 19(1), 143-150.
- Madison. (2003). Barrier function of the skin: "La Raison d'Être" of the epidermis. *Journal of Investigative Dermatology*, 121(2), 231-241.
- Mahdi, Conway, Mills, & Smith. (2016). Gellan gum fluid gels for topical administration of diclofenac. *International Journal of Pharmaceutics*, 515(1–2), 535-542.
- Maji, Lahiri, & Das. (2012). Study of hydrophilicity and stability of chemically modified PDMS surface using piranha and KOH solution. *Surface and Interface Analysis*, 44(1), 62-69.
- Makamba, Kim, Lim, Park, & Hahn. (2003). Surface modification of poly(dimethylsiloxane) microchannels. *Electrophoresis*, 24(21), 3607-3619.

- Mangelsdorf, Kielhorn, & Organization. (2006). *Dermal Absorption: Dermal Absorption*: World Health Organization.
- Markovic, Vladimirov, Cudina, Odovic, & Karljickovic-Rajic. (2012). A PAMPA assay as fast predictive model of passive human skin permeability of new synthesized corticosteroid C-21 esters. *Molecules*, 17(1), 480-491.
- Másson, Sigfússon, & Loftsson. (2002). Fish Skin as a Model Membrane to Study Transmembrane Drug Delivery with Cyclodextrins. *Journal of inclusion phenomena and macrocyclic chemistry*, 44(1), 177-182.
- Meckfessel, & Brandt. (2014). The structure, function, and importance of ceramides in skin and their use as therapeutic agents in skin-care products. *J Am Acad Dermatol*, 71(1), 177-184.
- Menon, Cleary, & Lane. (2012). The structure and function of the stratum corneum. *International Journal of Pharmaceutics*, 435(1), 3-9.
- Mertz, & Sloan. (2014). The Flux of Select NSAIDs through Silicone Membranes from Mineral Oil. *Pharmaceutics*, 6(3), 354-365.
- Miki, Ichitsuka, Yamada, Kimura, Egawa, Seki, Juni, Ueda, & Morimoto. (2015). Development of a membrane impregnated with a poly(dimethylsiloxane)/poly(ethylene glycol) copolymer for a high-throughput screening of the permeability of drugs, cosmetics, and other chemicals across the human skin. *European Journal of Pharmaceutical Sciences*, 66, 41-49.
- Misra, & Shahiwala. (2014). *Applications of Polymers in Drug Delivery* (1 ed.). Shropshire: Ismithers Rapra.
- Mitragotri. (2003). Modeling skin permeability to hydrophilic and hydrophobic solutes based on four permeation pathways. *Journal of Controlled Release*, 86(1), 69-92.
- Mitragotri, Anissimov, Bunge, Frasch, Guy, Hadgraft, Kasting, Lane, & Roberts. (2011). Mathematical models of skin permeability: An overview. *International Journal of Pharmaceutics*, 418(1), 115-129.
- Mohammed, Matts, Hadgraft, & Lane. (2012). Variation of Stratum Corneum Biophysical and Molecular Properties with Anatomic Site. *The AAPS Journal*, 14(4), 806-812.
- Mojumdar, Gooris, & Bouwstra. (2015). Phase behavior of skin lipid mixtures: The effect of cholesterol on lipid organization. *Soft Matter*, 11(21), 4326-4336.
- Mojumdar, Kariman, van Kerckhove, Gooris, & Bouwstra. (2014). The role of ceramide chain length distribution on the barrier properties of the skin lipid membranes. *Biochimica et Biophysica Acta (BBA) - Biomembranes*, 1838(10), 2473-2483.
- Moss, & Cronin. (2002). Quantitative structure–permeability relationships for percutaneous absorption: re-analysis of steroid data. *International Journal of Pharmaceutics*, 238(1), 105-109.
- Moss, Gullick, & Wilkinson. (2015). *Predictive Methods in Percutaneous Absorption*. Berlin: Springer.
- Netzlaff, Kaca, Bock, Haltner-Ukomadu, Meiers, Lehr, & Schaefer. (2007). Permeability of the reconstructed human epidermis model Episkin® in comparison to various human skin preparations. *European Journal of Pharmaceutics and Biopharmaceutics*, 66(1), 127-134.
- Ng, & Lau. (2015). Skin Deep: The Basics of Human Skin Structure and Drug Penetration. In N. Dragicevic & H. I. Maibach (Eds.), *Percutaneous Penetration Enhancers Chemical Methods in Penetration Enhancement: Drug Manipulation Strategies and Vehicle Effects* (pp. 3-11). Berlin: Springer
- Ng, Rouse, Sanderson, & Eccleston. (2010). A Comparative study of transmembrane diffusion and permeation of ibuprofen across synthetic membranes using franz diffusion cells. *Pharmaceutics*, 2(2), 209-223.
- Ng, Rouse, Sanderson, & Eccleston. (2012). The relevance of polymeric synthetic membranes in topical formulation assessment and drug diffusion study. *Arch Pharm Res*, 35(4), 579-593.
- Ng, Rouse, Sanderson, Meidan, & Eccleston. (2010). Validation of a static Franz diffusion cell system for in vitro permeation studies. *AAPS PharmSciTech*, 11(3), 1432-1441.
- Nguyen, Hang, Wang, Tian, Wang, McCarthy, & Chen. (2014). Simple and Improved Approaches to Long-Lasting, Hydrophilic Silicones Derived from Commercially Available Precursors. *ACS Applied Materials and Interfaces*, 6(24), 22876-22883.
- Nguyen, Tran, & Lee. (2016). Thermally robust and biomolecule-friendly room-temperature bonding for the fabrication of elastomer-plastic hybrid microdevices. *Lab on a chip*, 16(17), 3251-3259.

- Nicoli, Penna, Padula, Colombo, & Santi. (2006). New transdermal bioadhesive film containing oxybutynin: In vitro permeation across rabbit ear skin. *International Journal of Pharmaceutics*, 325(1), 2-7.
- Nishikawa, Yamamoto, Kojima, Kikuo, Fujii, & Sakai. (2008). Stable immobilization of rat hepatocytes as hemispheroids onto collagen-conjugated poly-dimethylsiloxane (PDMS) surfaces: Importance of direct oxygenation through PDMS for both formation and function. *Biotechnology and Bioengineering*, 99(6), 1472-1481.
- Norlén. (2006). Stratum corneum keratin structure, function and formation – a comprehensive review. *International Journal of Cosmetic Science*, 28(6), 397-425.
- Notman, & Anwar. (2013). Breaching the skin barrier — Insights from molecular simulation of model membranes. *Advanced Drug Delivery Reviews*, 65(2), 237-250.
- OECD. *Test No. 428: Skin Absorption: In Vitro Method*: OECD Publishing.
- OECD. *Test No. 431: In Vitro Skin Corrosion: Reconstructed Human Epidermis (RHE) Test Method*: OECD Publishing.
- OECD. *Test No. 439: In Vitro Skin Irritation: Reconstructed Human Epidermis Test Method*: OECD Publishing.
- Oliveira, Beezer, Hadgraft, & Lane. (2010). Alcohol enhanced permeation in model membranes. Part I. Thermodynamic and kinetic analyses of membrane permeation. *International Journal of Pharmaceutics*, 393(1–2), 61-67.
- Oliveira, Hadgraft, & Lane. (2012). The role of vehicle interactions on permeation of an active through model membranes and human skin. *International Journal of Cosmetic Science*, 34(6), 536-545.
- Ottaviani, Martel, & Carrupt. (2006). Parallel artificial membrane permeability assay: A new membrane for the fast prediction of passive human skin permeability. *Journal of Medicinal Chemistry*, 49(13), 3948-3954.
- Özgüney, Karasulu, Kantarci, Sözer, Güneri, & Ertan. (2006). Transdermal delivery of diclofenac sodium through rat skin from various formulations. *AAPS PharmSciTech*, 7(4), 39-45.
- Partidos, Beignon, Mawas, Belliard, Briand, & Muller. (2003). Immunity under the skin: potential application for topical delivery of vaccines. *Vaccine*, 21(7–8), 776-780.
- Patzelt, Mak, Jung, Knorr, Meinke, Richter, Rühl, Cheung, Tran, & Lademann. (2017). Do nanoparticles have a future in dermal drug delivery? *Journal of Controlled Release*, 246, 174-182.
- Pellett, Castellano, Hadgraft, & Davis. (1997). The penetration of supersaturated solutions of piroxicam across silicone membranes and human skin in vitro. *Journal of Controlled Release*, 46(3), 205-214.
- Pineau, Guillard, Fauconneau, Favreau, Marty, Gaudin, Vincent, Marraud, & Marty. (2012). In vitro study of percutaneous absorption of aluminum from antiperspirants through human skin in the Franz™ diffusion cell. *Journal of Inorganic Biochemistry*, 110, 21-26.
- Pinto, Minas, & Correia-Neves. (2015). *PDMS biofunctionalization study for the development of a microfluidic device: Application to salivary cortisol*.
- Potts, & Guy. (1992). Predicting skin permeability. *Pharmaceutical Research*, 9(5), 663-669.
- Powell. (2007). Skin physiology. *The Foundation Years*, 3(5), 193-196.
- Pranitha, & Lakshmi. (2014). Towards a correlation between polar surface area of drugs with Ex-vivo transdermal flux variability. *Iranian Journal of Pharmaceutical Sciences*, 10(2), 47-60.
- Proksch, Brandner, & Jensen. (2008). The skin: an indispensable barrier. *Experimental Dermatology*, 17(12), 1063-1072.
- Prottey. (1976). Essential fatty acids and the skin. *British Journal of Dermatology*, 94(5), 579-587.
- Pugh, Roberts, & Hadgraft. (1996). Epidermal permeability - penetrant structure relationships: 3. The effect of hydrogen bonding interactions and molecular size on diffusion across the stratum corneum. *International Journal of Pharmaceutics*, 138(2), 149-165.
- Qvist, Hoeck, Kreilgaard, Madsen, & Frokjaer. (2000). Evaluation of Göttingen minipig skin for transdermal in vitro permeation studies. *European Journal of Pharmaceutical Sciences*, 11(1), 59-68.
- Rabionet, Gorgas, & Sandhoff. (2014). Ceramide synthesis in the epidermis. *Biochim Biophys Acta*, 1841(3), 422-434.

- Ravenzwaay, & Leibold. (2004). A comparison between in vitro rat and human and in vivo rat skin absorption studies. *Human & Experimental Toxicology*, 23(9), 421-430.
- Roskos. (1989). The effect of ageing on percutaneous absorption in man. *Journal of pharmacokinetics and biopharmaceutics*, 17, 617-630.
- Roy, Fujiki, & Fleitman. (1993). Permeabilities of alkyl p-aminobenzoates through living skin equivalent and cadaver skin. *Journal of Pharmaceutical Sciences*, 82(12), 1266-1268.
- Salvador, & Chisvert. (2007). *Analysis of Cosmetic Products* (Vol. 1st). Oxford: Elsevier Science.
- Sankar, Murthy, Das, Sathya, Nankar, Venugopalan, & Doble. (2017). Polydimethyl siloxane based nanocomposites with antibiofilm properties for biomedical applications. *Journal of Biomedical Materials Research - Part B Applied Biomaterials*, 105(5), 1075-1082.
- Santos, Watkinson, Hadgraft, & Lane. (2011). Enhanced permeation of fentanyl from supersaturated solutions in a model membrane. *International Journal of Pharmaceutics*, 407(1), 72-77.
- Schmook, Meingassner, & Billich. (2001). Comparison of human skin or epidermis models with human and animal skin in in-vitro percutaneous absorption. *International Journal of Pharmaceutics*, 215(1-2), 51-56.
- Schreiber, Mahmoud, Vuia, Rübhelke, Schmidt, Schaller, Kandárová, Haberland, Schäfer, Bock, et al. (2005). Reconstructed epidermis versus human and animal skin in skin absorption studies. *Toxicology in Vitro*, 19(6), 813-822.
- Sekkat, Kalia, & Guy. (2002). Biophysical Study of Porcine Ear Skin In Vitro and Its Comparison to Human Skin In Vivo. *Journal of Pharmaceutical Sciences*, 91(11), 2376-2381.
- Seo, & Lee. (2006). Effects on wettability by surfactant accumulation/depletion in bulk polydimethylsiloxane (PDMS). *Sensors and Actuators, B: Chemical*, 119(1), 192-198.
- Shahzad, Louw, Gerber, & du Plessis. (2015). Breaching the skin barrier through temperature modulations. *Journal of Controlled Release*, 202(0), 1-13.
- Shin, Shin, & Yoo. (2013). Attachment of alginate microcapsules onto plasma-treated PDMS sheet for retrieval after transplantation: Alginate Microcapsules onto Plasma-Treated PDMS Sheet. *Biotechnology and Applied Biochemistry*, 60(6), 617-622.
- Shumilov, Touitou, Godin, Ainbinder, Yosha, & Tsahor-Ohayon. (2009). Evaluation of a polysiloxane-collagen biphasic membrane: A model for in vitro skin permeation studies. *Journal of Drug Delivery Science and Technology*, 19(4), 289-294.
- Simon, Amaro, Healy, Cabral, & de Sousa. (2016). Comparative evaluation of rivastigmine permeation from a transdermal system in the Franz cell using synthetic membranes and pig ear skin with in vivo-in vitro correlation. *International Journal of Pharmaceutics*, 512(1), 234-241.
- Singh, & Singh. (1993). Transdermal drug delivery by passive diffusion and iontophoresis: A review. *Medicinal Research Reviews*, 13(5), 569-621.
- Sinkó, Garrigues, Balogh, Nagy, Tsinman, Avdeef, & Takács-Novák. (2012). Skin-PAMPA: A new method for fast prediction of skin penetration. *European Journal of Pharmaceutical Sciences*, 45(5), 698-707.
- Sinkó, Kökösi, Avdeef, & Takács-Novák. (2009). A PAMPA Study of the Permeability-Enhancing Effect of New Ceramide Analogues. *Chemistry & Biodiversity*, 6(11), 1867-1874.
- Stahl, Niedorf, & Kietzmann. (2009). Characterisation of epidermal lipid composition and skin morphology of animal skin ex vivo. *European Journal of Pharmaceutics and Biopharmaceutics*, 72(2), 310-316.
- Stahl, Niedorf, & Kietzmann. (2011). The correlation between epidermal lipid composition and morphologic skin characteristics with percutaneous permeation: an interspecies comparison of substances with different lipophilicity. *Journal of Veterinary Pharmacology and Therapeutics*, 34(5), 502-507.
- Sugibayashi, Todo, Oshizaka, & Owada. (2009). Mathematical Model to Predict Skin Concentration of Drugs: Toward Utilization of Silicone Membrane to Predict Skin Concentration of Drugs as an Animal Testing Alternative. *Pharmaceutical Research*, 27(1), 134.
- Synovec, Wasdo, & Sloan. (2013). The effect of lipid and aqueous solubilities on flux of nicotinic acid esters from water through silicone membrane. *Drug Development and Industrial Pharmacy*, 39(9), 1494-1497.
- Tan, Nguyen, Chua, & Kang. (2010). Oxygen plasma treatment for reducing hydrophobicity of a sealed polydimethylsiloxane microchannel. *Biomicrofluidics*, 4(3).

- Tan, Zhang, Wu, Fang, & He. (2009). The Enhancing Effect of Ion-pairing on the Skin Permeation of Glipizide. *AAPS PharmSciTech*, 10(3), 967.
- Taubert, Mano, Rodríguez-Cabello, & Rodríguez-Cabello. (2013). *Biomaterials Surface Science* (2 ed.). Weinheim: Wiley.
- Tayar, Tsai, Testa, Carrupt, Hansch, & Leo. (1991). Percutaneous penetration of drugs: A quantitative structure-permeability relationship study. *Journal of Pharmaceutical Sciences*, 80(8), 744-749.
- Thakoersing, Danso, Mulder, Gooris, El Ghalbzouri, & Bouwstra. (2012). Nature versus nurture: does human skin maintain its stratum corneum lipid properties in vitro? *Experimental Dermatology*, 21(11), 865-870.
- Thomas, Majumdar, Wasdo, Majumdar, & Sloan. (2007). The effect of water solubility of solutes on their flux through human skin in vitro: An extended Flynn database fitted to the Roberts–Sloan equation. *International Journal of Pharmaceutics*, 339(1), 157-167.
- Tobin. (2006). Biochemistry of human skin—our brain on the outside. *Chem Soc Rev*, 35(1), 52-67.
- Trommer, & Neubert. (2006). Overcoming the Stratum Corneum: The Modulation of Skin Penetration (pp. 106-121). London.
- Trotta, Ugazio, Peira, & Pulitano. (2003). Influence of ion pairing on topical delivery of retinoic acid from microemulsions. *Journal of Controlled Release*, 86(2), 315-321.
- Tyler, Hook, Pelster, Williams, Alexander, & Arlinghaus. (2017). Development and characterization of a stable adhesive bond between a poly(dimethylsiloxane) catheter material and a bacterial biofilm resistant acrylate polymer coating. *Biointerphases*, 12(2), 02C412.
- Uchida, Kadhum, Kanai, Todo, Oshizaka, & Sugibayashi. (2015). Prediction of skin permeation by chemical compounds using the artificial membrane, Strat-M™. *European Journal of Pharmaceutical Sciences*, 67, 113-118.
- Varvaresou. (2006). Percutaneous absorption of organic sunscreens. *Journal of Cosmetic Dermatology*, 5(1), 53-57.
- Wang, Xu, & Chen. (2006). Nonionic surfactant dynamic coating of poly(dimethylsiloxane) channel surface for microchip electrophoresis of amino acids. *Analytica Chimica Acta*, 569(1), 188-194.
- Wasdo, Juntunen, Devarajan, & Sloan. (2009). A correlation of flux through a silicone membrane with flux through hairless mouse skin and human skin in vitro. *International Journal of Pharmaceutics*, 373(1), 62-67.
- Wasukan, Srisung, Kulthong, Boonrungsiman, & Maniratanachote. (2015). Determination of silver in personal care nanoproducts and effects on dermal exposure. *Journal of Nanoparticle Research*, 17(11), 425.
- Waters. (2015). Recent developments in skin mimic systems to predict transdermal permeation. *Current Pharmaceutical Design*, 21(20), 2735-2732.
- Waters, Dennis, Bibi, & Mitchell. (2013). Surfactant and temperature effects on paraben transport through silicone membranes. *Colloids and Surfaces B: Biointerfaces*, 108, 23-28.
- Wijmans, & Baker. (1995). The solution-diffusion model: a review. *Journal of Membrane Science*, 107(1), 1-21.
- Williams. (2006). In vitro studies—how good are they at replacing in vivo studies for measurement of skin absorption? *Environmental Toxicology and Pharmacology*, 21(2), 199-203.
- Wipff, Majd, Acharya, Buscemi, Meister, & Hinz. (2009). The covalent attachment of adhesion molecules to silicone membranes for cell stretching applications. *Biomaterials*, 30(9), 1781-1789.
- Wong, & Ho. (2009). Surface molecular property modifications for poly(dimethylsiloxane) (PDMS) based microfluidic devices. *Microfluidics and Nanofluidics*, 7(3), 291-306.
- Wood, Brown, & Jones. (2012). Understanding heat facilitated drug transport across human epidermis. *European Journal of Pharmaceutics and Biopharmaceutics*, 81(3), 642-649.
- Wosicka, & Cal. (2010). Targeting to the hair follicles: Current status and potential. *Journal of Dermatological Science*, 57(2), 83-89.
- Wu, Chen, Cheng, Lee, & Shu. (2008). Thermal decomposition of hydrogen peroxide in the presence of sulfuric acid. *Journal of Thermal Analysis and Calorimetry*, 93(1), 115-120.

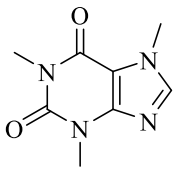
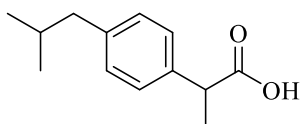
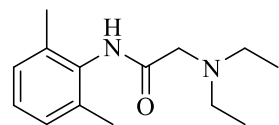
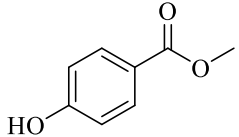
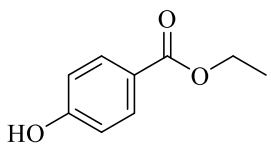
- Wu, He, Ren, Cai, Fang, & Feng. (2014). Development of functional biointerfaces by surface modification of polydimethylsiloxane with bioactive chlorogenic acid. *Colloids and Surfaces B: Biointerfaces*, 116, 700-706.
- Wu, Yuan, & Ding. (2011). Effect of polydimethylsiloxane surfaces silanized with different nitrogen-containing groups on the adhesion progress of epithelial cells. *Surface and Coatings Technology*, 205(10), 3182-3189.
- Yuan, & Capomacchia. (2005). The binary eutectic of NSAIDs and two-phase liquid system for enhanced membrane permeation. *Pharmaceutical Development and Technology*, 10(1), 1-10.
- Zhao, Lee, & Sen. (2012). Long-term retention of hydrophilic behavior of plasma treated polydimethylsiloxane (PDMS) surfaces stored under water and Luria-Bertani broth. *Sensors and Actuators, A: Physical*, 181, 33-42.
- Zilio, Sola, Damin, Faggioni, & Chiari. (2014). Universal hydrophilic coating of thermoplastic polymers currently used in microfluidics. *Biomedical Microdevices*, 16(1), 107-114.

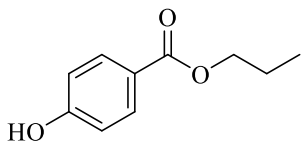
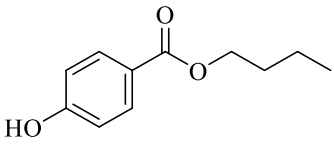
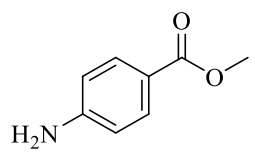
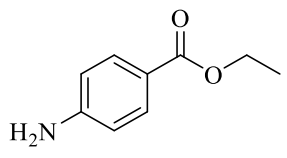
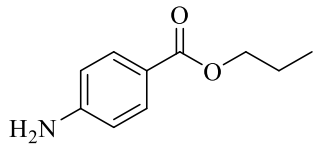
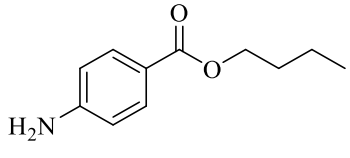
Chapter 2 Materials and Methods

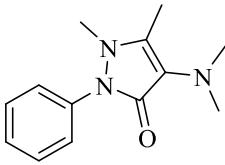
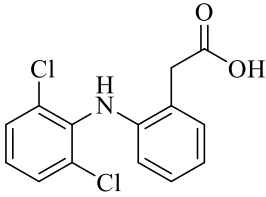
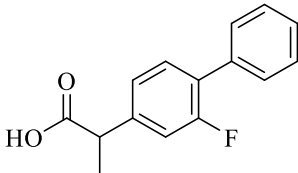
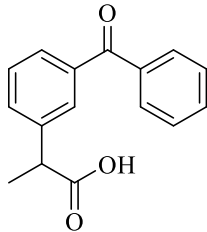
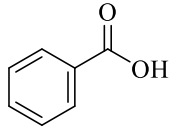
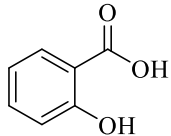
2.1 Materials

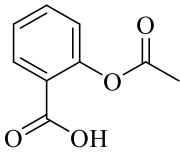
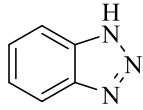
Silatos™ silicone sheeting, dimensions 150 x 200 x 0.13 mm, was purchased from ATOS medical. The sheeting consisted of a medical grade, non-sterile, poly(dimethylsiloxane) elastomer, with a density of 1102.6 kg m⁻³. Potassium phosphate dibasic (≥ 98 %), potassium phosphate monobasic (≥ 99 %), benzoic acid (≥ 99.5 %), benzocaine (≥ 99 %), benzotriazole (≥ 98.5 %), lidocaine (≥ 98 %), caffeine (≥ 99 %), acetyl salicylic acid (≥ 99 %), methyl 4-aminobenzoate (98 %), benzocaine (98 %), butamben (≥ 98 %), methyl 4-hydroxybenzoate (≥ 99 %), ethyl 4-hydroxybenzoate (99 %), butyl 4-hydroxybenzoate (≥ 99 %), (3-aminopropyl)triethoxysilane (≥ 98 %), (3-aminopropyl)trimethoxysilane (97 %), N_α-Boc-L-lysine (99 %), Boc-Lys(Z)-OH (> 98 %), and *N,N'*-dicyclohexylcarbodiimide (99 %) were purchased from Sigma Aldrich Ltd., Dorset, UK. Salicylic acid (> 99.5 %), propyl 4-hydroxybenzoate (≥ 99 %) and 4-dimethylaminoantipyrine (97 %), ethanol (> 99 %), dichloromethane (> 99 %), 4 N HCl in 1,4 -dioxane, 1,4-dioxane (99.8 %), HBr (33 % w/w) in glacial acetic acid, and ethyl acetate (> 99 %) were purchased from Fisher Scientific Ltd., Loughborough, UK. Risocaine (98 %) was purchased from Alfa Aesar, Lancashire, UK. Flurbiprofen (> 98 %), ketoprofen (> 98 %) and diclofenac (> 98 %) were purchased from Tokyo Chemical Industry Ltd. Ibuprofen (≥ 99 %) was purchased from BASF. All chemicals were used as supplied.

Table 2.1 Structure, molecular weight, $\log_{10} P$, charge, and λ_{\max} of pharmaceutical compounds used in permeation studies presented in this thesis.

Caffeine		
Abbreviation	CAF	
Molecular weight	194.19 g mol ⁻¹	
$\log_{10} P^i$	-0.13	
Charge	Cationic	
λ_{\max}	272 nm	
Ibuprofen		
Abbreviation	IBU	
Molecular weight	206.28 g mol ⁻¹	
$\log_{10} P^i$	3.72	
Charge	Anionic	
λ_{\max}	221 nm	
Lidocaine		
Abbreviation	LID	
Molecular weight	234.34 g mol ⁻¹	
$\log_{10} P^i$	3.63	
Charge	Cationic	
λ_{\max}^{ii}	230 nm	
Methyl Paraben		
Abbreviation	MP	
Molecular weight	152.15 g mol ⁻¹	
$\log_{10} P^i$	1.87	
Charge	Anionic	
λ_{\max}	254 nm	
Ethyl paraben		
Abbreviation	EP	
Molecular weight	166.17 g mol ⁻¹	
$\log_{10} P^i$	2.40	
Charge	Anionic	
λ_{\max}	254 nm	

Propyl paraben		
Abbreviation	PP	
Molecular weight	180.20 g mol ⁻¹	
log ₁₀ P ⁱ	2.93	
Charge	Anionic	
λ _{max}	254 nm	
Butyl paraben		
Abbreviation	BP	
Molecular weight	194.23 g mol ⁻¹	
log ₁₀ P ⁱ	3.46	
Charge	Anionic	
λ _{max}	254 nm	
Methyl 4-aminobenzoate		
Abbreviation	MAB	
Molecular weight	151.16 g mol ⁻¹	
log ₁₀ P ⁱ	1.41	
Charge	Cationic	
λ _{max}	287 nm	
Benzocaine		
Abbreviation	EAB	
Molecular weight	165.19	
log ₁₀ P ⁱ	1.95	
Charge	Cationic	
λ _{max}	287 nm	
Risocaine		
Abbreviation	PAB	
Molecular weight	179.22 g mol ⁻¹	
log ₁₀ P ⁱ	2.48	
Charge	Cationic	
λ _{max}	287 nm	
Butamben		
Abbreviation	BAB	
Molecular weight	193.24 g mol ⁻¹	
log ₁₀ P ⁱ	3.01	
Charge	Cationic	
λ _{max}	287 nm	

Aminopyrine		
Abbreviation	AMP	
Molecular weight	231.29 g mol ⁻¹	
log ₁₀ P ⁱ	0.76	
Charge	Cationic	
λ _{max}	264 nm	
Diclofenac		
Abbreviation	DF	
Molecular weight	296.15 g mol ⁻¹	
log ₁₀ P ⁱ	4.06	
Charge	Anionic/Cationic	
λ _{max}	275 nm	
Flurbiprofen		
Abbreviation	FP	
Molecular weight	244.26 g mol ⁻¹	
log ₁₀ P ⁱ	4.11	
Charge	Anionic	
λ _{max}	247 nm	
Ketoprofen		
Abbreviation	KTP	
Molecular weight	254.28 g mol ⁻¹	
log ₁₀ P ⁱ	2.81	
Charge	Anionic	
λ _{max}	261 nm	
Benzoic acid		
Abbreviation	BA	
Molecular weight	122.12 g mol ⁻¹	
log ₁₀ P ⁱ	1.89	
Charge	Anionic	
λ _{max}	228 nm	
Salicylic acid		
Abbreviation	SA	
Molecular weight	138.12 g mol ⁻¹	
log ₁₀ P ⁱ	2.06	
Charge	Anionic	
λ _{max}	234 nm	

Acetyl salicylic acid		
Abbreviation	ASA	
Molecular weight	180.16 g mol ⁻¹	
log ₁₀ P ⁱ	1.19	
Charge	Anionic	
λ _{max}	221 nm	
Benzotriazole		
Abbreviation	BTA	
Molecular weight	119.12 g mol ⁻¹	
log ₁₀ P ⁱ	1.34	
Charge	Cationic	
λ _{max}	260 nm	

ⁱ Chemspider, Royal Society of Chemistry.

ⁱⁱ Taken from Hatanka *et al.* and Uchida *et al.* (Hatanaka *et al.*, 2015; Uchida *et al.*, 2015)

2.2 Methods

2.2.1 Air Plasma Modification of Poly(dimethylsiloxane)

2.2.1.1 Membrane Preparation

Plasma treatment was performed using a Henniker Plasma HPT-100 Plasma Surface Treatment System. The system consisted of a cylindrical process chamber and an aluminium sample tray upon which the samples were placed centrally and equidistant from the plasma source. Plasma treatment was performed at a process pressure of 0.8 mBar, using air as the process gas, which was introduced at a flow rate of 8 SCCM. The plasma was ignited using a radiofrequency power supply set at an output of 100 W. For preliminary investigations, three treatment times were selected; these were 90, 120 and 150 seconds. Plasma treatment was performed on both sides of the membrane.

2.2.1.2 Water Contact Angle Analysis

The static water contact angle of unmodified PDMS and plasma modified PDMS following a 90 second plasma exposure time, was determined by the sessile drop method, using FTÅ1000 contact angle and surface measurement instrumentation. For all measurements, Barnstead™ ultrapure water was used, and a drop size of 2 µL. The experiment duration for each membrane type was 200 seconds, and measurements were taken at three surface locations per membrane.

2.2.1.3 Scanning Electron Microscopy (SEM)

SEM analysis was carried out using a JEOL 6060LV SEM. Samples were prepared for analysis by coating in a Quorum Technologies SC7620 Sputter coater equipped with an 80 % gold and 20 % palladium sputter target, for a total time of 30 seconds. SEM images were obtained in secondary electron mode, in triplicate, of unmodified PDMS membrane and plasma modified membrane, at a working distance of 15 mm and an acceleration voltage of 15 – 20 kV. The surface was examined for any obvious lesions or artefacts which may alter the permeability of the membrane.

2.2.1.4 Attenuated Total Reflectance – Fourier Transform Infrared Spectroscopy (ATR-FTIR)

ATR-FTIR analysis was carried out using a Nicolet 380 FTIR spectrometer in attenuated total reflectance mode, equipped with a diamond crystal internal reflection element, in the wavenumber

range 400 – 4000 cm^{-1} . Spectra were viewed in Omnic software version 9.2.106, and were collected as an average of 300 scans at 4 cm^{-1} resolution.

2.2.1.5 X-ray Photoelectron Spectroscopy (XPS)

X-ray photoelectron spectroscopic analysis of native and plasma treated PDMS was performed using a Kratos Axis Ultra DLD instrument with a monochromated aluminium source. Survey scans were performed between 1200 and 0 eV binding energy, at 160 eV pass energy and 0.5 eV intervals in order to determine surface composition. Two analysis points were selected per sample, with an analysis area of 700 μm by 300 μm . High-resolution spectra were obtained of O 1s, N 1s C 1s and Si 2p at the appropriate binding energy range at 20 eV pass energy and 0.05 eV intervals.

Quantification and curve fitting was performed using Casa XPS software, following the removal of the background using a Shirley function, and the use of calculated Schofield factors to account for the angle between the X-ray source and the sample, along with the variation of penetration depth with energy. The Levenburg-Marquadt algorithm was used to minimise the differences between the data points and the envelope i.e. a least squares fitting routine was used. Within the spectra for a given element, curves were constrained to have the same full width at half maximum. In the case of high-resolution spectra of the Si 2p orbital, two peaks corresponding to the Si 2p_{3/2} and Si 2p_{1/2} spin states were expected, with a peak area ratio of 0.5 and a separation of 0.63 eV. Thus, curve fits of spectra of the Si 2p envelope were constrained to pairs of symmetrical peaks with a fixed area ratio of 2:1.

2.2.1.6 Finite Dose Permeability Studies

Permeation experiments were carried out using custom made Franz cell apparatus. The cells had an orifice of 0.64 cm^2 and a receptor volume of 4 mL. Silatos™ silicone sheeting (dimensions 150 x 200 x 0.13 mm) was cut to appropriate size portions and sealed between the donor and receptor compartment using high vacuum silicone grease (Dow Corning®) and a clamp. Experiments were carried out in a water bath at 32 °C in accordance with OECD guideline 428. All donor and receptor solutions consisted of 0.05 M pH 7.4 phosphate buffer, prepared by dissolving 5.294 g of K_2HPO_4 and 2.666 g of KH_2PO_4 in 1 L of Barnstead™ ultrapure water. The pH was checked with a Jenway 3510 pH probe, and pH adjustment was performed with HCl where appropriate.

The donor solution was prepared by dissolving the permeant in buffer with a final concentration of $1000 \mu\text{g mL}^{-1}$, and the receptor solution consisted of 4 mL of pH 7.4 phosphate buffer in the absence of the permeant. 1.5 mL of donor solution was introduced to the donor compartments, which were subsequently occluded with Parafilm® to prevent evaporation. All solutions were sonicated and introduced to the Franz cell slowly using a syringe in order to minimise bubble formation. Prior to the introduction of donor solution, Franz cells were allowed to equilibrate for 30 minutes, and any bubbles removed by inversion of the cell. 0.6 mL of solution was removed from the receptor chamber at 45 minute intervals for a total of six hours, and replaced with fresh, pre-warmed receptor solution. Samples of receptor solution were analysed using a Cary 60 UV-Vis spectrophotometer, and the concentration of permeant in the receptor chamber was determined using the regression equation of a calibration graph constructed using standards covering the concentration range of all samples obtained in the permeation study ($R^2 \geq 0.99$). The cumulative mass of compound permeated after 6 hours was calculated, as in previous studies (Bhuiyan *et al.*, 2017). All experiments were performed in triplicate. Ibuprofen was selected as a model compound in order to make initial observations regarding the effect of plasma modification upon the permeation of drugs across PDMS membrane, along with the effect of altering the plasma treatment time. In order to observe the effect of varying physiochemical properties of the permeant, further studies were carried out utilising lidocaine, benzotriazole, caffeine and benzoic acid.

Statistical analysis was performed using IBM SPSS Version 22.0. Numerous studies have been performed to determine the frequency distribution of permeation data through silicone membranes, in order to establish appropriate statistical methods, and have found the data to fit a normal distribution (Frum *et al.*, 2007; Khan *et al.*, 2005). Thus, data was treated accordingly. The effect of treatment time on permeation was evaluated using one-way ANOVA ($\alpha = 0.05$), with Levene's test for equality of variance, and a post hoc Games-Howell test. Under circumstances whereby Levene's test revealed data heteroscedasticity, Welch's *F* was reported. An independent two tailed T-test and Levene's test for equality of variance was used to compare the cumulative mass of drug permeated through native and plasma treated PDMS ($\alpha = 0.05$) for each of the five compounds tested.

2.2.1.7 Infinite Dose Permeability Studies

Permeation experiments employing eighteen model pharmaceutical compounds were performed under infinite dose conditions to allow permeability coefficient (K_p) calculation, namely ibuprofen, lidocaine, benzoic acid, methyl paraben, ethyl paraben, propyl paraben, butyl paraben, methyl 4-aminobenzoate, benzocaine, risocaine, butamben, salicylic acid, acetyl salicylic acid, aminopyrine, caffeine, ketoprofen, flurbiprofen and diclofenac. Franz cells were used as described previously (Section 2.2.1.6), and experiments were performed in triplicate. Donor solution consisted of a saturated solution of drug in pH 7.4 phosphate buffered saline (0.15 M NaCl). Buffer was prepared by dissolving 7.385 g of dipotassium phosphate, 1.034 g of dihydrogen potassium phosphate and 8.766 g of sodium chloride in 1 L of Barnstead™ ultrapure water. pH adjustment was performed with HCl where appropriate.

The donor solution was prepared by the addition of excess quantities of drug to a 10 mL volumetric flask containing pH 7.4 phosphate buffered saline. The flasks were equipped with a Teflon stirrer bar and mounted on a magnetic stirrer plate in a water bath maintained at 32 °C for 24 hours, and subsequently filtered using a Minisart® cellulose acetate filter (pore size 0.45 µm). Receptor solution consisted of pH 7.4 phosphate buffered saline (0.15 M NaCl). All solutions were sonicated and introduced to the Franz cell slowly using a syringe in order to minimise bubble formation. Prior to the injection of donor solution, Franz cells were allowed to equilibrate for 30 minutes, and any bubbles removed by inversion of the cell. The donor chambers were filled with 1.5 mL of donor solution in the presence of excess drug to ensure maximum thermodynamic activity was maintained, and were occluded with Parafilm®. It was noted that the buffer failed to control pH, therefore all donor solution pH values were recorded in triplicate (Appendix 11). Samples were extracted from the receptor chamber at 30 minute intervals for a total of 6 hours and analysed using a Cary 60 UV-Vis spectrophotometer. The concentration of drug in the receptor chamber was determined as previously, using the regression equation of a calibration graph constructed using standards covering the concentration range of all samples obtained in the permeation study following appropriate dilution ($R^2 \geq 0.99$).

The mass of drug in the receptor chamber was corrected for the previous sample removal and the cumulative quantity of drug permeated per cm^2 was plotted versus time. The steady-state flux (J_{ss} , units $\mu\text{g cm}^{-2} \text{min}^{-1}$) was calculated from the gradient of the linear portion of the graph. The permeability coefficient (K_p , units cm min^{-1}) was obtained by normalisation of J_{ss} with the concentration of permeant in the donor chamber. The concentration of permeant in the donor solution was determined by extraction of an aliquot of donor solution prepared as described previously, followed by filtration using a Minisart® cellulose acetate filter (pore size $0.45 \mu\text{m}$), followed by appropriate dilution and subsequent quantification using a Cary 60 UV-Vis spectrophotometer, as described previously.

Statistical analysis was performed with IBM SPSS Version 22.0. An independent two tailed T-test and Levene's test for equality of variance was used to compare steady state flux (J_{ss}) through native and plasma treated PDMS ($\alpha = 0.05$), in line with findings from previous studies (Frum *et al.*, 2007; Khan *et al.*, 2005). This was further supported by a Shapiro-Wilk test for normality in both samples of J_{ss} data, and K_p data, obtained using plasma treated PDMS. In all cases $p > 0.05$ indicating no statistically significant deviations from normality. Correlation analysis was executed in line with that reported in similar studies (Lee *et al.*, 2010; Miki *et al.*, 2015; Uchida *et al.*, 2015). Bivariate correlation analysis with bootstrap confidence intervals was performed where appropriate in order to evaluate the effect of various physicochemical properties of the compounds tested on the reduction in K_p observed following plasma treatment. For all correlations reported as statistically significant, 95 % bias corrected accelerated (BCa) bootstrap confidence intervals, based on 1000 samples, for Pearson's correlation coefficient did not cross zero. Simple linear regression, with bootstrap confidence intervals, was performed in order to establish the relationship between the K_p^{native} , K_p^{plasma} and K_p^{human} . Similarly, in order to correlate the extent of permeation through human skin with various physicochemical properties, assumption-free Spearman's rho was computed.

2.2.2 N₂ Plasma Modification of Poly(dimethylsiloxane)

2.2.2.1 Membrane Preparation

Plasma treatment was carried out using a Henniker Plasma HPT-100 Plasma Surface Treatment System, as described previously (Section 2.2.1.1), operating at 100 W with N₂ as the process gas

(99.998 %, O₂ free). The process gas was introduced to the plasma process chamber at a flow rate of 8 SCCM, and the chamber was maintained at a pressure of 0.6 mBar. For preliminary investigations, four treatment times were selected i.e. 90, 150, 210 and 300 seconds.

2.2.2.2 Membrane Characterisation

SEM, ATR-FTIR and XPS analyses were conducted as described in Sections 2.2.1.3, 2.2.1.4, and 2.2.1.5, respectively.

2.2.2.3 Permeation Studies

Initial comparison with air plasma treatment, and preliminary studies determining treatment time effects were carried out as described in Section 2.2.1.7. In order to enable K_p calculation, the static, Franz type diffusion cell was substituted for a PermeGear flow-through type system (Figure 2.1) to enable the maintenance of sink conditions when using aqueous solutions of lipophilic compounds, and surpass the employment of solubility enhancers, which may interact with the membrane and obscure data interpretation. The system consisted of flow through type cells mounted on a heater block, the temperature of which was regulated by a water circulator unit mounted inside a water bath. Phosphate buffered saline (pH 7.4, 0.15 M NaCl) was pumped through the receptor chambers from a reservoir maintained at 32 °C by use of a hotplate stirrer and thermocouple. The cells had a diffusional area of 0.54 cm², and a flow rate of 12 ml hour⁻¹ was found to be adequate for all penetrants, in line with previous studies (Addicks *et al.*, 1987), with the exception of caffeine. In the case of caffeine, a flow rate of 4 mL hour⁻¹ was used to account for the lower flux and maintain sample concentrations above the limit of quantification of the analytical method. The concentration of analyte in the receptor medium was maintained at ≤ 10 % that of the donor solution. Donor solution consisted of a saturated solution of permeant in pH 7.4 PBS (0.15 M NaCl) with excess permeant present, prepared as described previously. The temperature under the membrane was measured using a thermocouple, and it was found that a circulating water temperature of 35.1 °C maintained a cell temperature of 32 °C.

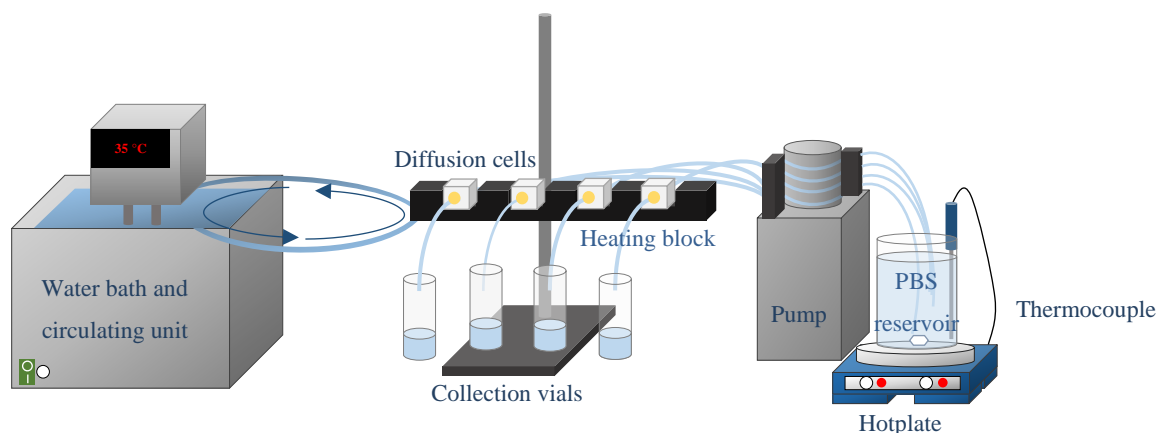


Figure 2.1 Schematic of the flow-through type system setup.

Quantitative analysis of the receptor solution was performed using RP-HPLC with a Shimadzu Prominence HPLC. The system consisted of a degasser (Shimadzu DGU-20A), pump (Shimadzu LC-20AT), an auto sampler (Shimadzu SIL-20A HT), a column oven (CTO-10AS VP Shimadzu), and a diode array detector (SPD-M20A Shimadzu). Data analysis was performed with LCSolutions software.

For analysis of all solutions containing parabens, aminobenzoate compounds and caffeine, mobile phase A consisted of 0.1 % H_3PO_4 in ultrapure water, and mobile phase B consisted of acetonitrile. For paraben compounds and caffeine, chromatography was performed using a LiChrosphere C18 column (4 x 250 mm, 5 μm). The ratios of mobile phase B:A were as follows: methyl paraben 35:65, ethyl paraben 35:65, propyl paraben 50:50, butyl paraben 50:50 and caffeine 20:80. A flow rate of 1.0 mL min^{-1} and an injection volume of 20 μL was used for all compounds. The oven was maintained at 40 $^\circ\text{C}$ for all analysis.

For analysis of all solutions containing aminobenzoate compounds, lidocaine and benzoic acid, chromatography was performed using a Waters X-Bridge C18 column (2.1 x 150 mm, 3.5 μm). For aminobenzoate compounds, the ratios of mobile phase B:A were as follows: methyl 4-aminobenzoate 30:70, ethyl 4-aminobenzoate 30:70, propyl 4-aminobenzoate 45:55 and butyl 4-aminobenzoate 45:55. For lidocaine analysis, mobile phase A consisted of 0.1 % H_3PO_4 containing 5 mM sodium 1-heptane sulfonate and mobile phase B consisted of acetonitrile. The ratio of mobile phase B:A was 30:70. For benzoic acid analysis, mobile phase A consisted of 45 mM KH_2PO_4 and 130 mM H_3PO_4 and mobile

phase B consisted of acetonitrile. The ratio of mobile phase B:A was 25:75. A flow rate of 0.3 mL min⁻¹ and an injection volume of 20 µL was used for all compounds. The oven was maintained at 40 °C for all analysis. All aqueous mobile phases were filtered prior to use.

The concentration of analyte in the receptor solution was determined from the regression equation of a plot of peak area versus concentration of a minimum seven standard solutions covering a minimum of 80 to 120 % of the analyte concentration. Linearity was determined by coefficients of determination ($R^2 \geq 0.999$), and intermediate and intra assay precision were determined for all methods using three determinations at three concentration levels. Limits of detection (LOD) and limits of quantification (LOQ) were determined using the standard deviation of the y-intercept of a regression line as recommended by the ICH Guidelines for Validation of Analytical Procedures (Appendix 13). The concentration of analyte in the donor solution was determined similarly, following filtration with a Minisart® cellulose acetate filter (pore size 0.45 µm) and appropriate dilution.

Statistical analysis was performed with IBM SPSS Version 22.0. Levene's test for the homogeneity of variance and one-way analysis of variance (One-way ANOVA) with a post hoc Bonferroni test were used to compare data obtained from studies evaluating the effect of N₂ plasma treatment time on the permeation of lidocaine and caffeine. Under circumstances whereby Levene's test revealed data heteroscedasticity, Welch's *F* was reported, and post hoc comparisons were performed using a Games-Howell test.

2.2.3 Lysine Functionalisation of Poly(dimethylsiloxane)

2.2.3.1 Lysine attachment to N₂ plasma treated PDMS using *N,N'*-Dicyclohexylcarbodiimide (DCC)

PDMS sheeting was cut to an appropriately sized square (4 cm x 4 cm) and was subject to N₂ plasma treatment for 90 seconds, on one side of the membrane, using a Henniker Plasma HPT-100 Plasma Surface Treatment System operating at 100 W with N₂ as the process gas, at a flow rate of 8 SCCM.

N₂ plasma treated PDMS was suspended in dichloromethane (DCM) (50 mL) for 2 minutes followed by submersion in a solution of Boc-Lys(Z)-OH in DCM (50 mL, 14.34 mM). *N,N'*-

dicyclohexylcarbodiimide (147.9 mg, 0.72 mmol) was then added, and the coupling reaction was allowed to proceed for two hours, followed by the removal of the disks from the solution and submersion in DCM (50 mL). The PDMS sheeting was suspended in 1,4-dioxane (50 mL) for 2 minutes, removed and suspended in 4 N HCl-dioxane for 30 minutes to achieve tert-butyloxycarbonyl (Boc) group removal. Again, the sheeting was suspended in 1,4-dioxane (50 mL) for cleaning purposes, before submersion in HBr in acetic acid (33 %) for removal of the carboxybenzyl (Z) protecting group. It was noted that the PDMS substrate disintegrated upon submersion in both 4 N HCl-dioxane and HBr in acetic acid therefore both the Boc and Z protecting groups were not removed. Samples were subject to ATR-FTIR, and XPS analysis as described in Sections 2.2.1.4 and 2.2.1.5, respectively. Further, the reaction was repeated, substituting DCM for EtOH.

A small permeation study was performed, endeavouring to observe the effect of the exposure of plasma treated PDMS to the permeation of a pharmaceutical compound, namely lidocaine. The study was performed according to the protocol outlined in Section 2.2.1.6, employing a donor solution of lidocaine in pH 7.4 phosphate buffered saline (0.15 M NaCl) at a concentration of 3000 $\mu\text{g mL}^{-1}$. PDMS was plasma treated according to Section 2.2.2.1, and immediately stored in 50 mL of dichloromethane, ethyl acetate, ethanol, or ultrapure water, for a duration of two hours. The membranes were blotted dry, and subsequently dried under vacuum at 70 °C for 15 minutes prior to mounting in the Franz cell.

2.2.3.2 Lysine attachment to alkoxy silane functionalised PDMS using *N,N'*-dicyclohexylcarbodiimide (PDMS-APTMS-Lys)

PDMS sheeting was cut to an appropriately sized square (4 cm x 4 cm) and was subject to plasma treatment for 90 seconds, on one side of the membrane, using a Henniker Plasma HPT-100 Plasma Surface Treatment System operating at 100 W with air as the process gas, at a flow rate of 8 SCCM. Alkoxy silane layer formation was performed as reported in other work (Pakstis *et al.*, 2010). Immediately after treatment, the PDMS sheeting was suspended in a solution of (3-aminopropyl)trimethoxysilane (APTMS) in absolute ethanol (1 % v/v, 50 mL) followed by the addition of 5 % v/v water. Samples were then incubated at 70 °C for 10 minutes, and then washed with

ethanol in deionised water (70 % v/v, 10 mL), and a further three times with deionised water (3 x 10 mL).

APTMS functionalised PDMS disks were suspended in DCM (50 mL) for 2 minutes followed by submersion in a solution of Boc-Lys(Z)-OH in DCM (50 mL, 14.34 mM). *N,N'*-dicyclohexylcarbodiimide (147.9 mg, 0.72 mmol) was then added, and the coupling reaction was allowed to proceed for 2 hours, followed by the removal of the disks from the solution and submersion in DCM (50 mL). Samples were subject to SEM, ATR-FTIR, and XPS analysis as described in Sections 2.2.1.3, 2.2.1.4 and 2.2.1.5, respectively.

2.2.3.3 Lysine attachment to PDMS using glutaraldehyde linker (PDMS-APTES-GA-Lys)

PDMS sheeting was cut to an appropriately sized square (4 cm x 4 cm) and was subject to plasma treatment for 90 seconds, on one side of the membrane, using a Henniker Plasma HPT-100 Plasma Surface Treatment System operating at 100 W with air as the process gas, at a flow rate of 8 SCCM. PDMS functionalisation with glutaraldehyde was performed according to reported methods (Farrell *et al.*, 2010; Kuddannaya *et al.*, 2013; Wipff *et al.*, 2009). The plasma pre-treated PDMS sheeting was submerged in a solution of (3-aminopropyl)triethoxysilane (APTES) (5 % v/v, 1.25 mL) in aqueous EtOH (94.7 % v/v, 23.75 mL). The solutions were maintained at 30 °C and gently agitated using a shaking water bath for one hour. The PDMS was then removed and washed with aqueous ethanol (94.7 % v/v, 10 mL) and cured at 60 °C for one hour. The PDMS was washed with pH 7.4 phosphate buffered saline (10 mL) and subsequently submerged in a solution of glutaraldehyde in pH 7.4 phosphate buffered saline (3 % v/v, 12.5 mL), and left for one hour at room temperature. Upon removal, the PDMS sheeting was washed with pH 7.4 phosphate buffered saline (10 mL). The PDMS sheeting was then submerged in a solution of N_{α} -Boc-L-lysine (0.397 M, 10 mL) over night at room temperature. Samples were subject to SEM, ATR-FTIR, and XPS analysis as described in Sections 2.2.1.3, 2.2.1.4 and 2.2.1.5, respectively.

2.2.3.4 Lysine-functionalised PDMS Permeation Studies

The permeability of PDMS-APTMS-Lys (Section 2.2.3.2) and PDMS-APTES-GA-Lys (Section 2.2.3.3) was investigated using the flow through type system, as described in Section 2.2.2.3. Four

model pharmaceutical compounds were employed namely butyl paraben, methyl 4-aminobenzoate, lidocaine, and benzoic acid, to encompass a range of physicochemical parameters.

References

- Addicks, Flynn, & Weiner. (1987). Validation of a Flow-Through Diffusion Cell for Use in Transdermal Research. *Pharmaceutical Research*, 4(4), 337-341.
- Bhuiyan, & Waters. (2017). Permeation of pharmaceutical compounds through silicone membrane in the presence of surfactants. *Colloids and Surfaces A: Physicochemical and Engineering Aspects*, 516, 121-128.
- Farrell, & Beaudoin. (2010). Surface forces and protein adsorption on dextran- and polyethylene glycol-modified polydimethylsiloxane. *Colloids and Surfaces B: Biointerfaces*, 81(2), 468-475.
- Frum, Eccleston, & Meidan. (2007). Evidence that drug flux across synthetic membranes is described by normally distributed permeability coefficients. *European Journal of Pharmaceutics and Biopharmaceutics*, 67(2), 434-439.
- Hatanaka, Yoshida, Kadhum, Todo, & Sugibayashi. (2015). In Silico Estimation of Skin Concentration Following the Dermal Exposure to Chemicals. *Pharmaceutical Research*, 32(12), 3965-3974.
- Khan, Frum, Sarheed, Eccleston, & Meidan. (2005). Assessment of drug permeability distributions in two different model skins. *International Journal of Pharmaceutics*, 303(1-2), 81-87.
- Kuddannaya, Chuah, Lee, Menon, Kang, & Zhang. (2013). Surface chemical modification of poly(dimethylsiloxane) for the enhanced adhesion and proliferation of mesenchymal stem cells. *ACS Applied Materials & Interfaces*, 5(19), 9777-9784.
- Lee, Conradi, & Shanmugasundaram. (2010). Development of an in silico model for human skin permeation based on a Franz cell skin permeability assay. *Bioorganic and Medicinal Chemistry Letters*, 20(1), 69-73.
- Miki, Ichitsuka, Yamada, Kimura, Egawa, Seki, Juni, Ueda, & Morimoto. (2015). Development of a membrane impregnated with a poly(dimethylsiloxane)/poly(ethylene glycol) copolymer for a high-throughput screening of the permeability of drugs, cosmetics, and other chemicals across the human skin. *European Journal of Pharmaceutical Sciences*, 66, 41-49.
- Pakstis, Dunkers, Zheng, Vorbürger, Quinn, & Cicerone. (2010). Evaluation of polydimethylsiloxane modification methods for cell response. *Journal of Biomedical Materials Research - Part A*, 92(2), 604-614.
- Uchida, Kadhum, Kanai, Todo, Oshizaka, & Sugibayashi. (2015). Prediction of skin permeation by chemical compounds using the artificial membrane, Strat-M™. *European Journal of Pharmaceutical Sciences*, 67, 113-118.
- Wipff, Majd, Acharya, Buscemi, Meister, & Hinz. (2009). The covalent attachment of adhesion molecules to silicone membranes for cell stretching applications. *Biomaterials*, 30(9), 1781-1789.

Chapter 3 The Effect of Air Plasma Treatment on the Permeation of Pharmaceutical Compounds through Poly(dimethylsiloxane)

3.1. Introduction

The oxidation of poly(dimethylsiloxane), typically performed using O₂ plasma treatment, is widely reported in literature for a plethora of applications, ranging from microfluidic device formation, to the formation of suitable substrates for cell culture applications (Gunda *et al.*, 2014; Kuddannaya *et al.*, 2013). The use of air as a process gas in plasma treatments aiming to generate surface silanol groups, and subsequent enhanced wettability and chemical reactivity, provides an alternative to O₂ based treatments, and offers financial advantages, along with more basic experimental setups. As such, it has received considerable attention. For instance, air plasma oxidation of PDMS has been used as a prerequisite to forming poly(vinyl alcohol) coatings, which have been shown to display enhanced stability of surface hydrophilicity (Li *et al.*, 2012), and have found use in the construction of microfluidic devices (Sharma *et al.*, 2007). Additionally, air plasma treatments have found use in tissue engineering, enabling heightened cell migration, which may assist complex tissue formation (Leclerc *et al.*, 2009), along with biomolecule immobilisation (Hu *et al.*, 2014), and more recently, in the support of lipid bilayers (Faysal *et al.*, 2017).

To date, the superior interactions between air plasma modified PDMS and biomolecules have not been capitalised for use in the production of artificial skin mimics for *in vitro* permeation studies. More simply, the enhanced properties of oxidised PDMS alone have not been considered with regards to such studies. For example, hydrogen bonding between penetrants and the polar head groups of fatty acids and ceramides in the intercellular lipid lamellae has long been known to be a determinant in the extent of percutaneous adsorption (Du Plessis *et al.*, 2002b). Work by Du Plessis *et al.* simulated hydrogen bonding effects in silicone membranes by membrane impregnation with solvents to maximise, and minimise, hydrogen bonding. Reductions in the diffusion coefficient of phenolic compounds were observed with increases in the number of hydrogen bonding groups in the penetrant, when the membrane was saturated with octanol. The authors noted that decreases in the diffusion

coefficient were likely to be as a result of membrane-penetrant hydrogen bonding, and were comparable to those observed in studies employing biological tissue. No such effect was observed when the membrane was impregnated with toluene and hydrogen bonding was minimised (Du Plessis *et al.*, 2001). The work emphasises the role of hydrogen bonding in the permeation of xenobiotics through biological tissue, and how polymeric skin mimics can be chemically adapted to enhance their performance in biomimetic systems. Nonetheless, since its publication, limited attempts have been made to incorporate such groups into the structure of PDMS more permanently, in order to enhance *in vitro-in vivo* correlation in skin permeability studies. Moreover, to date, only one body of work has been published aiming to imitate the crystalline nature of the stratum corneum intercellular lipids, by inclusion of more rigid, glassy domains within a polymeric skin mimic (Feldstein *et al.*, 1998). The use of plasma treatments is known to result in the formation of crystalline layers of SiO_x species (Bartalena *et al.*, 2012), thus, plasma treatments may be a promising tool in the development of appropriate skin mimics.

This chapter investigates the hypothesis that the air plasma treatment of PDMS membrane produces a barrier to permeation which is more similar to that of the intercellular lipid lamellae on the basis of its heteropolarity, crystallinity, and tortuosity (Figure 3.1).

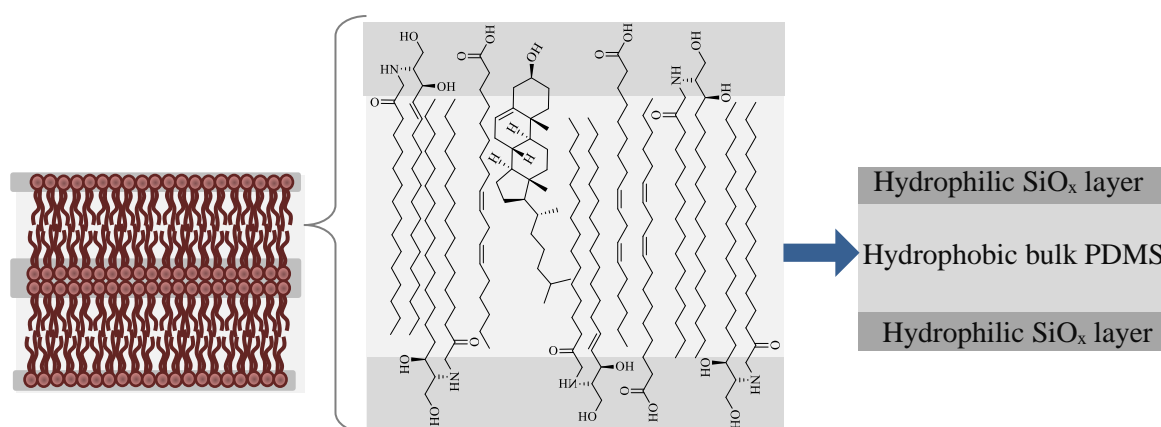


Figure 3.1 Intercellular lipid lamellae, taken from Benson *et al.* (Benson *et al.*, 2011), modelled using plasma treated PDMS.

In this chapter, the effect of the air plasma treatment of PDMS on the permeation of pharmaceutical compounds was evaluated using various compounds representing a wide range of therapeutic classes.

The Effect of Air Plasma Treatment on the Permeation of Pharmaceutical Compounds through
Poly(dimethylsiloxane)

The correlation between differences in permeation through native and plasma treated PDMS, and physicochemical properties of the permeant were investigated. Further, the permeability coefficients of eighteen compounds through both native and plasma treated PDMS were obtained from steady-state diffusion profiles, obtained under infinite dose conditions, and compared with a database of K_p values extracted from literature, whereby data had been collected under similar experimental conditions.

3.2. Results and Discussion

3.2.1. Membrane Characterisation

3.2.1.1. Water Contact Angle Analysis

The static water contact angle of PDMS pre and post modification was obtained in order to evaluate changes in surface hydrophilicity (Table 3.1). Native PDMS was found to display a static water contact angle of $112.26^\circ \pm 0.88$ (mean \pm standard deviation), characteristic of a hydrophobic substrate, and in line with reported data (Da Silva *et al.*, 2017; Maheshwari *et al.*, 2010; Mata *et al.*, 2005). The water contact angle of PDMS following a 90 second plasma treatment was found to be $60.74^\circ \pm 5.09$, indicative of a surface energy increase, in line with reported data (Mata *et al.*, 2005). The data confirms the formation of an overlying hydrophilic layer, and an underlying hydrophobic bulk substrate, or a ‘lamellar’ type structure of lipophilic native polymer and hydrophilic, oxidised polymer.

Table 3.1 Water contact angle analysis of native PDMS and PDMS following air plasma treatment.

Membrane	Mean water contact angle ($^\circ$)	Standard deviation
Native PDMS	112.26	0.88
Plasma treated PDMS	60.74	5.09

3.2.1.2. Attenuated Total Reflectance – Fourier Transform Infrared Spectroscopy (ATR-FTIR)

ATR-FTIR analysis was performed in order to confirm the surface chemical composition pre and post air plasma treatment (Table 3.2). The presence of surface methyl groups is confirmed by a symmetrical stretching vibration of the CH₃ group at 2962 cm^{-1} , and the asymmetric and symmetric deformation of the CH₃ group at 1413 and 1258 cm^{-1} , respectively, in the spectra of both native and air plasma treated PDMS. The Si-O-Si stretching vibration is observed in spectra of both membranes at 1006 cm^{-1} , along with absorptions at 786 and 701 cm^{-1} , confirming the presence of the O-SiCH₃ and C-SiCH₃ groups, respectively. The absence of the absorbance at 3300 cm^{-1} , indicative of the presence of hydroxyl groups, should be noted, and may be explained by the sampling depth of the spectroscopic technique. The penetration depth of the evanescent wave ranges from 700 nm to greater than 1 μm , orders of

magnitude greater than alternative techniques such as energy dispersive X-ray spectroscopy (EDX), X-ray photoelectron spectroscopy (XPS), secondary ion mass spectroscopy (SIMS) and ion scattering spectroscopy (ISS) (Vladkova, 2013), rendering the spectrum representative of the surface chemical composition of both the surface and underlying bulk substrate. For this reason, ATR-FTIR data is presented in this thesis supported by analysis from alternative surface characterisation methods.

Table 3.2 ATR-FTIR of native PDMS and PDMS following air plasma treatment.

Assignment	ν_{\max} (cm ⁻¹)	
	Native PDMS	Plasma treated PDMS
$\nu_s(\text{CH}_3)$	2962.3	2962.3
$\delta_{\text{as}}(\text{CH}_3)$	1412.6	1413.4
$\delta_s(\text{CH}_3)$	1258.2	1258.2
Si-O-Si	1006.3	1006.4
O-SiCH ₃	786.2	785.8
C-SiCH ₃	701.4	701.1

3.2.1.3. X-ray Photoelectron Spectroscopy (XPS)

Quantitative elemental composition of the PDMS surface pre- and post-modification was determined using XPS survey scans (Figure 3.2 and Figure 3.3), with data subsequently presented in the form of atomic percent (%) (Table 3.3). The O 1s, C 1s and Si 2p orbitals were identified at binding energies circa 530 eV, 282 eV and 100 eV, respectively, in both native PDMS and PDMS following 90 seconds plasma treatment, with an additional emission at a binding energy of 399 eV associated with the N 1s orbital in plasma treated PDMS. A carbon: oxygen: silicon atomic ratio of 2.1: 1.0: 1.2 was obtained for native PDMS, consistent with the theoretical ratio of 2: 1: 1, based on the chemical composition of the monomer unit. An increase in the atomic percent of oxygen post plasma treatment yields a C: O: Si atomic ratio of 1.0: 1.9: 1.4, and is consistent with the oxidative nature of air plasma treatments, and suggests up to 50 % conversion of surface methyl groups to silanol and carbonyl containing groups. The presence of ~ 0.6 % of nitrogen at the surface post plasma treatment, in comparison to < 0.1 %

pre-treatment, is unsurprising taking into account the chemical composition of air, i.e. 78 % nitrogen (Pandit *et al.*, 2010), and the reported use of nitrogen plasma treatments to obtain amine and imine functionalities (Hirata *et al.*, 2008; Vesel *et al.*, 2008; Wu *et al.*, 2011; Yang *et al.*, 2016).

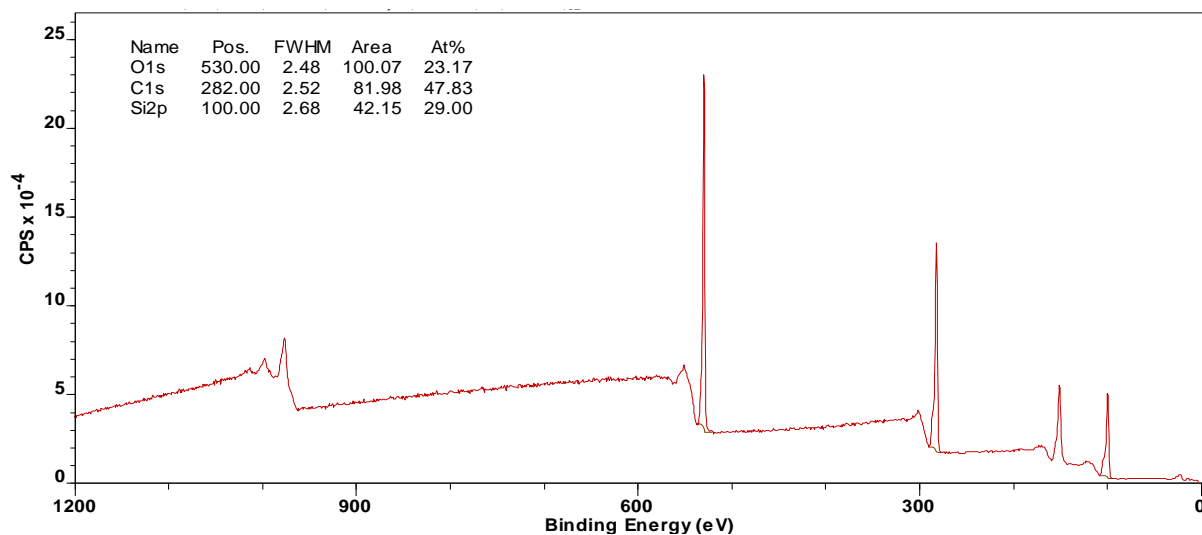


Figure 3.2 XPS survey scan of native PDMS.

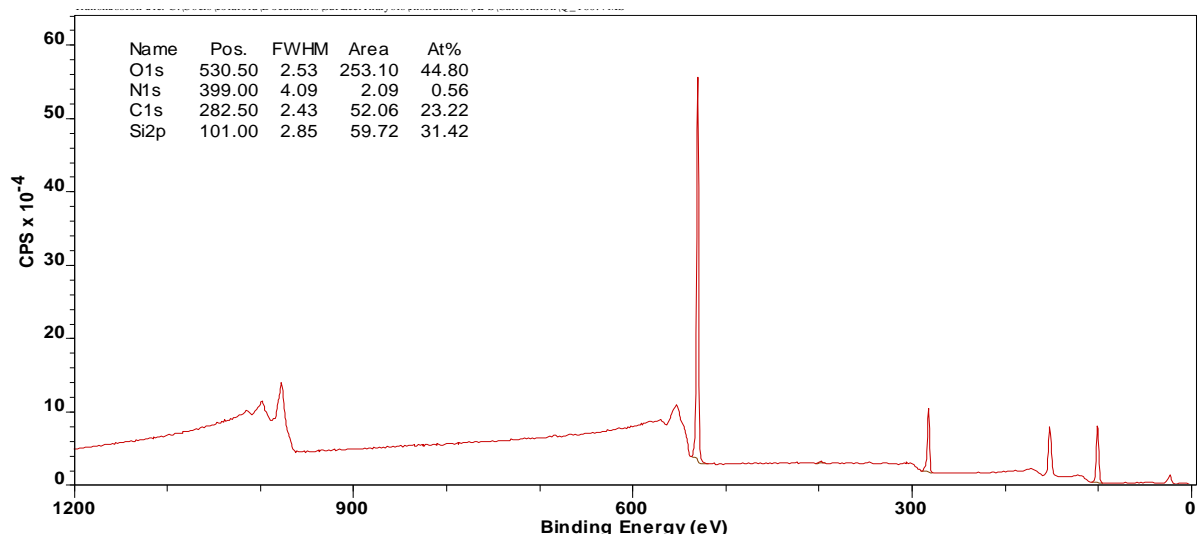


Figure 3.3 XPS survey scan of PDMS following a 90 second air plasma treatment.

Table 3.3 Atomic (%) of oxygen, nitrogen, carbon and silicon taken from XPS survey scans of native PDMS and PDMS following air plasma treatment.

Membrane	Sample	Atomic percent (%)			
		O	N	C	Si
Native PDMS	1	23.17	< 0.10	47.83	29.00
	2	22.79	< 0.10	48.92	28.28
Plasma treated PDMS	1	44.80	0.56	23.22	31.42
	2	44.11	0.61	24.49	30.79

High resolution spectra of the Si 2p, C 1s and N 1s peak were obtained prior to and following air plasma treatment (Figure 3.4 - Figure 3.9). The Si 2p peak can be deconvoluted by curve fitting into siloxane units containing one (mono), two (di), three (tri) or four (quaternary) oxygen atoms, and are given the notation M, D, T and Q respectively. An increase in binding energy of ~ 0.65 eV is expected for the substitution of a methyl group with an oxygen atom in a siloxy unit, however, curve fitting the Si 2p level is made more complex by the existence of two electron spin states (Si 2p_{3/2} and Si 2p_{1/2}), resulting in the occurrence of two symmetrical peaks per chemical state with a peak area ratio of 0.5 (Owen *et al.*, 2012). The peak at binding energy 102.32 eV and 102.41 in native and plasma treated PDMS, respectively, can be assigned to di siloxy units, supported by the 2.1: 1.0: 1.2 atomic ratio obtained in the survey scan. A decrease in the percent area of this peak, from 60.56 % in native PDMS, to 20.60 % following plasma treatment, can be attributed to a depletion in concentration of this siloxy unit in the top 10 nm of the substrate. This is further supported by an increase in the percent area of the emission at a binding energy ca.103.7 eV, which can be assigned to Q siloxy units, from 6.11 % in native PDMS to 46.08 % in plasma treated PDMS. The presence of a small percentage (6.11 %) of Q siloxane units in native PDMS is unsurprising since other work in the Waters research group has confirmed the basic nature of the native surface (Waters *et al.*, 2016).

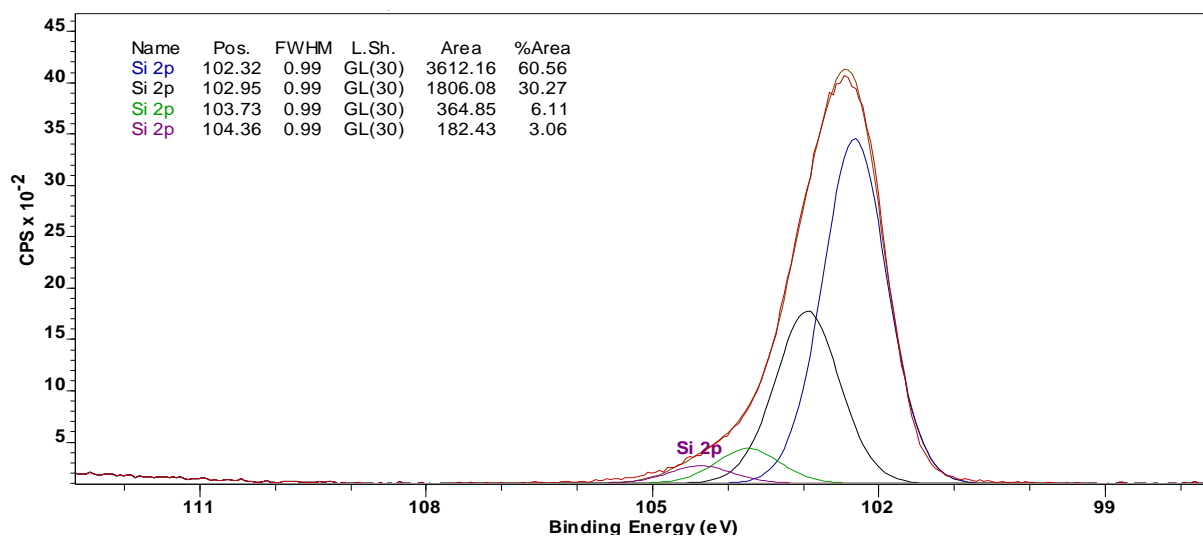


Figure 3.4. High resolution XPS spectrum of the Si 2p orbital in native PDMS.

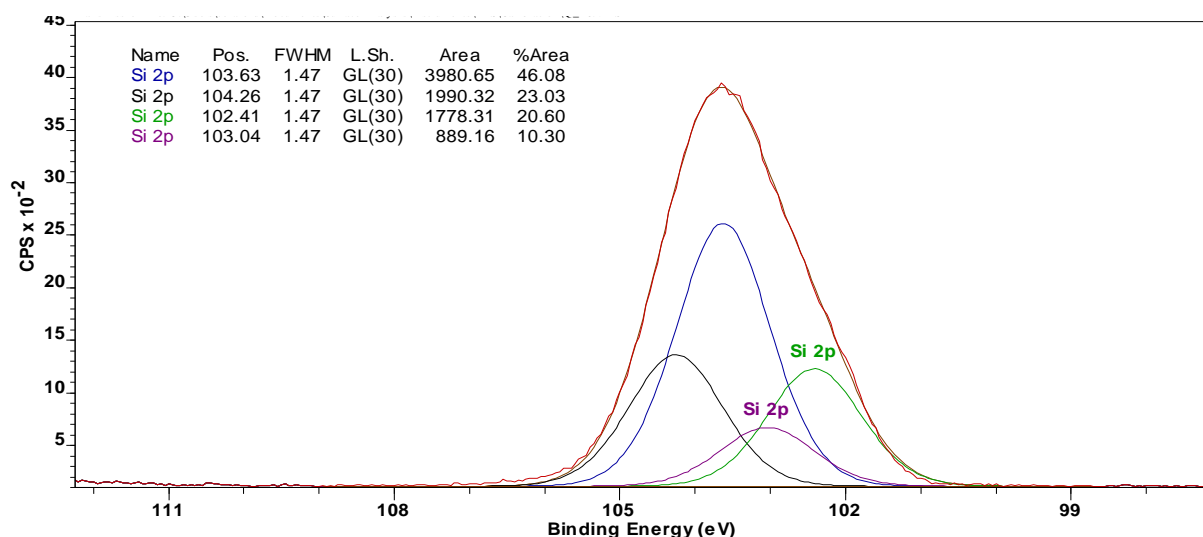


Figure 3.5. High resolution XPS spectrum of the Si 2p orbital in plasma treated PDMS.

Existing literature reports the deconvolution of C 1s spectra into alkyl carbon, amine, imine and nitrile, alcohol and ether, and carboxylic acid and ester groups (Wolf, 2012; Wu *et al.*, 2011). Expectedly, the high resolution XPS spectrum of the C 1s peak in native PDMS (Figure 3.6) contains one peak at 285 eV, corresponding to that of C-H groups. The XPS spectrum of the C 1s peak in plasma modified PDMS (Figure 3.7) contains two further peaks at 286.7 eV and 288.5 eV, with the former matching most closely those reported for alcohol, amine, and nitrile groups, and the latter matching most closely those reported for amide and carbonyl groups (Williams *et al.*, 2004; Wu *et al.*, 2011; Yang *et al.*, 2016).

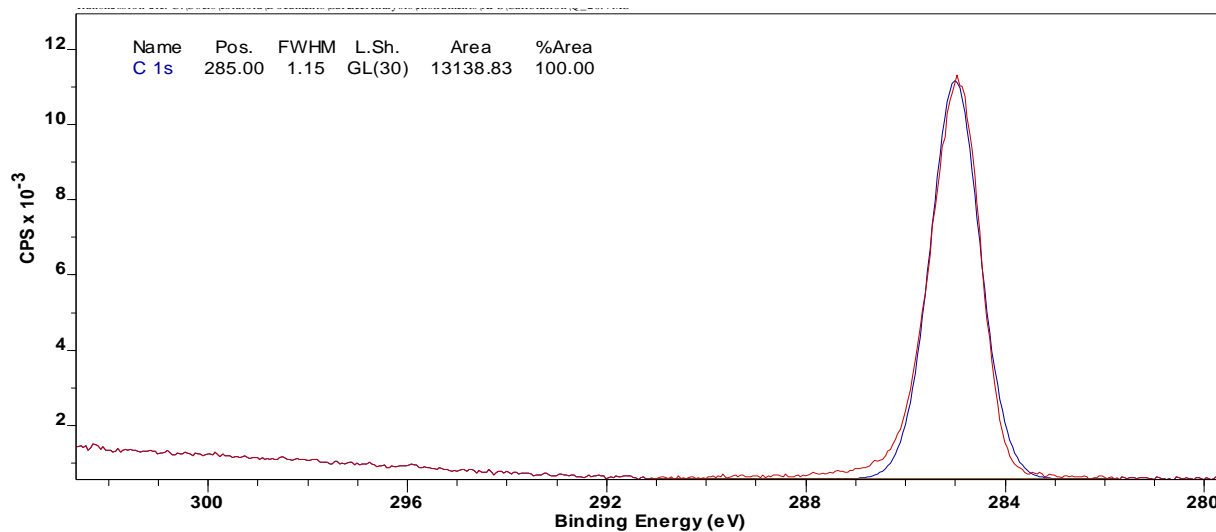


Figure 3.6. High resolution XPS spectrum of the C 1s orbital in native PDMS.

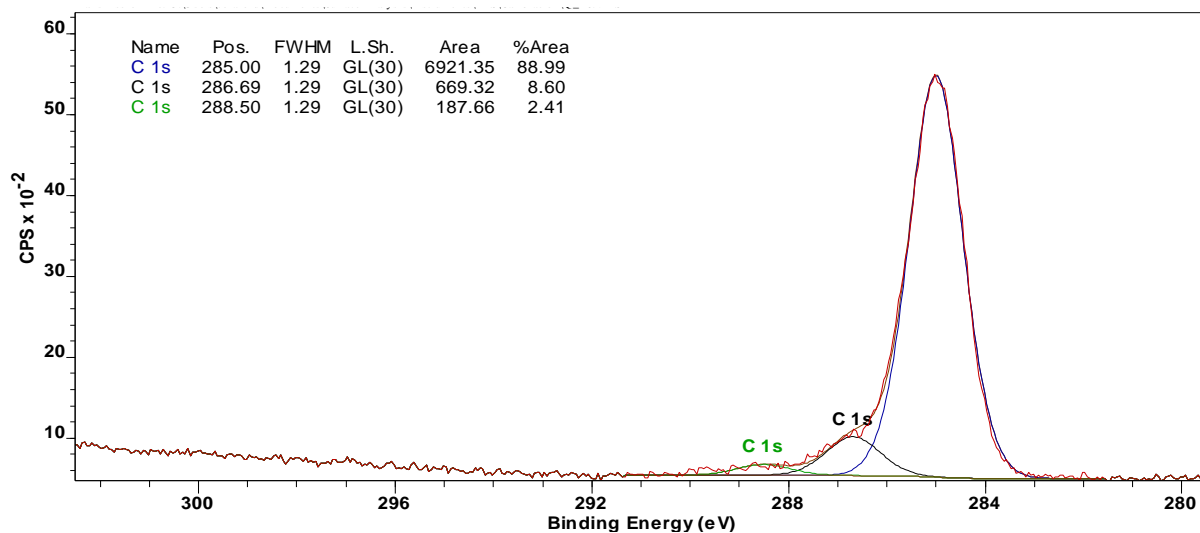


Figure 3.7. High resolution XPS spectrum of the C 1s orbital in plasma treated PDMS.

Given that carbon atoms represent ~ 24 % of the surface of PDMS post plasma treatment, 8.60 % of which are present as either alcohol, amine, or nitrile groups (> 2% of atoms overall), the peak at 286.7 eV cannot be accounted for entirely by amine or nitrile species, since this would necessitate a stoichiometric atomic percent of nitrogen, i.e. > 2 %. The lack of a peak in the high resolution XPS spectrum of the N 1s orbital in native PDMS is expected (Figure 3.8), and the presence of only one peak in the high resolution spectrum of the N 1s orbital at 400.79 eV (Figure 3.9) suggests that all nitrogen atoms are present in one chemical state i.e. amide groups. This is further supported by the peak at 288.50 eV in the high resolution spectrum of the C 1s orbital in plasma treated PDMS

representing 0.59 – 0.71 % of overall surface atoms (2.41 % and 3.07 % of carbon atoms in samples 1 and 2 respectively), and the presence of a stoichiometric percent of nitrogen (0.56 - 0.61 %). Only ~ 11 % of carbon atoms, comprising only 24 atomic % of the surface, i.e. 2.6 % overall, are in the oxidised state, suggesting that the majority of oxygen containing groups at the surface are present as silanol groups, more specifically, Q siloxane units.

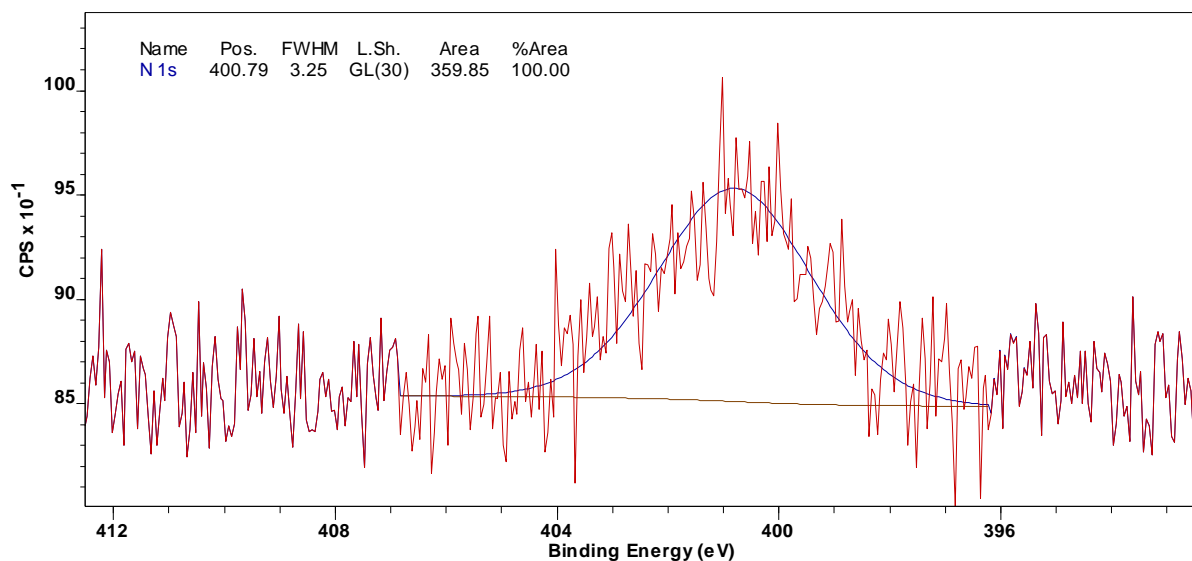


Figure 3.8. High resolution XPS spectrum of the N 1s orbital in native PDMS.

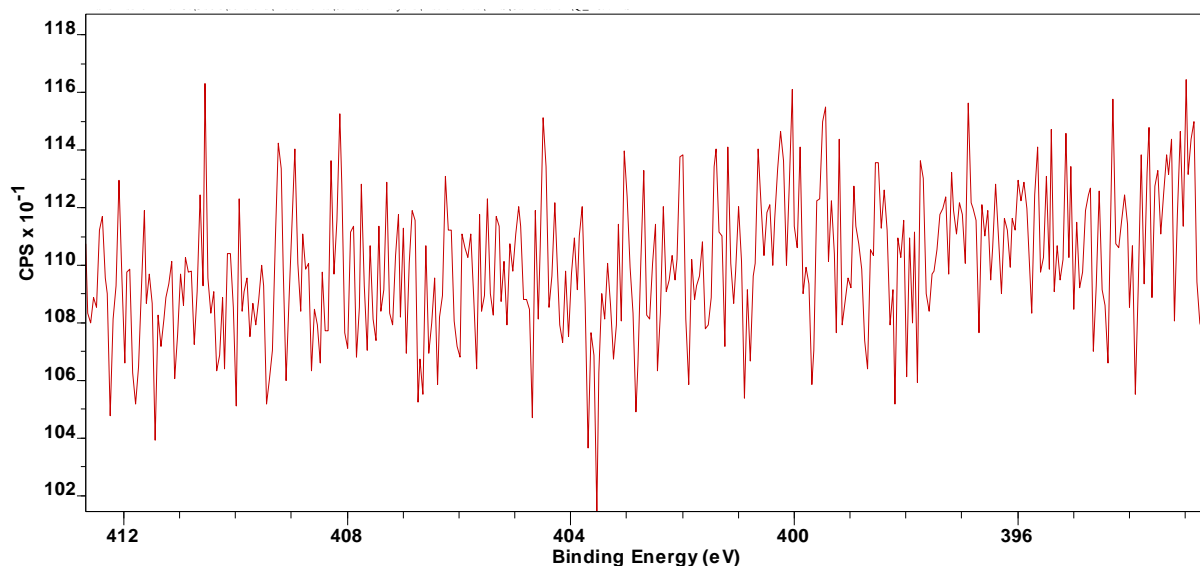


Figure 3.9. High resolution XPS spectrum of the N 1s orbital in plasma treated PDMS.

3.2.1.4. Scanning Electron Microscopy

Changes in surface morphology of PDMS upon plasma treatment, which may subsequently affect polymer permeability, were monitored using scanning electron microscopy, the general findings of which are presented in Figure 3.10.

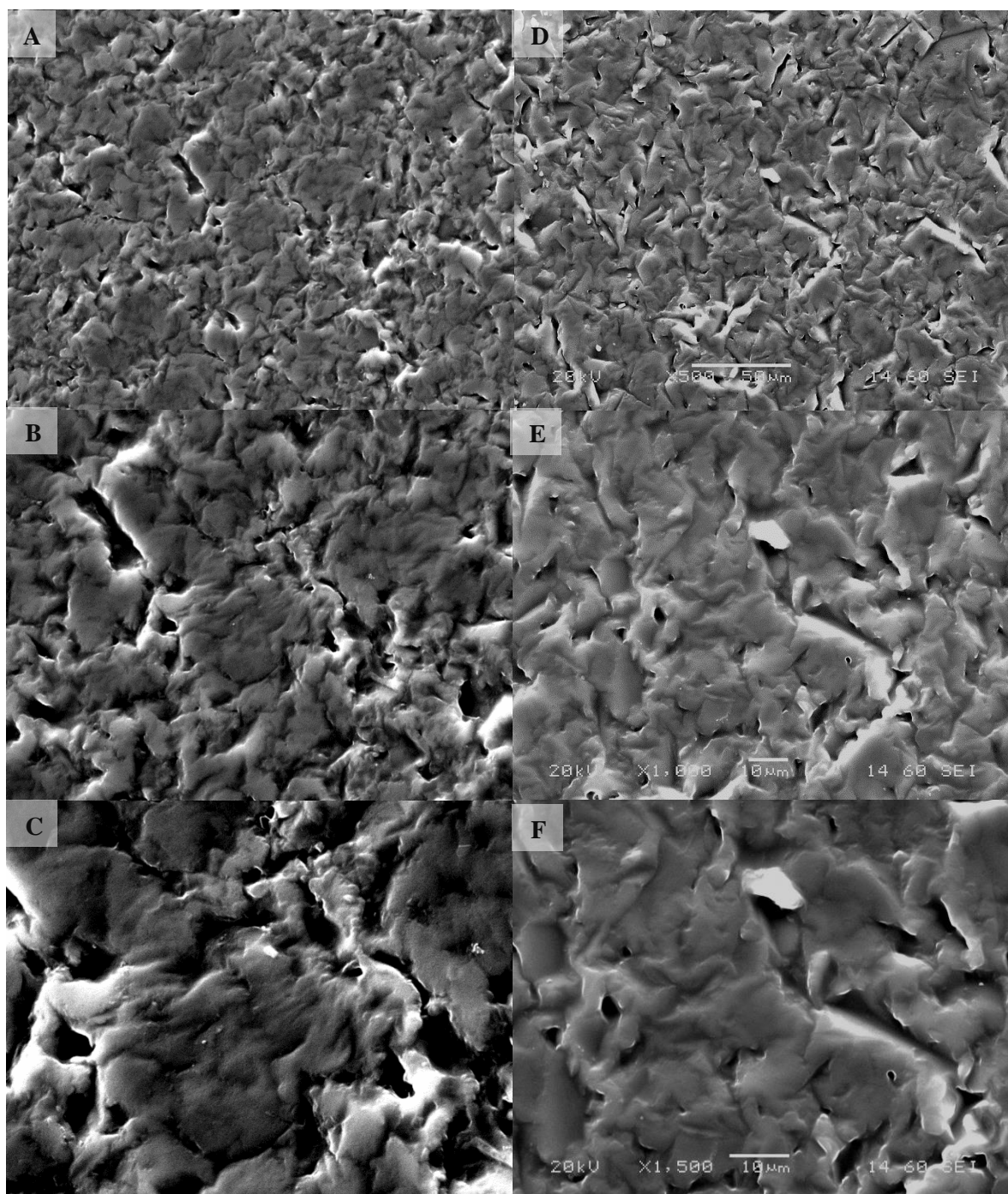


Figure 3.10 Scanning Electron Microscopy images of native PDMS (A-C, 500 X, 1000 X, and 1500 X magnification, respectively) and PDMS following 90 seconds plasma treatment (D-F, 500 X, 1000 X and 1500 X magnification, respectively).

Notably, an increase in wrinkling and cracking of the surface was observed following plasma treatment compared with native PDMS, in line with literature reports (Kaczorowski *et al.*, 2015). These phenomena can be correlated to the formation of an oxidised, silica-like surface following plasma oxidation, and the subsequent brittle nature of the surface, resulting in a contrast in elasticity and increased mechanical strain between the surface and the bulk (Cordeiro *et al.*, 2009; Lee *et al.*, 2017; Nania *et al.*, 2015).

3.2.2. Permeability Studies

3.2.2.1. Finite Dose Studies

The effect of plasma treatment time on the permeability of PDMS was investigated using the model drug ibuprofen (IBU). Three treatment times of 90, 120 and 150 seconds were employed, and the mean percent reduction in mass permeated was calculated, relative to permeation through native PDMS (Table 3.4).

Table 3.4 Effect of plasma treatment time on the permeation of the model drug ibuprofen
(mean \pm standard deviation).

Compound	Treatment time (seconds)	Cumulative mass permeated after 6 hours (μg)	Mean percent reduction in mass permeated (%)
IBU	0	63.22 \pm 2.23	N/A
	90	53.22 \pm 3.10	15.82
	120	39.60 \pm 15.52	37.36
	150	39.71 \pm 6.78	37.19

An overall statistically significant difference in the cumulative mass of IBU permeated after 6 hours was observed ($F(3,4.05) = 12.43, p = 0.017$). Levene's test for homogeneity of variance revealed data heteroscedasticity ($F(3,8) = 6.109, p = 0.018$); thus, a post hoc Games-Howell test was used to perform pairwise comparisons. A 15.82 % reduction in the cumulative mass of IBU permeating the membrane was observed upon employment of a 90 second air plasma pre-treatment ($p = 0.042$). A further 21.54 % mean decrease in permeation was observed upon a 30 second extension in treatment time, suggesting a greater extent of surface oxidation. However, an increase in the relative standard deviation (39.19 % for PDMS following 120 seconds plasma treatment compared with 3.54 % and 5.82 % for native PDMS and PDMS following a 90 second plasma treatment, respectively) suggests an increase in surface heterogeneity. Thus, a statistically insignificant difference in permeation was observed ($p = 0.560$). An additional 30 second increase in plasma treatment time yielded a statistically insignificant difference in the percent reduction in mass permeated when compared with the previous treatment time ($p = 1.00$). This may be explained by either the occurrence of complete surface oxidation at 120 seconds exposure time, or further oxidation occurring at prolonged treatment times, accompanied by phenomena which may increase permeability, such as cracking, observed previously (Figure 3.10).

In order to determine the effect of the properties of the permeant on the cumulative mass permeated after 6 hours, the permeation of five further compounds through native and plasma treated PDMS was investigated (Table 3.5). The five permeants cover a molecular weight range of 119.12 - 234.34 g mol⁻¹, a log₁₀ P range of -0.13 - 3.72, and represent both cationic and anionic charged states. A treatment time of 90 seconds was selected, according to preliminary data. A donor solution pH value of 7.4 was utilised for all compounds, in order to minimise pH gradients across the membrane, in line with that reported by other authors (Uchida *et al.*, 2015; Zhang *et al.*, 2012). Two pH values were selected in the case of one anionic compound, namely ibuprofen (IBU) and one cationic compound, namely lidocaine (LID), in order to investigate the effect of extent of ionisation on the change in cumulative mass observed following plasma treatment. A pH value of 6.0 was selected on the basis of the significant change in the extent of ionisation of each compound observed and its biological relevance

i.e the pH of skin has been shown to be depth-dependent and within the range of 5.5 – 8 (Wagner *et al.*, 2003).

Table 3.5 Cumulative mass of ibuprofen (IBU), lidocaine (LID), caffeine (CAF), benzocaine (EAB), benzoic acid (BA), and benzotriazole (BTA) permeated through native PDMS and PDMS following air plasma treatment (mean \pm standard deviation, 4 sig.fig., $n = 3$).

Compound	pH	Cumulative mass permeated after 6 hours (μg)	
		Native PDMS	Plasma treated PDMS
IBU	7.4	63.22 \pm 2.24	53.22 \pm 3.10
	6.0	449.8 \pm 18.8	138.2 \pm 26.96
LID	7.4	348.9 \pm 20.8	95.07 \pm 7.93
	6.0	68.41 \pm 5.16	28.92 \pm 15.21
CAF	7.4	6.959 \pm 0.824	5.647 \pm 0.154
		5.323 \pm 0.688 ^a	5.054 \pm 1.046 ^a
EAB	7.4	819.3 \pm 12.8	526.9 \pm 15.8
BA	7.4	19.27 \pm 1.47	17.09 \pm 1.38
BTA	7.4	37.04 \pm 3.58	29.30 \pm 3.95

a. Recalculated at 5 hours 15 minutes.

Statistically significant differences in the cumulative mass permeated through PDMS following plasma treatment were observed for three of the six compounds tested i.e. ibuprofen (IBU), lidocaine (LID) and benzocaine (EAB). For LID, a 72.75 % reduction in permeation was observed following plasma treatment ($t(4) = 19.76$, $p < 0.001$) at pH 7.4, and a 57.73 % reduction in permeation was observed at pH 6.0 ($t(2.46) = 4.26$, $p = 0.035$). For IBU, a 70.99 % reduction in permeation was observed following plasma treatment ($t(4) = 16.43$, $p < 0.001$) at pH 6.0, and a 15.82 % reduction in permeation was observed ($t(4) = 4.54$, $p = 0.01$) at pH 7.4. For EAB, a 35.69 % reduction in mass permeated was observed following plasma treatment ($t(4) = 24.94$, $p < 0.001$).

In the case of, caffeine (CAF), a statistically significant reduction in permeation was observed after 6 hours, however, the final sampling interval represented only 1 of 8 for which permeation through native PDMS was higher than that through plasma treated PDMS, and was influenced by higher permeation in only one of three diffusion cells. This value was eliminated from the analysis, suspected of being erroneous. Values were recalculated based on the previous sampling interval, and no statistically significant differences in the cumulative mass permeated were observed ($t(4) = 0.374$, $p = 0.728$). Further, no statistically significant differences in permeation were observed for benzoic acid (BA) ($t(4) = 1.874$, $p = 0.134$) and benzotriazole (BTA) ($t(4) = 2.516$, $p = 0.066$). Notably, no statistically significant increases in permeation following plasma treatment were observed.

The three compounds displaying statistically significant differences in permeation through PDMS following plasma treatment were found to be those with the greatest cumulative mass permeated through native PDMS after 6 hours. Therefore, it may be inferred that properties which govern permeation through silicone membranes, such as $\log_{10} K_{O/W}$ ($\log_{10} P$) (Miki *et al.*, 2015), and the extent of ionisation (Waters *et al.*, 2016), may also influence the reduction in permeation observed following plasma treatment.

IBU, LID, and EAB represent the three compounds with the highest $\log_{10} P$ values i.e. 3.72, 3.63 and 1.95, respectively. CAF, BTA, and BA represent the three compounds with the lowest $\log_{10} P$ values i.e. -0.13, 1.34, and 1.89, respectively. It is widely accepted that the $\log_{10} P$, or $\log_{10} K_{O/W}$, of a compound influences the compounds ability to partition into both the stratum corneum i.e. the stratum corneum partition coefficient, K , (Section 1.5) (Moss *et al.*, 2015), and alternative lipophilic membranes (Waters *et al.*, 2016). Thus, the data may suggest that the oxidation of PDMS may exhibit some effect on the partitioning of the tested compounds on the ability of the permeant to partition into the membrane. The reduction in WCA observed following plasma treatment (Table 3.1) indicates the formation of a hydrophilic layer, and may suggest reduced solubility of lipophilic compounds in the superficial layer, reducing membrane partitioning.

Many active pharmaceutical ingredients (APIs) are known to be weak acids or bases. Increases in ionisation are known to significantly decrease the permeation of compounds through lipophilic

membranes, described by pH-partition theory (Baba *et al.*, 2017; Charifson *et al.*, 2014; Zhang *et al.*, 2017). Subsequently, studies aiming to determine the physicochemical parameters which may influence topical and transdermal delivery have considered the distribution coefficient, $\log_{10} D$, as a suitable descriptor of membrane partitioning (Avdeef, 2012; Baba *et al.*, 2017; Lee *et al.*, 2010). The effect of pH on the reduction in mass permeated following plasma treatment was investigated using LID and IBU. In the case of both compounds, the percent reduction was greatest at the pH at which the compound is least ionised i.e. pH 6.0 for IBU and pH 7.4 for LID, supporting the hypothesis that it is the permeation of the lipophilic, unionised form of the compound, that is most hindered following the plasma oxidation of PDMS. In neither case, an increase in ionisation resulted in an increase in the extent of permeation.

The treatment of PDMS with air plasma has been shown to primarily result in the formation of silanol groups, using X-ray photoelectron spectroscopy (Figure 3.2 - Figure 3.9). Silanol groups are known to be weakly acidic, with a pK_a of ~ 4 (Owen *et al.*, 2012). The Henderson-Hasselbalch equation can be used to determine the percent ionisation of weak acids, with known pK_a values at a determined pH, as follows:

$$pH = pK_a + \log_{10} \left(\frac{[A^-]}{[HA]} \right) \quad \text{Equation 3.1}$$

Taking a pK_a value of 4, at pH values of 7.4 and 6.0, $> 99\%$ of surface silanol groups are deprotonated. Hence, in both cases, the surface charge is primarily anionic. LID is a weak base, and is 79.92% ionised at pH 7.4 with a $\log_{10} D$ of 1.66. At pH 6.0, LID is 98.76% ionised, with a $\log_{10} D$ of 0.40. IBU is a weak acid and is 99.92% ionised at pH 7.4, and 98.04% ionised at pH 6.0, displaying $\log_{10} D$ values of 0.58 and 1.93, respectively (ACD/I-Lab). In both cases, the largest reduction in permeation was observed at the pH at which each compound displayed the greatest $\log_{10} D$. The difference in percent reduction across the pH ranges tested for each compound varies. The percent reduction in IBU permeation observed following plasma treatment increased by 55.17% over the pH range tested (from 15.82% at pH 7.4, to 70.99% at pH 6.0). The percent reduction in LID permeation observed following plasma treatment increased by 15.02% over the pH range tested (from 57.73% at pH 6.0, to 70.75%

at pH 7.4). Despite this, similar changes in $\log_{10} D$ are observed over the pH range tested i.e. 1.26 units for LID, and 1.35 units for IBU. Assuming a relationship between the $\log_{10} D$ of the penetrant and the percent reduction in permeation observed following plasma treatment, the percent reduction in permeation of LID is high (57.73 %) at a $\log_{10} D$ of just 0.40, compared with a percent reduction of just 15.82 % at a similar $\log_{10} D$ of 0.58 in the case of IBU. LID is known to readily form ion pairs in solution, thus, the $\log_{10} D$ of primarily cationic LID may be a poor descriptor for the distribution of ion pairs (Wood *et al.*, 2012).

It is conceivable that the mechanism by which plasma oxidation of PDMS reduces the permeation of pharmaceutical compounds is complex and varies for each compound, similar to the multitude of complex interactions between xenobiotics and ionogenic groups in the stratum corneum (Du Plessis *et al.*, 2002a, 2002b). For example, in the case of anionic compounds, electrostatic repulsion between the surface and permeant may prevent membrane partitioning, as hypothesised in earlier work (Bhuiyan *et al.*, 2017; Waters *et al.*, 2013). On the contrary, electrostatic attraction between cationic permeants and the anionic PDMS surface may result in boundary layer formation, reduced partitioning, and retardation of diffusion. Importantly, following oxidation, PDMS appears to maintain its general impermeability towards ionised species, i.e. permeation through oxidised PDMS was reduced following increases in permeant ionisation. This is analogous to similar relationships observed with the stratum corneum (Baba *et al.*, 2017).

In any case, plasma treatment appears a promising method of reducing the permeation of pharmaceutical compounds through silicone skin mimics, the use of which often results in overestimations of the extent of percutaneous absorption that may be observed *in vivo*. In order to further characterise the complex interactions occurring, and evaluate the effect of plasma treatment on endpoints more broadly used in *in vitro* studies i.e. steady-state flux and the permeability coefficient, further studies using a more extensive body of compounds at an alternative dosing level were then performed.

3.2.2.2. Infinite Dose Studies

Diffusion cell experiments were performed under infinite dose conditions in order to acquire the steady-state flux (J_{ss}) of the compounds selected, and to facilitate calculation of the permeability coefficient (K_p) for each compound. The extensive use of K_p as a descriptor for skin permeation conveniently permits comparison of permeability data obtained using synthetic skin models with permeability data from literature obtained using human epidermal tissue, and is a useful measure for evaluating the predictive capability of *in vitro* models (Baba *et al.*, 2017; Miki *et al.*, 2015; Uchida *et al.*, 2015).

The body of compounds selected represents a range of therapeutic classes, namely antifungals, keratolytic agents, non-steroidal anti-inflammatories, analgesics, antipyretics and anaesthetics. Further, the data set represents a wide range of functionalities, including carboxyl, amide, amine, ester, phenyl, hydroxyl, imidazole and ketone groups, and contains two homologous series. The molecular weight of the compounds varies greater than 2 fold (138.12 - 296.15 g mol⁻¹), and the log₁₀ P of the compounds selected varies from -0.13 - 4.11; properties which have both been shown to heavily influence skin permeation (Potts *et al.*, 1992).

The steady-state flux (J_{ss}) values for all 18 compounds are presented in Table 3.6. Statistically significant differences in J_{ss} were found for all compounds in the dataset, with the exception of caffeine (CAF), acetyl salicylic acid (ASA), benzocaine (EAB) and risocaine (PAB) ($p > 0.05$, $\alpha = 0.05$). Markedly significant differences in J_{ss} were observed for benzoic acid (BA), lidocaine (LID) and ibuprofen (IBU) (Figure 3.11-Figure 3.13) ($p < 0.001$, $\alpha = 0.05$).

Table 3.6 Steady-state flux (J_{ss}) of ibuprofen (IBU), flurbiprofen (FLP), ketoprofen (KTP), caffeine (CAF), lidocaine (LID), benzoic acid (BA), salicylic acid (SA), acetyl salicylic acid (ASA) aminopyrine (AMP), methyl paraben (MP), ethyl paraben (EP), propyl paraben (PP), butyl paraben (BP), methyl 4-aminobenzoate (MAB), benzocaine (EAB), risocaine (PAB), butamben (BAB) and diclofenac (DF) through native PDMS and PDMS following air plasma treatment (mean \pm standard deviation, 4 sig.fig, $n = 3$).

Compound	J_{ss} ($\mu\text{g cm}^{-2} \text{min}^{-1}$)		<i>p</i> -value
	Native	Plasma	
IBU	5.461 \pm 0.284	2.491 \pm 0.272	< 0.001
FLP	0.9748 \pm 0.0307	0.7940 \pm 0.0650	0.012
KTP	0.3308 \pm 0.0204	0.2737 \pm 0.0131	0.015
CAF	0.1908 \pm 0.0107	0.2215 \pm 0.0299	0.169
LID	13.34 \pm 0.64	8.487 \pm 0.456	< 0.001
BA	9.813 \pm 0.399	5.379 \pm 0.427	< 0.001
SA	5.052 \pm 0.317	3.972 \pm 0.123	0.005
ASA	1.584 \pm 0.068	1.239 \pm 0.100	0.08
AMP	9.295 \pm 0.549	4.978 \pm 0.736	0.001
MP	2.191 \pm 0.066	1.760 \pm 0.091	0.003
EP	2.223 \pm 0.031	1.813 \pm 0.135	0.007
PP	1.907 \pm 0.022	1.266 \pm 0.091	0.005
BP	2.211 \pm 0.117	1.892 \pm 0.140	0.039
MAB	6.577 \pm 0.525	5.015 \pm 0.478	0.019
EAB	4.257 \pm 0.156	4.392 \pm 0.093	0.267
PAB	4.121 \pm 0.143	4.142 \pm 0.190	0.889
BAB	2.480 \pm 0.150	2.012 \pm 0.200	0.032
DF	0.1181 \pm 0.0064	0.1088 \pm 0.0054	0.125

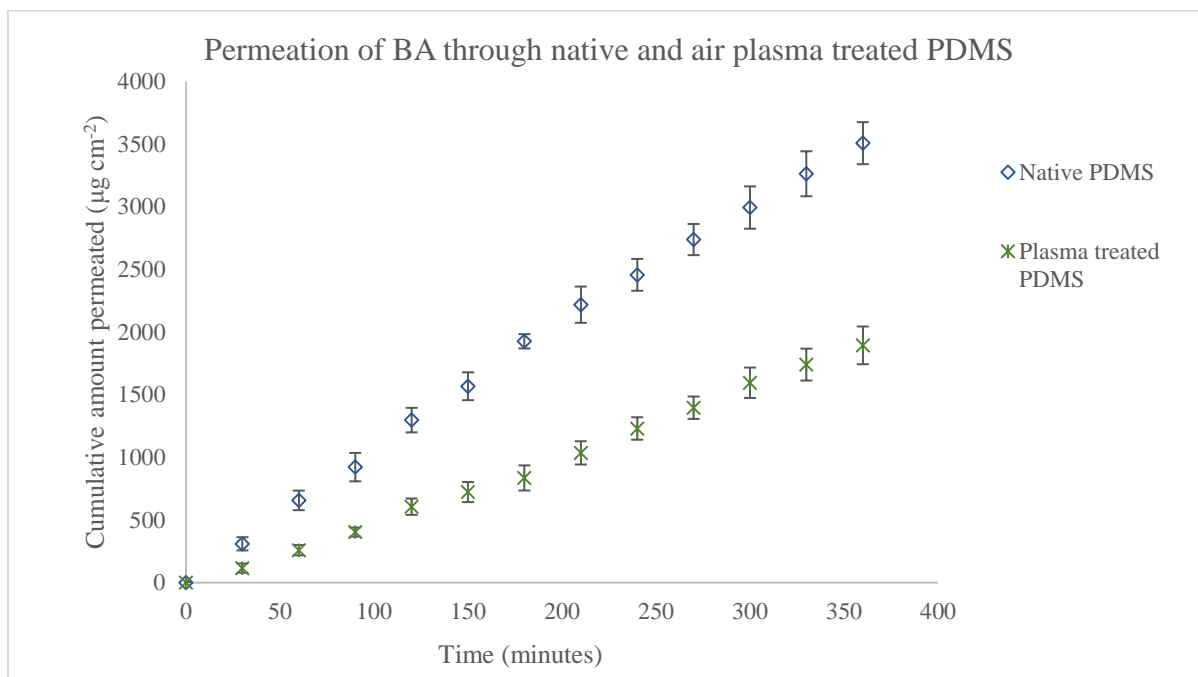


Figure 3.11 Steady-state flux of benzoic acid through native PDMS and PDMS following air plasma treatment (mean \pm standard deviation, $n = 3$).

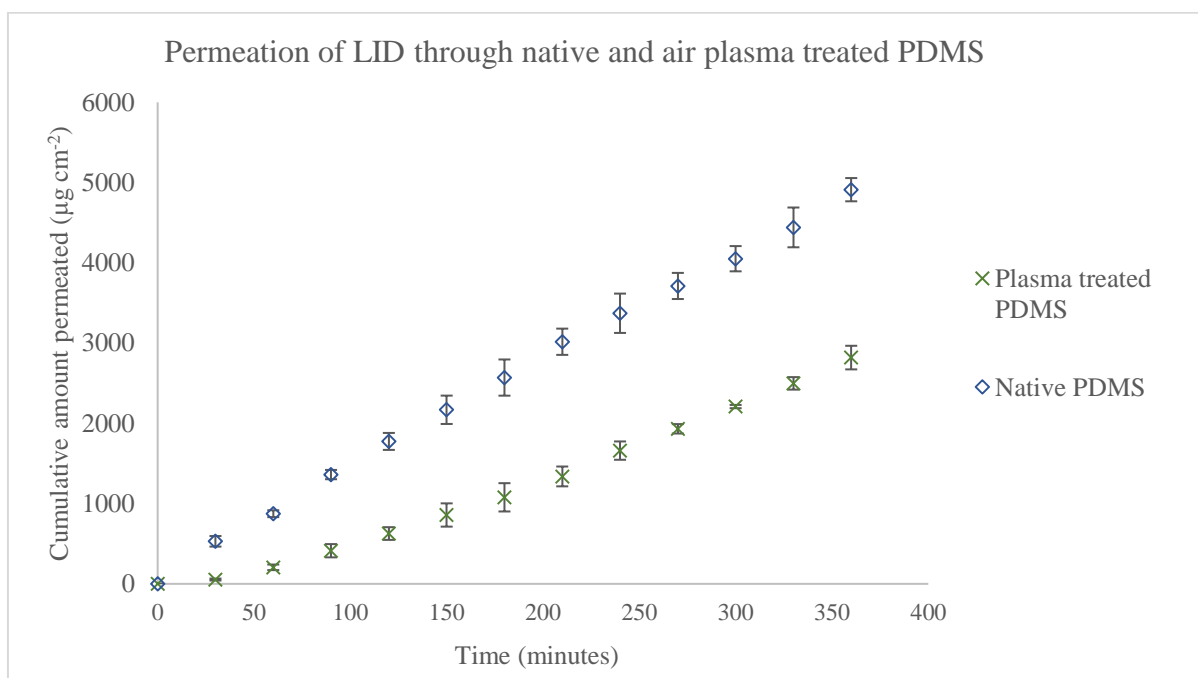


Figure 3.12 Steady-state flux of lidocaine through native PDMS and PDMS following air plasma treatment (mean \pm standard deviation, $n = 3$).

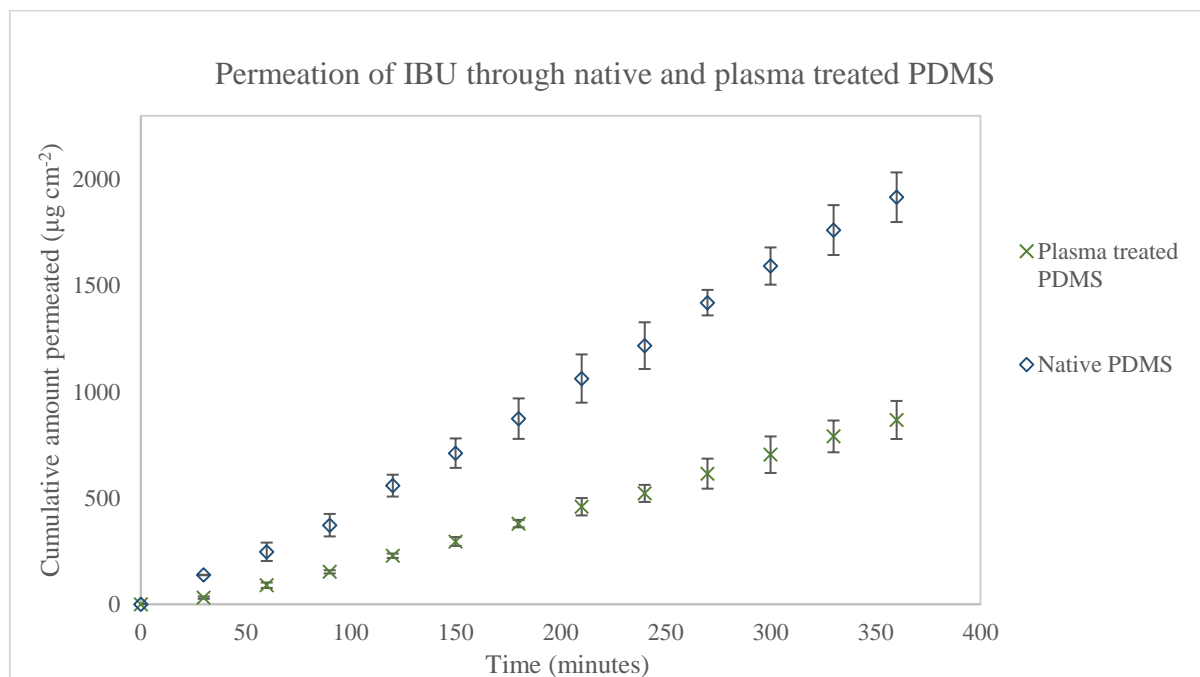


Figure 3.13 Steady-state flux of ibuprofen through native PDMS and PDMS following air plasma treatment (mean \pm standard deviation, $n = 3$).

The concentration of permeant in the donor chamber was determined as described in Section 2.2.1.7, and is presented in Table 3.7. Since PDMS is in many cases more permeable than human epidermal tissue, receptor chamber concentrations are often much higher during static permeation experiments using the synthetic substitute than those using isolated biological tissue. This can be particularly problematic with high $\log_{10} P$ compounds, for which aqueous solubility is very low, but permeability through a lipophilic barrier is high. It can be seen in Table 3.7 such an effect was observed with butyl paraben (BP), benzocaine (EAB), risocaine (PAB) and butamben (BAB). This is somewhat unsurprising since these compounds are amongst the highest $\log_{10} P$, and lowest percent ionised of the compounds tested, parameters both known to influence permeation through lipophilic, non-porous membranes, and limit solubility in physiologically conducive receptor solutions. The linearity of the permeation profiles for these compounds was inspected, and $R^2 \geq 0.99$ for all four compounds, indicating maintenance of steady-state conditions. Thus, steady-state fluxes (J_{ss}) (Table 3.6) and permeability coefficients (K_p) (Table 3.8) were calculated for all compounds in this dataset. Such data treatment may be appropriate for intra-dataset comparative purposes, however, caution must be

exercised when correlating this data with external datasets, such as literature K_p values, for which sink conditions were maintained throughout the course of the study.

Table 3.7 Concentration of ibuprofen (IBU), flurbiprofen (FLP), ketoprofen (KTP), caffeine (CAF), lidocaine (LID), benzoic acid (BA), salicylic acid (SA), acetyl salicylic acid (ASA) aminopyrine (AMP), methyl paraben (MP), ethyl paraben (EP), propyl paraben (PP), butyl paraben (BP), methyl 4-aminobenzoate (MAB), benzocaine (EAB), risocaine (PAB), butamben (BAB) and diclofenac (DF) in the donor chamber (C_{donor}), and receptor chamber after 6 hours ($C_{receptor}$) quoted to 4 significant figures (mean \pm standard deviation, 4 sig.fig., $n = 3$), and the time at which the receptor chamber exceeded 10 % saturation.

Compound	Membrane	C_{donor} (mg mL ⁻¹)	$C_{receptor}$ (μ g mL ⁻¹)	$t_{10\%}$ (mins)
LID	Native	3.694 \pm 0.039	365.6 \pm 3.2	> 360
	Plasma		241.7 \pm 26.4	> 360
IBU	Native	4.585 \pm 0.025	150.6 \pm 12.4	> 360
	Plasma		70.86 \pm 8.04	> 360
BA	Native	8.625 \pm 0.008	253.0 \pm 9.7	> 360
	Plasma		147.7 \pm 12.9	> 360
SA	Native	7.703 \pm 0.053	148.0 \pm 9.0	> 360
	Plasma		112.9 \pm 1.8	> 360
ASA	Native	12.62 \pm 0.26	41.76 \pm 3.08	> 360
	Plasma		33.54 \pm 3.22	> 360
AMP	Native	46.32 \pm 0.72	262.1 \pm 10.1	> 360
	Plasma		146.4 \pm 22.2	> 360
CAF	Native	21.59 \pm 0.28	5.036 \pm 0.125	>360
	Plasma		5.933 \pm 0.229	> 360
DF	Native	1.938 \pm 0.048	3.007 \pm 0.384	> 360
	Plasma		2.860 \pm 0.038	> 360

Table 3.7 continued.

Compound	Membrane	C_{donor} (mg mL ⁻¹)	C_{receptor} ($\mu\text{g mL}^{-1}$)	$t_{10\%}$ (mins)
FLP	Native	4.494 ± 0.051	25.99 ± 1.44	> 360
	Plasma		22.16 ± 1.37	> 360
KTP	Native	9.301 ± 0.119	9.319 ± 0.600	> 360
	Plasma		8.033 ± 0.608	> 360
MP	Native	3.094 ± 0.154	59.55 ± 1.33	> 360
	Plasma		43.60 ± 1.65	> 360
EP	Native	1.209 ± 0.031	57.06 ± 1.17	> 360
	Plasma		50.78 ± 2.00	> 360
PP	Native	0.4839 ± 0.0068	50.13 ± 2.59	300
	Plasma		34.69 ± 4.92	> 360
BP	Native	0.3105 ± 0.0020	57.03 ± 2.25	102
	Plasma		52.96 ± 4.58	181
MAB	Native	1.804 ± 0.018	167.3 ± 16.0	> 360
	Plasma		139.9 ± 8.3	> 360
EAB	Native	0.8901 ± 0.0076	112.6 ± 5.9	162
	Plasma		121.4 ± 4.1	191
PAB	Native	0.7489 ± 0.0091	106.3 ± 1.6	123
	Plasma		98.47 ± 12.2	250
BAB	Native	0.2256 ± 0.0005	67.63 ± 5.11	59
	Plasma		55.42 ± 3.54	86

K_p values were calculated by the normalisation of J_{ss} (Table 3.6) with C_{donor} (Table 3.7), according to Equation 1.5, and the resultant values are presented in Table 3.8. Further, the mean percentage reduction in K_p was calculated according to Equation 3.2:

$$\text{Mean percent reduction in } K_p = \left(\frac{K_p^{\text{native}} - K_p^{\text{plasma}}}{K_p^{\text{native}}} \right) \times 100 \quad \text{Equation 3.2}$$

To assist in the understanding of the varying effect of plasma treatment on different compounds, bivariate correlation analysis was performed, endeavouring to evaluate the relationship between the mean percent reduction in K_p with physicochemical parameters of the penetrant. Physicochemical parameters known to influence the extent of permeation through synthetic lipophilic membranes and epidermal tissue i.e. $\log_{10} P$, molecular weight, $\log_{10} D$, polar surface area (PSA), the extent of ionisation, and hydrogen bond donor (HBD) and acceptor (HBA) count, and hydrogen bond donor acidity (HB_{acid}) and basicity (HB_{basic}) were compiled and are summarised in Table 3.9 (Baba *et al.*, 2017; Cronin *et al.*, 1998; Lee *et al.*, 2010; Potts *et al.*, 1992; Pranitha *et al.*, 2014; Zhang *et al.*, 2017). It was noted that the buffer failed to control pH upon saturation with permeant, therefore the pH was recorded (Appendix 11) to enable the accurate determination of various parameters i.e. $\log_{10} D$ and percent ionisation.

Table 3.8 K_p values of ibuprofen (IBU), flurbiprofen (FLP), ketoprofen (KTP), caffeine (CAF), lidocaine (LID), benzoic acid (BA), salicylic acid (SA), acetyl salicylic acid (ASA) aminopyrine (AMP), methyl paraben (MP), ethyl paraben (EP), propyl paraben (PP), butyl paraben (BP), methyl 4-aminobenzoate (MAB), benzocaine (EAB), risocaine (PAB), butamben (BAB) and diclofenac (DF) obtained with native (K_p^{native}) and air plasma (K_p^{plasma}) treated PDMS. (mean \pm standard deviation, $n = 3$).

Compound	K_p^{native} ($\times 10^{-4} \text{ cm min}^{-1}$)	K_p^{plasma} ($\times 10^{-4} \text{ cm min}^{-1}$)	Mean reduction in K_p (%)
IBU	11.91 \pm 0.54	5.432 \pm 0.514	54.39
FLP	2.169 \pm 0.063	1.767 \pm 0.1264	18.53
KTP	0.3557 \pm 0.0193	0.2944 \pm 0.0126	17.23
CAF	0.0884 \pm 0.0044	0.1026 \pm 0.0120	-28.25
LID	36.11 \pm 1.54	22.98 \pm 1.09	36.36
BA	11.38 \pm 0.40	6.236 \pm 0.428	45.20
SA	6.560 \pm 0.359	5.158 \pm 0.142	21.37
ASA	1.255 \pm 0.051	0.9821 \pm 0.0709	21.75
AMP	2.007 \pm 0.106	1.075 \pm 0.139	46.44
MP	7.092 \pm 0.363	5.698 \pm 0.359	19.66
EP	18.40 \pm 0.47	15.00 \pm 1.03	18.48
PP	39.43 \pm 0.62	26.17 \pm 1.65	33.63
BP	71.21 \pm 3.28	60.94 \pm 3.91	14.42
MAB	36.45 \pm 2.54	27.80 \pm 2.31	23.73
EAB	47.83 \pm 1.56	49.35 \pm 0.98	-3.18
PAB	55.04 \pm 1.75	55.31 \pm 2.27	-0.49
BAB	109.9 \pm 5.8	89.21 \pm 7.67	18.83
DF	0.6099 \pm 0.0316	0.5618 \pm 0.0272	7.89

Table 3.9 Percent ionised, polar surface area (PSA), $\log_{10} D$, and $\log_{10} P$, hydrogen bond donor (HBD) and acceptor (HBA) count, and hydrogen bond acidity (HB_{acid}), and basicity (HB_{basic}) of ibuprofen (IBU), flurbiprofen (FLP), ketoprofen (KTP), caffeine (CAF), lidocaine (LID), benzoic acid (BA), salicylic acid (SA), acetyl salicylic acid (ASA) aminopyrine (AMP), methyl paraben (MP), ethyl paraben (EP), propyl paraben (PP), butyl paraben (BP), methyl 4-aminobenzoate (MAB), benzocaine (EAB), risocaine (PAB), butamben (BAB) and diclofenac (DF).

Compound	Percent ionised (%) (i)	PSA (\AA^2) (ii)	$\log_{10} D$ (i)	$\log_{10} P$ (ii)	HBD (ii)	HBA (ii)	HB_{acid} (iii)	HB_{basic} (iii)
LID	28.47	36	2.10	3.63	1	3	0.07	1.24
IBU	99.37	37	1.44	3.72	1	2	0.08	3.31
BA	55.73	37	1.40	1.89	1	2	0.02	2.75
SA	66.61	58	1.95	2.06	2	3	0.08	2.74
ASA	50.00	64	1.09	1.19	1	4	0.71	0.67
AMP	0.25	27	-0.52	0.76	0	4	0.00	1.60
CAF	0.00	58	0.11	-0.13	0	6	0.08	1.25
DF	99.89	49	1.85	4.06	2	3	0.03	3.35
FLP	99.66	37	1.48	4.11	1	2	0.07	3.36
KTP	98.84	54	1.00	2.81	1	3	0.01	3.39
MP	5.94	47	1.93	1.87	1	3	0.71	0.46
EP	7.36	47	2.33	2.40	1	3	0.66 ^a	0.72 ^a
PP	5.94	47	2.85	2.93	1	3	0.74	0.43
BP	7.36	47	3.18	3.46	1	3	0.74	0.43
MAB	0.00	52	1.39	1.41	2	3	0.30	0.72
EAB	0.00	52	1.79	1.95	2	3	0.31	0.69
PAB	0.00	52	2.21	2.48	2	3	0.23 ^a	0.77 ^a
BAB	0.00	52	2.50	3.01	2	3	0.30	0.68

- (i) ACD/I-Lab. Calculated at the pH of the donor solution (Appendix 11).
- (ii) Chemspider
- (iii) Zhang *et al.*, 2017. Where available, data was taken for the macrospecies, based on the percent ionisation at the donor solution pH. Values marked with ^a were unavailable, and were calculated using ACD/I-Lab Absolv module.

The most extensive correlation was found between the mean reduction in K_p (%) and PSA, and is demonstrated in Figure 3.14. Pearson's correlation coefficient ($r = -0.652$, $p = 0.003$, $[-0.847, -0.374]$) indicated a large effect of PSA on the reduction in K_p observed, significant at both the $\alpha = 0.05$ and $\alpha = 0.01$ level. Further, 42.3 % of the variance in the mean reduction in K_p (%) can be accounted for by PSA ($R^2 = 0.423$).

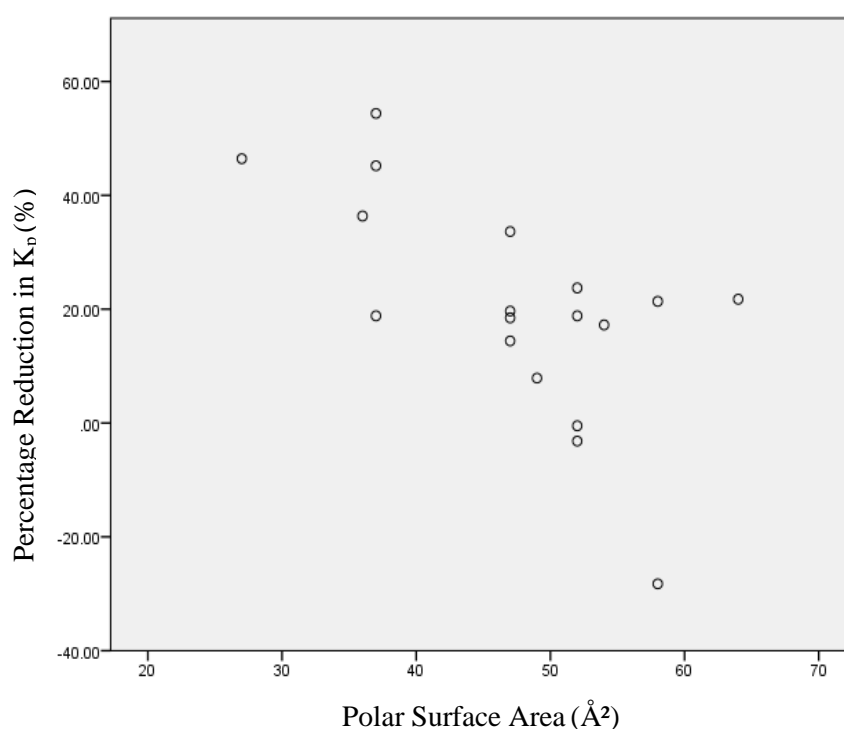


Figure 3.14 Plot of percent reduction in K_p (%) versus polar surface area (PSA) ($R^2 = 0.423$, $n = 18$).

The correlation indicates that, in general, the introduction of silanol groups to the surface of PDMS had the greatest effect on compounds with the lowest polar surface area (PSA), and the smallest effect on compounds with the greatest polar surface area. The introduction of Si-OH groups at the surface of PDMS, thus, hinders the permeation of pharmaceutical compounds with the lowest surface area of polar functionalities, such as nitrogen-, oxygen-containing groups. Similar dependences on PSA have been observed with epithelial barriers; Shanmugasundaram *et al.* report a negative correlation between PSA and the human skin permeability coefficients of 61 compounds ($R^2 = 0.46$) (Lee *et al.*, 2010), and

work by Palm *et al.* highlighted the dependence of fraction absorbed (FA) in humans, following oral administration, on PSA (Palm *et al.*, 1997).

The presence of hydrophilic groups at the surface of PDMS, introduced via physical adsorption, has previously been shown to reduce the permeation of pharmaceutical compounds, hypothesised to be a consequence of reduced partitioning of the permeant into the membrane (Bhuiyan *et al.*, 2017; Waters *et al.*, 2013). Based on the above findings, the partitioning of compounds with a high polar surface area, therefore, may be less affected by the introduction of polar functionalities to the surface of PDMS. Conversely, compounds with a low polar surface area may display low partitioning into the outermost, hydrophilic polymer layers. One explanation for the lack of permeability increases is that the diffusion of compounds with high PSAs that may display enhanced partitioning into the outer layers, may be limited by diffusion through the underlying, hydrophobic bulk.

No statistically significant bivariate correlations were found for $\log_{10} D$ ($r = -0.001$, $p = 0.996$, [-0.614, 0.578]), $\log_{10} P$ ($r = 0.287$, $p = 0.248$, [-0.455, 0.726]), percent ionised ($r = 0.269$, $p = 0.281$ [-0.185, 0.608]), MW ($r = -0.043$, $p = 0.866$, [-0.401, 0.415]), HBD ($r = -0.147$, $p = 0.561$, [-0.796, 0.458]), and HBA ($r = -0.498$, $p = 0.035$, [-0.850, 0.451]), HB_{acid} ($r = -0.071$, $p = 0.781$, [-0.465, 0.357]) and HB_{basic} ($r = 0.251$, $p = 0.315$, [-0.149, 0.608])

3.2.3. Comparison with Human Skin Data

The K_p values obtained using both synthetic membranes i.e. native and plasma treated, were compared with a library of K_p values collated from permeability studies reported in literature employing excised skin. Appropriate K_p values were identified on the basis of experimental setup, and the data were scrutinised according to the following factors: tissue type, experimental temperature, dose, receptor solution composition, and donor solution composition. The resultant library is presented in Appendix 14, and the K_p values selected for comparison are summarised in Table 3.10.

Multiple authors have reported the lack of standardised permeability data in literature, and emphasised the importance of performing comparisons made with literature permeability coefficients on smaller datasets, which are more standardised in terms of experimental procedures, and human skin source and

preparation technique (Provin *et al.*, 2015; Sinkó *et al.*, 2012). Exceptions to this were made where appropriate; For example, data for LID was available from Uchida *et al.* (Uchida *et al.*, 2015), however, the authors report obtaining the hydrochloride salt, thus this data was substituted with data from another source reporting use of the free base (Miki *et al.*, 2015).

All donor solutions were aqueous (either buffers or purified/deionised water) in order to exclude the possibility of excipients altering the barrier function of the skin. Where possible, K_p values were selected whereby the author had reported no pH adjustment to the donor phase, and the donor and receptor phase matched that of permeation studies employing synthetic substitutes i.e. pH 7.4 phosphate buffered saline. The K_p value of a compound is known to be heavily influenced by pH, and the subsequent extent of ionisation. The overall K_p of a compound is known to be a sum of the permeability coefficients of the macro- and microspecies present (Zhang *et al.*, 2017):

$$K_p^{\text{total}} = (K_p^{\text{union}} \times F^{\text{union}}) + (K_p^{\text{ion}} \times F^{\text{ion}}) \quad \text{Equation 3.3}$$

Where K_p^{union} and F^{union} are the permeability coefficient of the unionised species and the fraction unionised, respectively, and K_p^{ion} and F^{ion} are the corresponding values for the ionised species.

Given that the stratum corneum is orders of magnitude less permeable to the ionised form of a compound, it is clear that variations in the pH of the vehicle may have a profound effect on the observed permeability coefficient (Bartosova *et al.*, 2012). Similar relationships have also been observed in silicone membranes (Waters *et al.*, 2016). The influence of vehicle pH was considered particularly important for compounds at pH values considerably close to the pKa, or for which significant fraction was known to be ionised. For example, BA has a pKa of 4.1, and is 55.73 % ionised at a donor solution pH of 4.2 (ACD/I-Lab). Zhang *et al.* report a similar donor solution pH of 4.0. Adjustment to a pH of 7.4 would yield a percent ionisation of 99.95 % (ACD/I-Lab). Deviations from the buffer pH for the remaining compounds for which K_p values were abstracted from the same source were comparable to those obtained in this study, thus were deemed more suitable than those published by Miki *et al.* (Miki *et al.*, 2015).

Two compounds were removed from the data set on the basis of insufficient data for comparison with external datasets. A minimum of four data points prior to the receptor solution concentration exceeding 10 % that of the donor was considered adequate to ensure steady-state conditions were attained, and to enable calculation of K_p . In the case of butamben (BAB) and butyl paraben (BP), only two and three data points, respectively, were obtained. As such, K_p values for these compounds were not correlated with those from literature, whereby sink conditions were reported.

Table 3.10 Permeability coefficients extracted from literature for lidocaine (LID), ibuprofen (IBU), benzoic acid (BA), salicylic acid (SA), acetylsalicylic acid (ASA), aminopyrine (AMP), caffeine (CAF), diclofenac (DF), flurbiprofen (FLP), ketoprofen (KTP), methyl paraben (MP), ethyl paraben (EP), propyl paraben (PP) methyl 4-aminobenzoate (MAB), benzocaine (EAB) and risocaine (PAB).

Compound	Permeability Coefficient ($\times 10^{-4} \text{ cm min}^{-1}$)	Source
LID	4.209	(Miki <i>et al.</i> , 2015)
IBU	0.560	(Zhang <i>et al.</i> , 2012)
BA	2.940	(Zhang <i>et al.</i> , 2012)
SA	2.301	(Degim <i>et al.</i> , 1998)
ASA	0.085	(Walker <i>et al.</i> , 1997)
AMP	0.198	(Uchida <i>et al.</i> , 2015)
CAF	0.108	(Uchida <i>et al.</i> , 2015)
DF	0.167	(Degim <i>et al.</i> , 1998)
FLP	0.379	(Zhang <i>et al.</i> , 2012)
KTP	1.17	(Zhang <i>et al.</i> , 2012)
MP	1.49	(Uchida <i>et al.</i> , 2015)
EP	2.32	(Uchida <i>et al.</i> , 2015)
PP	2.18	(Uchida <i>et al.</i> , 2015)

Table 3.10 continued.

Compound	Permeability Coefficient ($\times 10^{-4} \text{ cm min}^{-1}$)	Source
MAB	11.0	(Uchida <i>et al.</i> , 2015)
EAB	12.1	(Uchida <i>et al.</i> , 2015)
PAB	13.4	(Uchida <i>et al.</i> , 2015)

Bivariate correlation analysis and simple linear regression was performed in order to evaluate the extent of correlation between K_p^{human} and K_p^{native} , and K_p^{human} and K_p^{plasma} . Pearson's correlation coefficient revealed a large effect size and a statistically significant correlation between K_p^{human} and K_p^{native} ($r = 0.869$, $p = < 0.001$, $[0.621, 0.988]$) (Figure 3.15).

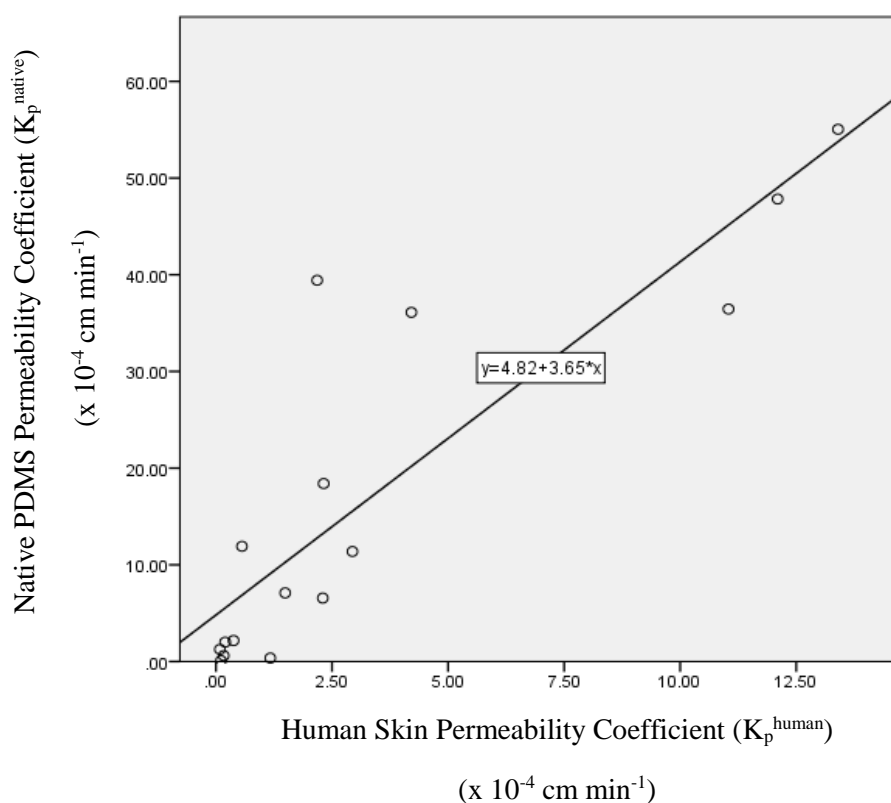


Figure 3.15 Plot of permeability coefficients through native PDMS (K_p^{native}) versus human skin (K_p^{human}) ($R^2 = 0.75$, $n = 16$).

Bivariate correlation analysis was also performed in order to evaluate the extent of correlation between K_p^{human} and K_p^{native} for values of K_p^{human} whereby no correlation was expected, serving as a negative control. For example, values of K_p^{human} for FLP, KTP, and BA taken from Zhang *et al.* were substituted for values reported by other authors (Miki *et al.* in the case of FLP and KTP, and Degim *et al.* in the case of BA) whereby the pH of the donor solution differed significantly from that observed for K_p^{native} , or no control of the pH was reported i.e. an aqueous solution was used. Further, the value of K_p^{human} corresponding to LID reported by Miki *et al.* was substituted with that from Uchida *et al.* whereby the hydrochloride salt was used. Expectedly, Pearson's correlation coefficient revealed no statistically significant correlation between K_p^{human} and K_p^{native} ($r = -0.030$, $p = < 0.912$, $[-0.316, 0.914]$).

An increase in correlation was observed between permeability coefficients obtained using human skin, and the synthetic skin mimic, following plasma treatment ($r = 0.925$, $p = < 0.001$, $[0.750, 0.990]$), indicating an increase in predictive capability of the skin mimic (Figure 3.16).

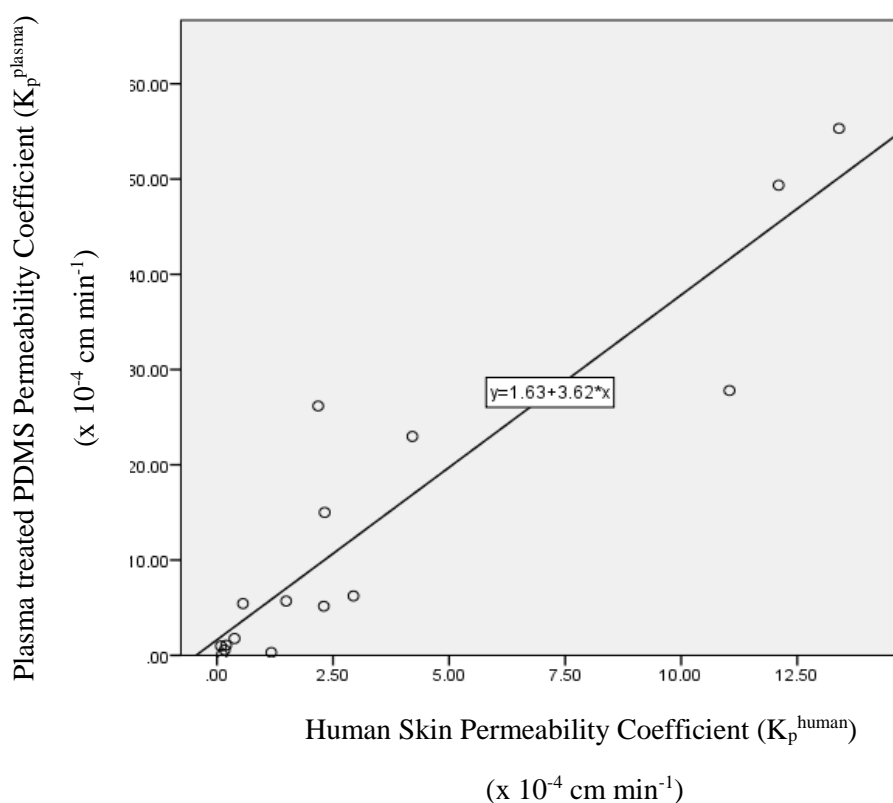


Figure 3.16 Plot of permeability coefficients through plasma treated PDMS (K_p^{plasma}) versus human skin (K_p^{human}) ($R^2 = 0.86$, $n = 16$).

Bivariate correlation analysis was also performed in order to compare physicochemical properties which may influence permeation through both synthetic systems and human skin. A statistically significant relationship was observed between K_p^{native} and $\log_{10} D$ ($r = 0.553, p = 0.026, [0.226, 0.794]$), and K_p^{native} and percent ionisation ($r = -0.550, p = 0.027, [-0.862, -0.191]$). Similar relationships were observed between K_p^{plasma} and percent ionisation ($r = -0.549, p = 0.027, [-0.797, -0.283]$), and K_p^{plasma} and $\log_{10} D$ ($r = 0.486, p = 0.056, [0.156, 0.813]$), the latter of which was marginally insignificant at the $\alpha = 0.05$ level. The negative value of Pearson's correlation coefficient with regards to the relationship between permeation through both synthetic systems and the extent of ionisation indicates the negative effect of ionisation on permeation through the two synthetic substitutes, and has been shown previously (Waters *et al.*, 2016). A similar relationship was observed between K_p^{human} and percent ionisation, however, was insignificant at the $\alpha = 0.05$ level ($r = -0.415, p = 0.110, [-0.885, 0.302]$). The limited correlation may indicate greater sensitivity of silicone based skin mimics to ionisation compared with human skin, as a result of the presence of more continuous hydrophilic routes through the stratum corneum, such as the polar head groups of the stratum corneum intercellular lipid lamellae. Conversely, it may indicate that the percent ionisation values presented in Table 3.9 are a poorer representation of the extent of ionisation observed in literature studies employing human skin tissue. The percent ionisation values were corrected for compounds which the authors noted significant deviations in donor solution pH, and no increase in correlation was observed ($r = -0.406, p = 0.118, [-0.847, 0.254]$), supporting the hypothesis that silicone membranes are more sensitive to permeant ionisation. A similar dependence of the permeability coefficient on $\log_{10} D$ was observed with data obtained using human skin ($r = 0.518, p = 0.040, [0.121, 0.765]$). Correction of $\log_{10} D$ for reported pH values yielded a similar relationship ($r = 0.518, p = 0.040, [-0.008, 0.831]$).

Statistically significant correlations between K_p and HB_{basic} were observed for native PDMS ($r = -0.568, p = 0.022, [-0.832, -0.278]$) and plasma treated PDMS ($r = -0.553, p = 0.026, [-0.755, -0.351]$). No statistically significant correlations were observed between K_p and HB_{acid} for native PDMS ($r = 0.244, p = 0.363, [-0.148, 0.702]$), or plasma treated PDMS ($r = 0.215, p = 0.425, [-0.220, 0.845]$). Values for HB_{acid} and HB_{basic} were corrected for any changes in the macrospecies present based on the

reported donor solution pH i.e. for LID and BA, the values were substituted for those for the ionised and neutral species, respectively, from Zhang *et al.* (Zhang *et al.*, 2017). No statistically significant correlations were observed between K_p and HB_{basic} ($r = -0.419$, $p = 0.106$, $[-0.695, 0.006]$) or HB_{acid} ($r = 0.388$, $p = 0.137$, $[-0.140, 0.727]$), in the case of human skin.

Two homologous series' were included in the dataset presented in this work, analogous to other studies aiming to quantify the effect of various physicochemical properties of permeation through human skin and alternative models (Baba *et al.*, 2017; Du Plessis *et al.*, 2002b; Uchida *et al.*, 2015). The inclusion of homologous series provides a useful method of observing the effects of parameters such as $\log_{10} P$ and molecular weight, on skin permeation, in the absence of more complex interactions arising from the inclusion of alternative functional groups, such as hydrogen bond acidity and basicity. In this work, this was performed using two series of alkyl benzoate based compounds. In general, the permeability coefficients of alkyl 4-aminobenzoates through native PDMS were greater than alkyl 4-hydroxybenzoates. A similar relationship was observed in human skin, and is represented graphically in Figure 3.17.

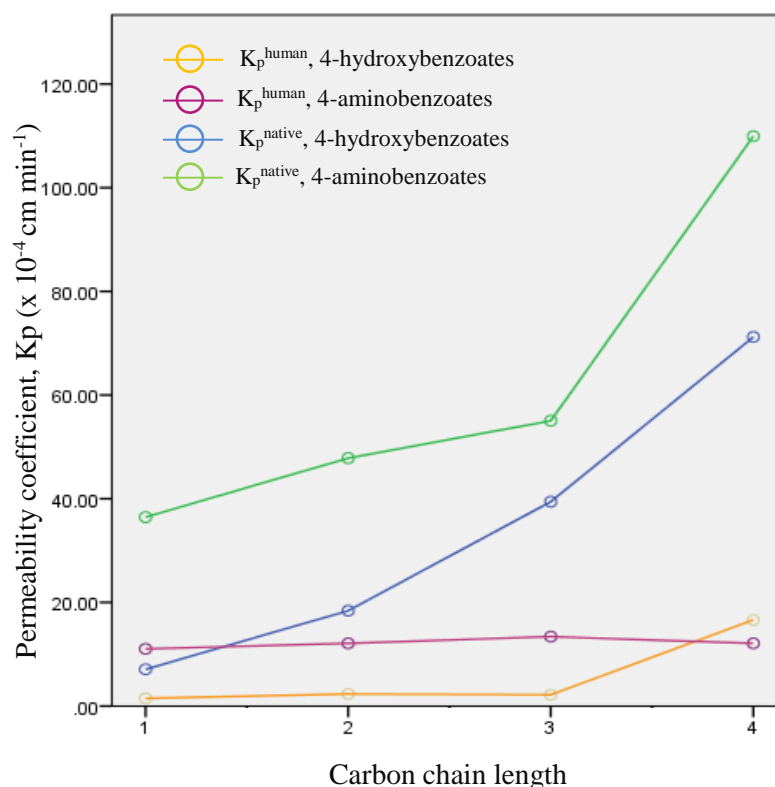


Figure 3.17 Permeability coefficients of alkyl 4-amino- and 4-hydroxy- benzoates as a function of carbon chain length.

The permeability coefficients of compounds through native PDMS increased with increases in carbon chain length, within each series. Increasing carbon chain length represents an increase in $\log_{10} P$ and molecular weight. Increases in $\log_{10} P$ are known to be concomitant with increases in the permeability coefficient, and increases in molecular weight, or molecular volume, are known to contribute negatively to the permeability coefficient, described in pioneering work by Potts and Guy (Potts *et al.*, 1992). In this work, decreases in K_p , as a result of increases in molecular volume, appear to be largely offset by increases in $\log_{10} P$. This is also represented mathematically in the Potts and Guy model by the varying magnitude of the coefficients associated with each parameter i.e. 0.71 for $\log_{10} K_{O/W}$, and -0.0061 for molecular weight (Potts *et al.*, 1992). The magnitude of the increase in K_p associated with the extension of the carbon chain length appears to be larger at longer chain lengths, particularly with regards to permeation through PDMS. This effect is particularly evident between a chain length of three and four carbons in the alkyl 4-aminobenzoate series. It must also be considered that a loss of sink conditions in the experiment employing butyl 4-aminobenzoate may have resulted in boundary layer control and an underestimation of K_p . It is, therefore, plausible that this effect is more prominent than that displayed in Figure 3.17. This effect is somewhat unsurprising, given the lack of hydrophilic domains within the native PDMS structure, in contrast to the stratum corneum, noted previously by Cronin *et al.* Interestingly, the author notes that polymeric systems containing ‘alternating hydrophobic and hydrophilic layers’ may provide skin mimics of greater mechanistic relevance (Cronin *et al.*, 1998). In any case, a similar relationship has been observed previously with the permeation of alkyl 4-aminobenzoates through silicone membranes by Addicks *et al.* (Addicks *et al.*, 1987).

The permeability coefficients of compounds from both series displayed similar trends through plasma treated PDMS, and are represented graphically in Figure 3.18. As previously, alkyl 4-aminobenzoates show greater permeability coefficients than alkyl 4-hydroxybenzoates, and the permeability coefficient increases with increasing chain length.

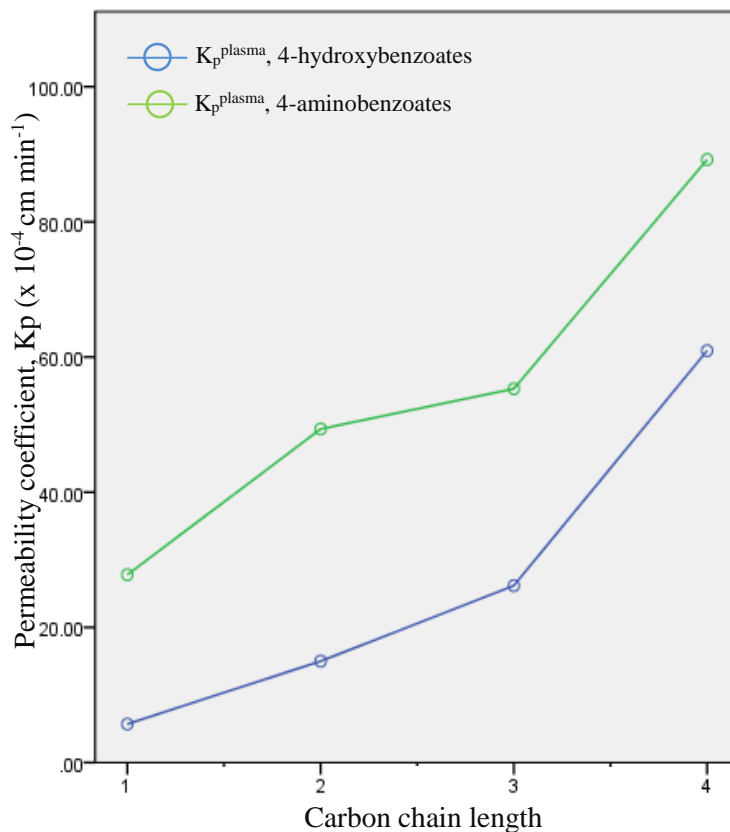


Figure 3.18 Permeability coefficients of alkyl 4-aminobenzoates through plasma treated PDMS.

The effect of plasma treatment on the permeation of alkyl benzoate based compounds appears to be somewhat variable. The mean percent reduction in K_p following plasma treatment in the case of methyl 4-hydroxybenzoate (MP), ethyl 4-hydroxybenzoate (EP), methyl 4-aminobenzoate (MAB) and butyl 4-aminobenzoate (BAB) were similar, with values of 19.66 %, 18.48 %, 23.73 %, and 18.83 %, respectively. The mean percent reduction in K_p with respect to butyl 4-hydroxybenzoate (BP) was marginally lower, displaying a value of 14.42 %. The greatest mean percent reduction was observed with propyl 4-hydroxybenzoate, with a value of 33.63 %. No statistically significant reductions were observed in the case of ethyl 4-aminobenzoate and propyl 4-aminobenzoate (Table 3.6). Despite the variable degree of reduction in K_p observed, all eight compounds display similar values of PSA, shown previously to correlate well with the extent of reduction in value of K_p (Figure 3.14). Limited correlation with other physicochemical parameters found previously, which vary within the homologous series, such as MW, HB_{acid} , HB_{basic} and $\log_{10} P$, may indicate the source of variability is the plasma process. For example, alterations in the composition of the process gas in the case of air

plasma, such as increases or decreases in the amount of water vapour present, may limit the reproducibility of the PDMS surfaces obtained (Chau *et al.*, 2011). It is therefore, a logical progression of the work presented in this thesis to evaluate the effect of administering greater control of the composition of the plasma process gas by use of well-defined process gases, such as those provided by commercially obtained cylinders.

3.3. Conclusions

Despite the multitude of advantages associated with the replacement of biological tissue with silicone based skin mimics in *in vitro* permeation studies, such as limited ethical criticism, legal status, heightened availability, greater reproducibility, and the consequent ease of data deconvolution, the overestimation in percutaneous absorption observed with such systems continues to be a drawback. Therefore, a major aim of the work presented in this chapter was to determine a suitable method of chemically modifying the structure of PDMS, in order to reduce the permeation of pharmaceutical compounds, and subsequently reduce, or eliminate, overestimations of percutaneous absorption. Statistically significant reductions in the steady-state flux, J_{ss} , of fourteen pharmaceutical compounds were observed, for thirteen of which overestimations in percutaneous adsorption had been observed upon comparison with suitable data from literature. No statistically significant increases in permeation were observed following plasma treatment, deeming the method compatible with permeation studies. Further, the work endeavoured to produce a mechanistically substantiated model of the stratum corneum, based on the heteropolar structure of the intercellular lipid lamellae and surrounding corneocytes. Physical and chemical characterisation, using water contact angle analysis, X-ray photoelectron spectroscopy, attenuated total reflectance-Fourier transform infrared spectroscopy, and scanning electron microscopy was performed in order to confirm the presence of polar, silanol species into the overall apolar structure of the PDMS bulk. Thus, the resultant membrane may provide a more tortuous barrier to permeation, analogous to the stratum corneum.

Bivariate correlation analysis was performed in order to evaluate the predicting capability of both the native and modified PDMS skin mimic. A library of *ex vivo* human skin permeability data was collated from literature, and refined according to the reported experimental procedure. An increase in

correlation was observed between permeability coefficients extracted from literature (K_p^{human}), and experimentally determined permeability coefficients using the plasma modified membrane (K_p^{plasma}) ($R^2 = 0.86$), compared with the native PDMS membrane ($R^2 = 0.75$). Various physicochemical properties of the compounds in the data set were considered, and it was found that the percent reduction in K_p observed was heavily influenced by polar surface area (PSA) ($r = -0.652$, $p = 0.003$ [-0.847, -0.374]).

Furthermore, the compatibility of the plasma modification method used in this work with permeation studies, and the increased chemical reactivity of plasma treated PDMS, renders the work an appropriate platform for the production of more biorelevant surfaces via subsequent wet chemical methods.

References

- Addicks, Flynn, & Weiner. (1987). Validation of a Flow-Through Diffusion Cell for Use in Transdermal Research. *Pharmaceutical Research*, 4(4), 337-341.
- Avdeef. (2012). *Absorption and Drug Development: Solubility, Permeability, and Charge State* (2 ed.). US: Wiley.
- Baba, Ueno, Hashida, & Yamashita. (2017). Quantitative prediction of ionization effect on human skin permeability. *International Journal of Pharmaceutics*, 522(1), 222-233.
- Bartalena, Loosli, Zambelli, & Snedeker. (2012). Biomaterial surface modifications can dominate cell-substrate mechanics: The impact of PDMS plasma treatment on a quantitative assay of cell stiffness. *Soft Matter*, 8(3), 673-681.
- Bartosova, & Bajgar. (2012). Transdermal drug delivery in vitro using diffusion cells. *Current Medicinal Chemistry*, 19(27), 4671-4677.
- Benson, & Watkinson. (2011). *Topical and Transdermal Drug Delivery : Principles and Practice*. Hoboken, NJ, USA: John Wiley & Sons.
- Bhuiyan, & Waters. (2017). Permeation of pharmaceutical compounds through silicone membrane in the presence of surfactants. *Colloids and Surfaces A: Physicochemical and Engineering Aspects*, 516, 121-128.
- Charifson, & Walters. (2014). Acidic and basic drugs in medicinal chemistry: a perspective. *Journal of medicinal chemistry*, 57(23), 9701-9717.
- Chau, Millare, Lin, Upadhyayula, Nuñez, Xu, & Vullev. (2011). Dependence of the quality of adhesion between poly(dimethylsiloxane) and glass surfaces on the composition of the oxidizing plasma. *Microfluidics and Nanofluidics*, 10(4), 907-917.
- Cordeiro, Zschoche, Janke, Nitschke, & Werner. (2009). Functionalization of poly(dimethylsiloxane) surfaces with maleic anhydride copolymer films. *Langmuir*, 25(3), 1509-1517.
- Cronin, Dearden, Gupta, & Moss. (1998). An investigation of the mechanism of flux across polydimethylsiloxane membranes by use of quantitative structure-permeability relationships. *Journal of Pharmacy and Pharmacology*, 50(2), 143-152.
- Da Silva, Zhang, Schelcher, Winter, Guyon, Tabeling, Bonn, & Tatoulian. (2017). Study of the Stability and Hydrophilicity of Plasma-Modified Microfluidic Materials. *Plasma Processes and Polymers*, 14(3), 1-15.
- Degim, Pugh, & Hadgraft. (1998). Skin permeability data: Anomalous results. *International Journal of Pharmaceutics*, 170(1), 129-133.
- Du Plessis, Pugh, Judefeind, & Hadgraft. (2001). The effect of hydrogen bonding on diffusion across model membranes: consideration of the number of H-bonding groups. *European Journal of Pharmaceutical Sciences*, 13(2), 135-141.
- Du Plessis, Pugh, Judefeind, & Hadgraft. (2002a). The effect of the nature of H-bonding groups on diffusion through PDMS membranes saturated with octanol and toluene. *European Journal of Pharmaceutical Sciences*, 15(1), 63-69.
- Du Plessis, Pugh, Judefeind, & Hadgraft. (2002b). Physico-chemical determinants of dermal drug delivery: Effects of the number and substitution pattern of polar groups. *European Journal of Pharmaceutical Sciences*, 16(3), 107-112.
- Faysal, Park, Nguyen, Garcia, & Subramaniam. (2017). Lipid Bilayers Are Long-Lived on Solvent Cleaned Plasma-Oxidized poly(dimethyl)siloxane (ox-PDMS). *PLOS ONE*, 12(1), 1-16.
- Feldstein, Raigorodskii, Iordanskii, & Hadgraft. (1998). Modeling of percutaneous drug transport in vitro using skin-imitating Carbosil membrane. *Journal of Controlled Release*, 52(1-2), 25-40.
- Gunda, Singh, Norman, Kaur, & Mitra. (2014). Optimization and characterization of biomolecule immobilization on silicon substrates using (3-aminopropyl)triethoxysilane (APTES) and glutaraldehyde linker. *Applied Surface Science*, 305, 522-530.
- Hirata, & Ichiki. (2008). Introduction of Amino Groups on Poly(dimethylsiloxane) Surface Using Low-pressure Nitrogen-based Inductively Coupled Plasma. *Journal of Photopolymer Science and Technology*, 21(5), 705-710.

- Hu, Ma, Zhang, & Wang. (2014). Small molecule - Folic acid modification on nanopatterned PDMS and investigation on its surface property. *Biomedical Microdevices*, 16(3), 487-497.
- Kaczorowski, Szymanski, Batory, & Niedzielski. (2015). Effect of plasma treatment on the surface properties of polydimethylsiloxane. *Journal of Applied Polymer Science*, 132(11), 41635.
- Kuddannaya, Chuah, Lee, Menon, Kang, & Zhang. (2013). Surface chemical modification of poly(dimethylsiloxane) for the enhanced adhesion and proliferation of mesenchymal stem cells. *ACS Applied Materials & Interfaces*, 5(19), 9777-9784.
- Leclerc, Duval, Pezron, & Nadaud. (2009). Behaviors of liver and kidney explants from chicken embryos inside plasma treated PDMS microchannels. *Materials Science and Engineering: C*, 29(3), 861-868.
- Lee, Conradi, & Shanmugasundaram. (2010). Development of an in silico model for human skin permeation based on a Franz cell skin permeability assay. *Bioorganic and Medicinal Chemistry Letters*, 20(1), 69-73.
- Lee, Hong, Park, Lee, & Kim. (2017). A simple fabrication process for stepwise gradient wrinkle pattern with spatially-controlled wavelength based on sequential oxygen plasma treatment. *Microelectronic Engineering*, 176, 101-105.
- Li, Wang, & Shen. (2012). Chemical modification on top of nanotopography to enhance surface properties of PDMS. *Surface and Coatings Technology*, 206(8-9), 2161-2167.
- Maheshwari, Kottantharayil, Kumar, & Mukherji. (2010). Long term hydrophilic coating on poly(dimethylsiloxane) substrates for microfluidic applications. *Applied Surface Science*, 257(2), 451-457.
- Mata, Fleischman, & Roy. (2005). Characterization of polydimethylsiloxane (PDMS) properties for biomedical micro/nanosystems. *Biomedical microdevices*, 7(4), 281-293.
- Miki, Ichitsuka, Yamada, Kimura, Egawa, Seki, Juni, Ueda, & Morimoto. (2015). Development of a membrane impregnated with a poly(dimethylsiloxane)/poly(ethylene glycol) copolymer for a high-throughput screening of the permeability of drugs, cosmetics, and other chemicals across the human skin. *European Journal of Pharmaceutical Sciences*, 66, 41-49.
- Moss, Gullick, & Wilkinson. (2015). *Predictive Methods in Percutaneous Absorption*. Berlin: Springer.
- Nania, Matar, & Cabral. (2015). Frontal vitrification of PDMS using air plasma and consequences for surface wrinkling. *Soft matter*, 11(15), 3067-3075.
- Owen, & Dvornic. (2012). *Silicone Surface Science* (Vol. 4). Dordrecht: Springer Netherlands.
- Palm, Stenberg, Luthman, & Artursson. (1997). Polar Molecular Surface Properties Predict the Intestinal Absorption of Drugs in Humans. *Pharmaceutical Research*, 14(5), 568-571.
- Pandit, & Yeung. (2010). Failure of oxygenation *Core Topics in Critical Care Medicine* (pp. 232).
- Potts, & Guy. (1992). Predicting skin permeability. *Pharmaceutical Research*, 9(5), 663-669.
- Pranitha, & Lakshmi. (2014). Towards a correlation between polar surface area of drugs with Ex-vivo transdermal flux variability. *Iranian Journal of Pharmaceutical Sciences*, 10(2), 47-60.
- Provin, Nicolas, Grégoire, & Fujii. (2015). A Microfluidic Diffusion Cell for Fast and Easy Percutaneous Absorption Assays. *Pharmaceutical Research*, 32(8), 2704-2712.
- Sharma, Dhayal, Govind, Shivaprasad, & Jain. (2007). Surface characterization of plasma-treated and PEG-grafted PDMS for micro fluidic applications. *Vacuum*, 81(9), 1094-1100.
- Sinkó, Garrigues, Balogh, Nagy, Tsinman, Avdeef, & Takács-Novák. (2012). Skin-PAMPA: A new method for fast prediction of skin penetration. *European Journal of Pharmaceutical Sciences*, 45(5), 698-707.
- Uchida, Kadhum, Kanai, Todo, Oshizaka, & Sugibayashi. (2015). Prediction of skin permeation by chemical compounds using the artificial membrane, Strat-M™. *European Journal of Pharmaceutical Sciences*, 67, 113-118.
- Vesel, Mozetic, & Zalar. (2008). XPS characterization of PTFE after treatment with RF oxygen and nitrogen plasma. *Surface and Interface Analysis*, 40(3-4), 661-663.
- Vladkova. (2013). *Surface Engineering of Polymeric Biomaterials* (Vol. 1). Shropshire: Ismithers Rapra.

- Wagner, Kostka, Lehr, & Schaefer. (2003). pH profiles in human skin: influence of two in vitro test systems for drug delivery testing. *European Journal of Pharmaceutics and Biopharmaceutics*, 55(1), 57-65.
- Walker, Hulme, Rippon, Walmsley, Gunnigle, Lewin, & Winsey. (1997). In vitro model(s) for the percutaneous delivery of active tissue repair agents. *Journal of Pharmaceutical Sciences*, 86(12), 1379-1384.
- Waters, & Bhuiyan. (2016). Ionisation effects on the permeation of pharmaceutical compounds through silicone membrane. *Colloids and Surfaces B: Biointerfaces*, 141, 553-557.
- Waters, Dennis, Bibi, & Mitchell. (2013). Surfactant and temperature effects on paraben transport through silicone membranes. *Colloids and Surfaces B: Biointerfaces*, 108, 23-28.
- Williams, Wilson, & Rhodes. (2004). Stability of plasma-treated silicone rubber and its influence on the interfacial aspects of blood compatibility. *Biomaterials*, 25(19), 4659-4673.
- Wolf. (2012). *Atmospheric Pressure Plasma for Surface Modification* (Vol. 1. Aufl.;1;). Massachusetts: Wiley-Scrivener.
- Wood, Brown, & Jones. (2012). Understanding heat facilitated drug transport across human epidermis. *European Journal of Pharmaceutics and Biopharmaceutics*, 81(3), 642-649.
- Wu, Yuan, & Ding. (2011). Effect of polydimethylsiloxane surfaces silanized with different nitrogen-containing groups on the adhesion progress of epithelial cells. *Surface and Coatings Technology*, 205(10), 3182-3189.
- Yang, & Yuan. (2016). Investigation on the mechanism of nitrogen plasma modified PDMS bonding with SU-8. *Applied Surface Science*, 364, 815-821.
- Zhang, Abraham, & Liu. (2017). An equation for the prediction of human skin permeability of neutral molecules, ions and ionic species. *International Journal of Pharmaceutics*, 521(1-2), 259-266.
- Zhang, Chen, Scriba, Abraham, Fahr, & Liu. (2012). Human skin permeation of neutral species and ionic species: Extended linear free-energy relationship analyses. *Journal of Pharmaceutical Sciences*, 101(6), 2034-2044.

Chapter 4 The Effect of Nitrogen Plasma Treatment on the Permeation of Pharmaceutical Compounds through Poly(dimethylsiloxane)

4.1. Introduction

The suitability of poly(dimethylsiloxane) (PDMS) substrates in cell culture applications and tissue engineering has generated significant interest in plasma technologies and modification, with benefits ranging from increased cell adhesion, to controlled differentiation in three-dimensional tissues. Nitrogen-containing plasmas are of particular interest to such studies, providing a simple route to aminated surfaces which previously may display poor reactivity to biomolecules. The use of nitrogen-containing plasmas simultaneously allows for the introduction of functional groups typical of proteins (Salerno *et al.*, 2009), along with groups suitable for covalent coupling with peptides, or extracellular matrix proteins such as collagen, resulting in a more accurate representation of the micro-environment *in vivo* (Xu *et al.*, 2011).

Work by Yang *et al.* used an N₂ plasma treatment to enhance the reactivity of PDMS towards an epoxy group-containing photoresist for use in microfluidic channels. The group confirmed successful PDMS amination using ATR-FTIR and X-ray photoelectron spectroscopy (XPS). A peak at 399.7 eV in the high resolution N 1s XPS spectrum of N₂ plasma treated PDMS was attributed to surface amine functionalities. A peak at 286.4 eV in the high resolution C 1s spectra, along with a signal at 1100 – 1040 cm⁻¹ in the ATR-FTIR spectrum, led the group to conclude that amine functionalisation had occurred at carbon atoms in the polysiloxane structure (Yang *et al.*, 2016). Williams *et al.* performed similar work, aiming to control the thrombogenicity of PDMS-based medical devices. The authors compared the surface chemistry of medical grade PDMS following plasma treatments performed using O₂, Ar, N₂, and NH₃ process gases. Regarding both the N₂ and NH₃ plasma treatments, four new binding energies were observed in the C 1s spectra compared with the untreated polymer, indicating the presence of similar surface functionalities. In both cases, the signal consisting of the greatest atomic percent was that at a binding energy of 286 eV, which the authors assigned as either primary, or

secondary, amine groups. Of interest to this project, the group stored the membranes in phosphate buffered saline for one month and noted the presence of all four binding energies observed previously, with around three-quarters of the surface amine groups still present (Williams *et al.*, 2004).

Nitrogen containing plasmas are of particular interest to this project, since such processes are known to introduce amine groups, which are highly abundant in the stratum corneum proteinaceous environment, and may provide suitable sites for the covalent coupling of biomolecules. In the previous chapter, the introduction of primarily silanol groups to the surface of PDMS via an air plasma treatment was found to reduce the permeation of pharmaceutical compounds. Upon the employment of the resultant membrane as a skin mimic in permeation studies, an increase correlation with a self-collated library of literature permeability coefficients obtained using excised human skin was observed. In this chapter, similar plasma treatments using an N₂ process gas have been performed in order to observe the effect of N₂ plasma treatments on the permeation of pharmaceutical compounds.

4.2. Results and Discussion

4.2.1. Membrane Characterisation

4.2.1.1. Attenuated Total Reflectance-Fourier Transform Infrared Spectroscopy (ATR-FTIR)

ATR-FTIR analysis was performed, in order to confirm the surface chemical composition of PDMS following N₂ plasma treatment, and permit comparison with both native PDMS, and PDMS following air plasma treatment. Data corresponding to N₂ plasma treated PDMS is presented in Table 4.1, along with data corresponding to native PDMS, as presented previously (Table 3.2).

Table 4.1 ATR-FTIR of native PDMS and PDMS following N₂ plasma treatment.

Assignment	ν_{\max} (cm ⁻¹)	
	Native PDMS	N ₂ plasma treated PDMS
$\nu_s(\text{CH}_3)$	2962.3	2962.1
$\delta_{\text{as}}(\text{CH}_3)$	1412.6	1412.4
$\delta_s(\text{CH}_3)$	1258.2	1258.2
Si-O-Si	1006.3	1005.7
O-SiCH ₃	786.2	785.1
C-SiCH ₃	701.4	701.2

The presence of surface methyl groups is confirmed by a symmetrical stretching vibration of the CH₃ group at 2962.1 cm⁻¹, and the asymmetric and symmetric deformation of the CH₃ group at 1412.4 and 1258.2 cm⁻¹, respectively. The Si-O-Si stretching vibration is observed at 1005.7 cm⁻¹, along with absorptions at 785.1 and 701.2 cm⁻¹, confirming the presence of the O-SiCH₃ and C-SiCH₃ groups, respectively. As found previously, no additional adsorptions were observed associated with the surface functionalisation of PDMS, thus, the data was further supplemented with that obtained using X-ray photoelectron spectroscopy.

4.2.1.2. X-ray Photoelectron Spectroscopy (XPS)

As discussed previously (Section 3.2.1.3), quantitative elemental composition of the PDMS surface pre- and post-modification was determined using XPS survey scans (Figure 4.1). The O 1s, C 1s, Si 2p, and N 1s orbitals were identified at binding energies circa 530 eV, 282 eV, 100 eV, and 399 eV, respectively, with data subsequently presented in the form of atomic percent (%) (Table 4.2). Data corresponding to native and air plasma treated PDMS, determined previously (Table 3.3), is also summarised in Table 4.2 to enable facile comparison with previous data.

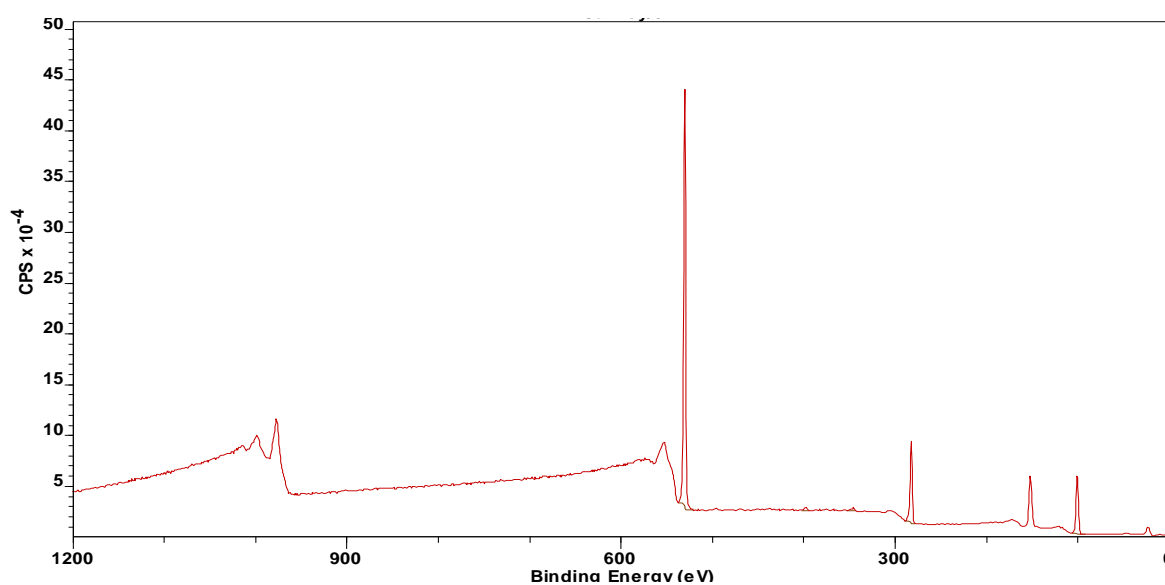


Figure 4.1 XPS survey scan of N₂ plasma treated PDMS.

Table 4.2 Atomic percent (%) of oxygen, nitrogen, carbon, and silicon at the surface of native, air plasma treated, and N₂ plasma treated PDMS taken from XPS survey scans.

Membrane	Sample	Atomic percent (%)			
		O	N	C	Si
Native PDMS	1	23.17	< 0.1	47.83	29.00
	2	22.79	< 0.1	48.92	28.28

Table 4.2 continued.

Membrane	Sample	Atomic percent (%)			
		O	N	C	Si
Air plasma treated PDMS	1	44.80	0.56	23.22	31.42
	2	44.11	0.61	24.49	30.79
Nitrogen plasma treated PDMS	1	44.49	0.87	25.86	28.44
	2	44.20	0.83	26.21	28.45

A decrease in the atomic percent of carbon, from 47.83 – 48.92 % in native PDMS to 25.86 – 26.21 % following N₂ plasma treatment, is consistent with the nature of plasma treatments and findings published in other work (Williams *et al.*, 2004). Unexpectedly, this was accompanied by a considerable increase in atomic percent of oxygen, from 22.79 – 23.17 % in native PDMS, to 44.11 – 44.80 % in N₂ treated PDMS, and is similar to that observed following air plasma treatment (44.20 – 44.49 %). A small increase in atomic percent of nitrogen present following N₂ plasma treatment (0.83 – 0.87 %) was observed, in comparison to that observed following air plasma treatment (0.56 – 0.61 %) (Table 4.2).

High resolution XPS spectra of the C 1s, N 1s, and Si 2p orbitals were also obtained and are presented in Figure 4.2, Figure 4.3, and Figure 4.4, respectively. Three signals were identified in the high resolution XPS spectrum on the C 1s orbital in N₂ plasma treated PDMS (Figure 4.2), at binding energies of 285.00 eV, 286.62 eV, and 288.43 eV, comparable to those obtained following air plasma modification of PDMS (Figure 3.7). As found previously, the signal at 285.00 corresponds to that of C-H bonds, and the signal at 288.43 corresponds to carbonyl containing units, i.e. C=O or O-C=O (Vesel *et al.*, 2008; Yang *et al.*, 2016). Literature reports the binding energy of the C-N group to occur in the range of 285.5-286.4 eV (Vesel *et al.*, 2008; Yang *et al.*, 2016), close to the binding energy observed at 286.62 eV in this work. On the basis that multiple authors have observed the formation of primary amine groups at the surface of PDMS following N₂ plasma treatments, the signal at this binding

energy may be attributed to the formation of primary amines (Williams *et al.*, 2004). The binding energies of C-O and C=N groups are reported to be markedly similar, at 285.5 eV, and 285.5 eV-286.6 eV (Vesel *et al.*, 2008; Yang *et al.*, 2016), respectively, and may suggest that the signals associated with these functionalities are unresolvable, particularly since nitrogen-containing groups represent, at most, 0.87 % of groups at the surface in this instance.

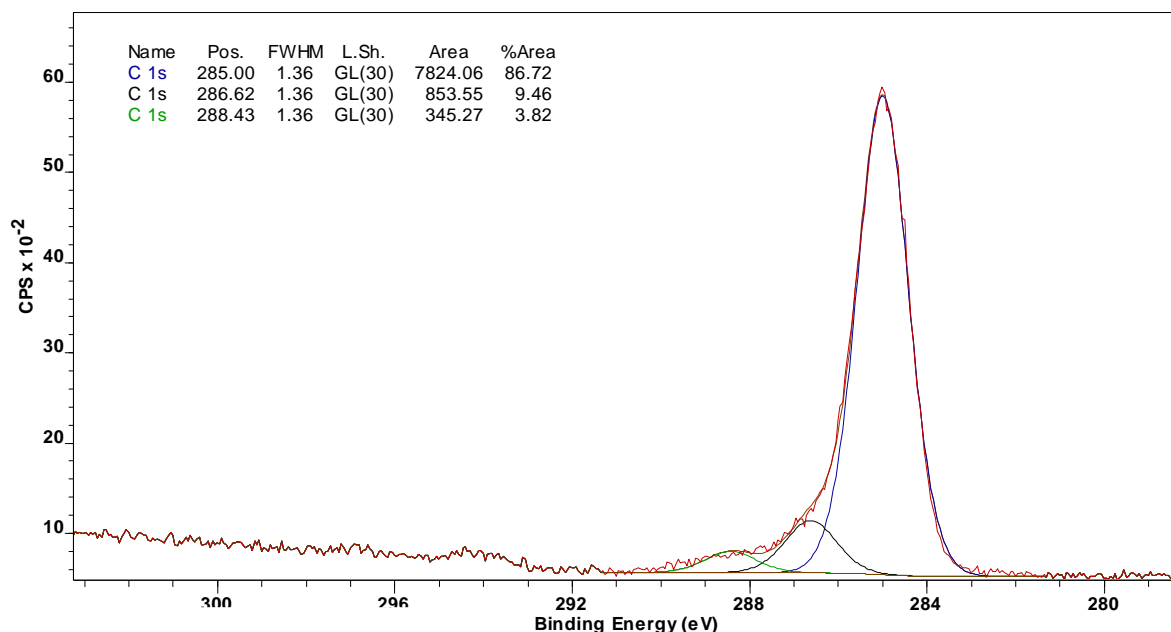


Figure 4.2 High resolution XPS spectrum of the C 1s orbital in N₂ plasma treated PDMS.

Only one signal was observed in the high resolution XPS spectrum of the N 1s orbital in N₂ plasma treated PDMS (Figure 4.3), similar to spectra of the N 1s orbital obtained following air plasma treatment (Figure 3.9). The signal was observed at a lower binding energy of 400.23 eV, compared with a binding energy of 400.79 eV observed following air plasma treatment. A reduction in binding energy may suggest the presence of fewer electron-withdrawing groups, such as oxygen, attached at the neighbouring carbon atom, and is consistent with the presence of amine groups at the surface as opposed to amide groups, on par with observations made in other work (Williams *et al.*, 2004).

The oxidative nature of N₂ plasma treatments was somewhat unanticipated given the known composition of the process gas i.e. 99.998 % N₂ (oxygen free), and numerous reports of N₂ plasmas resulting in the formation of PDMS surfaces displaying amine group functionality (Vesel *et al.*, 2008; Williams *et al.*, 2004; Yang *et al.*, 2016). Other authors note the occurrence of surface oxidation during

N₂ plasma treatment, and attribute this to the presence of residual air and/or H₂O in the plasma chamber, or oxygen entrapped within the polymer (Egitto *et al.*, 2006; Owen *et al.*, 1994). The findings in this work appear to match those by Owen *et al.* whom observed a surface atomic percent of oxygen of 48.7 % following the radiofrequency N₂ plasma treatment of PDMS (Owen *et al.*, 1994).

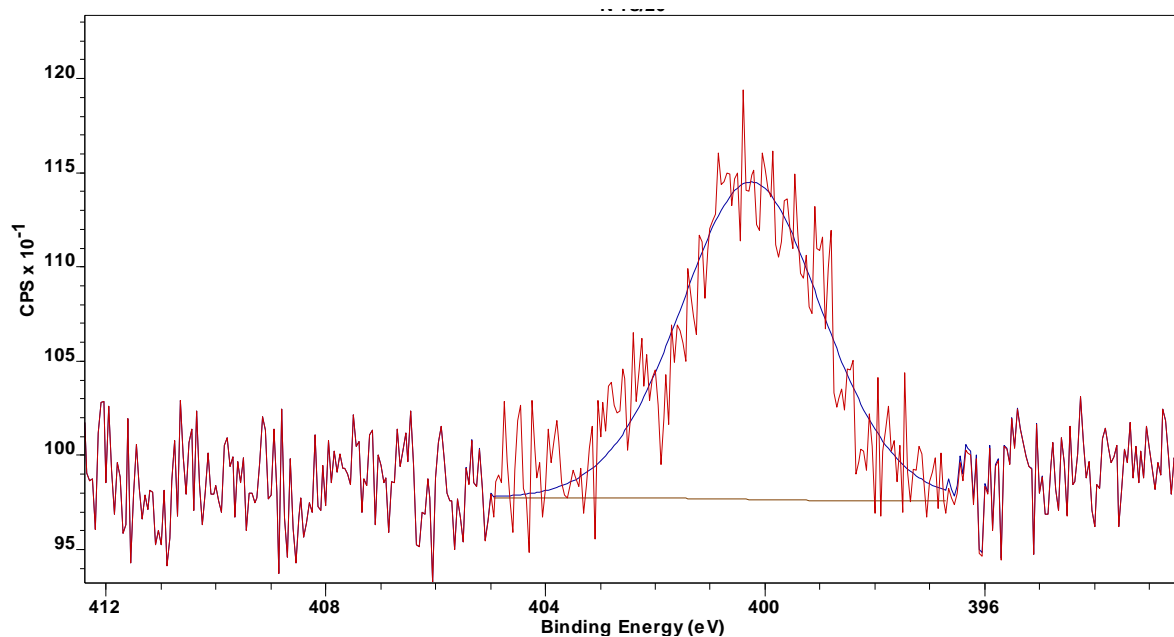


Figure 4.3 High resolution XPS spectrum of the N 1s orbital in N₂ plasma treated PDMS.

Four signals were identified in the high resolution XPS spectrum of the Si 2p orbital in N₂ plasma treated PDMS (Figure 4.4), at binding energies of 102.34 eV, 102.97 eV, 103.61 eV, and 104.24 eV. Based on the observed oxidative nature of the N₂ plasma treatment performed in this work, the presence of two emissions at 103.61 eV and 104.24 eV, with a peak area ratio of 0.5, is unsurprising, and is indicative of the presence of quaternary (Q) siloxane units, in line with previous observations (Figure 3.5).

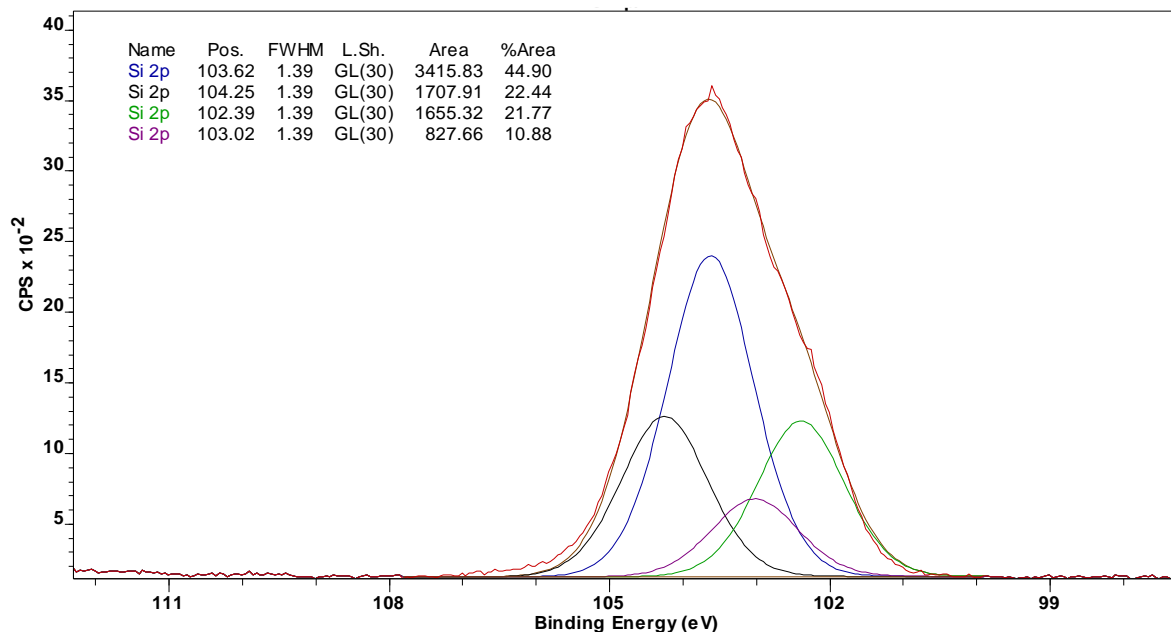


Figure 4.4 High resolution XPS spectrum of the Si 2p orbital in N₂ plasma treated PDMS.

4.2.1.3. Scanning Electron Microscopy

Scanning electron microscopy images of PDMS post-N₂ plasma treatment (Figure 4.5) were collected to facilitate the comparison of the surface morphology of PDMS following N₂ plasma treatment with both native PDMS, and PDMS following air plasma treatment (Figure 3.10). Interestingly, at an N₂ plasma treatment time of 90 seconds, cracking and surface wrinkling is observed to a lesser extent than the corresponding treatment employing air plasma. Further, images were collected following three exposure times (90, 150 and 300 seconds) in order to evaluate the effect of treatment time on surface morphology, and identify any correlation between surface morphology and drug permeation (Figure 4.5).

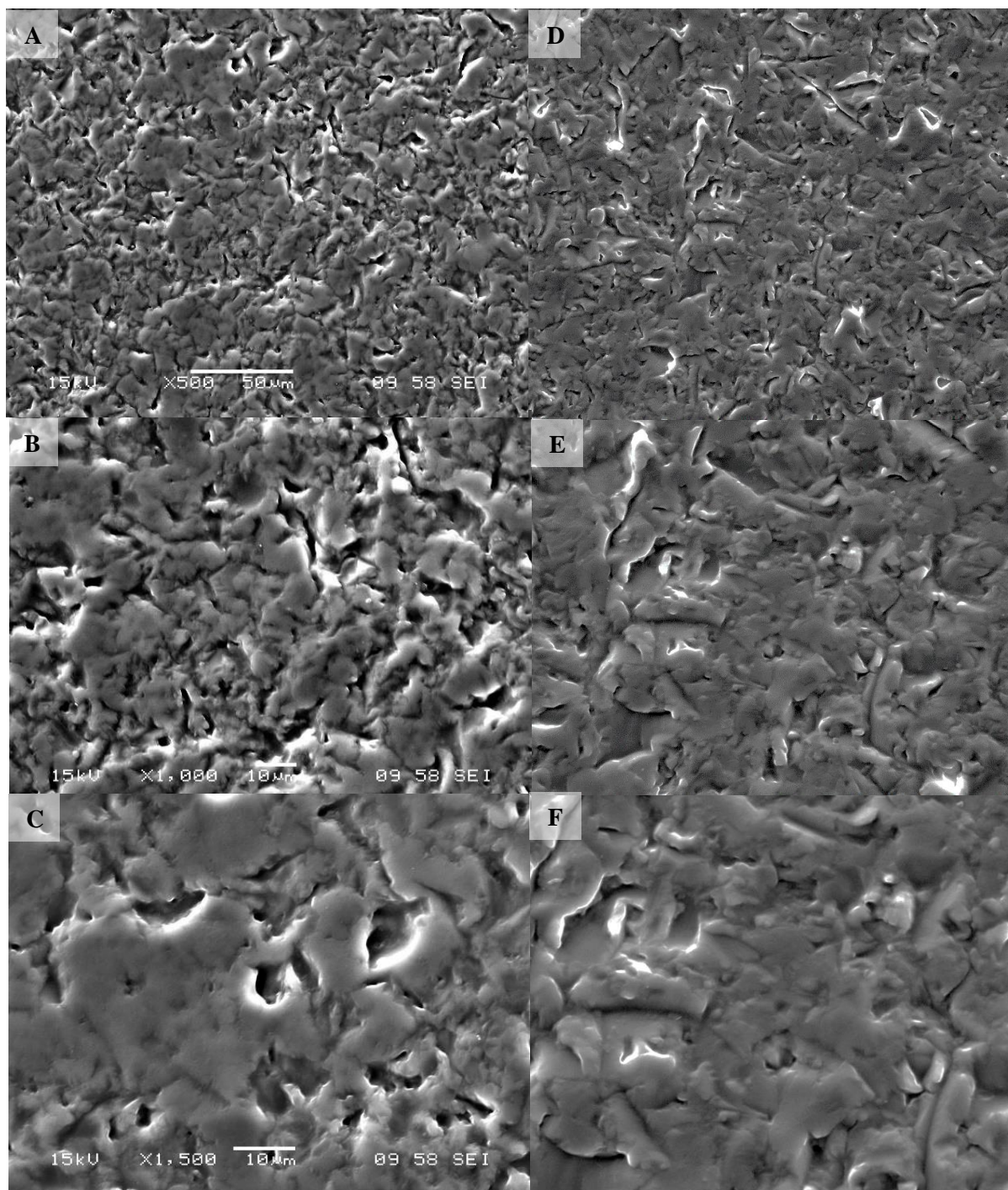


Figure 4.5 Scanning Electron Microscopy images of PDMS following 90 seconds N₂ plasma treatment (A-C, 500 X, 1000 X and 1500 X magnification, respectively) and 150 seconds N₂ plasma treatment (D-F, 500 X, 1000 X and 1500 X magnification respectively).

Changes in the morphological properties of the polymer are particularly evident at an N₂ plasma treatment time of 300 seconds (Figure 4.6). The polymer surface appears distinctly cracked and wrinkled, in contrast to the surface at the previous treatment times (Figure 4.5). Based on data obtained previously using X-ray photoelectron spectroscopy (Section 4.2.1.2.), this may be attributed to brittle SiO_x layer formation, and increased mechanical strain between the surface and the bulk (Cordeiro *et al.*, 2009; Lee *et al.*, 2017; Nania *et al.*, 2015).

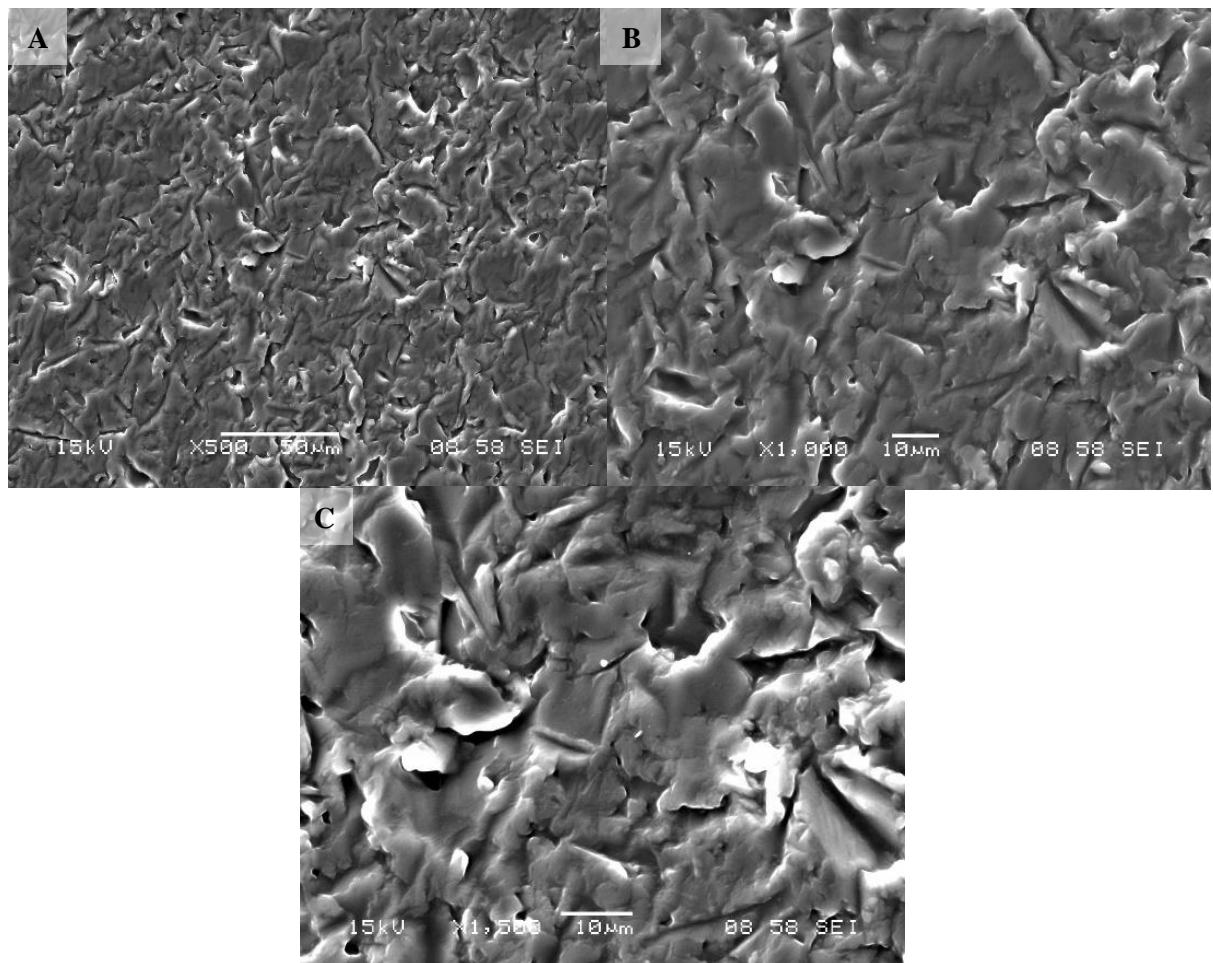


Figure 4.6 Scanning Electron Microscopy images of PDMS following 300 seconds N₂ plasma treatment at 500 X (A), 1000 X (B) and 1500 X (C) magnification.

4.2.2. Permeation study

4.2.2.1. Treatment time determination

Previous work (Chapter Three) demonstrated the potential of air plasma treatments to reduce the permeation of pharmaceutical compounds through PDMS, a frequently employed skin mimic with which over-estimations of percutaneous absorption are often observed. However, overestimations in the permeability coefficient were still observed following air plasma treatment; thus, alternative plasma treatments, which may offer the potential to reduce permeation further, and simultaneously introduce biorelevant sites, are of considerable interest to this work. Work by Nania *et al.*, investigating the effect of various experimental parameters on surface wrinkling of glass-elastomer bilayers formed following exposure of PDMS to plasma, found that a plasma process gas consisting of an equimolar mixture of nitrogen and oxygen resulted in slower hydrophilic ‘glassy layer’ formation, in comparison to that obtained using solely oxygen. The authors attributed this to a reduction in kinetics of the surface oxidation reaction, since the concentration of the ‘active species’ was considerably reduced following N₂ introduction (Nania *et al.*, 2015). Such findings suggest that changes in process gas composition may result in a necessity for various plasma treatment times for purposes related to those presented in this thesis.

Initial comparisons between N₂ and air plasma treated PDMS were performed employing two compounds from the previous compound library, namely lidocaine and caffeine (Table 4.3). The former previously displayed a 36.36 % reduction in K_p following plasma treatment, and a 5.5 fold over-estimation in K_p based on comparison with suitable literature data i.e. $K_p^{\text{plasma}}/K_p^{\text{human}}$. The latter displayed no reduction in permeation upon air plasma pre-treatment, and a ratio of 0.95 was observed between K_p^{human} and K_p^{plasma} .

Table 4.3 Steady state flux (J_{ss}) of lidocaine (LID) and caffeine (CAF) through N_2 plasma treated PDMS, at various treatment times.

Compound	Process gas	Plasma treatment time (seconds)	J_{ss} ($\mu\text{g cm}^{-2} \text{min}^{-1}$)
LID	N/A	0	13.34 ± 0.64
	Air	90	8.487 ± 0.456
	N_2	90	10.81 ± 0.56
	N_2	150	5.488 ± 1.034
	N_2	210	6.172 ± 1.359
	N_2	300	11.35 ± 1.61
CAF	N/A	0	0.1908 ± 0.0107
	Air	90	0.2215 ± 0.0300
	N_2	90	0.2023 ± 0.0294
	N_2	150	0.1774 ± 0.0143

A statistically significant difference in the steady state flux (J_{ss}) of lidocaine through PDMS following N_2 and air plasma treatment was observed ($t(4) = -5.573$, $p = 0.005$) (Figure 4.7). The permeation of LID through PDMS appeared to be affected to a lesser extent by an N_2 plasma pre-treatment, in comparison to an air plasma pre-treatment i.e. J_{ss} values of $10.81 \pm 0.56 \mu\text{g cm}^{-2} \text{min}^{-1}$ and $8.487 \pm 0.456 \mu\text{g cm}^{-2} \text{min}^{-1}$, respectively, were obtained. Since a 5.5 fold overestimation in the permeability coefficient of LID was observed previously upon comparison with literature data obtained using epidermal tissue, a major objective of the work presented in this chapter was to further reduce the permeation of pharmaceutical compounds. Thus, the effect of extended N_2 plasma treatment times were also investigated (Table 4.3).

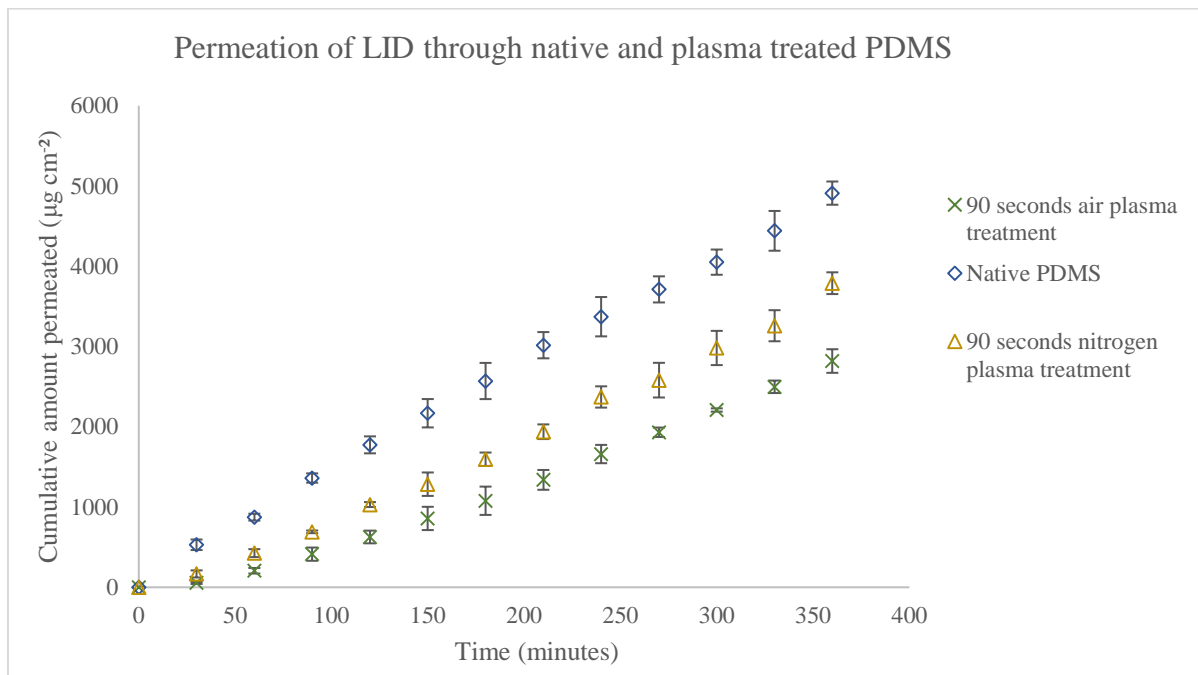


Figure 4.7 Permeation of lidocaine (LID) through native PDMS, and PDMS following a 90 second air and N₂ plasma treatment (mean ± standard deviation, $n = 3$).

Statistically significant differences in steady state flux (J_{ss}) were observed following alterations in the treatment time ($F(3,8) = 19.21$, $p = 0.001$). An increase in N₂ plasma treatment time, from 90 to 150 seconds, resulted in a statistically significant reduction in J_{ss} , from $10.81 \pm 0.56 \mu\text{g cm}^{-2} \text{min}^{-1}$ to $5.49 \pm 1.03 \mu\text{g cm}^{-2} \text{min}^{-1}$ ($p = 0.003$). A further 60 second extension in treatment time to 210 seconds resulted in no statistically significant difference in J_{ss} from the previous treatment time i.e. 150 seconds ($p = 0.898$). A further increase in N₂ plasma treatment time to 300 seconds resulted in a statistically significant increase compared with the previous treatment time, i.e. from $6.17 \pm 1.36 \mu\text{g cm}^{-2} \text{min}^{-1}$ to $11.35 \pm 1.61 \mu\text{g cm}^{-2} \text{min}^{-1}$ ($p = 0.003$). There was no statistically significant difference in the J_{ss} of LID through PDMS following a 300 second N₂ plasma treatment, compared with that obtained following a 90 second N₂ plasma treatment ($p = 0.944$).

Permeation data correlate well with the findings of scanning electron microscopy analysis (Figure 4.5 and Figure 4.6); statistically significant decreases in permeation were observed at intermediate treatment times i.e. 90 and 150 seconds, followed by increases in permeation at extended treatment times i.e. 300 seconds, consistent with a decrease in integrity of the membrane. These findings are also

consistent with findings in previous work regarding SiO_x layer formation. Smith *et al.* noted that the uppermost surface of PDMS is subject to the greatest plasma exposure, resulting in a superficial silica-like layer, which provides protection to the underlying substrate. This superficial protective layer results in only a finite modified-layer thickness being achievable, hypothesised to be in the range of 8-10 nm (Owen *et al.*, 1994). Longer treatment times have also been reported to be accompanied by increased cracking, as seen in Figure 4.6 (Juárez-Moreno *et al.*, 2015). Applying these observations to the data presented in Table 4.3, it would appear that maximum layer thickness occurs between an N₂ plasma treatment time of 90 and 150 seconds, above which the effect of crack formation on the permeation of pharmaceutical compounds supersedes that of hydrophilic layer formation. These findings correlate well with data presented previously with a different permeant, namely ibuprofen (Table 3.4). Thus, a treatment time of 150 seconds was selected as the most appropriate for this work, above which, the permeation of pharmaceutical compounds may become controlled by structural damage to the membrane.

The effect of a 150 second N₂ plasma treatment on the permeation of another pharmaceutical compound, namely caffeine, was also investigated (Table 4.3). Interestingly, caffeine displays no statistically significant differences in J_{ss}, regardless of the duration of plasma treatment ($F(2,6) = 1.191$, $p = 0.084$). Considering this observation in the context of the plasma modification process, it may be taken that the permeation of caffeine is unhindered by hydrophilic layer introduction, independent of the hydrophilic layer thickness i.e. the permeation of caffeine is controlled by permeation through the underlying hydrophobic bulk substrate. Similar results were also obtained previously following air plasma treatment (Table 3.8). In order to further understand these findings, along with the effect of further physicochemical properties on the permeation of pharmaceutical compounds, permeation studies employing a wider range of penetrants should be performed.

4.2.2.2. Permeability Coefficient (K_p) Determination

Permeation experiments were performed on a subset of pharmaceutical compounds employed previously. The body of compounds displayed a MW range 121.12 – 234.34 g mol⁻¹, a log₁₀ P range of

-0.13 – 3.63, a $\log_{10} D$ range of 0.11 – 3.18, and represented both anionic and cationic charge states. The percentage reduction in K_p observed previously, following the air plasma treatment of PDMS, was found to correlate well with the polar surface area (PSA) of the penetrant ($r = -0.652$, $p = 0.003$ [-0.847, -0.374]). The percentage reduction in K_p appeared variable for each compound within two homologous series', namely alkyl 4-aminobenzoates and alkyl 4-hydroxybenzoates. It was hypothesised that, since the PSA of each compound within each series was similar, this variability may be attributed to limited control of the chemical composition of the process gas. Thus, the two homologous series' were included in the body of compounds used for this work.

It was noted in previous work that the maintenance of sink conditions in the static cell was problematic (Table 3.7), in particular for high $\log_{10} P$ and $\log_{10} D$ compounds, for which flux through the lipophilic membrane is high, but solubility in aqueous receptor fluids is low. Thus, the static Franz cell type system was substituted for a flow-through type system (Figure 2.1). This would also circumvent the need for solubility enhancers, such as surfactants, which have been shown to influence permeation through silicone membranes (Bhuiyan *et al.*, 2017; Waters *et al.*, 2013), and may introduce artefacts to the data.

Preliminary temperature measurements found the temperature distributions throughout the two cell types to vary. It was found that, with the glass, non-jacketed Franz type cells, a water bath temperature of 32.9 ± 0.1 °C maintained a membrane temperature of 31.7 ± 0.4 °C, in line with the recommendations made by OECD Guideline 428 (32 ± 1 °C). In order to maintain a comparable membrane temperature in the flow-through type system (31.5 ± 0.2 °C), a water circulating temperature of 35.1 ± 0.5 °C, and a temperature of 34.1 ± 0.1 °C at the point of contact between the cell and the heater block was required.

Further, temperature measurements were performed across the donor chambers. The donor chamber temperature varied by up to 1.6 °C from the closest point in contact with the membrane to the furthest in the Franz cell, i.e. the height of the donor solution in the chamber, and by 2.4 °C in the flow through type system. For this reason, permeation experiments through native PDMS were repeated not only for

compounds shown to yield receptor chamber concentrations $\geq 10\%$ (Table 3.7), but for all compounds chosen in this study. Subsequently, comparisons between native and plasma treated PDMS were only performed between data gathered on the same cell system. An international study using quasi-standardised methods, aiming to identify sources of variation in diffusion cell studies, found a fourfold difference in the average flux of methyl paraben through silicone membrane between laboratories. The study also identified statistically significant differences in flux values obtained using static and flow-through cells ($\alpha = 0.05$). The authors noted that these differences could be attributed to differences in the precise membrane temperature, despite general control of the diffusion cell temperature (Chilcott *et al.*, 2005). The effect of variation in temperature regulation protocols is demonstrated in Figure 4.8, using two pharmaceutical compounds, namely risocaine (PAB) and butyl paraben (BP). ‘Temperature unregulated’ refers to the scenario in which the circulating water bath temperature was maintained at 32.0 °C, i.e. general control of the diffusion cell temperature. ‘Temperature regulated’ refers to the scenario in which the membrane temperature was measured using a thermocouple, and the circulating water bath temperature was adjusted accordingly to obtain a suitable precise membrane temperature i.e. 31.5 ± 0.2 °C.

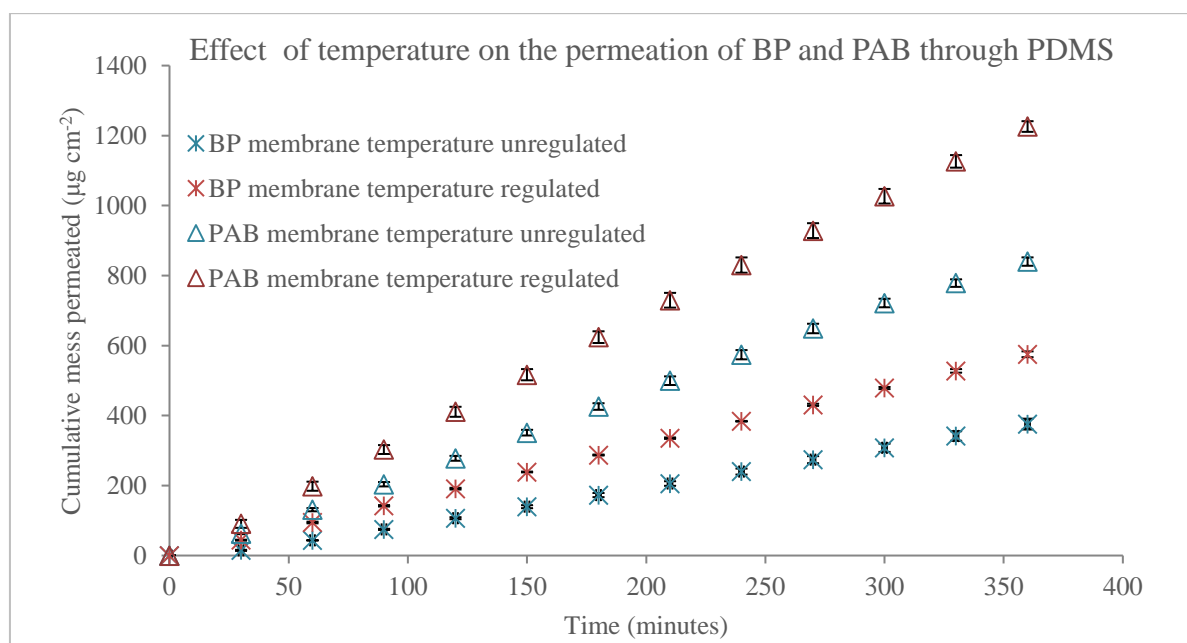


Figure 4.8 Effect of temperature on the permeation of butyl paraben (BP) and risocaine (PAB) through native PDMS.

Statistically significant differences in steady state flux (J_{ss}) were obtained for each mode of temperature regulation in the case of both risocaine ($t(4) = -37.28$, $p = < 0.001$), and butyl paraben ($t(4) = -21.11$, $p = < 0.001$) i.e. values of J_{ss} were significantly lower when the circulating water temperature was 32 °C, in comparison to 35 °C. The data reaffirms remarks made by other authors, advising that data comparisons should preferentially be performed using smaller, more standardised bodies of permeation data, since the diffusion cell types, dimensions, and subsequently, temperature distributions, are known to vary (Ng *et al.*, 2010; Provin *et al.*, 2015; Sinkó *et al.*, 2012). Values of steady state flux (J_{ss}), along with permeability coefficients (K_p) were obtained for a further nine compounds, employing a water circulating temperature of 35 °C, and are presented in Table 4.4.

Table 4.4 Steady state flux (J_{ss}) and permeability coefficient (K_p) of methyl paraben (MP), ethyl paraben (EP), propyl paraben (PP), butyl paraben (BP), methyl 4-aminobenzoate (MAB), benzocaine (EAB), risocaine (PAB), butamben (BAB), lidocaine (LID), caffeine (CAF) and benzoic acid (BA) through native and N₂ plasma treated PDMS (mean ± standard deviation, 4 sig.fig., $n = 3$).

Compound	J_{ss} ($\mu\text{g cm}^{-2} \text{min}^{-1}$)		K_p ($\times 10^{-4} \text{cm min}^{-1}$)	
	Native	N ₂ Plasma	Native	N ₂ Plasma
MP	1.355 ± 0.080	0.7565 ± 0.0143	4.646 ± 0.395	2.593 ± 0.290
EP	1.648 ± 0.033	1.097 ± 0.094	13.49 ± 0.82	8.978 ± 0.849
PP	1.560 ± 0.054	1.131 ± 0.079	31.25 ± 1.03	22.65 ± 1.40
BP	1.603 ± 0.015	1.238 ± 0.235	52.34 ± 0.43	40.43 ± 6.64
MAB	4.585 ± 0.126	4.326 ± 0.028	22.21 ± 0.99	20.95 ± 0.79
EAB	5.088 ± 0.074	2.462 ± 0.161	42.12 ± 2.81	20.38 ± 1.77
PAB	3.439 ± 0.037	2.280 ± 0.139	56.64 ± 1.25	37.56 ± 2.12
BAB	1.819 ± 0.052	0.8424 ± 0.1190	101.9 ± 3.7	84.24 ± 0.12
LID	16.40 ± 0.42	6.271 ± 0.237	41.75 ± 1.05	15.93 ± 0.54

Table 4.4 continued.

Compound	J_{ss} ($\mu\text{g cm}^{-2} \text{min}^{-1}$)		K_p ($\times 10^{-4} \text{cm min}^{-1}$)	
	Native	N_2 Plasma	Native	N_2 Plasma
CAF	0.2022 ± 0.0044	0.1969 ± 0.0122	0.0906 ± 0.0096	0.0882 ± 0.0104
BA	8.970 ± 0.695	3.879 ± 0.348	10.48 ± 0.71	4.533 ± 0.356

K_p values through native PDMS using the flow-through type system were found to correlate well with those obtained previously using the static, Franz type system (Table 3.8) ($r = 0.976$, $p < 0.001$, [0.885, 0.997]). The percent reduction in the permeability coefficient (K_p) following N_2 plasma treatment was calculated according to Equation 3.2, and is presented in Table 4.5, along with the percentage reduction in K_p following air plasma treatment, obtained previously (Table 3.8).

Table 4.5 Percent reduction in the permeability coefficient (K_p) of methyl paraben (MP), ethyl paraben (EP), propyl paraben (PP), butyl paraben (BP), methyl 4-aminobenzoate (MAB), benzocaine (EAB), risocaine (PAB), butamben (BAB), benzoic acid (BA), lidocaine (LID), and caffeine (CAF) following air and N_2 plasma treatment.

Compound	Mean percent K_p reduction following N_2 plasma treatment (%)	Mean percent K_p reduction following air plasma treatment (%)
MP	44.19	19.66
EP	33.45	18.48
PP	27.52	33.63
BP	22.76	14.42
MAB	5.67	23.73
EAB	51.61	-3.18
PAB	33.69	-0.49
BAB	17.33	18.83
LID	61.84	36.36

Table 4.5 continued

Compound	Mean percent K_p reduction following N_2 plasma treatment (%)	Mean percent K_p reduction following air plasma treatment (%)
CAF	2.88	-28.25
BA	56.75	45.20

Notable increases in the percent reduction in K_p were observed for seven of the eleven compounds i.e methyl paraben (MP), ethyl paraben (EP), butyl paraben (BP), benzocaine (EAB), risocaine (PAB), lidocaine (LID) and benzoic acid (BA), with two further compounds displaying reductions on par with those observed during air plasma treatment i.e. propyl paraben (PP) and butamben (BAB). Although an increase in the percent reduction in K_p for caffeine (CAF) was observed, no statistically significant differences in permeation were observed with regards to either air plasma treatment (Table 3.6), or N_2 plasma treatment ($F(2,6) = 1.191, p = 0.084$). The most notable reduction in K_p was observed with LID (Figure 4.9), for which a 61.84 % reduction in K_p was observed, almost twice that observed following air plasma treatment.

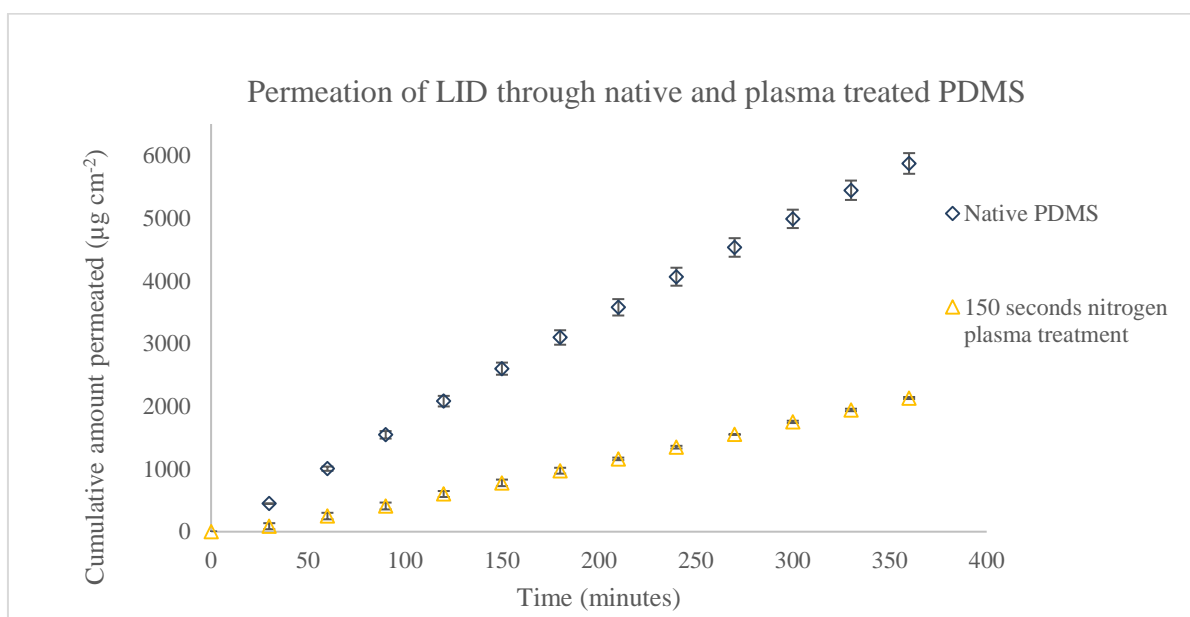


Figure 4.9 Permeation of lidocaine (LID) through native PDMS, and PDMS following a 150 second N_2 plasma treatment (mean \pm standard deviation, $n = 3$).

The pH of the donor solution was measured for each compound, as previously (Appendix 11), and was found to not differ from that obtained in previous work, with respect to each compound. Thus, the physicochemical properties of permeants presented in Table 3.9 were considered suitable descriptors for correlation analysis. As previously undertaken, bivariate correlation analysis was performed between the percent reduction in K_p , and the physicochemical data presented in Table 3.9. The most extensive correlation was found between the mean reduction in K_p (%) and polar surface area (PSA). Pearson's correlation coefficient ($r = -0.739$, $p = 0.009$, $[-0.973, -0.026]$) indicated a large effect of PSA on the reduction in K_p observed, significant at both the $\alpha = 0.05$ and $\alpha = 0.01$ level. Further, 54.6 % of the variance in the mean reduction in K_p (%) can be accounted for by PSA ($R^2 = 0.546$). These results are somewhat unsurprising, given the previous correlation observed between PSA and the percent reduction in K_p ($r = -0.652$, $p = 0.003$ $[-0.847, -0.374]$), and the similarities in the surface chemical composition of air plasma treated and N_2 plasma treated PDMS (Sections 3.2.1 and 4.2.1). The correlation observed here indicates a large, negative dependence of the reduction in K_p on the PSA, indicating that the permeation of high PSA compounds through PDMS is less effected by an N_2 plasma pre-treatment in comparison to that of low PSA compounds.

In contrast to data obtained using an air plasma treatment, a statistically significant bivariate correlation was observed between the percent reduction in K_p and percent ionisation ($r = 0.630$, $p = 0.038$, $[0.047, 0.873]$). The positive correlation coefficient indicates that greater reductions in K_p were observed with compounds displaying a greater extent of ionisation. In this dataset, the most extensively ionised compounds were lidocaine (LID) and benzoic acid (BA), displaying percent ionisation values of 28.47 % and 55.73 %, respectively (Table 3.9). Further, the pH values of the saturated suspensions were 8.32, and 4.16, respectively (Appendix 11). Using the Henderson-Hasselbalch equation (Equation 3.1), and taking a pKa of 4.0 (Owen *et al.*, 2012), the percent of surface silanol groups ionised was 100 % and 55.73 %, when the donor solution consisted of LID and BA, respectively. In these scenarios therefore, it may be taken that electrostatic interactions i.e. attraction in the case of cationic LID, and repulsion in the case of BA, between penetrants and ionogenic groups in the modified PDMS membrane may contribute to a reduction in permeation. These observations, however should be considered in the

context of research undertaken. Whilst the range in polar surface area (PSA) of the penetrants used for this work is very similar to that observed in previous work, i.e. 36 – 64 in the case of air plasma, and 37 – 58 in the case of N₂ plasma (Table 3.9), the same conclusion cannot be drawn for the extent of ionisation. The compounds in the dataset used in this work displayed a percent ionisation of 0 - 55.73 %, but the range was twice as large in previous work employing air plasma (0 – 99.89 %) (Table 3.9). Thus, caution must be exercised when making broad conclusions regarding the effect of ionisation using this dataset.

As previously found, no statistically significant correlations were observed between the percent reduction in K_p and molecular weight ($r = -0.045$, $p = 0.895$, [-0.050, 0.442]), hydrogen bond donor count ($r = 0.096$, $p = 0.779$, [-0.059, 0.369]), hydrogen bond acceptor count ($r = -0.557$, $p = 0.075$, [-0.892, -0.283]), hydrogen bond acidity ($r = 0.130$, $p = 0.702$, [-0.581, 0.684]), hydrogen bond basicity ($r = 0.393$, $p = 0.232$, [0.047, 0.873]) $\log_{10} D$ ($r = 0.166$, $p = 0.625$, [-0.821, 0.606]), or $\log_{10} P$ ($r = 0.403$, $p = 0.219$, [-0.072, 0.361]).

4.2.2.3. Comparison with human skin.

Permeability coefficients (K_p) through native PDMS obtained using the flow through system correlate well with human skin permeability coefficients extracted from literature (Table 3.10) ($r = 0.711$, $p = 0.014$, [0.249, 0.995]). The correlation observed is marginally weaker than that observed between K_p values obtained using the static, Franz type diffusion cells, and the same body of literature values ($r = 0.780$, $p = 0.005$, [0.413, 0.997]), which was significant at both the $\alpha = 0.05$ and the $\alpha = 0.01$ level. Varying degrees of correlation between literature permeability data and the data presented herein may be attributed to discrepancies in the experimental protocols employed; for example, all authors (Table 3.10) report the use of Franz type diffusion cells, as opposed to flow through type systems. Furthermore, despite all authors reporting an experimental temperature, no authors report a precise membrane temperature. Uchida *et al.*, Walker *et al.* and Zhang *et al.* report general control of the cell temperature by use of a water bath or incubator maintained at 32 °C, in contrast to Degim *et al.* whom report maintaining a receiver chamber temperature of 37 °C, which has been shown in other work to

provide a membrane temperature of 32 °C (Akomeah, 2007; Degim *et al.*, 1998; Miki *et al.*, 2015; Uchida *et al.*, 2015; Walker *et al.*, 1997; Zhang *et al.*, 2012). Such subjective interpretation of OECD Test Guideline 428, which states that the membrane temperature should be maintained at 32 °C, and that to achieve this, different cell designs may require different experimental temperatures, may result in variable data. This also highlights a typical problem with QSPR models, and one of numerous reasons why these models have failed to completely replace *in vitro* studies. The models are usually developed on older, existing databases of permeation data, collated from multiple authors and sources. For example, work published by Baba *et al.* in 2017, aiming to quantify the effects of ionisation on skin permeation, used permeability coefficients extracted from 68 sources, published as early as 1973 (Baba *et al.*, 2017). Whilst studies have found small, standardised sets of *in vitro* data to correlate well with *in vivo* data (Mohammed *et al.*, 2014), the effect of the use of multiple experimental procedures should be considered when analysing data from numerous authors.

Although the use of N₂ plasma treatment resulted in a percentage reduction in K_p either on par with, or greater than, that offered by air plasma treatment (Table 4.5), no increase in correlation with human skin data was obtained in comparison to that observed with native PDMS ($r = 0.691, p = 0.019, [0.325, 0.995]$) (Figure 4.10).

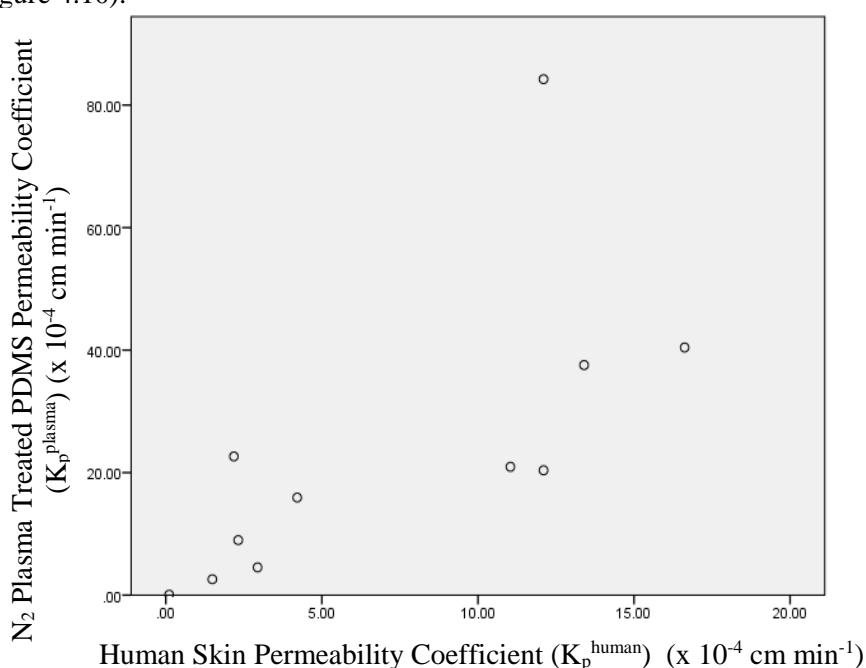


Figure 4.10 Plot of permeability coefficients through N₂ plasma treated PDMS (K_p^{plasma}) versus human skin (K_p^{human}) ($R^2 = 0.48, n = 11$).

4.3. Conclusion

The surface of PDMS was modified using an N₂ plasma treatment, endeavouring to produce a lamellae type polymeric structure containing biorelevant functional groups for use in *in vitro* skin permeation studies. Chemical characterisation of the surface following N₂ plasma treatment was performed using X-ray photoelectron spectroscopy (XPS) and attenuated total reflectance - Fourier transform infrared spectroscopy (ATR-FTIR). N₂ plasma treatment was found to primarily result in PDMS surface oxidation, as opposed to amination reported by other authors (Williams *et al.*, 2004; Yang *et al.*, 2016). This was hypothesised to be a consequence of the presence of residual H₂O and oxygen present within the plasma chamber and polymer, reported in other work (Egitto *et al.*, 2006; Owen *et al.*, 1994).

The surface morphology of N₂ plasma modified PDMS was analysed using scanning electron microscopy, the findings of which were observed to correlate well with preliminary permeation studies employing lidocaine (LID), and previous data obtained following air plasma treatment. A statistically significant reduction in LID permeation was observed following a 90 second N₂ plasma treatment, analogous to results obtained previously using an air plasma treatment. An extension in treatment time to 150 seconds resulted in a further statistically significant reduction in permeation, greater than that obtained previously using an air plasma treatment. A 210 second N₂ plasma treatment time was found to yield an insignificant difference in LID permeation, followed by a statistically significant increase in permeation following a 300 second plasma treatment, compared with the previous treatment time, owing to extensive surface cracking, observed during scanning electron microscopy analysis. Thus, permeation studies using ten further compounds from the previous dataset, in which PDMS (following 150 seconds N₂ plasma treatment) was used as the barrier to permeation, were performed. Greater extents of K_p reduction compared with those obtained following air plasma treatment were observed for seven out of eleven compounds, meeting a primary objective of the work presented in this chapter i.e. to further reduce the overestimation in permeation observed with PDMS skin mimics. However, no increases in correlation were observed following comparison with a library of literature permeability coefficients obtained using human epidermal tissue.

Conversely, a small increase in the atomic percent of nitrogen was observed following N₂ plasma treatment, which may suggest the presence of a small number of amine group containing surface sites, suitable for biomolecule conjugation. These findings may suggest that N₂ modified PDMS may provide a suitable platform for the production of biorelevant skin mimics, such as those containing protein-lipid bilayers.

References

- Akomeah. (2007). Variability in Human Skin Permeability In Vitro: Comparing Penetrants with Different Physicochemical Properties. *Journal of pharmaceutical sciences*, 96(4), 824-834.
- Baba, Ueno, Hashida, & Yamashita. (2017). Quantitative prediction of ionization effect on human skin permeability. *International Journal of Pharmaceutics*, 522(1), 222-233.
- Bhuiyan, & Waters. (2017). Permeation of pharmaceutical compounds through silicone membrane in the presence of surfactants. *Colloids and Surfaces A: Physicochemical and Engineering Aspects*, 516, 121-128.
- Chilcott, Barai, Beezer, Brain, Brown, Bunge, Burgess, Cross, Dalton, Dias, et al. (2005). Inter- and intralaboratory variation of in vitro diffusion cell measurements: An international multicenter study using quasi-standardized methods and materials. *Journal of Pharmaceutical Sciences*, 94(3), 632-638.
- Cordeiro, Zschoche, Janke, Nitschke, & Werner. (2009). Functionalization of poly(dimethylsiloxane) surfaces with maleic anhydride copolymer films. *Langmuir*, 25(3), 1509-1517.
- Degim, Pugh, & Hadgraft. (1998). Skin permeability data: Anomalous results. *International Journal of Pharmaceutics*, 170(1), 129-133.
- Egitto, & Matienzo. (2006). Transformation of Poly(dimethylsiloxane) into thin surface films of SiO_x by UV/Ozone treatment. Part I: Factors affecting modification. *Journal of Materials Science*, 41(19), 6362-6373.
- Juárez-Moreno, Ávila-Ortega, Oliva, Avilés, & Cauich-Rodríguez. (2015). Effect of wettability and surface roughness on the adhesion properties of collagen on PDMS films treated by capacitively coupled oxygen plasma. *Applied Surface Science*, 349, 763-773.
- Lee, Hong, Park, Lee, & Kim. (2017). A simple fabrication process for stepwise gradient wrinkle pattern with spatially-controlled wavelength based on sequential oxygen plasma treatment. *Microelectronic Engineering*, 176, 101-105.
- Miki, Ichitsuka, Yamada, Kimura, Egawa, Seki, Juni, Ueda, & Morimoto. (2015). Development of a membrane impregnated with a poly(dimethylsiloxane)/poly(ethylene glycol) copolymer for a high-throughput screening of the permeability of drugs, cosmetics, and other chemicals across the human skin. *European Journal of Pharmaceutical Sciences*, 66, 41-49.
- Mohammed, Matts, Hadgraft, & Lane. (2014). In Vitro–In Vivo Correlation in Skin Permeation. *Pharmaceutical Research*, 31(2), 394-400.
- Nania, Matar, & Cabral. (2015). Frontal vitrification of PDMS using air plasma and consequences for surface wrinkling. *Soft matter*, 11(15), 3067-3075.
- Ng, Rouse, Sanderson, Meidan, & Eccleston. (2010). Validation of a static Franz diffusion cell system for in vitro permeation studies. *AAPS PharmSciTech*, 11(3), 1432-1441.
- Owen, & Dvornic. (2012). *Silicone Surface Science* (Vol. 4). Dordrecht: Springer Netherlands.
- Owen, & Smith. (1994). Plasma treatment of polydimethylsiloxane. *Journal of Adhesion Science and Technology*, 8(10), 1063-1075.
- Provin, Nicolas, Grégoire, & Fujii. (2015). A Microfluidic Diffusion Cell for Fast and Easy Percutaneous Absorption Assays. *Pharmaceutical Research*, 32(8), 2704-2712.
- Salerno, Piscioneri, Laera, Morelli, Favia, Bader, Drioli, & De Bartolo. (2009). Improved functions of human hepatocytes on NH₃ plasma-grafted PEEK-WC–PU membranes. *Biomaterials*, 30(26), 4348-4356.
- Sinkó, Garrigues, Balogh, Nagy, Tsinman, Avdeef, & Takács-Novák. (2012). Skin–PAMPA: A new method for fast prediction of skin penetration. *European Journal of Pharmaceutical Sciences*, 45(5), 698-707.
- Uchida, Kadhum, Kanai, Todo, Oshizaka, & Sugibayashi. (2015). Prediction of skin permeation by chemical compounds using the artificial membrane, Strat-M™. *European Journal of Pharmaceutical Sciences*, 67, 113-118.
- Vesel, Junkar, Cvelbar, Kovac, & Mozetic. (2008). Surface modification of polyester by oxygen- And nitrogen-plasma treatment. *Surface and Interface Analysis*, 40(11), 1444-1453.

- Walker, Hulme, Rippon, Walmsley, Gunnigle, Lewin, & Winsey. (1997). In vitro model(s) for the percutaneous delivery of active tissue repair agents. *Journal of Pharmaceutical Sciences*, 86(12), 1379-1384.
- Waters, Dennis, Bibi, & Mitchell. (2013). Surfactant and temperature effects on paraben transport through silicone membranes. *Colloids and Surfaces B: Biointerfaces*, 108, 23-28.
- Williams, Wilson, & Rhodes. (2004). Stability of plasma-treated silicone rubber and its influence on the interfacial aspects of blood compatibility. *Biomaterials*, 25(19), 4659-4673.
- Xu, Li, Zhong, Zha, Wu, Liu, Xiao, Jiang, Zhang, & Chen. (2011). Amide-linkage formed between ammonia plasma treated poly(D,L-lactide acid) scaffolds and bio-peptides: Enhancement of cell adhesion and osteogenic differentiation in vitro. *Biopolymers*, 95(10), 682-694.
- Yang, & Yuan. (2016). Investigation on the mechanism of nitrogen plasma modified PDMS bonding with SU-8. *Applied Surface Science*, 364, 815-821.
- Zhang, Chen, Scriba, Abraham, Fahr, & Liu. (2012). Human skin permeation of neutral species and ionic species: Extended linear free-energy relationship analyses. *Journal of Pharmaceutical Sciences*, 101(6), 2034-2044.

Chapter 5 A Comparative Study of Biomolecule Conjugation Methods

5.1 Introduction

The wet chemical modification of poly(dimethylsiloxane) (PDMS) following plasma-based surface activation is used extensively as an approach to tailoring the interactions between the polymer substrate and specific biomolecules, looking to enhance biocompatibility and expand the possible applications of PDMS, particularly within the field of cytology. For example, various proteins have been immobilised at the surface of PDMS, e.g. fibronectin, laminin, and collagen (Kuddannaya *et al.*, 2013; Pakstis *et al.*, 2010), resulting in ‘biphasic’ membrane formation, enhanced cell adhesion and proliferation, and, in the case of myoglobin, sandwich immunoassay development (Gunda *et al.*, 2014).

Attempts to produce, and utilise, biphasic systems consisting of polymers and appropriate biomolecules are sparsely reported for *in vitro* skin permeation studies, despite the plethora of literature reporting the development of such systems for alternative applications. ‘Biphasic’, or ‘composite’ systems consisting entirely of synthetic materials, such as PDMS and poly(2-hydroxyethyl methacrylate) (PHEMA) copolymer membranes, have received interest as skin mimics for *in vitro* permeation studies, attributed to their hypothesised ability to represent both the hydrophobic and hydrophilic microdomains present in the human stratum corneum (Tomomi *et al.*, 1992; Yamaguchi *et al.*, 1997). However, this interest has not been extended to polymer-biomolecule composite systems. An example of such limited reports, published by Shumilov *et al.*, evaluated the suitability of INTEGRA® regeneration template, an FDA approved membrane for the treatment of burns and use in reconstructive surgery, as a surrogate for excised epidermal tissue in permeation studies. The biphasic template consists of a lipophilic polysiloxane layer and an underlying hydrophilic collagen layer, and following its use in permeation studies employing eight model compounds, good correlation was observed between flux through the template and flux through excised epidermal tissue ($R^2 = 0.8517$). The authors further noted that the membrane was advantageous in terms of uniformity, reduced safety

concerns, and storage. However, the sourcing of collagen from bovine tendon leads to the requirement of animal tissue, opposing the 'Replacement' principle of the '3 R's' (Shumilov *et al.*, 2009).

The stratum corneum has long been known to be the rate limiting barrier to xenobiotic permeation, forty percent of which consists of protein, eighty percent of which is known to be keratin (Lee *et al.*, 2010; Tobin, 2006). To date, a limited body of work has considered the relevance of keratin containing membranes for *in vitro* skin permeation studies. For example, work by Selmin *et al.*, reporting the development of a model skin consisting of keratin and ceramides for use in *in vitro* skin permeation studies, considered the permeation of only three penetrants, namely ibuprofen, propranolol, and testosterone (Selmin *et al.*, 2012). However, the work highlights an interesting feature of keratin; keratin can be obtained from sheep wool using various extraction procedures, and, in contrast to the collagen used in the INTEGRA® template, is readily available non-sacrificially. Moreover, arguably keratin-containing membranes are more relevant to such studies since eighty percent of the protein content of the stratum corneum is known to be keratin (Lee *et al.*, 2010). The authors accredit the successful use of the INTEGRA® membrane to the representation of the lipophilic stratum corneum and underlying hydrated dermis (Shumilov *et al.*, 2009), however, the stratum corneum is known to be the rate limiting barrier to the permeation of most penetrants (Godin *et al.*, 2007). Other interesting examples of work with keratin include the laser ablation of keratin membranes endeavouring to produce 'brick and mortar' patterned surfaces for use in the assessment of moisturising products i.e. permeation was not considered (Haq *et al.*, 2015).

Despite the large number of reported PDMS-biomolecule conjugation protocols, to date no work has been published reporting the use of such protocols for the development of suitable skin mimics. Further, it was hypothesised that PDMS-protein bilayers may provide a more tortuous pathway for permeation, analogous to the stratum corneum (Figure 5.1). For example, whilst the stratum corneum is known to be around 20 µm thick, the path length of diffusion is known to be in the range of 300-900 µm (Lane, 2013).

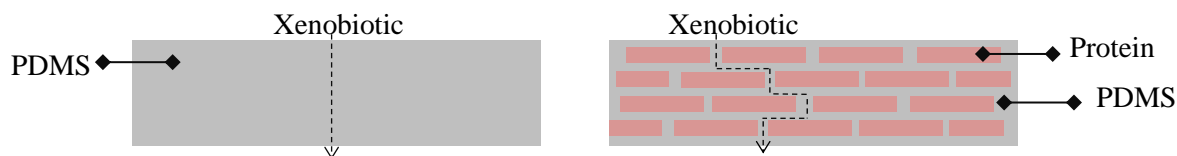


Figure 5.1 Permeation of a xenobiotic through PDMS (left) and PDMS-protein biphasic membrane (right).

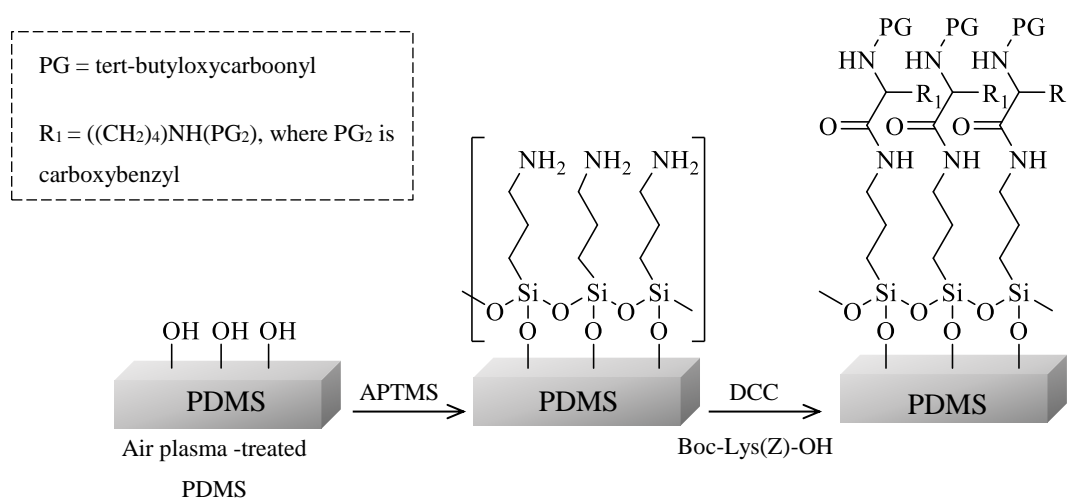
In this work, three biomolecule conjugation approaches were compared, whereby lysine was used as a model biomolecule, based on its abundance in keratin and its commercial availability (Candi *et al.*, 1998; Wang *et al.*, 2016). Furthermore, lysine provides the most common covalent binding sites in the immobilisation of proteins on polymeric substrates, since lysine residues are typically abundant on the exterior structure of protein molecules (Kim *et al.*, 2013; Migneault *et al.*, 2004).

The first approach involved the generation of an amide linkage between lysine and silanised PDMS by use of a carbodiimide coupling reagent, namely *N,N'*-dicyclohexylcarbodiimide (DCC), according to protocols conventionally used in solid phase peptide synthesis (SPPS). DCC has traditionally provided an attractive route to the generation of peptides in one-pot systems, since the *N,N'*-dicyclohexylurea side product is poorly soluble, and can be readily eliminated from the reaction by filtration, in contrast to those obtained using alternative carbodiimide reagents, such as diisopropyl carbodiimide and 1-ethyl-3-(3'-dimethylamino)carbodiimide hydrochloride (Montalbetti *et al.*, 2005). In this work, a setup was chosen analogous to that employed in SPPS whereby the polymeric resin, in this case membrane, was amine-functionalised, and the amino acid was 'anchored' at the C terminus (Knud J. Jenson, 2013; Muttenthaler *et al.*, 2015). The second approach reflected a similar setup, differing only by the method of surface amine group generation i.e. N_2 plasma was used instead of an alkoxy silane reagent. Finally, a more extensively reported method endeavouring to achieve permanent biomolecule adhesion to PDMS membranes was evaluated, namely the use of a glutaraldehyde linker molecule, surpassing the need for a coupling reagent.

5.2. Results and Discussion

5.2.1. Alkoxysilane Layer Formation and *N, N'*-Dicyclohexylcarbodiimide Coupling to Lysine.

In this section, an amine terminated alkoxysilane layer was formed, according to reported methods (Pakstis *et al.*, 2010), followed by the *N, N'*-dicyclohexylcarbodiimide (DCC) coupling of lysine (Scheme 5.1). In order to prevent peptide formation both the N_α and N_ϵ were protected with tert-butyloxycarbonyl and carboxybenzyl groups, respectively.



Scheme 5.1 Silanisation and sequential lysine functionalisation of PDMS.

5.2.1.1. Alkoxysilane Layer Formation

5.2.1.1.1. Attenuated Total Reflectance - Fourier Transform Infrared Spectroscopy (ATR-FTIR)

An amine terminated alkoxysilane self-assembled monolayer (SAM) was generated on the surface of PDMS using (3-aminopropyl)trimethoxysilane (APTMS) in order to provide reactive sites for potential biomolecule anchoring, according to methods reported previously by other authors (Lin *et al.*, 2010; Pakstis *et al.*, 2010). Successful SAM formation was confirmed by the presence of characteristic bands in the ATR-FTIR spectrum of APTMS silanised PDMS, summarised in Table 5.1.

Table 5.1 Summary of ATR-FTIR spectrum of APTMS silanised PDMS (PDMS-APTMS).

Assignment	ν_{\max} (cm^{-1})
$\nu_{\text{as}}(\text{NH}_2)$	3350.0
$\nu_{\text{s}}(\text{CH}_3)$	2961.9
$\delta_{\text{s}}(\text{NH}_2)$	1567.9
$\delta_{\text{s}}(\text{CH}_2)$	1488.0
$\delta_{\text{as}}(\text{CH}_3)$	1412.2
$\delta_{\text{s}}(\text{CH}_3)$	1258.1
Si-O-Si	1004.6
O-SiCH ₃	784.4
C-SiCH ₃	700.0

The presence of surface methyl groups was confirmed, as discussed previously (Sections 3.2.1.2 and 4.2.1.1), by a symmetrical stretching vibration of the CH₃ group at 2961.9 cm^{-1} , and the asymmetric and symmetric deformation of the CH₃ group at 1412.2 and 1258.1 cm^{-1} , respectively. The Si-O-Si stretching vibration was observed at 1004.6 cm^{-1} , along with absorptions at 784.4 and 700.0 cm^{-1} , confirming the presence of the O-SiCH₃ and C-SiCH₃ groups, respectively. The formation of an N-H stretching band at $\sim 3350 \text{ cm}^{-1}$, the presence of asymmetric bending deformation of the methylene group at 1488.0 cm^{-1} , along with the presence of an in plane deformation vibration of the NH₂ group of a primary amine at 1567.9 cm^{-1} , is indicative of successful surface functionalisation. The $\nu(\text{C-N})$ of a primary amine group, expected to appear at 1220-1020 cm^{-1} was not observed in the ATR-FTIR spectrum of APTMS functionalised PDMS, most likely as it is orders of magnitude smaller than the Si-CH₃ and Si-O-Si bands observed in this region.

5.2.1.1.2. X-ray Photoelectron Spectroscopy (XPS)

X-ray photoelectron spectroscopic analysis of APTMS silanised PDMS was performed in order to observe changes in the surface chemical composition of PDMS following SAM formation. The surface

atomic percent of oxygen, nitrogen, carbon, and silicon were obtained from XPS survey scans (Table 5.2) (Appendix 3).

Table 5.2 Atomic percent (%) of oxygen, nitrogen, carbon and silicon at the surface of native PDMS, PDMS following a 90 second air plasma treatment, and subsequent APTMS functionalisation, taken from XPS survey scans.

Membrane	Sample	Atomic percent (%)			
		O	N	C	Si
Native PDMS	1	23.17	< 0.1	47.83	29.00
	2	22.79	< 0.1	48.92	28.28
Plasma treated PDMS	1	44.80	0.56	23.22	31.42
	2	44.11	0.61	24.49	30.79
APTMS silanised PDMS (PDMS-APTMS)	1	22.01	6.89	49.64	21.46
	2	22.63	6.24	48.51	22.62

An overall increase in the atomic percent of nitrogen, from 0.6 % in air plasma treated PDMS, to > 6 % following treatment with APTMS, is indicative of successful alkoxy silane layer formation, in support of ATR-FTIR findings (Table 5.1), and is similar in magnitude to increases observed in similar work (Pakstis *et al.*, 2010). This is further supported by an increase in the atomic percent of carbon following silanisation, from ~23 – 24 % in air plasma treated PDMS, to ~ 49 – 50 % in silanised PDMS, which was anticipated given the structure of the organosilane.

The high resolution spectrum of the C 1s orbital (Figure 5.2) contains four signals at binding energies of 285.00 eV, 285.80 eV, 286.70 eV and 288.35 eV. The signals at 285.00 eV, 286.70 and 288.35 eV have been assigned previously, as methyl, alcohol and carbonyl containing groups, respectively (Section 3.2.1.3). The signal at 285.80 eV can be assigned to the primary amine of the silanising

reagent, and is within the range of values reported in literature for groups containing C-N bonds i.e. 285.5 – 286.4 eV (Vesel *et al.*, 2008; Yang *et al.*, 2016).

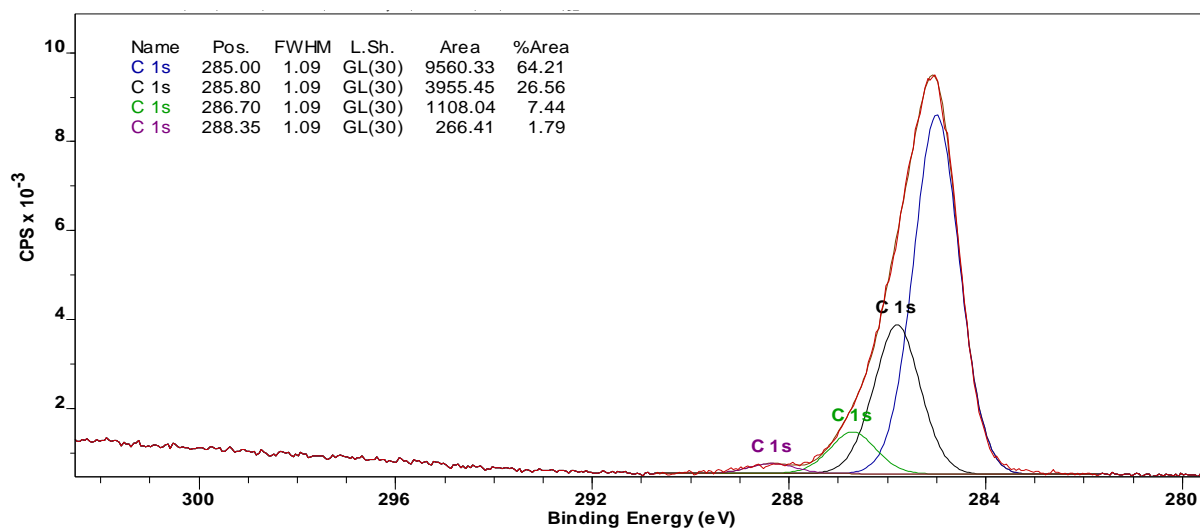


Figure 5.2 High resolution XPS spectrum of the C 1s orbital in APTMS silanised PDMS.

Two peaks are observable at binding energies of 399.59 eV and 401.23 eV in the high resolution XPS spectra of the N 1s orbital in silanised PDMS (Figure 5.3), representing 91.69 atomic % and 8.31 atomic %, respectively. The peak at 399.59 eV can be assigned to primary amine functionalities, supported by similar findings in literature (Hirata *et al.*, 2008; Yang *et al.*, 2016). The peak at the higher binding energy can be assigned to amide functionalities introduced during plasma processing, as noted previously (Section 3.2.1.3). This is supported by the relative quantity of the signal matching that of plasma introduced nitrogen-containing functionalities. Considering the signal at 401.23 eV represents 8.31 % of 6.89 atomic % of nitrogen in the sample, this signal accounts for an overall atomic percentage of ~ 0.57 %, in line with the data obtained for plasma processed PDMS (Table 3.3). Furthermore, the higher binding energy of the group is expected, taking into account the increase in binding energy associated with an increase in electronegativity of neighbouring atoms i.e. oxygen.

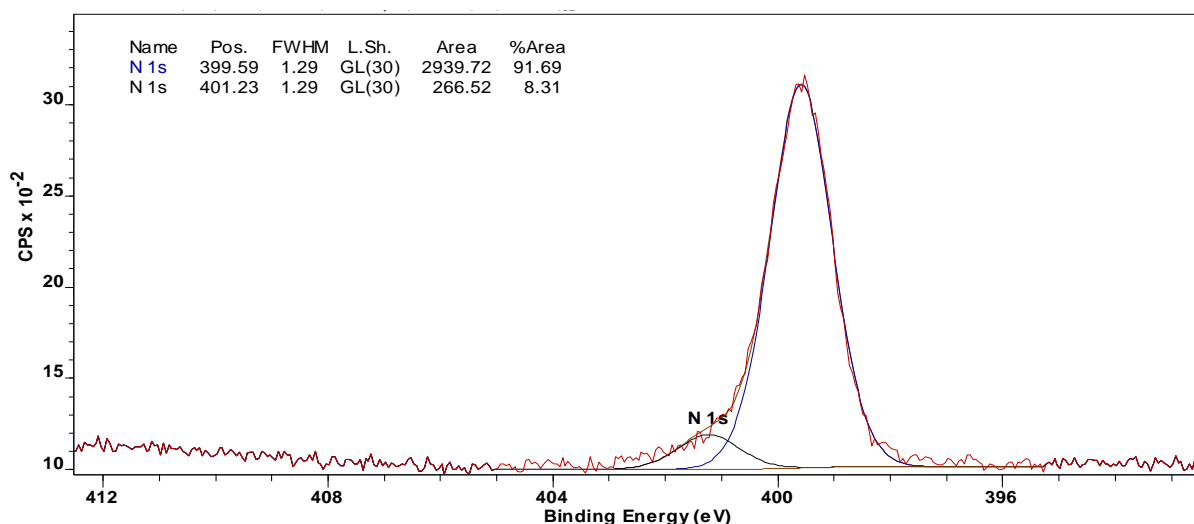


Figure 5.3 High resolution XPS spectrum of the N 1s orbital in APTMS silanised PDMS.

5.2.1.1.3. Scanning Electron Microscopy

Scanning electron microscopy images of alkoxy silane functionalised PDMS were obtained in support of chemical analysis, in order to confirm monolayer formation, and observe changes in the morphological characteristics of the membrane (Figure 5.4). To date, reported examples of alkoxy silane functionalisation of PDMS have generally considered the effect of SAM formation on the wettability and chemical reactivity of the substrate, along with the behaviour of cells cultured on the substrate, but have displayed limited interest in the overall membrane integrity (Karakoy *et al.*, 2014; Kuddannaya *et al.*, 2013; Pakstis *et al.*, 2010). General consideration of the membrane integrity of PDMS following various chemical treatments is of heightened interest to this project, since mechanical strain, structural damage, and crack formation, may result in increases in permeability.

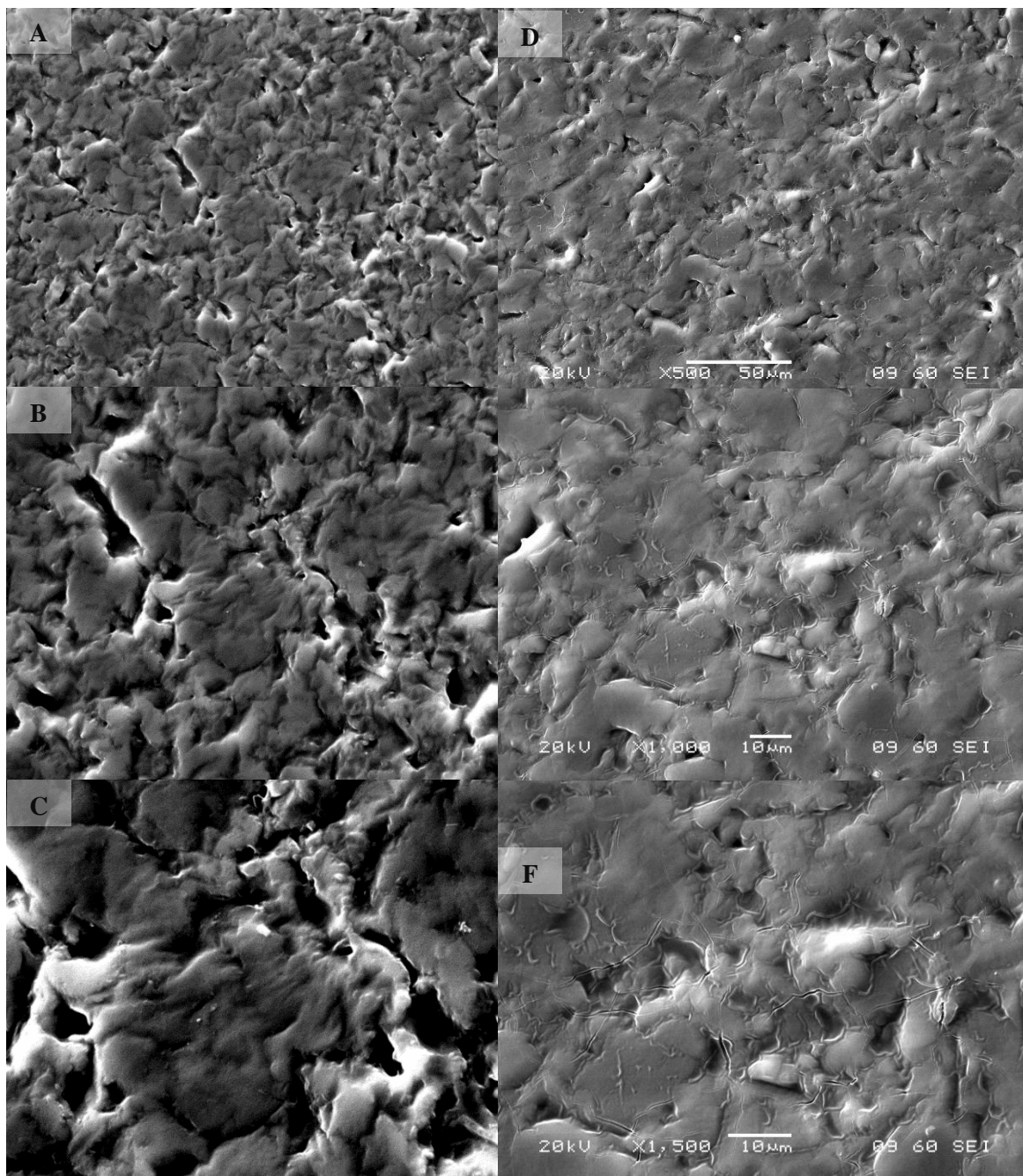


Figure 5.4 APTMS silanised PDMS at a magnification of 500 X (A), 1000 X (B), and 1500 X (C) Scanning Electron Microscopy images of PDMS following 90 seconds air plasma treatment (A-C, 500 X, 1000 X, and 1500 X magnification, respectively) and APTMS silanised PDMS.

Successful silane layer formation is apparent in Figure 5.4 along with surface cracking, which is readily observable at a magnification of 1500 X. Surface cracking may be attributed to mechanical strain between the surface and the bulk, in line with observations made previously (Cordeiro *et al.*, 2009).

5.2.1.2. *N, N'*-Dicyclohexylcarbodiimide coupling to Lysine

A dicyclohexylcarbodiimide coupling reaction between Boc-Lys(Z)-OH and APTMS functionalised PDMS was performed. The surface chemical composition was determined in order to confirm the occurrence of successful coupling between the amine terminated SAM (Section 4.1.1.1) and lysine using ATR-FTIR and XPS.

5.2.1.2.1. Attenuated Total Reflectance - Fourier Transform Infrared Spectroscopy (ATR-FTIR)

ATR-FTIR analysis of PDMS following APTMS layer formation and lysine coupling was performed in order to confirm the occurrence of successful coupling (Table 5.3). The results of ATR-FTIR analysis of both APTMS functionalised PDMS and Boc-Lys(Z)-OH are also presented in Table 5.3 to enable facile identification of surface functionality.

Table 5.3 ATR-FTIR analysis of APTMS functionalised PDMS, Boc-Lys(Z)-OH, and Boc-Lys(Z)-OH functionalised PDMS.

Assignment	ν_{\max} (cm^{-1})		
	APTMS functionalised PDMS (PDMS-APTMS)	Boc-Lys(Z)-OH	Boc-Lys(Z)-OH functionalised PDMS (PDMS-APTMS-Lys)
$\nu(\text{N-H})$	~ 3335	3337.1	3307.3
$\nu_{\text{as}}(\text{CH}_3)$	2961.6	2975.9	2962.0
$\nu(\text{C=O})$	N/A	1678.8	1651.2
		1738.2	1695.1
$\delta(\text{NH}_2)$	1567.3	N/A	N/A
$\nu(\text{C-N})$	N/A	1551.2	1531.1
$\delta_{\text{s}}(\text{CH}_2)$	1486.1	1456.1	1455.0
Si-CH ₃	1258.3	N/A	1257.9
Si-O-Si	1003.7	N/A	1004.1
O-SiCH ₃	784.4	N/A	784.6
C-SiCH ₃	699.9	N/A	698.1

A band at 1695.1 cm^{-1} in the ATR-FTIR spectrum of Boc-Lys(Z)-OH functionalised PDMS, and 1678.8 cm^{-1} in the ATR-FTIR spectrum of Boc-Lys(Z)-OH is indicative of the carbonyl group of the carbamate group present in both the tert-butyloxycarbonyl (Boc) and carboxybenzyl (Z) protecting group. The presence of an absorbance at 1651.2 cm^{-1} in the ATR-FTIR spectrum of Boc-Lys(Z)-OH functionalised PDMS is indicative of a carbonyl group in an amide link to the substrate. Furthermore, the presence of the symmetric stretch of the carbonyl group in the ATR-FTIR spectrum of Boc-Lys(Z)-OH at 1738.2 cm^{-1} , and its absence in the spectrum of Boc-Lys(Z)-OH functionalised PDMS confirms the covalent attachment of the amino acid to the surface. The presence of this signal additionally confirms that signals representative of the carbamate-containing protecting groups are not present as a result of the physisorption of lysine to PDMS.

An absorbance between 1570-1515 cm^{-1} present in both Boc-Lys(Z)-OH and Boc-Lys(Z)-OH functionalised PDMS i.e. at 1551.2 cm^{-1} and 1531.1 cm^{-1} , respectively, is indicative of the presence of a secondary amide, present as a consequence of protection of both former primary amine sites. The $\nu(\text{C-N})$ of a primary amine group appears at a lower frequency than that of amides (1220-1020 cm^{-1}), and is not observed in the ATR-FTIR spectrum of APTMS silanised PDMS, most likely as it is orders of magnitudes smaller than the Si-CH₃ and Si-O-Si bands observed in this region. However, the presence of asymmetric bending deformation of the methylene group at 1486.1 cm^{-1} indicates successful silanisation, along with the presence of an in-plane deformation vibration of the NH₂ group of a primary amine at 1567.3 cm^{-1} in the ATR-FTIR spectrum of silanised PDMS.

5.2.1.2.2. X-ray Photoelectron Spectroscopy (XPS)

X-ray photoelectron spectroscopic analysis was also performed in order to confirm changes in the surface elemental composition of APTMS functionalised PDMS following coupling to Boc-Lys(Z)-OH. Surface atomic percent of oxygen, carbon, nitrogen and silicon were obtained from survey scans (Appendix 4), and are presented in Table 5.4.

Table 5.4 Atomic percent (%) of oxygen, nitrogen, carbon and silicon at the surface of Boc-Lys(Z)-OH APTMS functionalised PDMS (PDMS-APTMS-Lys), taken from XPS survey scans.

Membrane	Sample	Atomic %			
		O	C	N	Si
PDMS-APTMS-Lys	1	24.41	51.38	4.89	19.32
	2	25.30	51.14	5.02	18.54

A small increase in the atomic percent of carbon, and a decrease in both the atomic percent of nitrogen and silicon at the surface of PDMS, is indicative of successful coupling, and is consistent with the structure of Boc-Lys(Z)-OH. In order to further confirm the occurrence of coupling, high resolution XPS spectra of the C 1s (Figure 5.5) and N 1s (Figure 5.6) orbitals were obtained, enabling the assignment of surface functionality.

Four peaks are resolvable in the high resolution XPS spectrum of the C 1s orbital in APTMS Boc-Lys(Z)-OH functionalised PDMS at binding energies of 285.00 eV, 286.48 eV, 289.69 eV and 287.82 eV. The signals at binding energies of 285.00 eV and 286.48 eV have been assigned previously to methyl, and alcohol groups, respectively (Sections 3.2.1.3 and 4.2.1.2). The notable absence of a signal at 285.80 eV, assigned previously as C-N the primary amine of APTMS, may suggest successful amide linkage to the amino acid. The two signals at binding energies of 287.82 eV and 289.69 eV, absent from the analogous spectrum for APTMS functionalised PDMS, match most closely those observed for carbonyl functionalities (Vesel *et al.*, 2008; Yang *et al.*, 2016). The binding energy of the former signal most closely matches that of amide groups, and the latter is markedly similar to reported values for carbamate groups i.e. 289.60 eV, present in the carboxybenzyl (Z) and tert-butyloxycarbonyl (Boc) protecting groups (Bittrich *et al.*, 2014), supporting the occurrence of successful Boc-Lys(Z)-OH functionalisation.

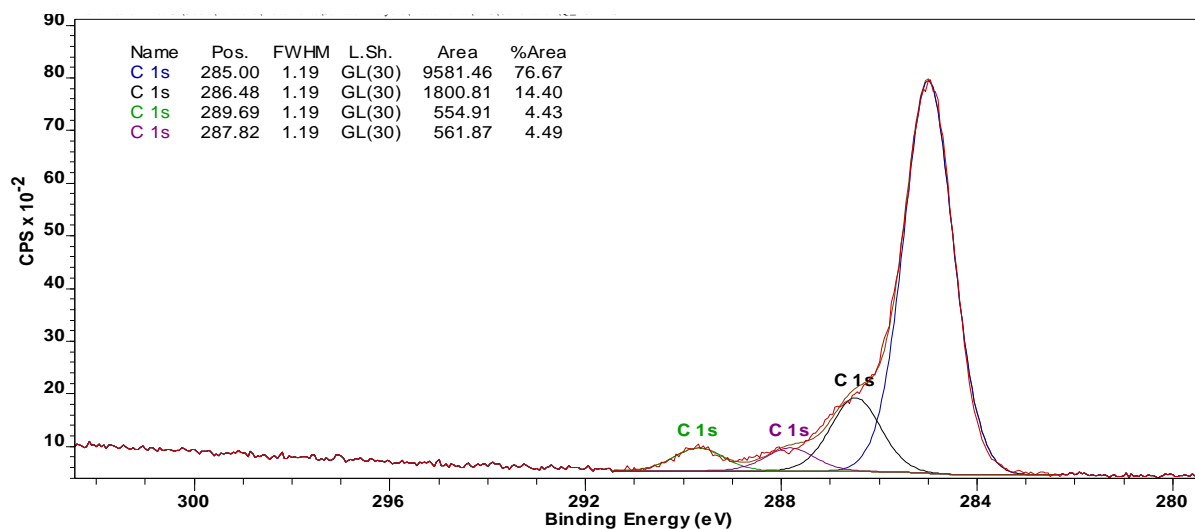


Figure 5.5 High resolution XPS spectrum of the C 1s orbital in APTMS-Boc-Lys(Z)-OH functionalised PDMS.

The presence of only one peak in the high resolution XPS spectrum of the N 1s orbital of APTMS silanised PDMS (Figure 5.3), and the presence of an additional peak at 401.88 eV in the N 1s spectrum of Boc-Lys(Z)-OH functionalised PDMS is indicative of successful surface modification. Furthermore, the higher chemical shift of the additional signal is concomitant with the addition of nitrogen atoms with neighbouring electron withdrawing groups i.e. amide and carbamate groups.

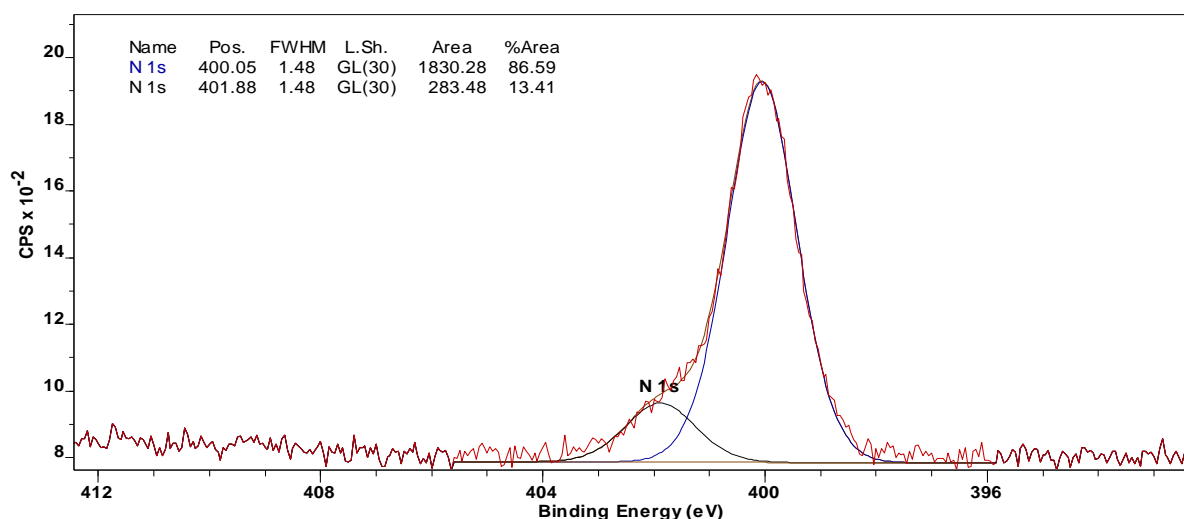
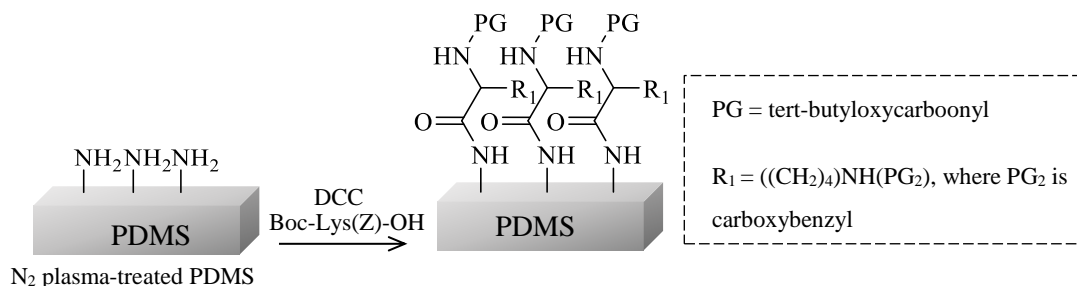


Figure 5.6 High resolution XPS spectrum of the N 1s orbital in APTMS-Boc-Lys(Z)-OH functionalised PDMS.

5.2.2. Coupling of Lysine to N₂ Plasma-Treated PDMS

Direct coupling of Boc-Lys(Z)-OH to PDMS, following surface amination using an N₂ plasma treatment, was explored as a potential route to immobilising amine-group containing biomolecules at the surface of PDMS, surpassing the requirement for a surface silanisation step (Scheme 5.2).



Scheme 5.2 Lysine functionalisation of N₂ plasma treated PDMS.

5.2.2.1. Attenuated Total Reflectance – Fourier Transform Infrared Spectroscopy (ATR-FTIR)

ATR-FTIR analysis of N₂ plasma treated PDMS following functionalisation with Boc-Lys(Z)-OH was performed in order to assign surface functionality. Data corresponding to Boc-Lys(Z)-OH functionalised PDMS is presented in Table 5.5, along with data corresponding to N₂ plasma treated PDMS to enable facile comparison.

Table 5.5 ATR-FTIR analysis of N₂ plasma treated PDMS prior to, and following, coupling with Boc-Lys(Z)-OH.

Assignment	ν_{\max} (cm ⁻¹)	
	N ₂ plasma treated PDMS	Boc-Lys(Z)-OH functionalised PDMS
$\nu_s(\text{CH}_3)$	2962.1	2962.2
$\nu(\text{C}=\text{O})$	N/A	1693.8
$\delta_{\text{as}}(\text{CH}_3)$	1412.4	1412.2
$\delta_s(\text{CH}_3)$	1258.2	1258.2
Si-O-Si	1005.7	1005.4
O-SiCH ₃	785.1	785.2
C-SiCH ₃	701.2	700.9

The presence of surface methyl groups was confirmed by a symmetrical stretching vibration of the CH₃ group at 2962.2 cm⁻¹, and the asymmetric and symmetric deformation of the CH₃ group at 1412.2 and 1258.2 cm⁻¹. The Si-O-Si stretching vibration is observed at 1005.4 cm⁻¹, along with absorptions at 785.2 and 700.9 cm⁻¹, confirming the presence of the O-SiCH₃ and C-SiCH₃ groups, respectively. An additional absorbance is observed at 1693.8 cm⁻¹, attributed to the stretching vibration of the carbonyl of a carbamate group present in the carboxybenzyl (Z) and tert-butyloxycarbonyl (Boc) protecting groups. As expected, this absorption is absent from the spectra of both N₂ plasma treated PDMS and APTMS silanised PDMS, and is present in the ATR-FTIR spectrum of APTMS silanised PDMS following coupling to Boc-Lys(Z)-OH (Table 5.3). Furthermore, this finding supports the presence of amine groups at the surface of PDMS following plasma treatment, as hypothesised following XPS analysis (Section 4.2.1.2).

5.2.2.2. X-ray Photoelectron Spectroscopy (XPS)

X-ray photoelectron spectroscopic analysis was performed in support of ATR-FTIR analysis, in order to confirm surface modification, and assign chemical functionality. Elemental composition was

obtained from XPS survey scans (Appendix 8 and Appendix 9), and is presented in Table 5.6. The physical adsorption, or physisorption, of ‘dynamic modifiers’ such as surfactants (Section 1.7.2) (Wang *et al.*, 2006), and proteins (Pakstis *et al.*, 2010) has recurrently been used as a modest approach to tailoring the surface properties of PDMS. Multiple authors have reported the limited robustness of such protocols, accredited to the known desorption of the modifier over time (Pakstis *et al.*, 2010). In order to confirm that characteristic signals in both the ATR-FTIR and XPS spectra were not present as a consequence of van der Waals interactions between the amino acid and plasma modified surface i.e. physisorption, the coupling reaction was performed according to two protocols. The former protocol employed the use of an aprotic solvent, namely dichloromethane, i.e. *N,N'*-dicyclohexylcarbodiimide coupling was known to occur, and the latter employed a protic solvent, namely ethanol, in which coupling was not possible.

Table 5.6 Atomic percent (%) of oxygen, nitrogen, carbon and silicon at the surface of N₂ plasma treated PDMS following coupling to Boc-Lys(Z)-OH in dichloromethane and ethanol, taken from XPS survey scans.

Membrane	Sample	Atomic percent (%)			
		O	N	C	Si
Boc-Lys(Z)-OH functionalised PDMS (Dichloromethane)	1	23.82	6.48	58.58	11.12
	2	24.17	6.85	58.05	10.93
Boc-Lys(Z)-OH functionalised PDMS (Ethanol)	1	42.83	0.74	27.42	29.01
	2	41.64	0.92	29.05	28.05

An increase in the atomic percent of nitrogen from 0.83 - 0.87 in N₂ plasma treated PDMS (Table 4.2), to 6.48 - 6.85 %, was observed following surface modification using dichloromethane. Additionally, an increase in carbon percent was observed, resulting in an atomic percent of carbon greater than that observed following both XPS analysis of N₂ plasma treatment (25.86 – 26.21 %), and native PDMS

(47.83 – 48.92 %), i.e. 58.05 – 58.58 atomic %. These results were anticipated in the event of successful coupling, given the structure of the amino acid. No such changes were observed following employment of a protic reaction solvent, and the values of atomic percent of carbon, oxygen, nitrogen, and silicone were all markedly similar to those observed previously, following N₂ plasma treatment alone (Table 4.2). From these results, it may be inferred that successful coupling has occurred. In order to further support this conclusion, high-resolution XPS spectra of the C 1s and N 1s orbitals were obtained.

The high resolution spectrum of the C 1s orbital in Boc-Lys(Z)-OH functionalised PDMS (dichloromethane) (Figure 5.7) is markedly similar to that obtained following coupling of Boc-Lys(Z)-OH to APTMS silanised PDMS (Figure 5.5) i.e. two signals at binding energies circa 288 and 290 eV were observed, associated with carbonyl containing functionalities. The high resolution spectrum of the C 1s orbital in Boc-Lys(Z)-OH functionalised PDMS (ethanol) (Figure 5.8) was notably similar to that observed following N₂ plasma treatment alone (Figure 4.2), with regards to both the binding energies of the observed signals, and the percent area (%) of each. These observations further reaffirm the occurrence of successful coupling in dichloromethane, and the absence of coupling in ethanol.

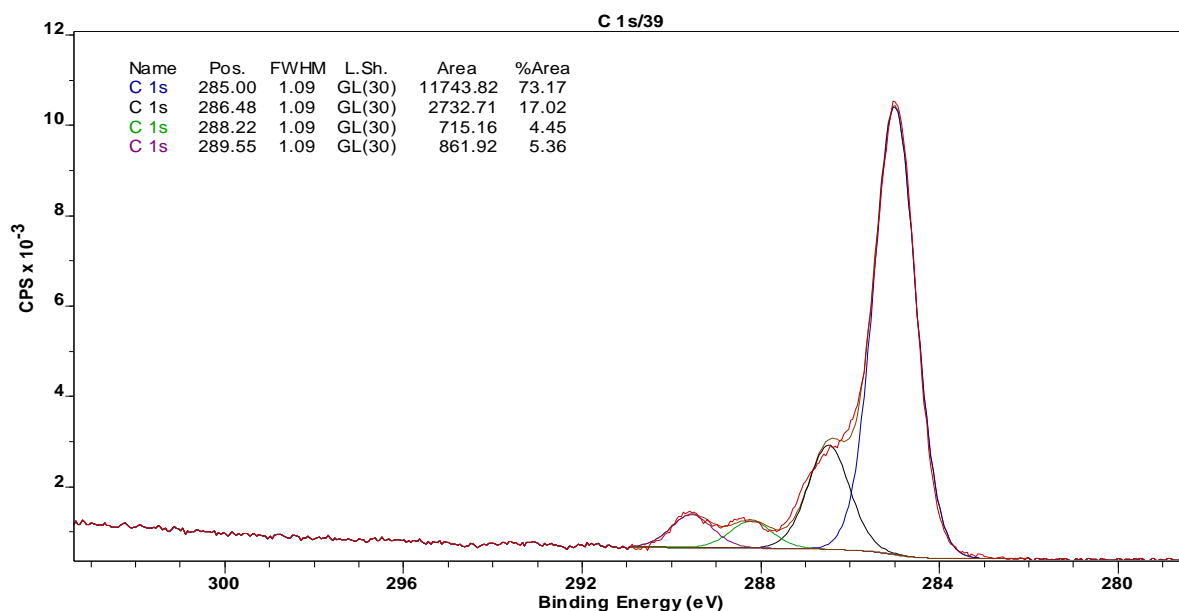


Figure 5.7 High resolution XPS spectrum of the C 1s orbital in Boc-Lys(Z)-OH functionalised PDMS (dichloromethane).

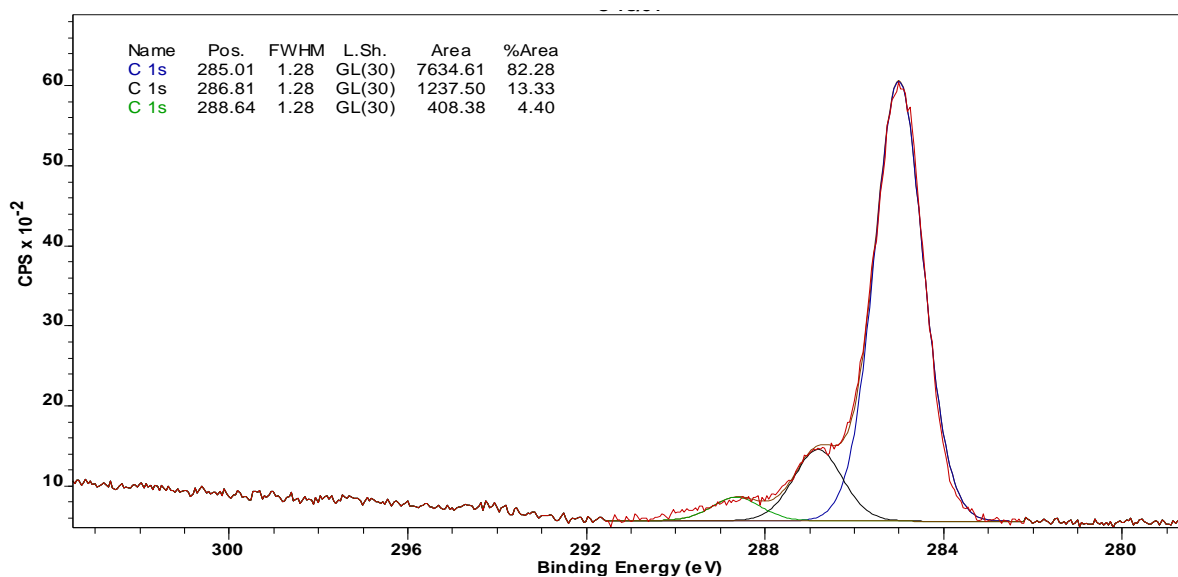


Figure 5.8 High resolution XPS spectrum of the C 1s orbital in Boc-Lys(Z)-OH functionalised PDMS (ethanol).

Analogous to the C 1s spectra, the high resolution XPS spectrum of the N 1s orbital in Boc-Lys(Z)-OH functionalised PDMS (dichloromethane) (Figure 5.9) was similar to that obtained following coupling of Boc-Lys(Z)-OH to APTMS silanised PDMS (Figure 5.6). Two signals were present, in contrast to the spectra obtained corresponding to Boc-Lys(Z)-OH functionalised PDMS (ethanol) (Figure 5.10) for which only one signal was observed, analogous to the spectrum obtained following N₂ plasma treatment (Figure 4.3).

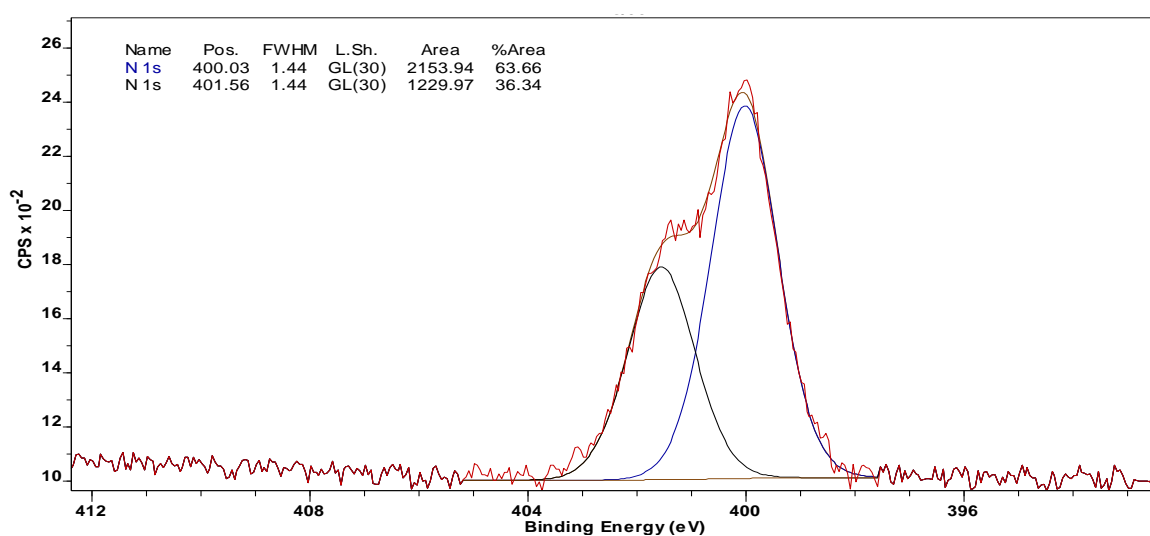


Figure 5.9 High resolution XPS spectrum of the N 1s orbital in Boc-Lys(Z)-OH functionalised PDMS (dichloromethane).

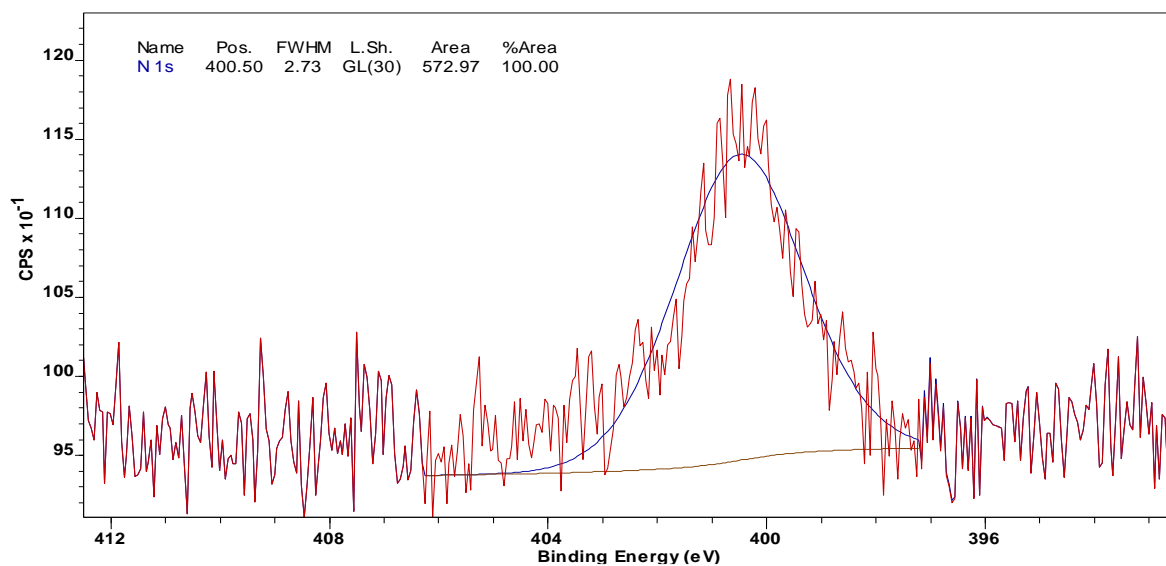


Figure 5.10 High resolution XPS spectrum of the N 1s orbital in Boc-Lys(Z)-OH functionalised PDMS (ethanol).

Exposure of plasma-treated, or UV-O₃-treated PDMS to aqueous solutions has repeatedly been investigated as a method of overcoming hydrophobic recovery, the success of which is thought to be attributed to hydrogen bonding between surface silanol groups and the solution, which may prevent the reorientation of polar functional groups towards the bulk (Ma *et al.*, 2011; Williams *et al.*, 2004; Zhao *et al.*, 2012). Thus, in this work, it was hypothesised that the exposure of PDMS to non-polar solvents may result in the reorientation of hydrophilic species towards the bulk, affecting the extent of permeation through the membrane. The effect of exposure of N₂ plasma treated PDMS to various solvents on the membrane permeability was investigated using the model compound lidocaine (LID). The cumulative mass of LID permeated through native PDMS, PDMS following N₂ plasma treatment, PDMS following storage in dichloromethane (DCM), and PDMS following storage in ethanol (EtOH) was calculated, and is presented in Table 5.7. A further aprotic solvent i.e. ethyl acetate (EtOAc), and a further protic solvent i.e. ultrapure water, were selected for comparative purposes. A storage time of three hours was selected, on par with the duration of the DCC coupling reaction.

Table 5.7 Effect of exposure of N₂ plasma treated PDMS to various solvents on the cumulative mass of lidocaine (LID) permeated after 6 hours (mean \pm standard deviation, 4 sig.fig. $n = 3$).

Plasma treatment time	Solvent treatment	Cumulative mass permeated (μg)
0	None	1292 \pm 47
150	None	464.1 \pm 71.7
150	Dichloromethane	1184 \pm 69
150	Ethanol	512.5 \pm 102.1
150	Ethyl acetate	1406 \pm 90
150	Deionised water	532.9 \pm 141.5

An overall statistically significant difference in the cumulative mass of lidocaine (LID) permeated after 6 hours following exposure to various solvents was observed ($F(5,12) = 65.45$, $p < 0.0010$). Levene's test for homogeneity of variance revealed data homoscedasticity ($F(5,12) = 1.230$, $p = 0.354$); thus, a post hoc Bonferroni test was used to perform pairwise comparisons.

Statistically significant differences in LID permeation were found between native PDMS, compared with PDMS following N₂ plasma treatment ($p < 0.001$), PDMS following storage in EtOH ($p < 0.001$), and PDMS following storage in ultrapure water ($p < 0.001$). No statistically significant differences were observed between permeation through N₂ plasma-treated PDMS, and plasma-treated PDMS following storage in EtOH ($p = 0.985$), and H₂O ($p = 0.934$). No statistically significant differences in permeation were observed following storage in EtOH compared with H₂O ($p = 1.00$) i.e no statistically significant differences in permeation were observed between PDMS following storage in the two protic solvents.

No statistically significant differences in permeation of LID were observed through native PDMS compared with PDMS following storage in DCM ($p = 0.704$), and following storage in EtOAc ($p =$

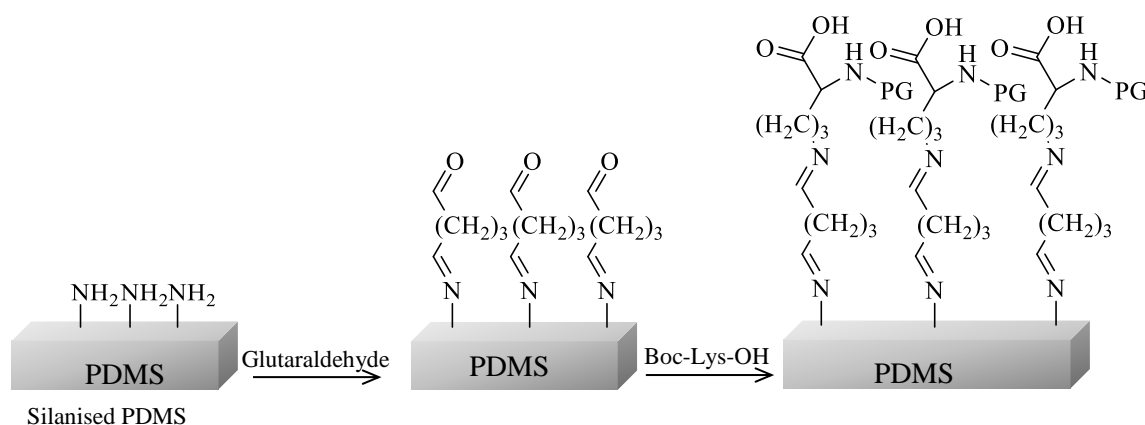
0.658) i.e. no statistically significant differences in permeation were observed between permeation through native PDMS and N₂ plasma-treated PDMS subsequently stored in either aprotic solvent. No statistically significant differences in permeation were observed between PDMS following storage in DCM compared with PDMS following storage in EtOAc ($p = 0.178$).

These findings suggest that the storage of N₂ plasma-treated PDMS in polar, protic solvents may prolong surface hydrophilicity, since such solvents can participate in hydrogen bonding with surface groups, on par with findings published by other authors (Ma *et al.*, 2011; Williams *et al.*, 2004; Zhao *et al.*, 2012). These findings must also be considered in the context of coupling reactions; if non-polar solvents, such as dichloromethane, result in the reorientation of amine groups towards the bulk, suitable surface groups available for biomolecule conjugation may become unavailable for reaction. Furthermore, non-polar solvents are known to swell PDMS (Lee *et al.*, 2003), and may facilitate the diffusion of oligomers to the surface, aiding hydrophobic recovery. These findings may further suggest that greater surface coverage may be achieved following reactions which can be performed in polar media.

5.2.3. Glutaraldehyde linker

The covalent attachment of glutaraldehyde to aminated PDMS surfaces is expansively used as a prerequisite to the immobilisation of biomolecules on PDMS substrates (Kuddannaya *et al.*, 2013; Shafieyan *et al.*, 2012; Wipff *et al.*, 2009). The reaction of glutaraldehyde with PDMS following amine functionalisation, for example with alkoxysilanes, can be performed in aqueous solution, typically isotonic pH 7.4 phosphate buffered saline, since many reports of biomolecule immobilisation on PDMS substrates are intended for cytological applications (Kuddannaya *et al.*, 2013). Protocols generally entail the submersion of PDMS substrates in 0.1 – 6 % solutions of glutaraldehyde for 15 – 60 minutes (Shafieyan *et al.*, 2012), followed by aqueous rinsing procedures, surpassing the need to consider the effect of exposure to organic solvents on PDMS membrane integrity. In this work, it was hypothesised that the use of a glutaraldehyde ‘linker’ molecule may provide a useful approach to circumventing the need for organic solvents, which may result in subsequent increases in permeability (Table 5.7), thought to be a consequence of accelerated hydrophobic recovery (Section 5.1.2.2). The use of

glutaraldehyde required the de-protection of either the α or ϵ amine group in Boc-Lys(Z)-OH, and the absence of a coupling reagent rendered the use of protecting groups redundant since peptide formation did not need to be evaded. However, signals from carbamate groups present in both the butoxycarbonyl (Boc) and carboxybenzyl (Z) in both the ATR-FTIR spectra and XPS spectra previously proved a useful marker for successful biomolecule immobilisation (Sections 5.2.1 and 5.2.2), thus, one of two protecting groups were removed i.e. N_α -Boc-L-lysine was used to enable comparison with previous spectra. Thus, PDMS was functionalised with (3-aminopropyl)triethoxysilane (APTES), followed by glutaraldehyde (GA), according to reported methods (Farrell *et al.*, 2010; Kuddannaya *et al.*, 2013; Wipff *et al.*, 2009), and was further functionalised with N_α -Boc-L-lysine i.e. PDMS-APTES-GA-Lys (Scheme 5.3), and was subject to ATR-FTIR, XPS, and SEM analysis, as performed previously.



Scheme 5.3 Lysine immobilisation at the surface of silanised PDMS following glutaraldehyde functionalisation, where PG = tert-butyloxycarbonyl.

5.2.3.1. Attenuated Total Reflectance - Fourier Transform Infrared Spectroscopy (ATR-FTIR)

Table 5.8 ATR-FTIR of native PDMS, and APTES silanised PDMS following glutaraldehyde and Boc-Lys(Z)-OH functionalisation (PDMS-APTES-GA-Lys).

Assignment	ν_{\max} (cm ⁻¹)	
	Native PDMS	PDMS-APTES-GA-Lys
$\nu(\text{N-H})$	N/A	3332.4
$\nu_{\text{as}}(\text{CH}_3)$	2962.3	2962.1
$\nu(\text{C=O})$	N/A	1698.8
$\nu(\text{C-N})$	N/A	1530.6
$\delta_{\text{s}}(\text{CH}_2)$	1412.6	1412.4
Si-CH ₃	1258.2	1258.2
Si-O-Si	1006.3	1005.7
O-SiCH ₃	786.2	785.1
C-SiCH ₃	701.4	701.2

An absorbance at 1530.6 cm⁻¹ in the ATR-FTIR spectrum of PDMS-APTES-GA-Lys is indicative of the presence of a secondary amide, and is markedly similar to that observed previously following Boc-Lys(Z)-OH functionalisation of APTMS silanised PDMS (1531.1 cm⁻¹) (Table 5.3), supporting the occurrence of successful amino acid functionalisation. Similarly, the presence of an absorption at 1698.8 cm⁻¹, comparable to that obtained previously following Boc-Lys(Z)-OH functionalisation i.e. at 1695.1 (Table 5.3), suggests the presence of a carbonyl group, indicating successful glutaraldehyde functionalisation, and may suggest successful Boc-Lys-OH functionalisation. As anticipated, the presence of surface methyl groups is confirmed by a symmetrical stretching vibration of the CH₃ group at 2962.1 cm⁻¹, and the asymmetric and symmetric deformation of the CH₃ group at 1412.4 and 1258.2 cm⁻¹, respectively. The Si-O-Si stretching vibration is observed at 1005.7 cm⁻¹, along with absorptions at 785.1 and 701.2 cm⁻¹, confirming the presence of the O-SiCH₃ and C-SiCH₃ groups, respectively.

5.2.3.2. X-ray Photoelectron Spectroscopy (XPS)

Quantitative elemental composition of the PDMS surface pre- and post-modification was determined using XPS survey scans (Appendix 5- Appendix 7), with data subsequently presented in the form of atomic percent (%) (Table 5.9). The O 1s, C 1s, N 1s and Si 2p orbitals were identified at binding energies circa 530 eV, 282 eV, 399 eV, and 100 eV, respectively.

Table 5.9 Atomic percent (%) of oxygen, nitrogen, carbon and silicon at the surface of APTES functionalised PDMS (PDMS-APTES), APTES-glutaraldehyde functionalised PDMS (PDMS-APTES-GA), and PDMS-APTES-GA following functionalisation with Boc-Lys-OH (PDMS-APTES-GA-Lys), taken from XPS survey scans.

Membrane	Sample	Atomic percent (%)			
		O	N	C	Si
PDMS-APTES	1	23.97	0.25	45.60	30.18
	2	23.96	< 0.10	45.63	30.40
PDMS-APTES-GA	1	21.59	3.61	57.73	17.07
	2	21.61	2.63	57.37	18.40
PDMS-APTES-GA-Lys	1	21.72	2.51	56.36	19.42
	2	23.51	2.69	54.01	17.49
	3	21.55	2.97	56.83	18.14
	4	22.56	3.25	55.03	18.09

An increase in the atomic percent (%) of nitrogen was observed following APTES silanisation (PDMS-APTES), compared with that obtained following similar analysis of native PDMS (Table 3.2). However, the increase in nitrogen observed was lower than that observed following air plasma treatment alone. Furthermore, the occurrence of this increase in only one of the duplicate samples

suggests surface heterogeneity, and an atomic percent of nitrogen lower than that of air plasma-treated PDMS suggests no attachment of APTES in the two sample areas tested, and may further suggest a degree of hydrophobic recovery occurring. These findings are supported by an increase in the atomic percent of nitrogen following glutaraldehyde functionalisation (PDMS-APTES-GA) i.e. the structure of glutaraldehyde is devoid of nitrogen. These results suggest a more extensive degree of silanisation, however, the nitrogen content observed was around half that observed previously following APTMS silanisation (Table 5.2). No significant changes in the surface chemical composition were observed following Boc-Lys-OH functionalisation (PDMS-APTES-GA-Lys), with regards to the atomic percent of carbon, oxygen, nitrogen and silicon. The identification of changes in surface chemistry on the basis of data obtained from survey scans proved problematic since samples were generally found to be heterogeneous in nature, supported by visual examination of the membrane (Figure 5.11), despite an increase in the number of samples tested with regards to PDMS-APTES-GA-Lys. Thus, high resolution XPS spectra were obtained in order to identify surface functionality (Figure 5.12 - Figure 5.17).

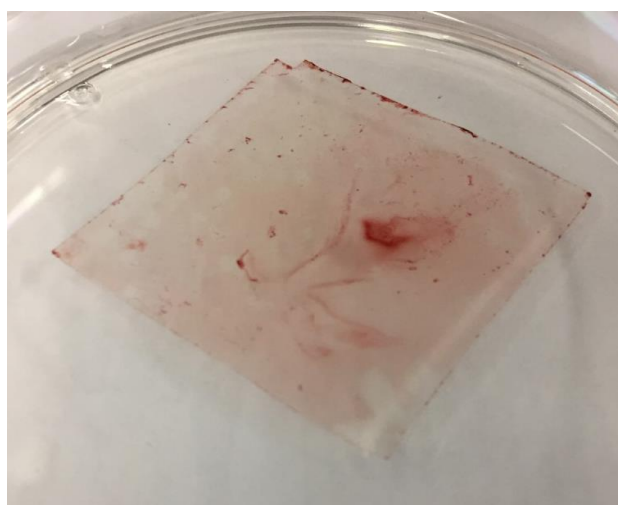


Figure 5.11 PDMS membrane following functionalisation with (3-aminopropyl)triethoxysilane, glutaraldehyde, and Boc-Lys-OH (PDMS-APTES-GA-Lys).

High resolution XPS spectra of the C 1s orbital in PDMS-APTES, PDMS-APTES-GA, and PDMS-APTES-GA-Lys were obtained, and are presented in Figure 5.12, Figure 5.13, and Figure 5.14, respectively. The high resolution XPS spectrum of the C 1s orbital in PDMS following silanisation with (3-aminopropyl)triethoxysilane (PDMS-APTES) (Figure 5.12) is markedly similar to that of

native PDMS (Figure 3.6), and suggests unsuccessful surface silanisation, supporting the findings of survey scans obtained at this sampling region on the substrate (Table 5.9).

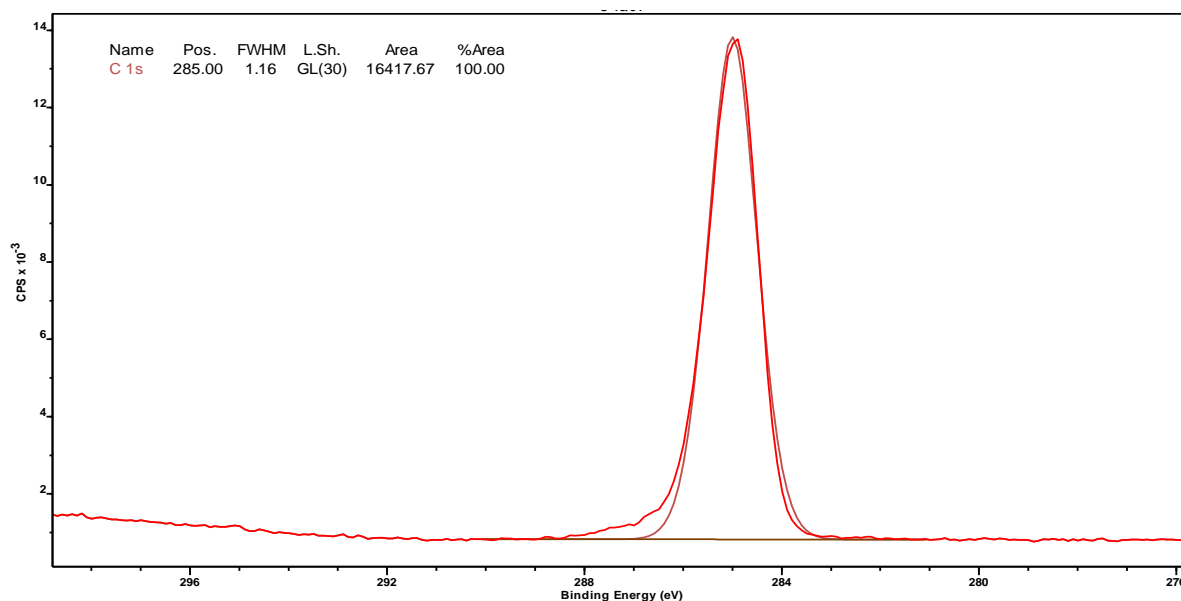


Figure 5.12 High resolution XPS spectra of the C 1s orbital in PDMS following (3-aminopropyl)triethoxysilane silanisation (PDMS-APTES).

The high resolution XPS spectrum of the C 1s orbital of PDMS-APTES following glutaraldehyde functionalisation (PDMS-APTES-GA) (Figure 5.13) contains four signals at binding energies of 284.99 eV, 285.82 eV, 286.83 eV and 288.03 eV, and is notably similar to that obtained previously following APTMS silanisation (Figure 5.2). Signals were previously assigned to methyl, amine, alcohol, and carbonyl-containing groups, respectively (Section 5.2.1.1.2). The atomic percent of the signal circa 288 eV, associated with carbonyl containing groups, is greater in PDMS-APTES-GA, in comparison to that obtained following APTMS silanisation (Figure 5.2) and air plasma treatment (Figure 3.7), as anticipated. The carbonyl signals obtained previously following APTMS silanisation and air plasma treatment, at binding energies of 288.35 eV and 288.50 eV, were attributed to amide groups introduced following plasma processing, based on the signal chemical shift, and the presence of a stoichiometric percent of nitrogen. The binding energy of the signal associated with carbonyl-containing functionalities is lower in the C 1s spectrum of PDMS-APTES-GA i.e. at 288.03 eV, than the corresponding spectra for air plasma treated and APTMS silanised PDMS i.e. at 288.50 and 288.35, respectively. The binding energy obtained herein more closely matches the range quoted for aldehyde

groups i.e. 287.81-288.06 eV, than that corresponding to amide groups i.e. 287.97 – 288.59 eV (Bittrich *et al.*, 2014), suggesting successful glutaraldehyde functionalisation, supporting the findings of ATR-FTIR spectroscopic analysis (Table 5.8).

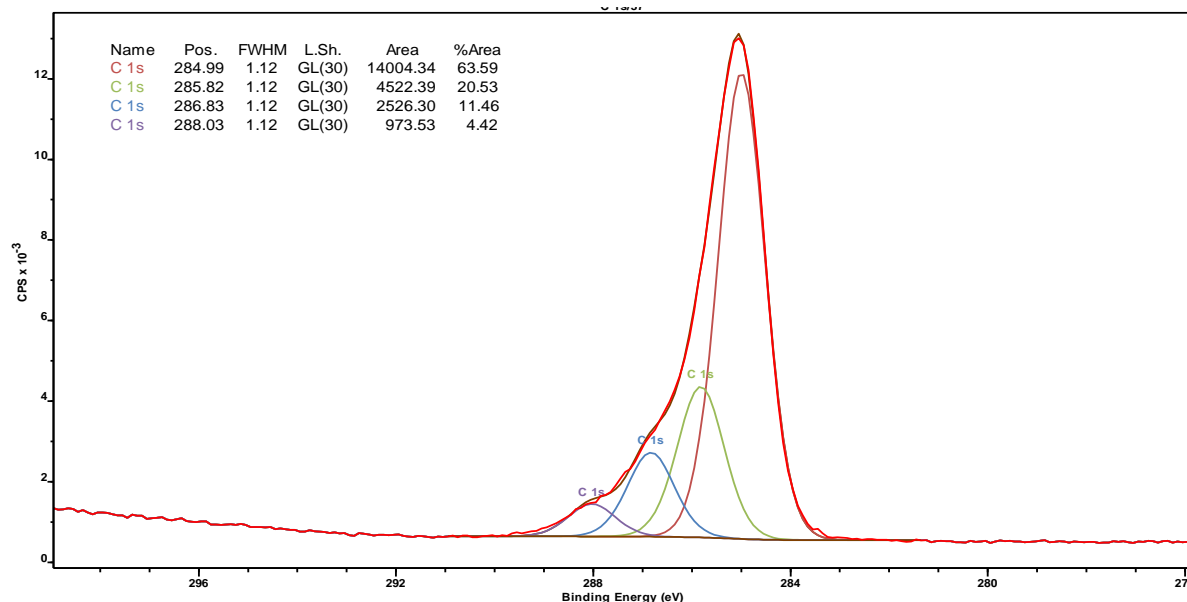


Figure 5.13 High resolution XPS spectrum of the C 1s orbital in PDMS following (3-aminopropyl)triethoxysilane silanisation and glutaraldehyde functionalisation (PDMS-APTES-GA). The high resolution XPS spectrum of the C 1s orbital in PDMS-APTES-GA-Lys (Figure 5.14) similarly contains four signals, at binding energies of 285.00 eV, 286.01 eV, 286.95 eV and 288.18 eV, matching those reported for methyl, amine, alcohol and carbonyl-containing groups, respectively. No significant deviations in the atomic percent of each signal were observed, in comparison with that obtained following similar analysis of PDMS-APTES-GA (Figure 5.13). Thus it was hypothesised that high resolution XPS spectra of the N 1s orbital would provide greater insight regarding the occurrence of surface lysine functionalisation (Figure 5.15 - Figure 5.17).

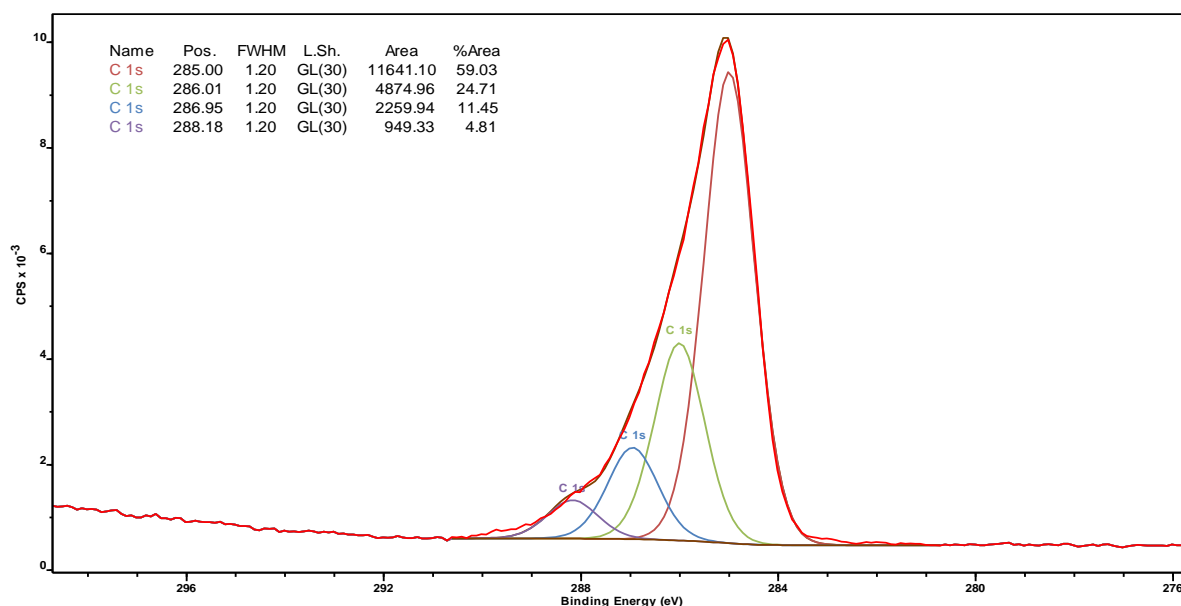


Figure 5.14 High resolution XPS spectrum of the C 1s orbital of PDMS following (3-aminopropyl)triethoxysilane silanisation, and functionalisation with glutaraldehyde and Boc-Lys-OH (PDMS-APTES-GA-Lys).

Only one peak was observed in the high resolution XPS spectrum of the N 1s orbital in PDMS-APTES. The binding energy is most similar to that obtained following APTMS silanisation i.e. 399.59 eV, matching that reported from primary amine groups (Figure 5.3), in comparison to that obtained corresponding to air plasma-treated PDMS i.e. 400.79 eV, matching that reported for amide groups (Figure 3.7) (Williams *et al.*, 2004).

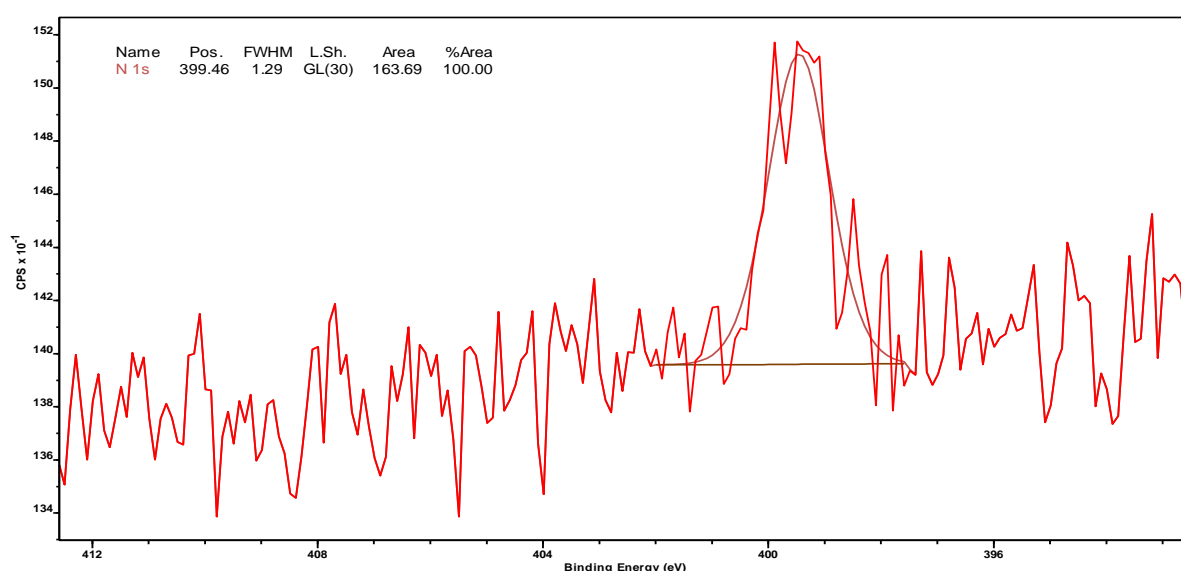


Figure 5.15 High resolution XPS spectrum of the N 1s orbital of PDMS following (3-aminopropyl)triethoxysilane silanisation (PDMS-APTES).

Two peaks were observable in the high resolution N 1s spectrum in PDMS-APTES-GA, as anticipated following the analysis of survey spectra and high resolution C 1s spectra (Table 5.9 and Figure 5.14, respectively) i.e. the sample appeared to be more extensively silanised. Furthermore, the binding energies of each signal, and the relative percent of each, were similar to values obtained previously following APTMS silanisation (Figure 5.3).

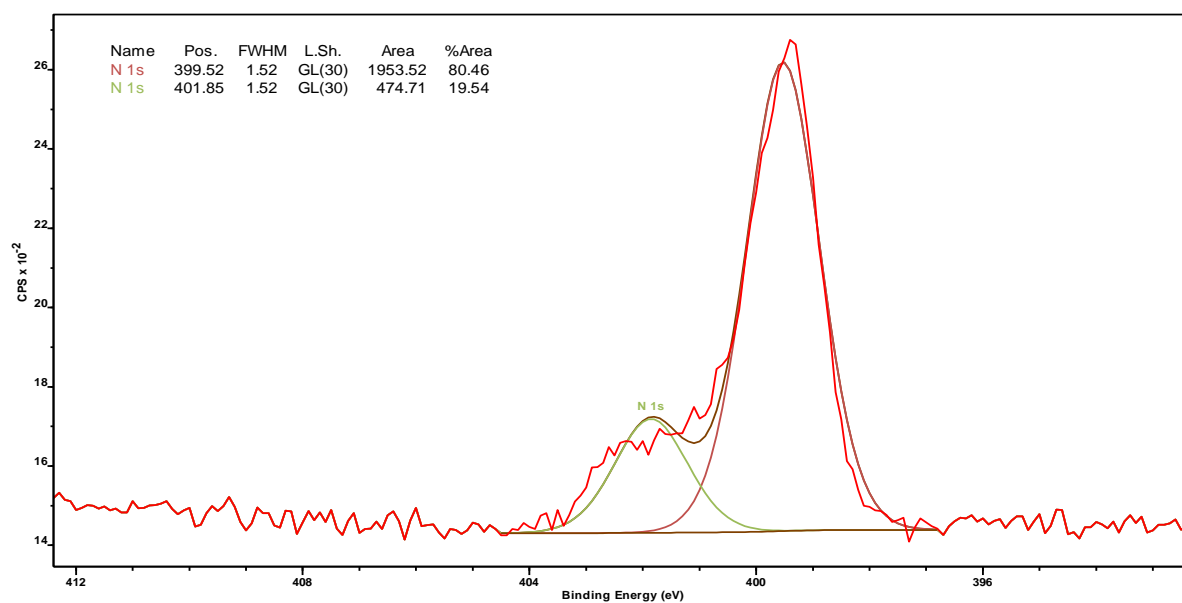


Figure 5.16 High resolution XPS spectrum of the N 1s orbital in PDMS following (3-aminopropyl)triethoxysilane silanisation and glutaraldehyde functionalisation (PDMS-APTES-GA).

A similar scenario was observed in the high resolution XPS spectrum of PDMS-APTES-GA-Lys (Figure 5.17), with two peaks at 399.69 eV and 401.78 eV, corresponding to amine and amide groups, respectively (Williams *et al.*, 2004). A small increase in the percent area of the latter signal was observed following coupling to Boc-Lys-OH and may suggest the presence of carbamate groups in the *tert*-butoxycarbonyl (Boc) protecting group.

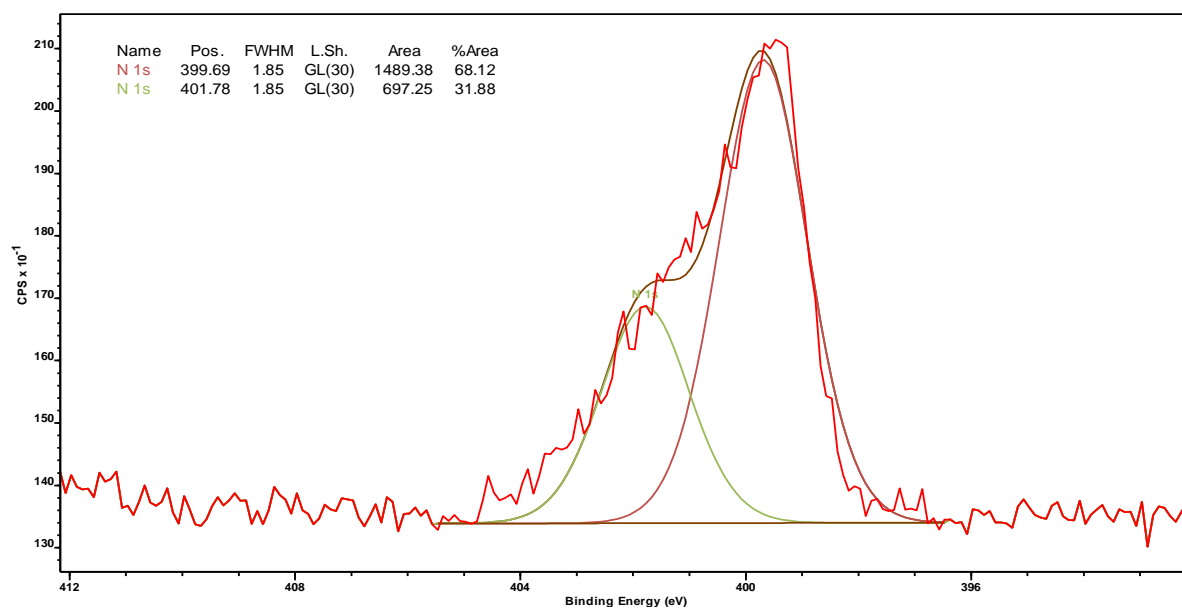


Figure 5.17 High resolution XPS spectrum of the N 1s orbital in PDMS following (3-aminopropyl)triethoxysilane silanisation and functionalisation with glutaraldehyde and Boc-Lys-OH (PDMS-APTES-GA-Lys).

5.2.3.3. Scanning Electron Microscopy

Scanning electron microscopy images of silanised PDMS following glutaraldehyde functionalisation (PDMS-APTES-GA) and following subsequent Boc-Lys-OH functionalisation (PDMS-APTES-GA-Lys) (Figure 5.18), were obtained in order to evaluate membrane integrity, and observe changes in surface morphology, which may affect the membrane permeability.

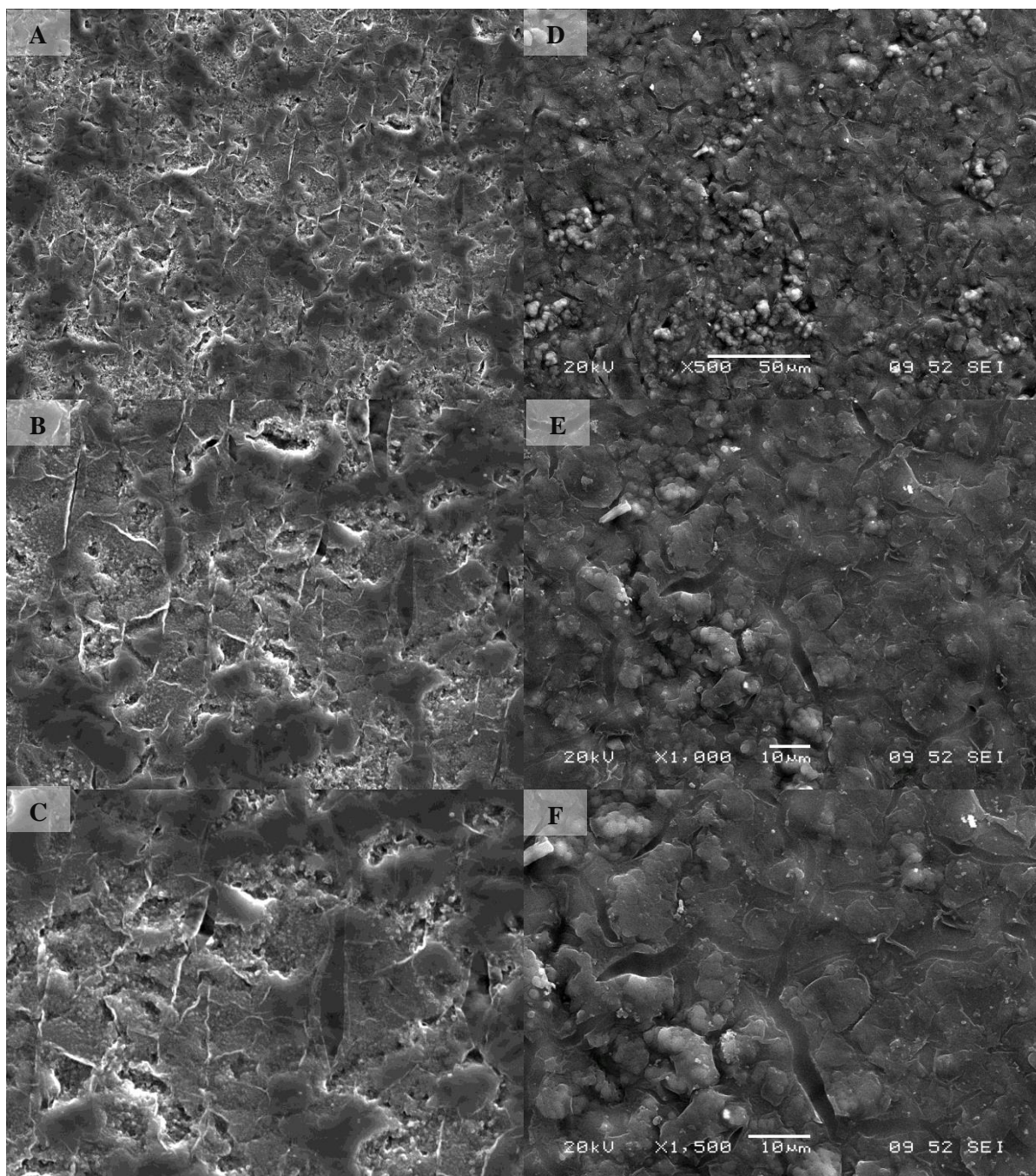


Figure 5.18 Scanning Electron Microscopy images of PDMS-APTES-GA (A-C, magnification 500 X, 100 X and 1500 X, respectively) and PDMS-APTES-GA-Lys (D-F, magnification 500 X, 100 X and 1500 X, respectively)

The morphology of the membrane following glutaraldehyde functionalisation is notably different from that observed immediately following silanisation (Figure 5.4) with an additional, heterogeneous superficial layer apparent. Similar observations were made following scanning electron microscopy

analysis of PDMS-APTES-GA following lysine functionalisation i.e. the membrane appeared different from silanised PDMS (Figure 5.4) and PDMS-APTES-GA (Figure 5.18).

5.3. Conclusions

In this chapter, three biomolecule immobilisation strategies were investigated for potential use in the attachment of biorelevant molecules to PDMS membranes, endeavouring to produce structurally relevant synthetic composite membranes for use in *in vitro* skin permeability studies. Keratinocytes represent more than 95 % of epidermal cells (McKittrick *et al.*, 2012), thus the attachment of keratin to PDMS is of heightened interest to this project. Lysine was selected as a model biomolecule to investigate the appropriateness of each immobilisation strategy, on the basis of its abundance in keratin, presence on the exterior structure of proteins, and commercial availability (Candi *et al.*, 1998; Kim *et al.*, 2013).

The silanisation of PDMS was performed, according to reported methods, endeavouring to generate surface amine groups for the coupling of lysine. An *N,N'*-dicyclohexylcarbodiimide coupling reaction was performed, according to protocols traditionally used in solid phase peptide synthesis. The presence of lysine at the surface of PDMS was confirmed following ATR-FTIR and XPS analysis, rendering the method a promising approach for the immobilisation of proteins. It was further hypothesised that the reaction could be extended to PDMS substrates following surface amination via an N₂ plasma treatment, surpassing the need for a surface silanisation step.

The direct coupling of lysine to N₂ plasma treated PDMS was found to be a convenient method of biomolecule attachment, however, despite the confirmation of the presence of lysine at the surface of the modified membrane using ATR-FTIR and X-ray photoelectron spectroscopy, the surface of PDMS was found to primarily be oxidised. Thus, in order to further extend this method to the covalent attachment of keratin, the adjustment of plasma conditions may be necessary i.e. the use of a custom made plasma generator, with which purge-vacuum cycles can be performed in order to remove residual air and water vapour. Furthermore, the exposure of N₂ plasma-treated PDMS to two aprotic solvents, namely dichloromethane and ethyl acetate, was found to result in an increase permeability, on par with

that obtained with native PDMS, hypothesised to be a consequence of the reorientation of polar surface groups. In order to enhance the degree of surface coverage, the use of coupling reagents with which coupling can be performed in polar solvents, such as *N*-(3-dimethylaminopropyl)-*N'*-ethylcarbodiimide hydrochloride (EDC), should be investigated prior to the utilisation of this method in the development of polymeric skin mimics i.e. the permeation of pharmaceutical compounds through membranes prepared using this approach will not be considered in this thesis.

The use of a glutaraldehyde 'linker' molecule was investigated as an approach to circumventing the need for aprotic solvents. Despite the frequency of reports, data deconvolution was problematic, attributed to the surface heterogeneity. An absorbance at 1530.6 cm^{-1} in the ATR-FTIR spectrum of PDMS-APTES-GA-Lys, markedly similar to that observed previously following lysine coupling to APTMS silanised PDMS, was indicative of the presence of a secondary amide, and suggested successful surface functionalisation. These findings were supported by an increase in the percent area of the signal associated with amide functionalities in the N 1s spectrum of PDMS-APTES-GA following lysine functionalisation i.e. PDMS-APTES-GA-Lys. Distinct changes in the morphological properties of the membrane were observed in the scanning electron microscopy images of PDMS following glutaraldehyde functionalisation and lysine functionalisation, in comparison to that observed following silanisation alone. Additionally, visual examination of the membrane supported the findings of other authors that glutaraldehyde may reduce substrate uniformity (Pakstis *et al.*, 2010). In any case, both the PDMS-APTMS-Lys and PDMS-APTES-GA-Lys membranes presented herein are of additional interest in permeation studies.

References

- Bittrich, Cometa, De Giglio, Di Mundo, Ditaranto, Eichhorn, Keller, Lednický, Mangolini, & Palumbo. (2014). *Polymer Surface Characterization*. Berlin/Boston: Walter De Gruyter.
- Candi, Tarcsa, Digiovanna, Compton, Elias, Marekov, & Steinert. (1998). A Highly Conserved Lysine Residue on the Head Domain of Type II Keratins is Essential for the Attachment of Keratin Intermediate Filaments to the Cornified cell Envelope through Isopeptide Crosslinking by Transglutaminases. *Proceedings of the National Academy of Sciences of the United States of America*, 95(5), 2067-2072.
- Cordeiro, Zschoche, Janke, Nitschke, & Werner. (2009). Functionalization of poly(dimethylsiloxane) surfaces with maleic anhydride copolymer films. *Langmuir*, 25(3), 1509-1517.
- Farrell, & Beaudoin. (2010). Surface forces and protein adsorption on dextran- and polyethylene glycol-modified polydimethylsiloxane. *Colloids and Surfaces B: Biointerfaces*, 81(2), 468-475.
- Godin, & Touitou. (2007). Transdermal skin delivery: predictions for humans from in vivo, ex vivo and animal models. *Adv Drug Deliv Rev*, 59(11), 1152-1161.
- Gunda, Singh, Norman, Kaur, & Mitra. (2014). Optimization and characterization of biomolecule immobilization on silicon substrates using (3-aminopropyl)triethoxysilane (APTES) and glutaraldehyde linker. *Applied Surface Science*, 305, 522-530.
- Haq, Khan, Dou, Alam, Attaullah, & Zari. (2015). Keratin film ablation for the fabrication of brick and mortar skin structure using femtosecond laser pulses. *Applied Physics A*, 120(4), 1415-1425.
- Hirata, & Ichiki. (2008). Introduction of Amino Groups on Poly(dimethylsiloxane) Surface Using Low-pressure Nitrogen-based Inductively Coupled Plasma. *Journal of Photopolymer Science and Technology*, 21(5), 705-710.
- Karakoy, Gultepe, Pandey, Khashab, & Gracias. (2014). Silane surface modification for improved bioadhesion of esophageal stents. *Applied Surface Science*, 311, 684-689.
- Kim, & Herr. (2013). Protein immobilization techniques for microfluidic assays (Vol. 7, pp. 41501). United States.
- Knud J. Jenson. (2013). *Peptide Synthesis and Applications* (2nd 2013 ed. Vol. 1047). Totowa, NJ: Humana Press.
- Kuddannaya, Chuah, Lee, Menon, Kang, & Zhang. (2013). Surface chemical modification of poly(dimethylsiloxane) for the enhanced adhesion and proliferation of mesenchymal stem cells. *ACS Applied Materials & Interfaces*, 5(19), 9777-9784.
- Lane. (2013). Skin penetration enhancers. *International Journal of Pharmaceutics*, 447(1-2), 12-21.
- Lee, Conradi, & Shanmugasundaram. (2010). Development of an in silico model for human skin permeation based on a Franz cell skin permeability assay. *Bioorganic and Medicinal Chemistry Letters*, 20(1), 69-73.
- Lee, Park, & Whitesides. (2003). Solvent Compatibility of Poly(dimethylsiloxane)-Based Microfluidic Devices. *Analytical Chemistry*, 75(23), 6544-6554.
- Lin, Freemantle, Kelly, Fielitz, Obare, & Ofoli. (2010). In situ immobilization of palladium nanoparticles in microfluidic reactors and assessment of their catalytic activity. *Nanotechnology*, 21(32), 1-8.
- Ma, Rivera, Hirasaki, & Biswal. (2011). Wettability control and patterning of PDMS using UV-ozone and water immersion. *Journal of Colloid and Interface Science*, 363(1), 371-378.
- McKittrick, Chen, Bodde, Yang, Novitskaya, & Meyers. (2012). The Structure, Functions, and Mechanical Properties of Keratin. *The Journal of The Minerals, Metals & Materials Society*, 64(4), 449-468.
- Migneault, Dartiguenave, Bertrand, & Waldron. (2004). Glutaraldehyde: Behavior in aqueous solution, reaction with proteins, and application to enzyme crosslinking. *BioTechniques*, 37(5), 790-802.
- Montalbetti, & Falque. (2005). Amide bond formation and peptide coupling. *Tetrahedron*, 61(46), 10827-10852.
- Muttenthaler, Albericio, & Dawson. (2015). Methods, setup and safe handling for anhydrous hydrogen fluoride cleavage in Boc solid-phase peptide synthesis. *Nature Protocols*, 10(7), 1067-1083.

- Pakstis, Dunkers, Zheng, Vorburger, Quinn, & Cicerone. (2010). Evaluation of polydimethylsiloxane modification methods for cell response. *Journal of Biomedical Materials Research - Part A*, 92(2), 604-614.
- Selmin, Cilurzo, Aluigi, Franzè, & Minghetti. (2012). Regenerated keratin membrane to match the in vitro drug diffusion through human epidermis. *Results in Pharma Sciences*, 2(1), 72-78.
- Shafieyan, Tiedemann, Goulet, Komarova, & Quinn. (2012). Monocyte proliferation and differentiation to osteoclasts is affected by density of collagen covalently bound to a poly(dimethyl siloxane) culture surface. *Journal of Biomedical Materials Research Part A*, 100A(6), 1573-1581.
- Shumilov, Toutilou, Godin, Ainbinder, Yosha, & Tsahor-Ohayon. (2009). Evaluation of a polysiloxane-collagen biphasic membrane: A model for in vitro skin permeation studies. *Journal of Drug Delivery Science and Technology*, 19(4), 289-294.
- Tobin. (2006). Biochemistry of human skin--our brain on the outside. *Chem Soc Rev*, 35(1), 52-67.
- Tomomi, Masami, Kenji, & Yasunori. (1992). Prediction of skin permeability of drugs. II. Development of composite membrane as a skin alternative. *International Journal of Pharmaceutics*, 79(1), 21-28.
- Vesel, Junkar, Cvelbar, Kovac, & Mozetic. (2008). Surface modification of polyester by oxygen- And nitrogen-plasma treatment. *Surface and Interface Analysis*, 40(11), 1444-1453.
- Wang, Xu, & Chen. (2006). Nonionic surfactant dynamic coating of poly(dimethylsiloxane) channel surface for microchip electrophoresis of amino acids. *Analytica Chimica Acta*, 569(1), 188-194.
- Wang, Yang, McKittrick, & Meyers. (2016). Keratin: Structure, mechanical properties, occurrence in biological organisms, and efforts at bioinspiration. *Progress in Materials Science*, 76, 229-318.
- Williams, Wilson, & Rhodes. (2004). Stability of plasma-treated silicone rubber and its influence on the interfacial aspects of blood compatibility. *Biomaterials*, 25(19), 4659-4673.
- Wipff, Majd, Acharya, Buscemi, Meister, & Hinz. (2009). The covalent attachment of adhesion molecules to silicone membranes for cell stretching applications. *Biomaterials*, 30(9), 1781-1789.
- Yamaguchi, Usami, Natsume, Aoyagi, Nagase, Sugibayashi, & Morimoto. (1997). Evaluation of Skin Permeability of Drugs by Newly Prepared Polymer Membranes. *Chemical and Pharmaceutical Bulletin*, 45(3), 537-541.
- Yang, & Yuan. (2016). Investigation on the mechanism of nitrogen plasma modified PDMS bonding with SU-8. *Applied Surface Science*, 364, 815-821.
- Zhao, Lee, & Sen. (2012). Long-term retention of hydrophilic behavior of plasma treated polydimethylsiloxane (PDMS) surfaces stored under water and Luria-Bertani broth. *Sensors and Actuators, A: Physical*, 181, 33-42.

Chapter 6 The Effect of Biomolecule Conjugation on the Permeation of Pharmaceutical Compounds.

6.1. Introduction

In the previous chapter, three biomolecule immobilisation strategies were compared as potential routes to PDMS-protein composite membranes for use in *in vitro* permeation studies. The silanisation of PDMS using (3-aminopropyl)triethoxysilane (APTMS) followed by the *N,N'*-dicyclohexylcarbodiimide (DCC) coupling of Boc-Lys(Z)-OH was found to be the most attractive method of surface modification, based on the abundance of surface amine groups available, and the apparent change in surface functionality following the coupling procedures, processes which were monitored using ATR-FTIR and X-ray photoelectron spectroscopy. Extension of this methodology to N₂ plasma-generated surface amine groups was less favourable, on the basis of the limited number of surface amine groups generated, and the apparent change in surface hydrophilicity following exposure to non-polar, aprotic solvents. However, this method still appears promising, providing amendments to the protocols can be performed i.e. removal of residual water vapour and O₂ from the polymer and plasma process chamber, and the substitution of DCC with an aqueous soluble coupling reagent. A further method of surface modification was investigated, selected on the basis of the wealth of literature reporting its successful employment (Kuddannaya *et al.*, 2013; Shafieyan *et al.*, 2012; Wipff *et al.*, 2009), and the lack of requirement for aprotic solvents. The findings of ATR-FTIR and XPS spectra were somewhat conflicting, attributed to the surface heterogeneity of the samples. Nonetheless, signals in the ATR-FTIR and XPS spectra indicated successful surface modification, and work by other authors finding the glutaraldehyde surface to be more hydrophilic than that observed following silanisation, rendered this technique promising (Pakstis *et al.*, 2010).

Work by Pakstis *et al.* aiming to screen surface modification methods suitable for the immobilisation of fibronectin and laminin, compared physisorption based, electrostatic based, and covalent bond generation based approaches to the production of substrates appropriate for the culture of smooth muscle cells. The authors noted the inadequate nature of physisorption based approaches for such purposes,

attributed to the known desorption of the surface ‘modifiers’ over time, and low protein density obtained. The authors further compared the protein density of (3-aminopropyl)trimethoxysilane modified PDMS (PDMS-APTMS), glutaraldehyde functionalised PDMS-APTMS, and PDMS following O₂ plasma treatment and sequential use of *N*-(3-dimethylaminopropyl)-*N'*-ethylcarbodiimide hydrochloride (EDC). The authors found that hydrogen bonding and electrostatic interactions between fibronectin and surface amine groups, generated following APTMS silanisation, resulted in both superior protein coverage, and substrate uniformity, in contrast to the surfaces obtaining following EDC coupling to plasma generated carbonyl groups, and following the use of the glutaraldehyde linker. Interestingly, the authors also note the hydrophilicity of the glutaraldehyde surface to be around twice that observed following plasma treatment, APTMS silanisation, and EDC treated, following protein attachment (Pakstis *et al.*, 2010).

The work by Pakstis *et al.* represents an interesting example of the tailoring, and comparison, of the surface properties of PDMS for a specific application, following various surface modification procedures. No such work has been performed evaluating the permeability of modified PDMS to pharmaceutical compounds. Thus, in this chapter, the permeability of (3-aminopropyl)trimethoxysilane functionalised PDMS following the covalent attachment of lysine (PDMS-APTMS-Lys), and PDMS following silanisation, glutaraldehyde functionalisation, and lysine attachment (PDMS-APTMS-GA-Lys) was investigated. Four model pharmaceutical compounds were employed to encompass a range of physicochemical parameters; an anionic and cationic compound, namely benzoic acid (BA) and lidocaine (LID), and two compounds displaying a low degree of ionisation with a high and low log₁₀ P values, namely methyl 4-aminobenzoate (MAB) and butyl paraben (BP). It was hypothesised that the use of PDMS-biomolecule bilayers in a permeation study may support the identification of a suitable method of protein immobilisation for the production of lamellae-type structures of PDMS, in conjunction with data obtained previously (Chapter 5).

6.2 Results and Discussion

6.2.1 *N,N'*-Dicyclohexylcarbodiimide Coupling of Lysine to Silanised PDMS (PDMS-APTMS-Lys)

The silanisation of PDMS using (3-aminopropyl)trimethoxysilane, following by the *N,N'*-dicyclohexylcarbodiimide coupling of Boc-Lys(Z)-OH appeared the most promising method of biomolecule immobilisation on the basis of the availability of surface amine groups, and the apparent change in surface functionalisation following lysine attachment. Thus, the permeability of the resultant membrane was of heightened interest to this work. Further, the surface modification of PDMS was performed on one side of the membrane, based on a ‘top-up’ type surface modification i.e. it was hypothesised that the production of a polymer-biomolecule bilayer, followed by repeated steps of the spin-coating of a PDMS layer, followed by further biomolecule immobilisation may provide a suitable future method of lamellae formation (Figure 6.1).



Figure 6.1 Proposed schematic of PDMS-biomolecule composite membrane formation.

Consequently, in order to compare permeation through lysine-modified substrates with air plasma modified substrates, data obtained in Table 3.6 i.e. steady state flux (J_{ss}) through air plasma-treated PDMS, was repeated, treating only one side of the membrane. Furthermore, the use of a flow-through type cell apparatus was found in earlier work to be a superior method of maintaining sink conditions, in comparison with static Franz cell type apparatus. Therefore, data corresponding to air plasma-treated PDMS, along with that corresponding to native PDMS and PDMS-APTMS-Lys, obtained using the former cell type, is presented in Table 6.1, in the form of steady state flux (J_{ss}).

Table 6.1 Steady state flux (J_{ss}) of lidocaine (LID), benzoic acid (BA), methyl aminobenzoate (MAB), and butyl paraben (BP) through native PDMS, PDMS following air plasma treatment, and PDMS following APTMS silanisation and lysine functionalisation (PDMS-APTMS-Lys) (mean \pm standard deviation, 4 sig.fig., $n = 3$).

Compound	Steady-state flux (J_{ss} , $\mu\text{g cm}^{-2} \text{min}^{-1}$)		
	Native PDMS	Air plasma-treated PDMS	PDMS-APTMS-Lys
LID	16.40 \pm 0.42	13.00 \pm 0.94	14.99 \pm 0.67
BA	8.970 \pm 0.695	7.356 \pm 0.529	8.801 \pm 0.259
MAB	4.585 \pm 0.126	2.964 \pm 0.100	3.141 \pm 0.058
BP	1.603 \pm 0.015	1.056 \pm 0.051	1.436 \pm 0.056

The steady state flux of each compound through native, plasma-treated, and lysine functionalised PDMS (PDMS-APTMS-Lys) was compared using one-way ANOVA. In all cases Levene's test for the homogeneity of variance was insignificant with respect to all compounds i.e. $p > 0.05$, thus a post hoc Bonferroni test was performed in order to identify differences in permeation between each membrane type. In all cases, an increase in permeation was observed following the DCC coupling of Boc-Lys(Z)-OH to APTMS silanised PDMS, in comparison to that obtained following plasma treatment alone, displayed graphically in Figure 6.2 and Figure 6.3 for methyl 4-aminobenzoate (MAB) and butyl paraben (BP), respectively.

In the case of MAB, an overall statistically significant difference in J_{ss} was observed ($F(2,6) = 301.062$, $p < 0.001$). Statistically significant differences in J_{ss} through native, and plasma-treated PDMS were observed ($p < 0.001$), in line with previous data obtained corresponding to PDMS plasma-treated on both sides of the membrane (Table 3.6). Furthermore, statistically significant differences in permeation through PDMS-APTMS-Lys were observed, in comparison with that through native PDMS ($p < 0.001$). However, a statistically significant increase in permeation was observed following APTMS-Lys functionalisation of PDMS, in comparison with that obtained following plasma treatment alone ($p =$

0.004). A similar situation was observed in the case of BP ($F(2,6) = 118.78$, $p < 0.001$), whereby statistically significant differences in J_{ss} through native and plasma-treated PDMS were observed ($p < 0.001$), along with statistically significant differences in permeation through PDMS-APTMS-Lys, in comparison with that obtained with native PDMS ($p = 0.011$). Furthermore, a statistically significant increase in J_{ss} was observed following APTMS-Lys functionalisation, in comparison with that obtained following air plasma treatment alone ($p < 0.001$).

In the case of lidocaine (LID), an overall statistically significant difference in flux through the three membranes were obtained ($F(2,6) = 17.87$, $p = 0.003$). A statistically significant difference in permeation through plasma treated PDMS was observed in comparison with that obtained through native PDMS ($p = 0.003$). A statistically significant difference in flux through plasma-treated PDMS and PDMS-APTMS-Lys was observed ($p = 0.042$), in contrast with that obtained between native PDMS and PDMS-APTMS-Lys ($p = 0.134$). A similar situation was observed in the case of benzoic acid (BA) ($F(2,6) = 8.127$, $p = 0.020$). A statistically significant difference in flux was observed between that obtained with native PDMS and plasma-treated PDMS ($p = 0.033$). A statistically significant increase in permeation was observed following APTMS-Lys functionalisation ($p = 0.048$), thus, no statistically significant difference in steady state flux through native PDMS and PDMS-APTMS-Lys was observed ($p = 1.000$).

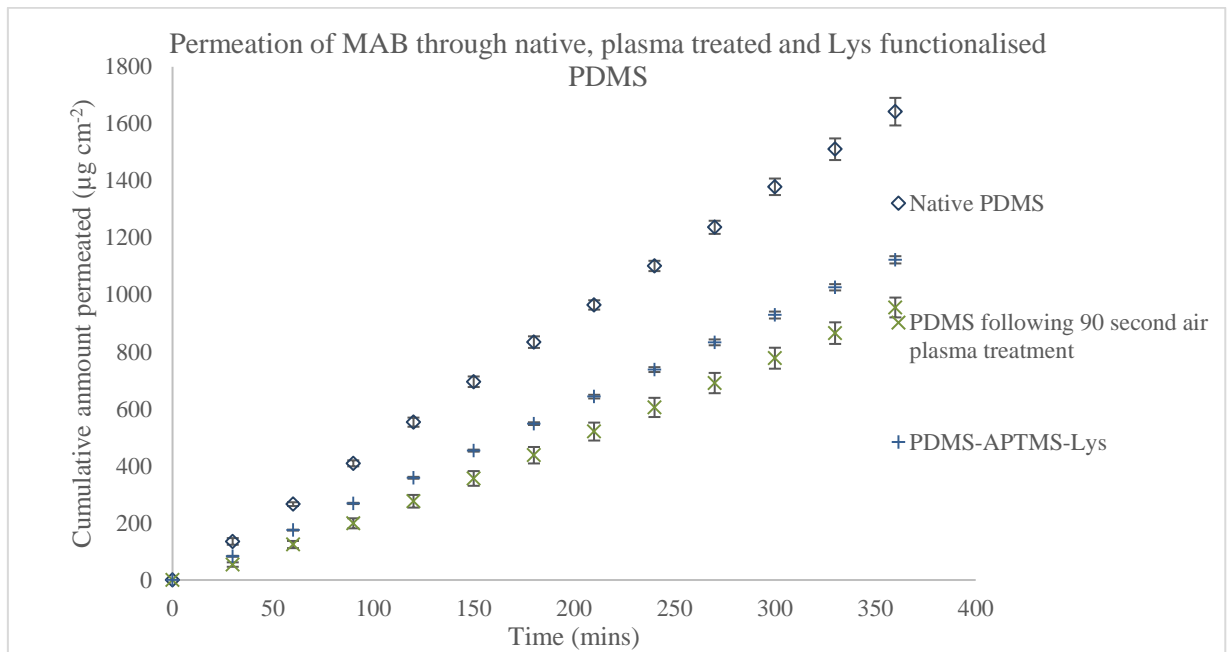


Figure 6.2 Permeation of methyl 4-aminobenzoate (MAB) through native PDMS, PDMS following air plasma treatment, and APTMS silanised PDMS following lysine functionalisation (PDMS-APTMS-Lys) (mean \pm standard deviation, $n = 3$).

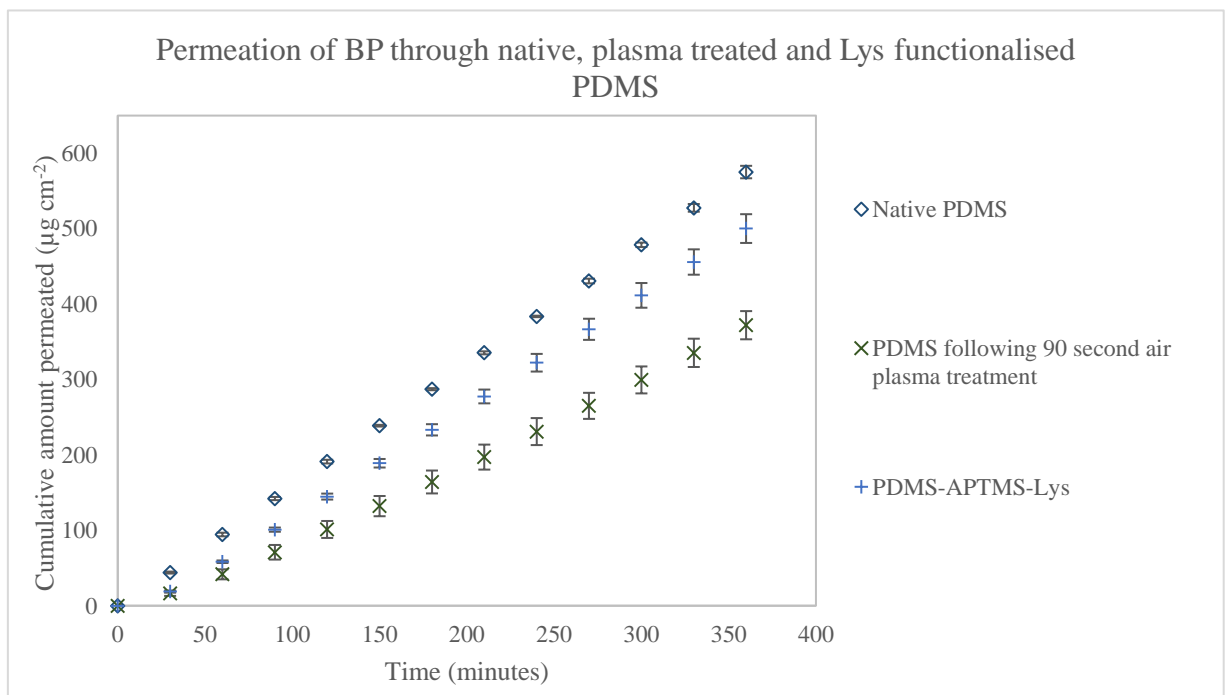


Figure 6.3 Permeation of butyl paraben (BP) through native PDMS, PDMS following air plasma treatment, and APTMS silanised PDMS following lysine functionalisation (PDMS-APTMS-Lys) (mean \pm standard deviation, $n = 3$).

In the case of all compounds tested, an increase in permeation was observed following APTMS-Lys functionalisation, with respect to that observed through plasma treated PDMS. Considering the findings presented in Table 5.7, the increase in permeation may be attributed to the hydrophobic recovery of PDMS and the reorientation of polar surface groups towards the bulk following exposure of plasma-treated and silanised PDMS to non-polar, aprotic solvents. No significant increases in permeation were observed with respect to that obtained through native PDMS. In order to further investigate these findings, the steady state flux of the same four compounds through silanised, glutaraldehyde and lysine functionalised PDMS (PDMS-APTES-GA-Lys) was considered i.e. all functionalisation reactions were performed in EtOH and phosphate buffered saline.

6.2.2. Use of Glutaraldehyde Linker (PDMS-APTES-GA-Lys).

The use of a glutaraldehyde linker molecule was explored as a facile approach to circumventing the need for non-polar, aprotic solvents, such as dichloromethane, and preventing the observed increase in membrane permeability (Table 5.7 and Table 6.1). Interestingly, work by Pakstis *et al.*, comparing multiple PDMS-biomolecule conjugation methods, found the surface of PDMS following functionalisation with glutaraldehyde and fibronectin to be more hydrophilic than plasma-treated PDMS, APTMS silanised PDMS, and PDMS functionalised with fibronectin using a carbodiimide coupling reagent, namely *N*-(3-dimethylaminopropyl)-*N'*-ethylcarbodiimide hydrochloride (EDC) (Pakstis *et al.*, 2010). In this work, the steady state flux of the same four compounds employed previously, namely lidocaine (LID), benzoic acid (BA), methyl 4-aminobenzoate (MAB) and butyl paraben (BP), was considered (Table 6.2).

Table 6.2 Steady state flux (J_{ss}) of lidocaine (LID), benzoic acid (BA), methyl aminobenzoate (MAB), and butyl paraben (BP) through native PDMS, PDMS following air plasma treatment, and PDMS following APTMS silanisation, glutaraldehyde and lysine functionalisation (PDMS-APTMS-GA-Lys) (mean \pm standard deviation, 4 sig.fig., $n = 3$).

Compound	Steady-state flux (J_{ss} , $\mu\text{g cm}^{-2} \text{min}^{-1}$)		
	Native PDMS	Air plasma-treated PDMS	PDMS-APTMS-GA-Lys
LID	16.40 \pm 0.42	13.00 \pm 0.94	9.612 \pm 0.454
BA	8.970 \pm 0.695	7.356 \pm 0.529	7.146 \pm 0.600
MAB	4.585 \pm 0.126	2.964 \pm 0.100	2.686 \pm 0.024
BP	1.603 \pm 0.015	1.056 \pm 0.051	1.047 \pm 0.069

The steady state flux of each compound through native, plasma-treated, and lysine functionalised PDMS (PDMS-APTMS-GA-Lys) was compared using one-way ANOVA. In all cases Levene's test for the homogeneity of variance was insignificant with respect to all compounds i.e. $p > 0.05$, thus a post hoc Bonferroni test was performed in order to identify differences in permeation between each membrane type.

In the case of LID, an overall statistically significant difference in flux through the three membranes was observed ($F(2,6) = 81.75$, $p < 0.001$). A statistically significant difference in flux through native PDMS and PDMS-APTMS-GA-Lys ($p < 0.001$) was observed, along with plasma-treated PDMS and PDMS-APTMS-GA-Lys ($p = 0.002$). In the case of MAB, an overall statistically significant difference in permeation was observed ($F(2,6) = 406.52$, $p < 0.001$). The steady state flux of MAB through native PDMS was found to differ to that through PDMS-APTMS-GA-Lys ($p < 0.0001$), however, no statistically significant differences in J_{ss} through plasma-treated PDMS and PDMS-APTMS-GA-Lys were observed ($p = 1.00$). Similar scenarios were also observed in the case of BP ($F(2,6) = 120.20$, $p < 0.001$), and BA ($F(2,6) = 7.536$, $p = 0.023$) i.e. statistically significant differences in permeation through native PDMS and PDMS-APTMS-GA-Lys were observed ($p < 0.001$ and $p < 0.023$ for BP and BA, respectively). No

statistically significant differences in permeation through plasma-treated PDMS and PDMS-APTES-GA-Lys were observed in the case of both compounds ($p = 1.00$).

In contrast to data obtained previously (Table 6.1, Figure 6.2 and Figure 6.3), no statistically significant increases in permeation were observed following APTES-GA-Lys functionalisation, in comparison to following plasma treatment alone, displayed graphically in Figure 6.4 and Figure 6.5 in the case of MAB and BP, respectively.

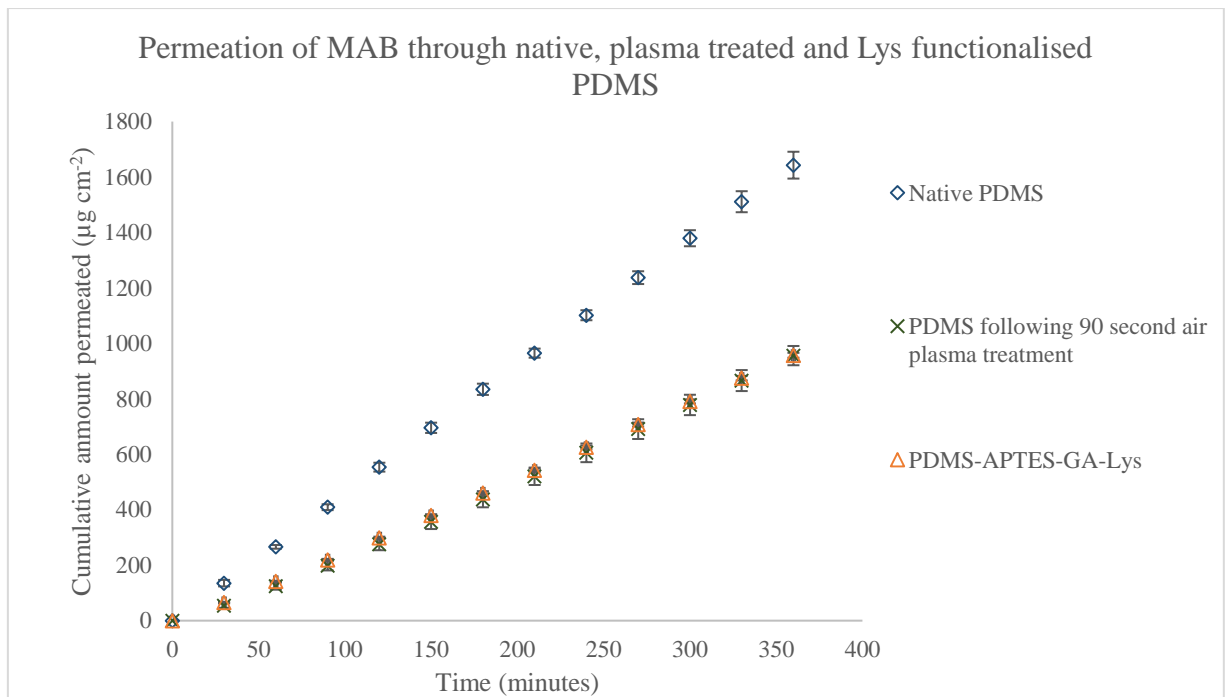


Figure 6.4 Permeation of methyl 4-aminobenzoate (MAB) through native PDMS, PDMS following air plasma treatment, and APTES silanised PDMS following glutaraldehyde and lysine functionalisation (PDMS-APTES-GA-Lys) (mean \pm standard deviation, $n = 3$).

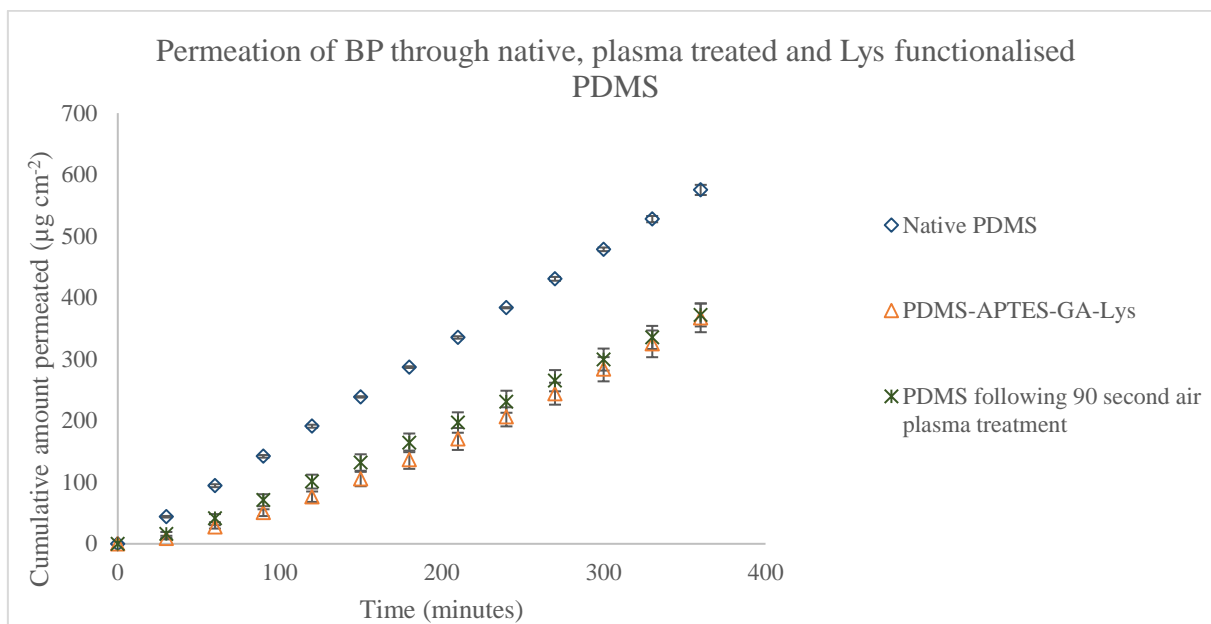


Figure 6.5 Permeation of butyl paraben (BP) through native PDMS, PDMS following air plasma treatment, and APTES silanised PDMS following glutaraldehyde and lysine functionalisation (PDMS-APTES-GA-Lys) (mean \pm standard deviation, $n = 3$).

A statistically significant reduction in permeation was observed in the case of only one of the four compounds tested in this study, namely lidocaine (LID). Considering the physicochemical properties of the penetrant, LID displays a polar surface area (PSA) of 36, close to that displayed by BA, i.e. 37, for which no statistically significant reduction in permeation was observed. Furthermore, LID displays a $\log_{10} P$ similar to that of BP i.e. 3.63 and 3.46, respectively. LID represents the only cationic compound in this study, with a saturated suspension above the initial buffer pH i.e. a pH of 8.3 (Appendix 11).

To date, no consensus has been reached regarding the mechanism of the reaction of glutaraldehyde with proteins. Although it is generally assumed that protein immobilisation on solid substrates occurs as a consequence of a reaction between the nucleophilic ϵ -amino groups of lysine residues on the exterior of proteins, no unanimity exists regarding the reactive glutaraldehyde species. As many as thirteen different forms of glutaraldehyde in solution have been noted, including α,β -unsaturated aldehydes and their resultant cyclic aldol condensation products, hydrated forms, cyclic hemiacetals and oligomers, polyglutaraldehyde structures including dimers, tetramers, and pentamers with a single available aldehyde group, and various aldol condensation polymeric products ranging in their degree of aldehyde, hydroxyl and carboxylic acid functionalisation (Migneault *et al.*, 2004). The relative proportion of each species in

solution has been found to be heavily dependent on solution pH, oxygen content, and concentration. For example, the dilution of a 70 % glutaraldehyde solution, known to contain a significant quantity of polymerised species, has been found to result in increased conversion to monomeric species (Kawahara *et al.*, 1992). Furthermore, in the pH range of 3.0 – 8.0, glutaraldehyde solutions have been found to consist mainly of monomeric, cyclic hemiacetals formed following the intramolecular reaction of a hydroxyl group with the carbonyl. Moreover, quandary surrounds the reaction via which glutaraldehyde mediated protein crosslinking occurs; both Micheal-type additions and Schiff base formation have been proposed as possible reaction mechanisms of glutaraldehyde based protein immobilisation, with the product of the latter represented in Scheme 5.3. Glutaraldehyde has been shown to react with multiple functional groups of proteins including thiol, phenol, amine and imidazole (Migneault *et al.*, 2004).

In this work, the surface was found to be heterogeneous, and the occurrence of a limited number of signals associated with N_α-Boc-L-lysine in the XPS and ATR-FTIR spectra of PDMS-APTES-GA-Lys (Section 5.2.3) may suggest the presence of free aldehyde groups. Considering this in the context of permeation studies, where the surface of modified PDMS may encounter a range of pH values of saturated suspensions or formulations, and penetrants may contain multiple functional groups known to react with glutaraldehyde, the use of glutaraldehyde for such purpose may be complex. For example, in the case of LID, the saturated suspension displayed a pH of 8.3. Schiff base formation is known to be reversible under basic conditions, and may result in increasing numbers of uncrosslinked glutaraldehyde molecules. The reduction of Schiff bases may be performed with sodium cyanoborohydride, resulting in the conversion of the imine to a secondary amine, which is stable to hydrolysis (Migneault *et al.*, 2004). It is apparent that knowledge of the mechanism of reaction of the amine group with glutaraldehyde serves as a prerequisite to the introduction of this step. The reduced nucleophilicity of amide groups, in comparison to that of amine groups, renders the reaction of lidocaine with glutaraldehyde unlikely in any case, however electrostatic interactions between deprotonated hydrated forms of glutaraldehyde and cationic lidocaine are highly likely.

The lack of permeability increase following lysine functionalisation may be attributed to a lack of hydrophobic recovery, as a consequence of the performance of all reactions in polar media i.e.

silanisation was performed in EtOH, and glutaraldehyde and lysine functionalisation was performed in phosphate buffered saline. Furthermore, the membrane heterogeneity observed previously (Section 5.2.3) did not appear to be problematic with regards to the permeation of pharmaceutical compounds i.e. coefficients of variation were all < 10 %, on par with those obtained following the employment of native and plasma-treated PDMS.

6.3. Conclusions

In this chapter, the permeation of pharmaceutical compounds through biomolecule-functionalised PDMS was considered. The silanisation of PDMS followed by the DCC coupling of lysine (PDMS-APTMS-Lys) appeared to be the most promising method of biomolecule conjugation, on the basis of the abundance of surface amine groups available for coupling, and distinct signals in the ATR-FTIR and XPS spectra following lysine functionalisation. However, increases in the permeation of four pharmaceutical compounds were observed following the employment of the membrane as a skin mimic in a flow-through cell type permeation study. It was hypothesised that such an increase was a consequence of the exposure of the polar PDMS surface to a non-polar solvent, namely dichloromethane, in support of earlier findings. Thus, the permeation of pharmaceutical compounds through PDMS functionalised with lysine via the use of a glutaraldehyde linker molecule (PDMS-APTES-GA-Lys) was considered. In contrast to the data obtained with PDMS-APTMS-Lys, no increase in permeation was observed following biomolecule immobilisation, attributed to the absence of non-polar solvents in the immobilisation process. A decrease in permeation was observed in the case of only one compound, namely lidocaine (LID), thought to be a consequence of interactions between cationic penetrant molecules and uncrosslinked glutaraldehyde molecules. In general, the immobilisation of lysine was found not to increase the permeation of pharmaceutical compounds, with respect to that through native PDMS. Such a finding indicates that, in the case of the compounds tested in this work, the overall rate of permeation appears to be largely controlled by permeation through the native bulk substrate. Since the objective of this work was to identify a suitable method of biomolecule attachment for the production of PDMS-protein lamellae structures, the aims of this work were met, despite no further decreases in permeation being observed in the case of three quarters of the compounds tested. Based on the surface

heterogeneity observed, and known complexity of the glutaraldehyde based protein immobilisation process, it may be taken that the immobilisation of biomolecules for the purpose of skin permeation studies should be performed using diimide based coupling reagents. It also must be noted that whilst no decrease in permeation was observed for lysine-PDMS bilayers, these findings cannot be extended to keratin-PDMS multilayers, rendering the continuation of this work promising, providing that a larger range of pharmaceutical compounds are tested.

References

- Kawahara, Ohmori, Ohkubo, Hattori, & Kawamura. (1992). The structure of glutaraldehyde in aqueous solution determined by ultraviolet absorption and light scattering. *Analytical Biochemistry*, 201(1), 94-98.
- Kuddannaya, Chuah, Lee, Menon, Kang, & Zhang. (2013). Surface chemical modification of poly(dimethylsiloxane) for the enhanced adhesion and proliferation of mesenchymal stem cells. *ACS Applied Materials & Interfaces*, 5(19), 9777-9784.
- Migneault, Dartiguenave, Bertrand, & Waldron. (2004). Glutaraldehyde: Behavior in aqueous solution, reaction with proteins, and application to enzyme crosslinking. *BioTechniques*, 37(5), 790-802.
- Pakstis, Dunkers, Zheng, Vorbürger, Quinn, & Cicerone. (2010). Evaluation of polydimethylsiloxane modification methods for cell response. *Journal of Biomedical Materials Research - Part A*, 92(2), 604-614.
- Shafieyan, Tiedemann, Goulet, Komarova, & Quinn. (2012). Monocyte proliferation and differentiation to osteoclasts is affected by density of collagen covalently bound to a poly(dimethyl siloxane) culture surface. *Journal of Biomedical Materials Research Part A*, 100A(6), 1573-1581.
- Wipff, Majd, Acharya, Buscemi, Meister, & Hinz. (2009). The covalent attachment of adhesion molecules to silicone membranes for cell stretching applications. *Biomaterials*, 30(9), 1781-1789.

Chapter 7 Conclusions and Future Work

A primary objective of the work presented in this thesis was to evaluate various polymer modification methods as potential approaches to producing a lamellae-type PDMS membranes, parallel to the structure of the stratum corneum, for use in *in vitro* skin permeation studies. The effect of the plasma treatment of PDMS on the permeation of pharmaceutical compounds, representing a range of physicochemical properties and therapeutic classes, was considered. The air plasma treatment of PDMS was found to result in the formation of polar surface functionalities, namely silanol groups, in line with literature reports (Chen *et al.*, 2007), and rendered the membrane less permeable to fourteen pharmaceutical compounds. Furthermore, an increase in correlation between permeability coefficients obtained using the synthetic substitute, and literature permeability coefficients obtained using excised human epidermal tissue, was observed.

It was further hypothesised that amine-functionalised PDMS surfaces may provide a useful platform for the attachment of biomolecules in order to enhance the biorelevance of PDMS skin mimics. Thus, an additional aim of the work presented in this thesis was to consider the effect of the N₂ plasma treatment of PDMS as a prerequisite to such work, on the basis of the large body of literature reporting the generation of surface amine groups following the N₂ plasma treatment of PDMS (Williams *et al.*, 2004; Yang *et al.*, 2016). With regards to the permeation of pharmaceutical compounds through N₂ plasma treated PDMS alone, a reduction in the permeation of nine pharmaceutical compounds was observed. No increase in correlation between permeability coefficients obtained using the synthetic substitute, and those obtained using epidermal tissue, was observed, despite the occurrence of greater reductions in the permeation of pharmaceutical compounds.

A third aim of the work presented in this thesis was to evaluate potential methods of immobilising amine group containing biomolecules at the surface of PDMS, to assist in the development of a method of producing a lipid-protein multilayer membrane, similar to the stratum corneum, appropriate for skin permeation assays. Two alkoxy silane based biomolecule immobilisation strategies were investigated, namely alkoxy silane layer formation followed by the *N,N'*-dicyclohexylcarbodiimide (DCC) coupling of Boc-Lys(Z)-OH (PDMS-APTMS-Lys), and alkoxy silane layer formation followed by Boc-Lys-OH

functionalisation using a glutaraldehyde 'linker' molecule (PDMS-APTES-GA-Lys). The silanisation of PDMS and sequential DCC coupling reaction method appeared to be the most promising in terms of the abundance of surface amine groups available, and distinct signals in the ATR-FTIR and XPS spectra, indicating successful lysine functionalisation. However, moderate increases in the permeation of pharmaceutical compounds were observed following the employment of the membrane as a skin mimic, with respect to permeation following plasma alone, thought to be a result of the exposure of PDMS to non-polar, aprotic solvents. No such increases in permeation were observed following the employment of PDMS-APTES-GA-Lys, selected on the basis of the performance of all functionalisation reactions in polar media, and the reported surface hydrophilicity (Pakstis *et al.*, 2010). Deconvolution of the surface analysis data, i.e. ATR-FTIR and XPS data, corresponding to the latter membrane type, was more problematic, attributed to the heterogeneity of the modified polymer surface. Thus, a logical progression of this work is to explore the potential of *N*-(3-dimethylaminopropyl)-*N'*-ethylcarbodiimide hydrochloride (EDC), an aqueous soluble diimide coupling reagent, in the production of biomolecule functionalised PDMS skin mimics, allowing for the performance of coupling in polar media, and potentially circumventing the permeability increase observed following the use of DCC.

The N₂ plasma treatment of PDMS was hypothesised to be a facile alternative to the air plasma treatment of PDMS and sequential silanisation reaction, in the generation of surface amine groups. A significant level of surface oxidation was observed i.e. the major species found to be introduced were silanol groups. It was hypothesised that the significant degree of surface oxidation was a consequence of residual air and water vapour in the polymer and the plasma process chamber. Upon employment of this membrane in the DCC coupling of Boc-Lys(Z)-OH, successful surface amino acid functionalisation at the limited number of surface amine sites was observed. In order to extend the use of N₂ plasma treatments to the immobilisation of biomolecules at the surface of PDMS, such as proteins, via amide bond formation, the use of a custom built plasma generator should be considered, allowing for more precise control over the resultant surface chemical functionality. For example, the plasma system utilised in this work performs only one chamber evacuation, via use of a vacuum pump, prior to the introduction of the process gas to the chamber and plasma ignition. Multiple purge-vacuum cycles may assist the removal of residual air and water vapour. The use of an in-line drying agent e.g. anhydrous calcium chloride

should be investigated as a modest approach to the removal of residual water vapour from the N₂ process gas. Additionally, the direct attachment of the plasma generator to an N₂ cylinder, for which the composition is more highly chemically characterised, should be considered as an alternative to the gas line system utilised in this work in order to minimise the influx of water vapour.

Sequential work should also consider alterations in the mechanical properties, such as the Young's modulus, of PDMS membranes following the physical and chemical based modification protocols explored in this thesis; variations in the elasticity of modified PDMS-based skin mimics may be correlated to crack formation, and subsequent increases in the permeation of pharmaceutical compounds. Following the exposure of PDMS membranes to oxidising plasma treatments, Si-CH₃ and Si-O bond cleavage is known to occur, inevitably resulting in alterations in the degree of cross-linking of polymer chains at the membrane surface i.e. quaternary siloxane units are formed (Owen *et al.*, 2012). At temperatures above the glass transition, polymers that are weakly cross-linked typically display 'rubber-like' behaviour, whilst polymers that are highly cross-linked display 'stiff viscoelastic' properties (Bergstrom, 2015). Such observations are particularly relevant to the development of PDMS-based polymeric skin mimics for which the glass transition temperature is low (-120 - -125 °C in the case of native PDMS) (Bosq *et al.*, 2014; Dollase *et al.*, 2003; Zhou *et al.*, 2010), and for which a range of storage and experimental temperatures may be employed.

Further logical progression of this work is the production of PDMS-biomolecule multilayers via multiple spin-coating and biomolecule immobilisation steps (Figure 6.1). Moreover, keratin extraction procedures should be optimised, allowing for keratin-PDMS multilayer formation. For example, keratin has successfully been extracted from sheep wool by sulfitolysis. Furthermore, it is hypothesised here that keratin from sheep wool may provide a suitable substitute for that in the stratum corneum barrier i.e. both are α -keratins, consisting of polypeptides in an α -helix conformation, in comparison to the β -pleated sheet conformation observed in reptilian and avian tissues, such as scales and feathers (Wang *et al.*, 2016). Although no further decreases in permeation were observed following biomolecule immobilisation in this work, these findings are not necessarily applicable to multilayers and/or alternative biomolecules. Other interesting progressions of this work include the possible 'corneocyte

patterning' of PDMS prior to biomolecule immobilisation, to enable a more accurate representation of the structural properties of the stratum corneum i.e. distinct proteinaceous regions surrounded by a continuous lipophilic region. The patterning of corneocyte bricks on the surface of PDMS may be possible by the production of a 'grid' or 'mesh' protective template that may be mounted onto the PDMS membrane prior to plasma processing (Figure 7.1). Since protected regions will be rendered chemically inert, it may be possible to selectively bio-functionalise the oxidised/aminated regions.

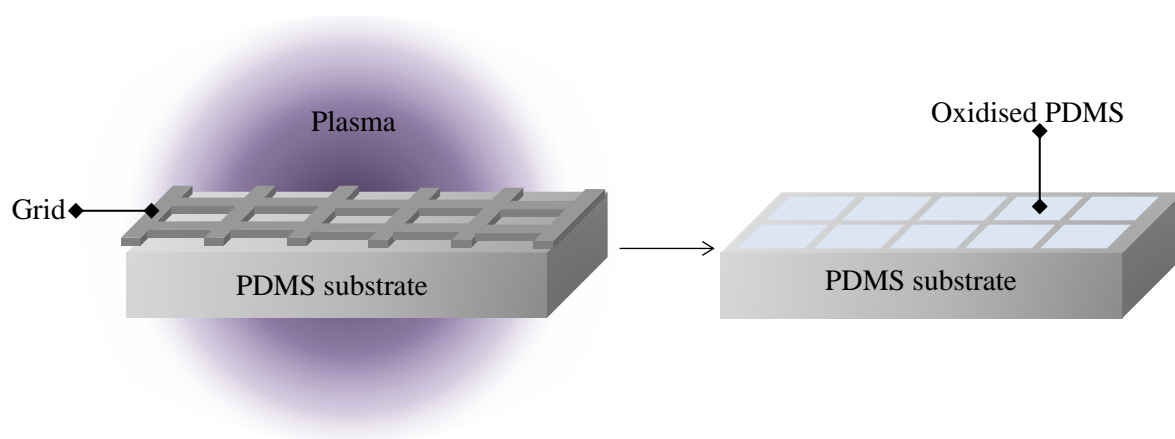


Figure 7.1 The corneocyte patterning of PDMS by use of a 'grid' template during plasma processing.

In summary, the aims of the work presented in this thesis were met i.e. the potential of the air plasma treatment of PDMS to produce lamellae-type structures suitable for skin permeation studies was investigated. Moreover, the potential of N_2 plasma treatment to aminate the surface of PDMS was considered, and three methods of biomolecule immobilisation were compared. Consequently, the work presented in this thesis provides a considerable insight of the effect of multiple biomolecule immobilisation strategies on the permeation of pharmaceutical compounds through PDMS. In general, plasma treatments appeared to reduce the permeation of pharmaceutical compounds through PDMS, a frequently employed skin mimic with which over estimations in percutaneous adsorption are often observed. The chemical immobilisation of lysine at the surface of PDMS did not significantly increase the permeation of pharmaceutical compounds, with respect to that through native PDMS, thus, the work may further facilitate the development of biorelevant polymeric skin mimics for use in permeation studies.

References

- Bergstrom. (2015). *Mechanics of Solid Polymers*: Elsevier Science.
- Bosq, Guigo, Persello, & Sbirrazzuoli. (2014). Melt and glass crystallization of PDMS and PDMS silica nanocomposites. *Physical chemistry chemical physics : PCCP*, 16(17), 783-784.
- Chen, & Lindner. (2007). The stability of radio-frequency plasma-treated polydimethylsiloxane surfaces. *Langmuir*, 23(6), 3118-3122.
- Dollase, Wilhelm, Spiess, Yagen, Yerushalmi-Rozen, & Gottlieb. (2003). Effect of Interfaces on the Crystallization Behavior of PDMS. *Interface Science*, 11(2), 199.
- Owen, & Dvornic. (2012). *Silicone Surface Science* (Vol. 4). Dordrecht: Springer Netherlands.
- Pakstis, Dunkers, Zheng, Vorbuerger, Quinn, & Cicerone. (2010). Evaluation of polydimethylsiloxane modification methods for cell response. *Journal of Biomedical Materials Research - Part A*, 92(2), 604-614.
- Wang, Yang, McKittrick, & Meyers. (2016). Keratin: Structure, mechanical properties, occurrence in biological organisms, and efforts at bioinspiration. *Progress in Materials Science*, 76, 229-318.
- Williams, Wilson, & Rhodes. (2004). Stability of plasma-treated silicone rubber and its influence on the interfacial aspects of blood compatibility. *Biomaterials*, 25(19), 4659-4673.
- Yang, & Yuan. (2016). Investigation on the mechanism of nitrogen plasma modified PDMS bonding with SU-8. *Applied Surface Science*, 364, 815-821.
- Zhou, Ellis, & Voelcker. (2010). Recent developments in PDMS surface modification for microfluidic devices. *Electrophoresis*, 31(1), 2-16.

Appendix 1

Conferences Attended

Lush Prize 2014 Conference- 'Is One R the new 3Rs?', London, UK, 2014.

APS Industrial Insights, Sandwich, UK, 2015.

APS International PharmSci, Nottingham, UK, 2015.

Bioinspired Materials, Manchester Metropolitan University, Manchester, UK, 2016.

Biorelevant, Royal Society of Chemistry, London, UK, 2016.

PGR Conference 2016, University of Huddersfield, Huddersfield, UK, 2016.

Poster Presentations

Plasma-treated Poly(dimethylsiloxane)-An Improved Surrogate for Human Skin - *Bioinspired Materials*, Manchester Metropolitan University, Manchester, UK, 2016.

Plasma-treated Poly(dimethylsiloxane)-An Improved Surrogate for Human Skin - *Biorelevant*, Royal Society of Chemistry, London, UK, 2016.

Peer Reviewed Publications

Effect of plasma surface treatment of poly(dimethylsiloxane) on the permeation of pharmaceutical compounds, *Journal of Pharmaceutical Analysis*, 7(5), 2017.

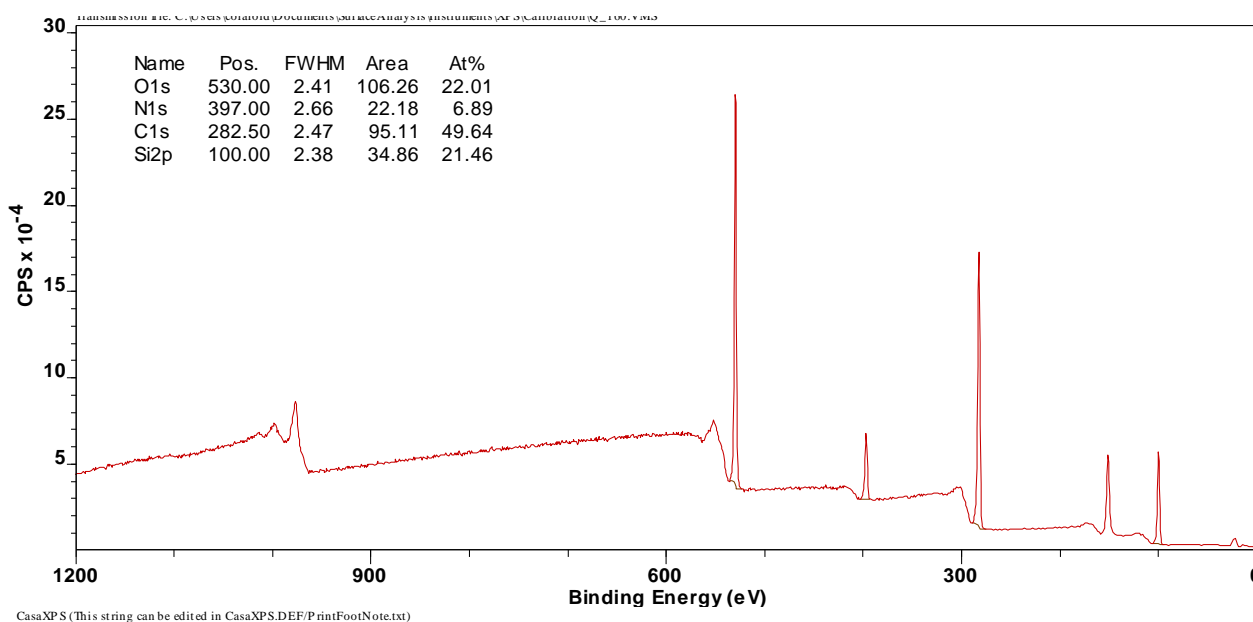
Appendix 2

Assumptions of statistical tests used in this thesis.

<u>Test</u>	<u>Assumptions</u>
Independent samples T-test	Normal distribution of the dependent variable, independence of observations, homogeneity of variance.
One-way analysis of variance (ANOVA)	Normal distribution of the dependent variable residuals, independence of observations, homogeneity of variance.
Levene's test for the homogeneity of variance	Independence of observations, variables are measured at the interval or ratio level.
Welch's <i>F</i> test	Normal distribution of the dependent variable residuals.
Pearson's correlation coefficient	Homoscedasticity, variables are measured at the interval or ratio level, approximate normal distribution of the variables.
Spearman's rho	Variables are measured at the ordinal, interval, or ratio level.
Post hoc Bonferroni test	Homogeneity of variance.
Post hoc-Games Howell	Heteroscedasticity of variance.

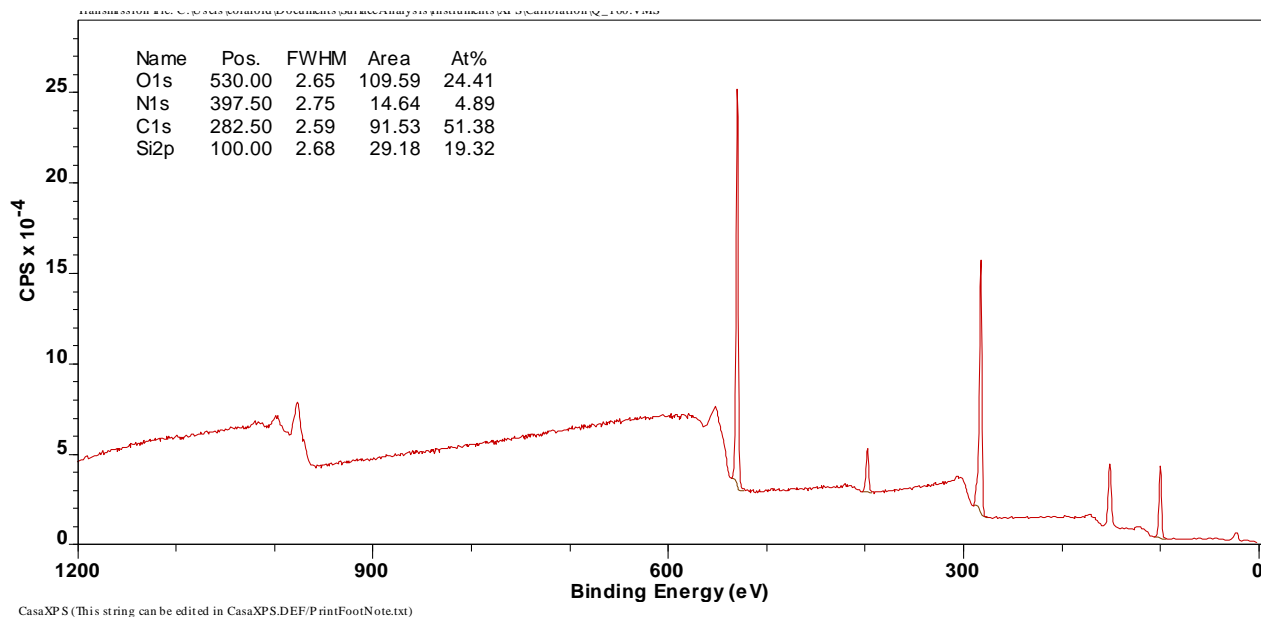
Appendix 3

XPS survey scan of APTMS silanised PDMS.



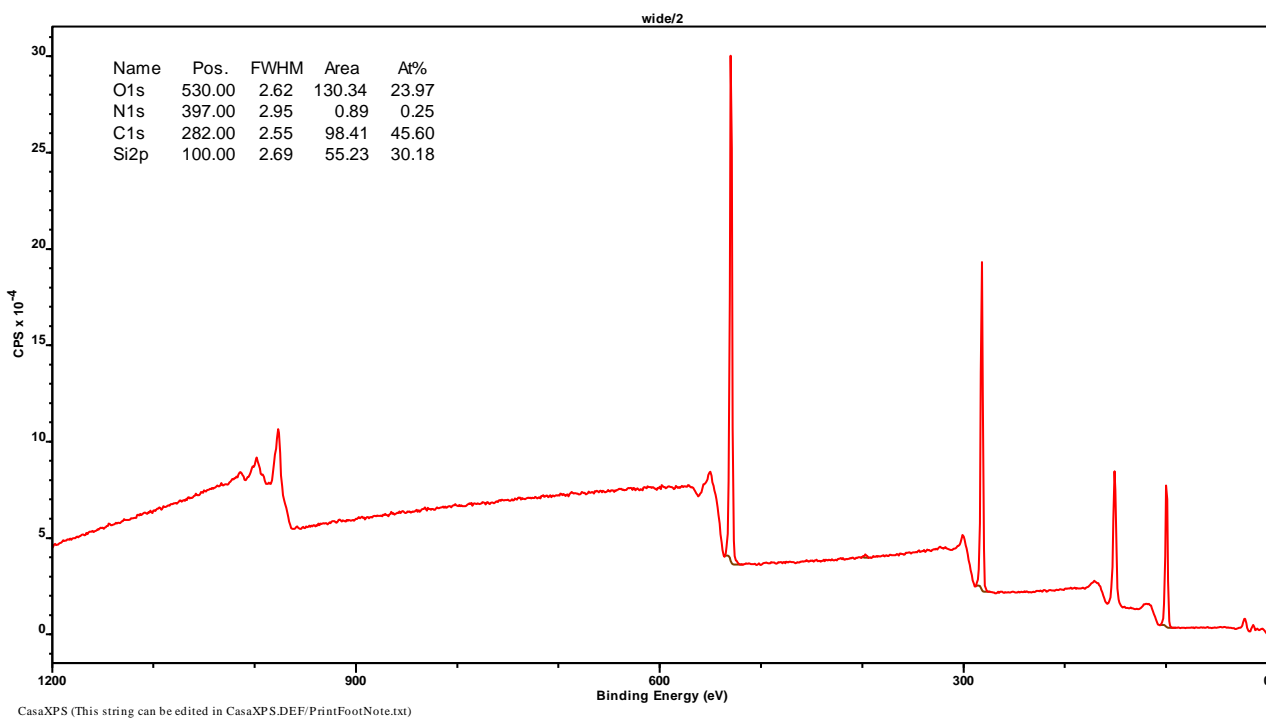
Appendix 4

XPS survey scan of PDMS-APTMS-Lys.



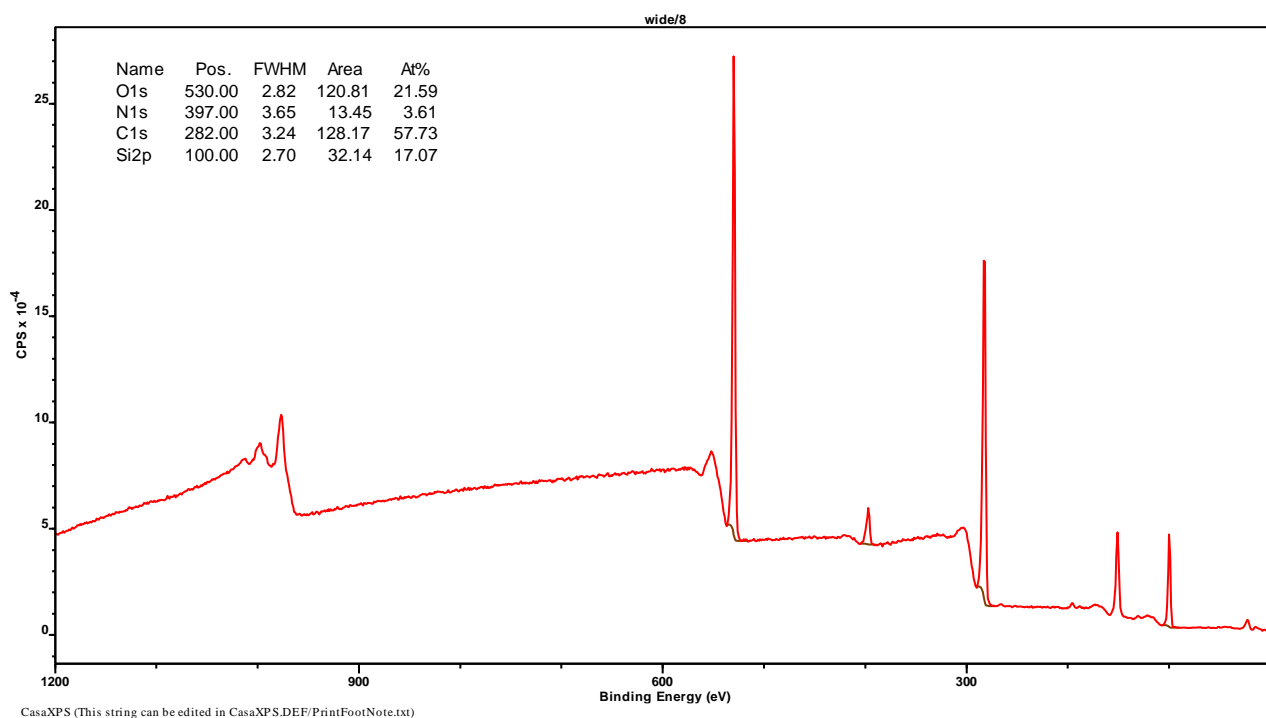
Appendix 5

XPS survey scan of PDMS-APTES.



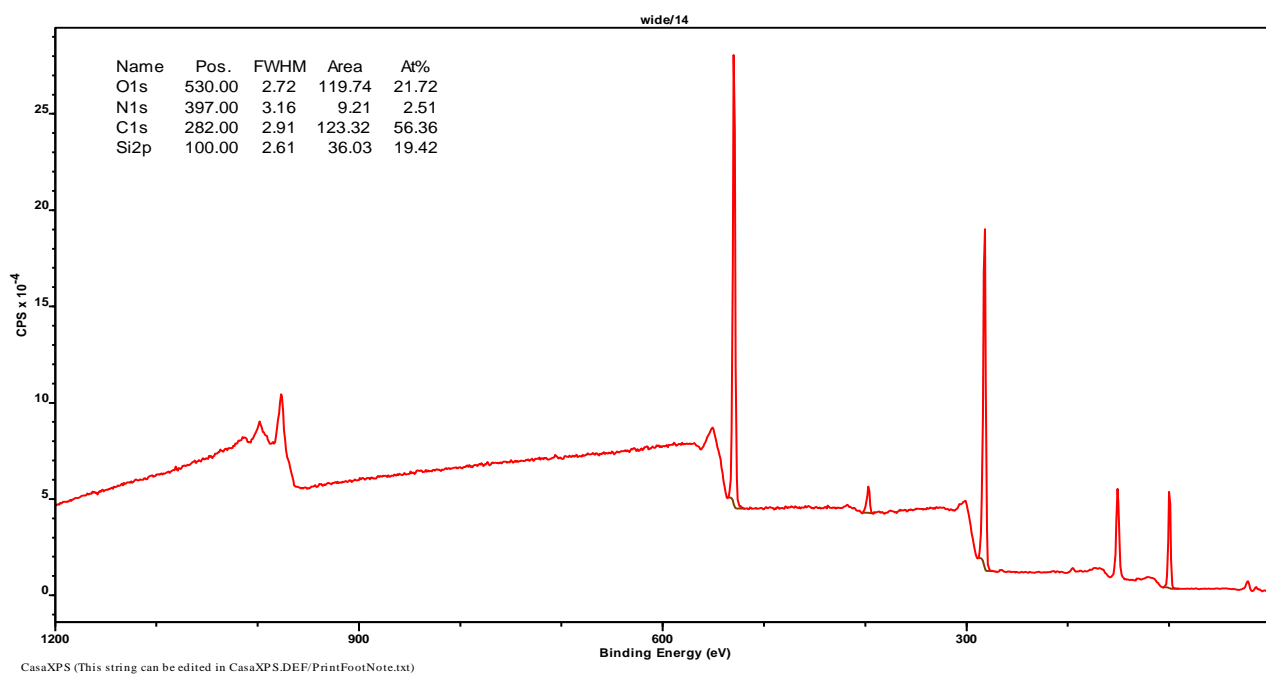
Appendix 6

XPS survey scan of PDMS-APTES-GA.



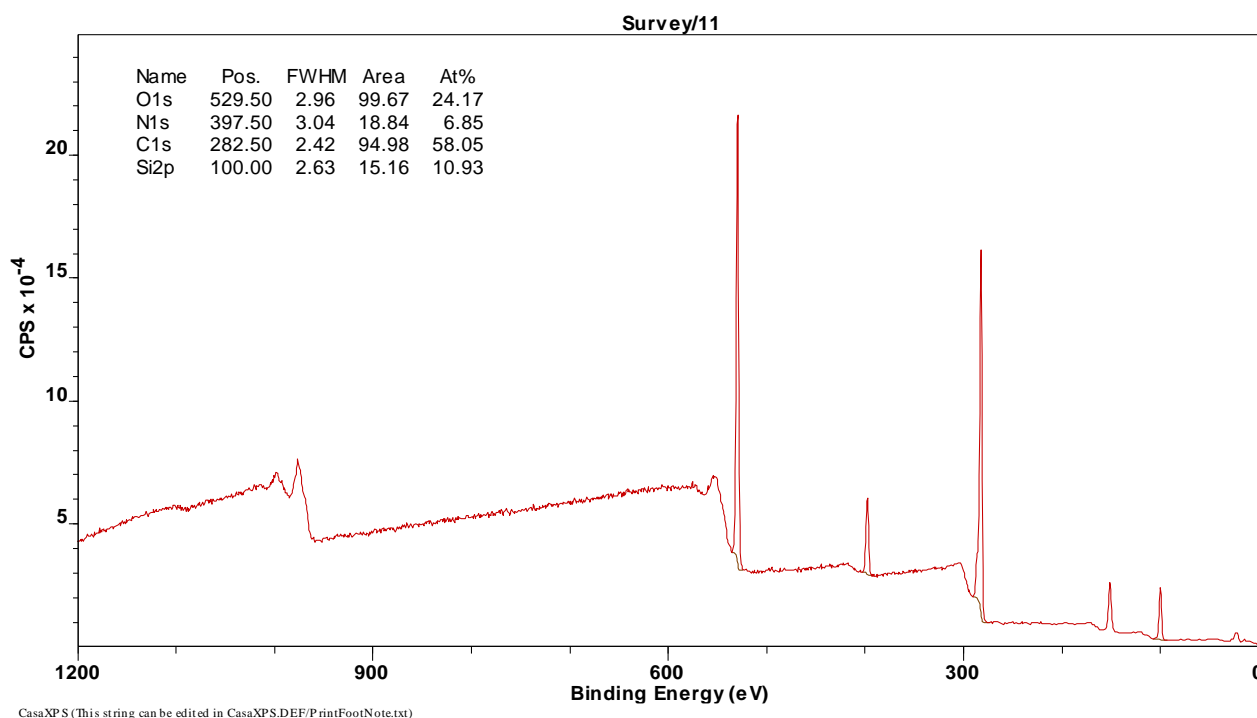
Appendix 7

XPS survey scan of PDMS-APTES-GA-Lys



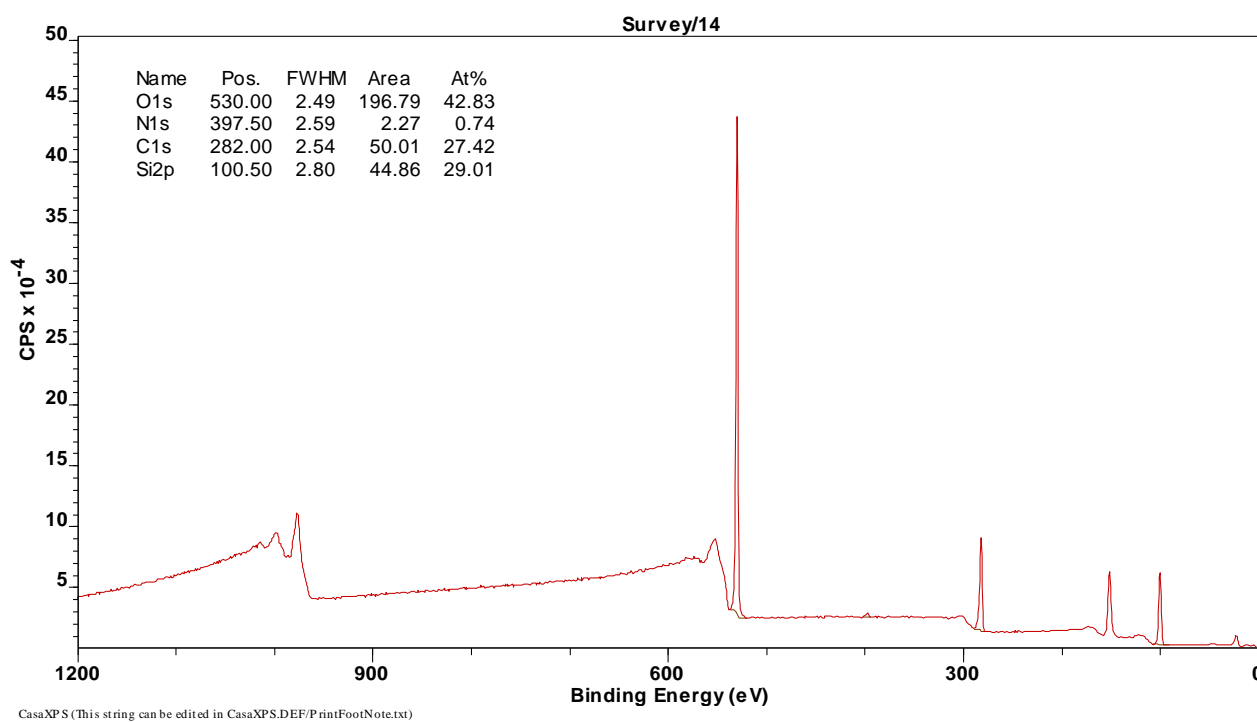
Appendix 8

Boc-Lys(Z)-OH functionalised PDMS (Dichloromethane).



Appendix 9

Boc-Lys(Z)-OH functionalised PDMS (EtOH).



Appendix 10

Specifications of PDMS, as provided by the manufacturer.

Product reference: 7458

Lot number: 1504028

Supplier: ATOS Medical

Sheet size: 150 x 200 mm

Sheet thickness: 0.13 mm

Grade: Medical grade (without polyester reinforcement)

Density: 1102.6 kg m⁻³

Tensile strength: 1038 psi

Percent elongation: 516 %

Extractables: Dichloromethane (4.8 % by weight loss), Ethanol (3.5 % by weight loss)

Trace metals analysis: None detectable

Crystallinity: No crystalline silica detected

Appendix 11

pH of saturated suspensions of ibuprofen (IBU), flurbiprofen (FLP), ketoprofen (KTP), caffeine (CAF), lidocaine (LID), benzoic acid (BA), salicylic acid (SA), acetyl salicylic acid (ASA), aminopyrine (AMP), methyl paraben (MP), ethyl paraben (EP), propyl paraben (PP), butyl paraben (BP), methyl 4-aminobenzoate (MAB), benzocaine (EAB), risocaine (PAB), butamben (BAB) and diclofenac (DF).

Compound	pH of saturated suspension (air plasma)	pH of saturated suspension (N ₂ plasma)
IBU	6.49 ± 0.01	N/A
FLP	6.58 ± 0.08	N/A
KTP	6.01 ± 0.01	N/A
CAF	7.52 ± 0.01	7.40 ± 0.00
LID	8.32 ± 0.03	8.33 ± 0.02
BA	4.16 ± 0.01	4.16 ± 0.00
SA	3.28 ± 0.02	N/A
ASA	3.45 ± 0.05	N/A
AMP	7.48 ± 0.05	N/A
MP	7.25 ± 0.00	7.27 ± 0.00
EP	7.35 ± 0.00	7.38 ± 0.00
PP	7.31 ± 0.01	7.37 ± 0.00
BP	7.37 ± 0.01	7.36 ± 0.00
MAB	7.38 ± 0.01	7.40 ± 0.00
EAB	7.39 ± 0.01	7.44 ± 0.00
PAB	7.41 ± 0.01	7.37 ± 0.00
BAB	7.36 ± 0.00	7.43 ± 0.01
DF	7.09 ± 0.01	N/A

Appendix 12

Concentration (mg mL^{-1}) of saturated solutions of caffeine (CAF), lidocaine (LID), benzoic acid (BA), methyl paraben (MP), ethyl paraben (EP), propyl paraben (PP), butyl paraben (BP), methyl 4-aminobenzoate (MAB), benzocaine (EAB), risocaine (PAB), and butamben (BAB).

Compound	Donor solution concentration (mg mL^{-1})
MP	2.929 ± 0.233
EP	1.226 ± 0.009
PP	0.4493 ± 0.0081
BP	0.3063 ± 0.0007
MAB	1.838 ± 0.017
EAB	1.213 ± 0.093
PAB	0.6074 ± 0.0139
BAB	0.1786 ± 0.0057
LID	3.931 ± 0.052
CAF	22.56 ± 2.54
BA	8.557 ± 0.111

Appendix 13

Linear range, linearity, intermediate precision, intra assay precision, limit of detection (LOD), and limit of quantification for high performance liquid chromatography methods used in the quantification of caffeine (CAF), lidocaine (LID), benzoic acid (BA), methyl paraben (MP), ethyl paraben (EP), propyl paraben (PP), butyl paraben (BP), methyl 4-aminobenzoate (MAB), benzocaine (EAB), risocaine (PAB), and butamben (BAB).

Compound	Range ($\mu\text{g mL}^{-1}$)	Linearity (R^2)	Intermediate precision RSD (%)	Intra assay precision RSD (%)	LOD ($\mu\text{g mL}^{-1}$)	LOQ ($\mu\text{g mL}^{-1}$)
MP	0.1 – 80	≥ 0.999	0.1 $\mu\text{g mL}^{-1}$: 9.15 10 $\mu\text{g mL}^{-1}$: 2.90 50 $\mu\text{g mL}^{-1}$: 2.57	0.1 $\mu\text{g mL}^{-1}$: 7.56 10 $\mu\text{g mL}^{-1}$: 0.07 50 $\mu\text{g mL}^{-1}$: 1.03	0.064	0.195
EP	0.1 – 100	≥ 0.999	0.1 $\mu\text{g mL}^{-1}$: 6.86 10 $\mu\text{g mL}^{-1}$: 2.27 50 $\mu\text{g mL}^{-1}$: 3.43	0.1 $\mu\text{g mL}^{-1}$: 1.44 10 $\mu\text{g mL}^{-1}$: 0.24 50 $\mu\text{g mL}^{-1}$: 0.35	0.047	0.142
PP	0.1 – 50	≥ 0.999	0.1 $\mu\text{g mL}^{-1}$: 5.26 10 $\mu\text{g mL}^{-1}$: 3.49 50 $\mu\text{g mL}^{-1}$: 2.24	0.1 $\mu\text{g mL}^{-1}$: 0.40 10 $\mu\text{g mL}^{-1}$: 0.21 50 $\mu\text{g mL}^{-1}$: 0.08	0.028	0.084
BP	0.1 – 50	≥ 0.999	0.1 $\mu\text{g mL}^{-1}$: 2.76 10 $\mu\text{g mL}^{-1}$: 2.39 50 $\mu\text{g mL}^{-1}$: 4.01	0.1 $\mu\text{g mL}^{-1}$: 1.87 10 $\mu\text{g mL}^{-1}$: 2.41 50 $\mu\text{g mL}^{-1}$: 1.07	0.056	0.169

Compound	Range ($\mu\text{g mL}^{-1}$)	Linearity (R^2)	Intermediate precision RSD (%)	Intra assay precision RSD (%)	LOD ($\mu\text{g mL}^{-1}$)	LOQ ($\mu\text{g mL}^{-1}$)
MAB	2.5 – 50	≥ 0.999	2.5 $\mu\text{g mL}^{-1}$: 4.17 10 $\mu\text{g mL}^{-1}$: 4.29 30 $\mu\text{g mL}^{-1}$: 5.14	2.5 $\mu\text{g mL}^{-1}$: 4.17 10 $\mu\text{g mL}^{-1}$: 4.29 30 $\mu\text{g mL}^{-1}$: 5.14	0.070	0.211
EAB	1 – 50	≥ 0.999	2.5 $\mu\text{g mL}^{-1}$: 4.59 10 $\mu\text{g mL}^{-1}$: 4.96 30 $\mu\text{g mL}^{-1}$: 7.33	2.5 $\mu\text{g mL}^{-1}$: 0.08 10 $\mu\text{g mL}^{-1}$: 0.14 30 $\mu\text{g mL}^{-1}$: 0.56	0.049	0.147
PAB	0.25 – 20	≥ 0.999	1 $\mu\text{g mL}^{-1}$: 8.66 2.5 $\mu\text{g mL}^{-1}$: 4.58 10 $\mu\text{g mL}^{-1}$: 5.03	1 $\mu\text{g mL}^{-1}$: 0.40 2.5 $\mu\text{g mL}^{-1}$: 0.76 10 $\mu\text{g mL}^{-1}$: 0.95	0.093	0.283
BAB	0.25 – 20	≥ 0.999	1 $\mu\text{g mL}^{-1}$: 8.68 2.5 $\mu\text{g mL}^{-1}$: 10.38 10 $\mu\text{g mL}^{-1}$: 8.17	1 $\mu\text{g mL}^{-1}$: 2.54 2.5 $\mu\text{g mL}^{-1}$: 2.58 10 $\mu\text{g mL}^{-1}$: 2.09	0.107	0.323
LID	0.6 – 60	≥ 0.999	0.6 $\mu\text{g mL}^{-1}$: 1.52 3 $\mu\text{g mL}^{-1}$: 6.17 15 $\mu\text{g mL}^{-1}$: 2.76	0.6 $\mu\text{g mL}^{-1}$: 0.8 3 $\mu\text{g mL}^{-1}$: 0.28 15 $\mu\text{g mL}^{-1}$: 0.43	0.030	0.092

Compound	Range ($\mu\text{g mL}^{-1}$)	Linearity (R^2)	Intermediate precision RSD (%)	Intra assay precision RSD (%)	LOD ($\mu\text{g mL}^{-1}$)	LOQ ($\mu\text{g mL}^{-1}$)
CAF	0.05 – 50	≥ 0.999	0.05 $\mu\text{g mL}^{-1}$: 15.45 2 $\mu\text{g mL}^{-1}$: 2.15 10 $\mu\text{g mL}^{-1}$: 4.07	0.25 $\mu\text{g mL}^{-1}$: 2.69 2 $\mu\text{g mL}^{-1}$: 12.39 10 $\mu\text{g mL}^{-1}$: 0.07	0.022	0.066
BA	0.05 – 60	≥ 0.999	5 $\mu\text{g mL}^{-1}$: 6.76 20 $\mu\text{g mL}^{-1}$: 4.81 40 $\mu\text{g mL}^{-1}$: 3.13	5 $\mu\text{g mL}^{-1}$: 0.17 20 $\mu\text{g mL}^{-1}$: 0.16 40 $\mu\text{g mL}^{-1}$: 0.08	0.126	0.381

Appendix 14

Permeability coefficients (K_p) of ibuprofen (IBU), flurbiprofen (FLP), ketoprofen (KTP), caffeine (CAF), lidocaine (LID), benzoic acid (BA), salicylic acid (SA), acetyl salicylic acid (ASA), aminopyrine (AMP), methyl paraben (MP), ethyl paraben (EP), propyl paraben (PP), butyl paraben (BP), methyl 4-aminobenzoate (MAB), benzocaine (EAB), risocaine (PAB), butamben (BAB) and diclofenac (DF) extracted from literature.

Compound	Permeability coefficient (K_p , cm min ⁻¹)			
IBU	6.0513 x 10 ⁻⁴ (Degim <i>et al.</i> , 1998) b, g.	5.60 x 10 ⁻⁵ (Zhang <i>et al.</i> , 2012) b, f.		
KTP	6.474 x 10 ⁻⁴ (Miki <i>et al.</i> , 2015) b, e.	1.170 x 10 ⁻⁴ (Zhang <i>et al.</i> , 2012) b, f.		
FLP	7.082 x 10 ⁻³ (Miki <i>et al.</i> , 2015) b, e.	3.786 x 10 ⁻⁵ (Zhang <i>et al.</i> , 2012) b, f.		
DF	1.67 x 10 ⁻⁵ (Degim <i>et al.</i> , 1998) b, g.			
LID	4.209 x 10 ⁻⁴ (Miki <i>et al.</i> , 2015) b, e.	4.0 x 10 ⁻⁷ (Trovatti <i>et al.</i> , 2012) b, i.	0.084 x 10 ⁻⁴ (Uchida <i>et al.</i> , 2015) c, p.	
CAF	1.08 x 10 ⁻⁵ (Uchida <i>et al.</i> , 2015) c, f.	1.267 x 10 ⁻⁶ (Schreiber <i>et al.</i> , 2005) c, j.	3.6 x 10 ⁻⁶ (Schäfer-Korting, 2006) d, j.	2.83 x 10 ⁻⁶ (Nanayakkara <i>et al.</i> , 2005) b, f.
BA	4.1865 x 10 ⁻⁴ (Degim <i>et al.</i> , 1998) b, h.	2.94 x 10 ⁻⁴ (Zhang <i>et al.</i> , 2012) b, g.		

Compound	Permeability coefficient (K_p , cm min^{-1})			
SA	2.3006×10^{-4} (Degim <i>et al.</i> , 1998) b, h.	1.4×10^{-5} (Smith <i>et al.</i> , 2000) b, k.	4.384×10^{-4} (Qvist <i>et al.</i> , 2000) b, l.	2.83×10^{-4} (Smith <i>et al.</i> , 2000) b, o.
ASA	8.5×10^{-6} (Walker <i>et al.</i> , 1997) c, n.			
AMP	1.98×10^{-5} (Uchida <i>et al.</i> , 2015) c, f.	1.854×10^{-5} (Miki <i>et al.</i> , 2015) b, e.		
MAB	1.104×10^{-3} (Uchida <i>et al.</i> , 2015) c, f.	3.8×10^{-4} (Roy <i>et al.</i> , 1993) a, e.		
EAB	1.21×10^{-3} (Uchida <i>et al.</i> , 2015) c, f.	3.3×10^{-4} (Roy <i>et al.</i> , 1993) a, e.		
PAB	1.34×10^{-3} (Uchida <i>et al.</i> , 2015) c, f.			
BAB	1.21×10^{-3} (Uchida <i>et al.</i> , 2015) c, f.	1.4×10^{-3} (Roy <i>et al.</i> , 1993) a, e.		
MP	1.49×10^{-4} (Uchida <i>et al.</i> , 2015) c, f.	5.67×10^{-4} (Nanayakkara <i>et al.</i> , 2005) b, f.	3.306×10^{-4} (Akomeah, 2007) b, f.	3.550×10^{-4} (Akomeah <i>et al.</i> , 2004) b, m.
EP	2.32×10^{-4} (Uchida <i>et al.</i> , 2015) c, f.			
PP	2.18×10^{-4} (Uchida <i>et al.</i> , 2015) c, f.			

Compound	Permeability coefficient (K_p , cm min^{-1})			
BP	2.12×10^{-4} (Uchida <i>et al.</i> , 2015) c, f.	1.564×10^{-3} (Nanayakkara <i>et al.</i> , 2005) b, f.	1.71×10^{-3} (Akomeah, 2007) b, f.	1.6619×10^{-3} (Akomeah <i>et al.</i> , 2004) b, m.

- a. 25 °C
- b. 37 °C.
- c. 32 °C.
- d. 33.5 °C.
- e. Donor solution: Saturated solution in purified water. Receptor solution: Purified water.
- f. Donor solution: Saturated solution in pH 7.4 phosphate buffered saline. Receptor solution: pH 7.4 phosphate buffered saline.
- g. Donor solution: Saturated solution in pH 7.4 phosphate buffered saline diluted to 80 % saturation. Receptor solution: pH 7.4 phosphate buffered saline.
- h. Donor solution: Aqueous solution. Receptor solution: pH 7.4 phosphate buffered saline.
- i. Donor solution: 2 % (w/w) aqueous solution. Receptor solution: Isotonic pH 7.4 phosphate buffered saline.
- j. Donor solution: 0.1 % in pH 7.4 phosphate buffered saline. Receptor solution: pH 7.4 phosphate buffered saline.
- k. Donor solution: 2 mg/mL solution in pH 5.13 McIlvaine buffer. Receptor solution: pH 5.13 McIlvaine buffer.
- l. Donor solution: 2 mg/ml solution in pH 7.4 phosphate buffer adjusted to pH 2.5. Receptor solution pH 7.4 phosphate buffer.
- m. Donor solution: Saturated solution in deionised water. Receptor solution: pH 7.4 phosphate buffered saline.
- n. Donor solution: Not stated. Receptor solution: distilled water.
- o. Donor solution: Saturated suspension in pH 3.14 McIlvaine buffer. Receptor solution: pH 5.13 McIlvaine buffer.
- p. Donor solution: Saturated solution in pH 7.4 phosphate buffered saline, adjusted to pH 7.9. Receptor solution: pH 7.4 phosphate buffered saline

References

- Akomeah. (2007). Variability in Human Skin Permeability In Vitro: Comparing Penetrants with Different Physicochemical Properties. *Journal of pharmaceutical sciences*, 96(4), 824-834.
- Akomeah, Nazir, Martin, & Brown. (2004). Effect of heat on the percutaneous absorption and skin retention of three model penetrants. *European Journal of Pharmaceutical Sciences*, 21(2-3), 337-345.
- Degim, Pugh, & Hadgraft. (1998). Skin permeability data: Anomalous results. *International Journal of Pharmaceutics*, 170(1), 129-133.
- Miki, Ichitsuka, Yamada, Kimura, Egawa, Seki, Juni, Ueda, & Morimoto. (2015). Development of a membrane impregnated with a poly(dimethylsiloxane)/poly(ethylene glycol) copolymer for a high-throughput screening of the permeability of drugs, cosmetics, and other chemicals across the human skin. *European Journal of Pharmaceutical Sciences*, 66, 41-49.
- Nanayakkara, Bartlett, Forbes, Marriott, Whitfield, & Brown. (2005). The effect of unsaturated fatty acids in benzyl alcohol on the percutaneous permeation of three model penetrants. *International Journal of Pharmaceutics*, 301(1-2), 129-139.
- Qvist, Hoeck, Kreilgaard, Madsen, & Frokjaer. (2000). Evaluation of Göttingen minipig skin for transdermal in vitro permeation studies. *European Journal of Pharmaceutical Sciences*, 11(1), 59-68.
- Roy, Fujiki, & Fleitman. (1993). Permeabilities of alkyl p-aminobenzoates through living skin equivalent and cadaver skin. *Journal of Pharmaceutical Sciences*, 82(12), 1266-1268.
- Schäfer-Korting. (2006). Reconstructed human epidermis for skin absorption testing: results of the german prevalidation study. *ATLA: alternatives to laboratory animals*, 34(3), 283-294.
- Schreiber, Mahmoud, Vuia, Rübhelke, Schmidt, Schaller, Kandárová, Haberland, Schäfer, Bock, et al. (2005). Reconstructed epidermis versus human and animal skin in skin absorption studies. *Toxicology in Vitro*, 19(6), 813-822.
- Smith, & Irwin. (2000). Ionisation and the effect of absorption enhancers on transport of salicylic acid through silastic rubber and human skin. *International Journal of Pharmaceutics*, 210(1-2), 69-82.
- Trovatti, Freire, Pinto, Almeida, Costa, Silvestre, Neto, & Rosado. (2012). Bacterial cellulose membranes applied in topical and transdermal delivery of lidocaine hydrochloride and ibuprofen: In vitro diffusion studies. *International Journal of Pharmaceutics*, 435(1), 83-87.
- Uchida, Kadhum, Kanai, Todo, Oshizaka, & Sugibayashi. (2015). Prediction of skin permeation by chemical compounds using the artificial membrane, Strat-M™. *European Journal of Pharmaceutical Sciences*, 67, 113-118.
- Walker, Hulme, Rippon, Walmsley, Gunnigle, Lewin, & Winsey. (1997). In vitro model(s) for the percutaneous delivery of active tissue repair agents. *Journal of Pharmaceutical Sciences*, 86(12), 1379-1384.
- Zhang, Chen, Scriba, Abraham, Fahr, & Liu. (2012). Human skin permeation of neutral species and ionic species: Extended linear free-energy relationship analyses. *Journal of Pharmaceutical Sciences*, 101(6), 2034-2044.

